University of Alberta

ALTERNATING CURRENT ELECTROCOAGULATION (AC/EC) OF FINE PARTICULATE SUSPENSIONS

by

Roy Oswald Ifill

A thesis submitted to the Faculty of Graduate Studies and Research
in partial fulfillment of the requirements for the degree of

Doctor of Philosophy
in
Chemical Engineering

Department of Chemical and Materials Engineering

Spring 2010
Edmonton, Alberta

Examining Committee

Dr. Thomas H. Etsell, Department of Chemical and Materials Engineering

Dr. Qi Liu, Department of Chemical and Materials Engineering

Professor L.R. Plitt, Department of Civil and Environmental Engineering

Dr. Mohamed Gamal El-Din, Department of Civil and Environmental Engineering

Dr. Michael A. Kessick, RJ Oil Sands Inc.

ABSTRACT

Poor settling of solids increases land requirement for tailings containment and imposes severe constraints on the water balance. Consequent to these considerations, the alternating current electrocoagulation (AC/EC) technique emerged as a candidate for enhancing the settling behaviour of suspensions in the mineral, coal and oil sands industries. Hence, a fundamental study of AC/EC was undertaken with aluminum electrodes. Ground silica (d_{50} = 20 µm), which formed a stable suspension, served as the model tailings solid at 5.0 wt % in water.

The AC/EC process consisted of two developmental stages: coagulation, marked by pH decrease in the silica suspension; and floc growth, characterized by pH increase from the minimum (*i.e.*, the end of coagulation). AC/EC enhanced the initial settling rate of silica by over three orders of magnitude, and exhibited remarkable flexibility by virtue of the wide range of process parameters that could be optimized. For example, AC/EC can be operated in either the indirect or direct mode. The settling behaviour of bentonite (estimated d_{50} < 1 µm) was more enhanced by indirect AC/EC, while that of silica benefited more from direct AC/EC.

Any condition that increased aluminum dosage (*e.g.*, current, retention time), increased the initial settling rate of silica. Over the feed water pH range of 3.0 to 9.1, AC/EC was effective in enhancing the settling behaviour of silica. AC/EC was also effective over a wide range of temperatures (23° to 85°C).

High electrical energy demand by AC/EC was observed throughout this study. Its optimization was beyond the scope of this work.

Dilution of a sample of Syncrude mature fine tailings (MFT) to 4.6 wt % solids sustained a stable suspension. Settling occurred after AC/EC treatment, a crystal-clear supernatant resulted and bitumen was recovered as froth. Entrained solids were easily spray-washed from the froth with water.

The settling behaviour of a Luscar Sterco fine coal tailings sample was not augmented by AC/EC, possibly due to contamination by the company's own electrocoagulation operation.

After having been stored dry for more than a year, electrocoagulated silica was an effective coagulant for as-received silica and Syncrude MFT.

ACKNOWLEDGMENTS

I take this opportunity to express my sincere gratitude to Dr. Nosa Egiebor and Prof. Verne Plitt for their guidance, suggestions and assistance towards the accomplishment of this research.

The efforts of Dr. Tom Etsell and Dr. Robert Hayes in guiding the update of this thesis for defence are gratefully acknowledged.

I am grateful to NSERC and the former Luscar Sterco for the financial support they provided.

Finally, I extend my profound gratitude to my family for their support of this endeavour.

TABLE OF CONTENTS

LIST OF TABLES

LIST OF FIGURES

LIST OF PLATES

CHAPTER 1
INTRODUCTION

1.1 BACKGROUND

A brief review of the impact of stable particulate suspensions on industrial and environmental processes illustrates the need for treatment options that are capable of significantly enhancing the dewatering characteristics of the solids.

1.1.1 Effects of Stable Particulate Suspensions on Industrial Processing

For about a century, colloidal solids have been known to stabilize emulsions (Briggs, 1921). In oil sands production, for example, bentonite stabilizes water-bitumen emulsions (Gelot *et al.*, 1984). Where such emulsions are to be broken, processing time and production costs are increased. In hydrometallurgical processes incorporating solvent extraction for metal recovery from leach liquor, the entrainment of fine solids in the aqueous phase promotes the formation of stable emulsions, also known as “crud formation”. Since this prevents rapid disengagement of the liquid phases in the settlers, emulsion formation incurs additional operating costs due to the substantial reduction of operating capacity, the addition of demulsifier, or the possible loss of dissolved metal and organic extractant if the emulsion is skimmed off.

In metal electrowinning operations, suspended particulates in the cells are highly undesirable since they impair the quality of the metal electrodeposit in which they become occluded.

Leach residue in hydrometallurgical plants is washed to recover leach reagent before disposal to the tailings pond. The washing operation is performed in a countercurrent decantation circuit, often with filtration as the final stage of solid-liquid separation. Clearly, the solids must dewater rapidly to maintain throughput.

The dewatering behaviour of tailings directly affects the utilization of the tailings pond, which is designed principally as a repository for the solids while permitting recycle of the supernatant water to the plant. A major requirement for

efficient operation is that the solids settle readily in the tailings pond. Poorly settling solids, therefore, severely restrict solution recycle and impose an exorbitant demand on land space for storage of the tailings slurry. This is the case with Syncrude's Mildred Lake operation where, by 1985, the Mildred Lake Settling Basin (MLSB) was growing annually by 25×10^6 m^3 (MacKinnon, 1986) and, by 1988, it was occupying a total area of 22 km^2 (MacKinnon, 1989). In its tailings plan submitted to the Energy Resources Conservation Board, Syncrude (2009) stated that the MLSB was occupying approximately 30 km^2 of land. In addition to this, there were the unquantified areas of land occupied by one other out-of-pit tailings storage facility, the Southwest Sand Storage (SWSS), and three in-pit tailings deposition areas, namely, West In-pit (WIP), East In-pit (EIP) and Southwest In-pit (SWIP).

1.1.2 Environmental Influence of Stable Particulate Suspensions

Colloids create turbidity which is undesirable in potable water. Because of their large surface area, colloids are strong adsorbents for metal ions, toxic organic compounds, viruses and radionuclides. These noxious adsorbates are thus transported over long distances in air, groundwater and surface water (Sawyer *et al.*, 1994).

The total suspended solids (TSS) concentration in wastewater, such as precipitates in process plant effluents, is indicative of the extent of pollution (Sawyer *et al.*, 1994). As expected, the load on filters and clarifiers increases with increasing TSS, making the dewatering behaviour of the solids a critical consideration. Volatile suspended solids (VSS) are most likely to contain a significant fraction of organic material, accounting for up to 80% of the TSS (Sawyer *et al.*, 1994). In environmental engineering practice, both the TSS and VSS constitute parameters by which activated sludge processes are controlled.

1.1.3 Removal of Suspended Particulates

In solid-liquid separation operations, such as thickening, clarification and filtration, chemical reagents are conventionally added in small doses to destabilize and aggregate colloidal and suspended solids. Reagents, such as alum and ferric sulphate, are widely used to promote aggregation of the particles into larger entities with enhanced dewatering characteristics. In practice,

however, this technique tends to become less effective in cold water or for colloidal particles. Reagent cost accounts for a sizeable fraction of the costs incurred in water treatment and mineral processing operations. For example, Montgomery (1985) quoted an annual reagent cost of approximately $120M for the American water treatment industry. It follows, therefore, that the identification of less expensive or more efficient means of coagulation/flocculation remains an important objective.

More recently, the conventional reagents have been giving way to their polymeric derivatives as coagulants, particularly for water and wastewater treatment. The derivatives have shown greater efficacy over a wider pH range and at lower temperatures. Consequently, much effort has gone into the study of such derivatives as polyaluminum chloride, PACl (Duan and Gregory, 2003; Wang *et al.*, 2002; Gregory and Duan, 2001), polyaluminum chloride sulphate, PACS (Gao and Yue, 2005), polyaluminum silicate chloride, PASC (Gao *et al.*, 2002), and basic aluminum sulphate, BAS (Solomentseva *et al.*, 2004).

It is instructive at this juncture to define “colloids”. Montgomery (1985) defines “colloidal solids” as particles having a diameter in the nominal range of 5 nm to 1 µm, whereas “suspended solids” are larger than 1 µm and dissolved solids are smaller than 5 nm. Other definitions (Everett, 1988; MacKinnon, 1986; van Olphen, 1977) place colloidal particles in the size range of 1 nm to 1 µm, while still others (*e.g.*, Masliyah, 1994) consider particles with diameters of 1 nm to 10 µm to be colloidal. It should be pointed out that only one dimension of a particle needs to be in the colloid range for the particle to be considered colloidal (Everett, 1988). Evidently, the definition of colloidal size is by no means rigid, but it is consistent with the concept that colloidal size denotes the minimum size a particle can attain without being in true solution.

Colloidal particles are generated by the following operations and processes (Sawyer *et al.*, 1994):

- drilling and blasting during mining operations;
- grinding in general and colloid milling in particular;
- aqueous ionic reactions, such as precipitation and application of the common-ion effect;
- molecular aggregation in solution, as in micelle formation (*e.g.*, soap and proteins); and

- natural weathering, as in the case of iron oxides and silicates, for example.

Microorganisms, such as viruses, bacteria and algae, are also considered to be colloidal. It is noteworthy that, although molecules of gelatine, albumin and humic materials dissolve in water, they are large enough to be considered colloidal and, therefore, not in true solution (Sawyer *et al.*, 1994).

For the purposes of this study, "coagulation" is defined as the destabilization of a particulate dispersion in a liquid phase, usually an aqueous medium. The definition implies that constraints on interparticle contact, engendered by electrostatic repulsion or steric hindrance, are eliminated or minimized such that aggregation can occur and dewatering is facilitated. "Flocculation" is defined as the aggregation of destabilized particulates into porous, 3-dimensional networks called "flocs". Coagulation is effected by inorganic reagents, such as alum, while flocculation is promoted by macromolecular compounds, such as starch. Hence, these definitions proposed by La Mer (1964) have been adopted in this study.

1.1.4 Electrocoagulation

Coagulation effected or aided by electrical means is connoted as "electrocoagulation". In the literature, a variety of terms is used to describe the process by which colloidal and suspended particles are caused, by electrical treatment with consumable anodes, to be dewatered more readily. "Electrocoagulation" (*e.g.*, Cañizares *et al.*, 2007; Holt *et al.*, 2005; Ghernaout *et al.*, 2008; Barkley *et al.*, 1993; Makarov *et al.*, 1987) is the most widely used term, mainly because many authors use "coagulation" and "flocculation" interchangeably. Other connotations of the technique include "electro-flocculation" (Harif and Adin, 2007; Ofir *et al.*, 2007a), "electrokinetically enhanced sedimentation" (Sauer and Davis, 1994), "electroprecipitation" (Jenke and Diebold, 1984), ""electrolytic flocculation" (Pretorius *et al.*, 1991), "electrochemical treatment" (Bejankiwar, 2002), and "electrolysis" (Grøterud and Smoczynski, 1992). In this study, preference is given to "electrocoagulation" in analogy with La Mer's (1964) definition.

1.2 LITERATURE REVIEW

1.2.1 Overview of Electrocoagulation

1.2.1.1 Direct and Alternating Current Electrocoagulation

Electrocoagulation can be achieved with direct current (DC) or alternating current (AC). Since alternating current oscillates between positive and negative values, one electrode (plate, rod, or other configuration) becomes the anode and the other the cathode between 0 and π radians of the cycle. Between π and 2π, however, the electrodes reverse polarity. In this way, both electrodes function alternately as anode and cathode in every cycle.

The performances of AC and DC electrocoagulation have not been compared experimentally, side by side, in the literature. Such a comparison would be expected to yield useful data, particularly in relation to the consumption of electrical energy. A brief overall comparison would show that alternating current electrocoagulation (AC/EC) can be powered directly from the mains, requiring only a transformer to regulate the current, as was done in this study. Direct current electrocoagulation (DC/EC), on the other hand, can be powered by a battery for laboratory purposes, with a rheostat for current adjustment. For large scale application, however, AC power would be the practical choice and rectifiers would be required to convert it to DC. It appears, therefore, that the operation of DC/EC on a commercial scale would incur higher capital expenditure than AC/EC, mainly for ancillary electrical equipment.

Electrophoresis (*i.e.*, the migration of charged particles under the influence of an imposed electric field) occurs during DC/EC. Upon arriving at the electrode of opposite polarity, the particles adhere thereto. With time, the particles coat the electrode, increasing its resistivity and reducing its effective area. One way of limiting this phenomenon is to reverse the electrode polarity periodically (Donini *et al.*, 1994; Perng *et al.*, 2007). With AC/EC, on the other hand, electrophoresis does not occur. Under quiescent conditions, the charged particles would oscillate about a mean position under the influence of the AC field. This mean position for colloidal particles would change randomly as a consequence of Brownian motion.

Anode passivation occurs during DC/EC (Mollah *et al.*, 2001). With operating time, the oxide layer becomes thicker, thus increasing the resistivity of the anode and the proportion of energy lost to passivation. These effects may be

minimized or eliminated by reversing the electrode polarity periodically (Donini *et al.*, 1994; Jiang *et al.*, 2002). In AC/EC, the frequent polarity reversal prevents passivation from occurring.

As electrocoagulation proceeds, pH changes occur in the solution. In the case of DC/EC under quiescent conditions, the pH was observed to drop into the strongly acidic range around the anode, while it rose to alkaline levels around the cathode (Moreno *et al.*, 2009; Cañizares *et al.*, 2007; Cañizares *et al.*, 2005a). Hence, under such pH conditions, iron anodes and aluminum cathodes experienced higher dissolution rates than those predicted by Faraday's Law.

Owing to water electrolysis, hydrogen gas is evolved at the cathode (Jenke and Diebold, 1984; Pretorius *et al.*, 1991; Przhegorlinskii *et al.*, 1987; Vik *et al.*, 1984) and oxygen at the anode (Cañizares *et al.*, 2005b; Cañizares *et al.*, 2009; Trompette and Vergnes, 2009; Mollah *et al.*, 2004; Perng *et al.*, 2007; Moreno *et al.*, 2009). Hence, gas evolution occurs at both electrodes in DC/EC and AC/EC. In AC/EC, however, gas evolution switches with the alternating polarity. In both cases, the same quantity of gas is released. In the main reaction, metal from the anode is oxidized and enters solution. Electrode reactions are discussed in Section 1.2.4.1.

1.2.1.2 Electrode Materials

Aluminum and iron (or steel) are the most frequently used materials for electrodes in electrocoagulation. They can be used together in the same cell if an advantage is perceived. Criteria for the selection of electrode materials are summarized below.

1. The material must oxidize electrolytically and dissolve in water. This criterion eliminates graphite as a potential electrode material and limits the candidate materials to metals.
2. The metal hydroxide should have a low K_{S0} (*i.e.*, K_{SP}) value for high utilization of the metal and, hence, minimization of its residual concentration in solution. The K_{S0} values for aluminum and iron hydroxides are: $Al(OH)_3$, $5x10^{-33}$; $Fe(OH)_2$, $1.8x10^{-15}$; $Fe(OH)_3$, $6x10^{-38}$ (Mortimer, 1986). This criterion justifies the preference for aluminum and iron (or steel) as electrode materials. Zinc has been tested, but the high K_{S0} value of $4.5x10^{-17}$ (Mortimer, 1986) resulted in elevated residual zinc concentrations in the treated water (Jenke and

Diebold, 1984). Of the iron hydroxides, $Fe(OH)_3$ is the more effective because of its lower K_{S0} value. During electrocoagulation, iron from the anode is oxidized to the ferrous state, requiring aeration (pH > ~3) for further oxidation to Fe(III). At high current densities, the rate of Fe(II) generation could outstrip the rate of oxygen solubility, reducing the utilization of the metal (Jenke and Diebold, 1984; Sanfan, 1991). Another constraint can arise from the reduced solubility of oxygen with increasing ionic strength of the solution. Criteria 1 and 2 will be treated in detail in the discussion of aqueous chemistry.

3. High electrical conductivity is a desirable property of the metal to reduce the energy lost as heat. Electrical conductivities for aluminum and iron at 273°K are 4.14×10^7 and 1.17×10^7 Siemens/metre (S/m), respectively. In contrast, that for carbon is about three orders of magnitude lower (7.27×10^4 S/m) at the same temperature (Weast, 1989).
4. The metal should be inexpensive and readily available.
5. The metal must not be toxic. This requirement eliminates lead as a potential electrode material.

1.2.1.3 Cell Design

Most of the testwork reported in the literature was performed with plate electrodes arranged in a manner identical to conventional electrolysis cells. Only a few studies were directed towards optimization of the cell design. A novel approach resulted in the fluidized-bed ACE Separator (Barkley *et al.*, 1993) which consisted of a series of hollow cylinders fabricated from 316 stainless steel and interconnected with polyethylene tubing. Alternate cylinders were connected to the same AC polarity and the assembly was operated in a vertical position. Aluminum shot, between 1.2 and 2.4 mm in diameter, was fluidized by the feed solution in continuous flow.

In another study (Pretorius *et al.*, 1991), three DC power connection configurations were examined. In one configuration sketched in Figure 1-1a, power was connected to the two outermost plate electrodes. Between these, adjacent pairs of electrodes were bridged but were not connected to the power supply. This arrangement induced the same polarity in a given electrode pair which, in turn, induced the opposite polarity in the next, adjacent pair. Another

design (Figure 1-1b) created cells in series by the connection of alternate electrodes, in parallel, to the power supply. This arrangement was identical to that in conventional electrolytic cells. The third design (Figure 1-1c) was like the first, but without bridging. Only the two outermost plates were monopolar. Each of the inner plates, however, was bipolar by induction, such that the obverse faces of a single plate were of opposite polarity.

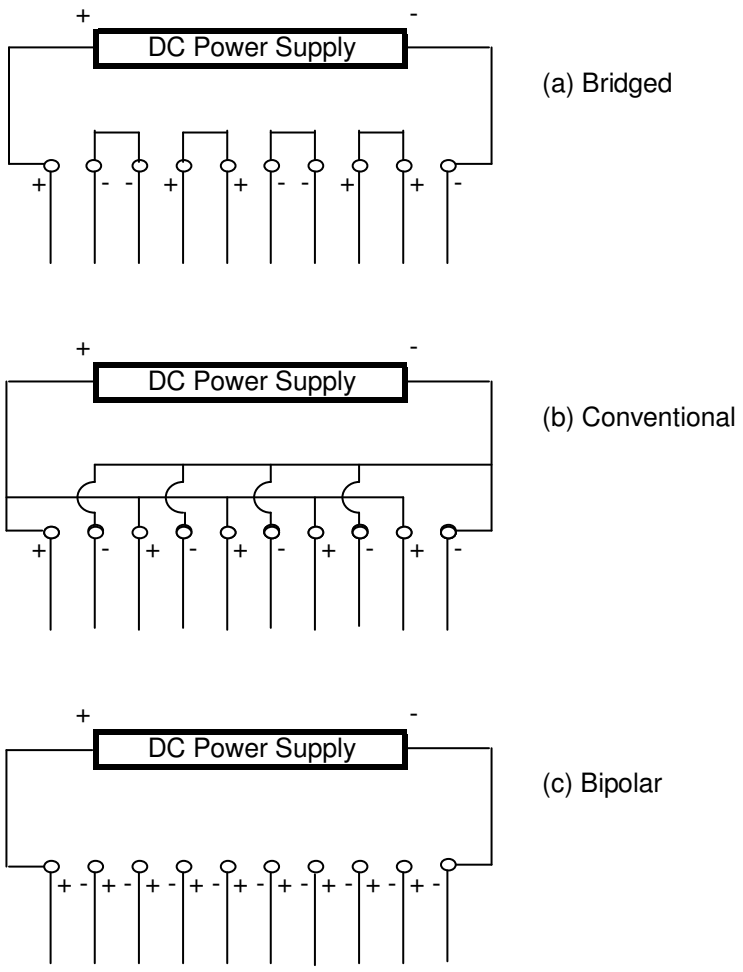

Figure 1-1. Power connection configurations (Pretorius et al., 1991).

Woytowich *et al.* (1993) described a concentric tube cell made of aluminum. A DC potential was imposed across the inner and outer tubes to electrocoagulate the solids in the wastewater flowing continuously through the annulus. The periodic reversal of polarity reportedly assisted with cleaning.

1.2.2 Electrocoagulation Performance

Besides destabilizing particulate suspensions, the electrocoagulation technique is capable of removing petroleum products, dissolved organic compounds, heavy metal ions, bacteria and certain anions (*e.g.*, fluoride, phosphate, silicate) from water (*e.g.*, Ivanishvili *et al.*, 1987; Renk, 1988). In addition, Parekh *et al.* (1992) attributed the capability for liquid-liquid separation (*i.e.*, demulsification) to the technique. Barkley *et al.* (1993) concurred, identifying a maximum oil concentration of 5% which could be treated effectively by electrocoagulation. They further stated that suspensions containing up to 10% solids could be electrocoagulated successfully.

Electrocoagulation plants were built and operated as early as 1889 in England, and later in the U.S. and Soviet Union, to treat sewage, wastewater and potable water. It is interesting to note that, in the English plants treating sewage and canal water, seawater was added to the feed to utilize the chlorine generated electrolytically for disinfection (Vik *et al.*, 1984). More recently, electrocoagulation was implemented in the meat, petroleum, edible oil and ink industries (Beck *et al.*, 1974).

1.2.2.1 Pilot Plant Tests

The technique has been demonstrated on the pilot plant scale in cleaning up 176 m^3 of bilge water from abandoned ships (Woytowich *et al.*, 1993). A modular, mobile unit of the concentric tube design was used. DC/EC treatment resulted in the removal of over 99% of total petroleum hydrocarbons, 71 to 99% of dissolved heavy metals and 73% of phosphorus. A 98% volume reduction resulted when the sludge was removed. Cost savings were estimated to be $185k USD and were attributed to the reduced electrical energy consumption in treating sea water (high conductivity).

In another pilot plant test, simulated wastewater that might result from soil washing operations was treated in the ACE Separator in 208-L batches (Barkley *et al.*, 1993). AC at 10 Hz was found to be optimal. Higher frequencies reportedly caused floc fragmentation, as did extended retention time. Unfortunately, no test data were presented in support of the frequency optimization, and the range of frequencies that was examined was not defined. Nevertheless, the fragmenting effect is expected to be similar for 60 Hz as for 10 Hz, both frequencies being in

the low range. The fragmenting effect of AC frequency reported by Barkley *et al.* (1993) was probably exacerbated by the grinding action of the fluidized aluminum shot. The authors did not comment on any floc-building property that AC frequency might have possessed or displayed. With extended retention time, flocs weaken mechanically as they grow, and fragment at some optimal size. Electrocoagulation increased the mean diameter from 2.2 µm (individual clay particles) to 230 µm (flocs) (Barkley *et al.,* 1993). Analyses of the wastewater before and after electrocoagulation treatment are reported in Table 1-1. Aluminum and stainless steel electrodes were observed to give comparable results.

Table 1-1. Wastewater analyses (Barkley et al., 1993).

Parameter	Feed, mg/L	Effluent, mg/L	Reduction, %
TSS	220	4.5	98
TOC*	130	6.6	95
Cu	0.30	0.085	72
Cd	0.50	0.15	70
Cr	0.31	0.024	92
Pb	0.72	0.09	88

*Total organic carbon

In another aspect of the work of Barkley *et al.* (1993), total recovery of TiO_2 from clarifier overflow was reported. These particles were less than 0.3 µm and were used to manufacture high-grade pigment. The addition of chemical coagulant was avoided because of detriment to the pigment quality. Thus, electrocoagulation satisfied a need for enhanced recovery (*i.e.*, improved settling rate) which could not be addressed with chemical coagulation.

Two pilot studies were performed in the U.S. at Superfund sites for the remediation of contaminated groundwater (Brewster and Passmore, 1994). DC/EC via steel electrodes was effective in attenuating the concentrations of Al, As, Ba, Cd, Cr, Cu, Pb, Hg, Ni, Se, Tl and Zn. Tables 1-2 and 1-3 report the test results obtained at a wood preservation site in South Carolina and a landfill site in New York State, respectively. The data show consistently significant reductions in metal concentration consequent to DC/EC treatment. Moreover, the treated water met the regional concentration limits, where these existed, for discharge.

Table 1-2. Wood preservation site in South Carolina (Brewster and Passmore, 1994).

Metal	Concentration, mg/L			TCLP* Leachate, mg/L	
	Influent	Effluent	Discharge Limit	DC/EC Solids	Limit
Al	0.10	< 0.05	35.0	no data	no data
Ba	0.23	< 0.005	no data	4.0	100.0
Cr	3.5	< 0.05	2.0	< 0.05	5.0

*Toxicity characteristic leaching procedure

Of particular interest are the results of the TCLP. This procedure is prescribed by the U.S. Environmental Protection Agency to assess the leachability of contaminants from solid residues. In all cases, where TCLP limits have been established, considerably less metal was leached from the DC/EC solids. Consequently, the solids were classified as non-hazardous. The TCLP leachate analyses in Tables 1-2 and 1-3 attest to how firmly the metal ions are bound to the iron hydroxide and hydrated iron oxide precipitates. Barium, the exception, was deduced by Brewster and Passmore (1994) to have been held by weak electrostatic attraction.

Table 1-3. Landfill site in New York State (Brewster and Passmore, 1994).

Metal	Concentration, mg/L			TCLP Leachate, mg/L	
	Influent	Effluent	Discharge Limit	DC/EC Solids	Limit
As	54.5	0.098	0.190	<0.5	5.0
Cd	0.26	<0.005	no data	<0.1	1.0
Cr	0.710	<0.01	no data	<0.5	5.0
Cu	0.055	<0.02	0.05	no data	no data
Pb	0.24	<0.005	0.009	<0.5	5.0
Hg	0.00024	<0.0002	0.0002	<0.02	0.2
Ni	0.415	0.024	no data	no data	no data
Se	16.0	<0.025	no data	<0.5	1.0
Tl	0.032	<0.005	no data	no data	no data
Zn	12.0	<0.01	no data	no data	no data

Brewster and Passmore estimated a total operating cost of $0.32 USD per 1000 gallons ($0.08 USD/$m^3$) after treating 28,336 gallons (107.3 m^3) of the

South Carolina groundwater. The current density was set to release from the electrodes an iron dosage of 20 mg/L, and sludge was generated at the rate of 1.36 lb per 1000 gallons (0.16 kg/m^3). It should be noted that power was supplied to the electrodes in the bipolar configuration (see Figure 1-1c).

1.2.2.2 Bench-scale Tests

Sea water (3,000 mg/L salinity) was electrocoagulated to reduce hardness and alkalinity, so that scaling would be minimized in electrodialysis and reverse osmosis equipment (Sanfan, 1991). DC/EC treatment reduced hardness and alkalinity by 40%. When the flocs were recycled to the electrocoagulation cell, a further reduction of 25 to 30% was achieved. Removal was observed to increase with aeration (iron anodes used) and current density. The immediate effect of increasing the latter was the increased quantity of metal (*i.e.*, dosage) dissolving from the plates.

Synthetic wastewater containing 30 mg/L P was treated in continuous flow by AC/EC via aluminum electrodes to remove phosphorus (Grøterud and Smoczynski, 1992). The AC frequency was modulated to 3.9 mHz (approaching DC conditions). Phosphorus removal was found to depend on current density, pH, flow rate and energy consumption. Removal increased with increasing current density and decreasing flow rate due to the increased dosage of aluminum from the plates. The water pH rose from 5.2 to as high as 9.0 during electrocoagulation. As the pH in the treated water increased from 8.7 to 9.0, phosphorus removal decreased. For a given degree of phosphorus removal, the energy consumption increased with flow rate because the current density had to be increased to compensate for the shortened retention time. The existence of a lower operating limit for current density was acknowledged but the value was not reported. Below this limit, electrocoagulation did not proceed. The authors anticipated that the energy consumption could be reduced by pH adjustment, NaCl addition to increase the water conductivity, and by optimization of the cell geometry.

DC/EC was applied with aluminum plates to decolourize water samples from three lakes; *i.e.*, to remove humic substances (Vik *et al.*, 1984). Decolourization, which was monitored by TOC analysis, was found to vary with pH as follows: zero below pH 3, slow above pH 6, and fastest at pH 4.8.

Wastewater from coal washing operations was treated by AC/EC (Parekh *et al.*, 1992). The water contained 0.3% solids with a median particle diameter of 1.8 µm. The zeta potential was high (-49.9 mV), suggesting a stable suspension of negatively charged coal particles. The suspension was treated under continuous, turbulent flow (N_{Re}~10^4). Test conditions were varied as follows: retention time, 20 to 60 s; current density, 124 to 310 A/m^2; voltage, 30 to 70 V at 60 Hz. The initial settling rate of the electrocoagulated coal increased with current density. In addition, about 90% of phosphate, 40% of dissolved nickel and virtually all of the dissolved copper were removed. Moreover, the electrocoagulated solids were, themselves, an effective coagulant when mixed in proportions as low as 25% with untreated suspension.

Dissolved metals were removed by DC/EC treatment of actual and synthetic samples of acid mine drainage (Jenke and Diebold, 1984). Steel, zinc and lead rod electrodes were tested. Dissolved copper and aluminum were completely removed, while zinc removal was hampered by the relatively high K_{S0} value of $Zn(OH)_2$. Zinc electrodes were capable of removing dissolved zinc from synthetic solution until an equilibrium concentration was reached. Removal of Mn and Mg was poor. In all cases, the pH increased by 10 units to 12.5 in 15 minutes' electrocoagulation. It is expected that redissolution of zinc from the sludge occurred at high pH values. The current density was not reported. Oxygen starvation occurred when the steel electrodes were used for more than 10 minutes. To prevent starvation, the natural induction of air into the solution should have been replaced or supplemented with air or oxygen sparging, or with the addition of hydrogen peroxide. The lead anode is reported to have become passivated quickly.

Samples of tar sand and oil shale wastewaters were electrocoagulated to reduce TOC and TSS concentrations (Renk, 1988). Details of the test conditions are scant. However, the retention time was reported to be under 20 s, suggesting a continuous flow system. Removal of TOC, oil and grease, TSS, and dissolved silica equalled or exceeded 98%. The toxicity of Syncrude tailings pond water was lowered, as determined by Microtox EC_{50}.

1.2.2.3 Comparison of Electrocoagulation and Chemical Coagulation

Electrocoagulation is considered to be easy to operate because the equipment tends to be simple (Un *et al.*, 2009; Yildiz *et al.*, 2008; Holt *et al.*, 2005). For a given aluminum dosage, electrocoagulation produces less sludge than does chemical coagulation. Since the technique removes a wide range of pollutants and does not introduce associated anions, as chemical coagulants do, electrocoagulation is viewed as being environmentally compatible.

In a direct comparison between electrocoagulation and chemical coagulation, meat processing wastewater was treated separately by DC/EC (Beck *et al.*, 1974) and by a chemical coagulant-flocculant combination of 200 mg/L ferric sulphate, 50 mg/L lime and 2 mg/L anionic polyelectrolyte (Swift's 400X™). During DC/EC, the fats, oils and grease floated with the microbubbles of gas generated and were skimmed off the surface. The analyses, summarized in Table 1-4, indicate the effectiveness of electrocoagulation.

Table 1-4. Test data from Beck et al. (1974).

Parameter	Electrocoagulation	Chemical Treatment
Total time for coagulation and floc recovery at 10% solids (min)	7	33
TSS in treated effluent (mg/L)	80 to 100	250 to 350
Fats, oils and grease in treated effluent (mg/L)	10 to 30	80 to 120
COD* after 7 min (mg/L)	625	1200

*Chemical oxygen demand

Further tests, in which chemical coagulation, chemical flocculation and electrocoagulation were combined, produced significantly improved performance over that of electrocoagulation alone. In addition, performance improved even further when the pH was adjusted.

The rising microbubbles of gas (*i.e.*, hydrogen and oxygen) assist in floating the solids to the surface where they can be skimmed off (Beck *et al.*, 1974; Belongia *et al.*, 1999). For effective flotation of the solids, termed "electroflotation" by some (Mollah *et al.*, 2004; Jiang *et al.*, 2002), the electrocoagulation current must be large enough to generate a dense cloud of

gas microbubbles (Un *et al.*, 2009; Holt *et al.*, 2002). At low current, the number density of microbubbles would be low, such that sedimentation becomes the dominant mode of solids separation (Holt *et al.*, 2002; Cañizares *et al.*, 2005b; Mollah *et al.*, 2004). Normally, sedimentation of solids from food wastewater is an unsatisfactory mode of separation, given that a major proportion of the solids is fatty, naturally buoyant and hydrophobic (Beck *et al.*, 1974).

Ivanishvili *et al.* (1987) reported that electrocoagulation demonstrated the greater effectiveness, was more amenable to automation, allowed the development of a simpler flowsheet, and did not increase the total dissolved solids (TDS) concentration in the treated water significantly. However, they added the qualification that the superiority of electrocoagulation was particularly valid for small capacity operations.

Vik *et al.* (1984) compared alum and electrocoagulation (with aluminum plates) for equal dosages of aluminum (6 mg/L) in decolourizing a lake water sample. They concluded that electrocoagulation was effective in decolourizing the sample at its natural pH of 4.8, while pH adjustment to 6.0 was prerequisite for chemical coagulation. The techniques were equally effective, but electrocoagulation produced a smaller volume of sludge. In a plant, this feature of electrocoagulation would effect a decrease in the design capacity of the sludge handling facilities, such as filtration. The pH was the same after chemical coagulation, but rose to 7.0 during electrocoagulation.

Barkley *et al.* (1993) compared electrocoagulation with chemical coagulation in which alum and an unidentified polyelectrolyte were tested. Electrocoagulation and the polyelectrolyte were four to five times as effective as alum in the removal of TSS and TS (total solids). In COD reduction, electrocoagulation was two to four times as effective as alum and the polyelectrolyte. The three methods demonstrated comparable performances in removing dissolved metals.

Kobya *et al.* (2007) estimated the cost of operating a plant to treat 1000 m^3 of textile plant wastewater per day. In the study, the performance of DC/EC was compared with that of chemical coagulation in removing turbidity and COD. Chemical coagulation was tested separately with alum, aluminum chloride, ferric sulphate and ferric chloride. The estimated total operating cost included direct costs (*e.g.*, electrode material and chemical coagulant) and indirect costs (*e.g.*,

labour and maintenance), supported by economic data taken from 2005Q3 for Turkey (where the study was undertaken). Over all, the operating cost for chemical coagulation was estimated to be 3.2 times that of DC/EC.

The flocs produced by electrocoagulation are reported to be stronger (*i.e.*, more shear-resistant) and denser than those generated by chemical coagulation (Barkley *et al.*, 1993). Tests showed that electrocoagulation produced 83% (by volume) less sludge than did chemical coagulation, and the sludge from electrocoagulation filtered 76% faster than that from chemical coagulation.

Whereas chemical coagulation requires a discrete addition of coagulant, electrocoagulation continuously adds coagulant that is generated *in situ*. Holt *et al.* (2002) tested DC/EC on a synthetic suspension of 1 g/L solids (67% kaolinite, 25% quartz, 3% illite/mica, the rest other minerals). They observed that DC/EC went through three stages, namely, lag, reactivity and stabilization. In the lag stage, the system entered an induction phase, during which the pH rose and then fell below its initial value, while the turbidity did not change significantly. In the reactive stage, the pH did not show any substantial change, but the turbidity dropped rapidly. Finally, in the stabilization stage, both the pH and turbidity levelled off.

Some evaluations show electrocoagulation to represent an alternative to chemical coagulation (Beck *et al.*, 1974; Renk, 1988; Woytowich *et al.*, 1993; Cañizares *et al.*, 2005b; Cañizares *et al.*, 2009; Harif *et al.*, 2006), but the economics are better only for small treatment plants (Holt *et al.*, 2005; Grøterud and Smoczynski, 1992; Ivanishvili *et al.*, 1987; Vik *et al.*, 1984). The improvement of the economics with decreasing plant size is, no doubt, related to energy consumption. This is most likely to be the pivotal challenge to the implementation of electrocoagulation on a large scale. However, the present status of development of the technology, together with the high cost of chemical coagulants, constitutes an argument for, at least, the partial replacement of chemical coagulation by electrocoagulation (Kobya *et al.*, 2007; Moreno *et al.*, 2009).

In the last decade, there appears to have been a resurgence of interest in the technique of electrocoagulation, directed almost exclusively at the treatment of water and wastewater (Zongo *et al.*, 2008; Yildiz *et al.*, 2008; Bejankiwar, 2002; Ofir *et al.*, 2007b; Ilhan *et al.*, 2008). A portion of the studies (Den and

Huang, 2006; Lai and Lin, 2003; Wang C-T. *et al*., 2009; Ghernaout *et al*., 2008) has examined solid-liquid separation in thin suspensions (*i.e*., up to ~2 wt % solids).

The review has revealed significant gaps in the published literature. For instance, all of the works referenced in the previous paragraph focussed on DC/EC. This author estimates that less than 2% of the research done in the last decade involved AC/EC. In addition, no published reports could be found post-1997 for the application of electrocoagulation to concentrated suspensions (*i.e*., >2 wt % solids) for the enhancement of the solid-liquid separation characteristics. One might reasonably expect that such studies would hold great interest for the mineral industry.

1.2.3 Colloidal Behaviour

Consistent with the behaviour of solid surfaces, particles acquire a surface charge upon dispersion or suspension in an aqueous medium (Everett, 1988). The sign and magnitude of the charge depend on its origin and on the chemistry of the dispersion medium. Usually, the sign of the charge is the same for particles of one material, and the particles of most materials carry a negative charge (Riddick, 1968). Some clays, such as kaolinite, are exceptional in that a single platelet can have negatively charged basal surfaces and positively charged edge surfaces (Everett, 1988; van Olphen, 1977). However, charges of the same sign create electrostatic repulsion which prevents or opposes close approach and collision of particles. This is one mechanism by which particulate suspensions are stabilized. Another stabilization mechanism is steric hindrance in which flagellae presented by high molecular weight polymers, which are adsorbed onto the particle surface, physically limit the proximity of approach of the particles (Gregory, 1993; Masliyah, 1994).

Colloidal stability is a thermodynamically metastable condition which could persist for long periods of time. Remarkably, the original gold sols (*i.e*., stable particulate dispersions of gold in aqueous media), that were prepared by Michael Faraday in the 1850's, still exist at the Royal Institution in London (Everett, 1988). The forces influencing the stability of suspensions are both repulsive and attractive, the latter type generally being denoted as London-van der Waals forces. In most of the literature, they are called van der Waals forces.

Influences on particle stability are discussed in subsequent sections of this thesis.

1.2.3.1 Origins of Particle Surface Charge

Particle surface charge originates from (Everett, 1988):

- isomorphous substitution in the crystal lattice,
- specific ion adsorption onto the particle surface,
- ionization of surface groups,
- differential dissolution of ions from sparingly soluble crystals, and
- charged crystal surfaces.

Isomorphous substitution refers to the replacement of an ion in the crystal lattice by another of different valency, the substitution being made possible by the similarity in ionic radii (Putnis and McConnell, 1980). In clays, for example, Al^{3+} (ionic radius, 0.51 Å) commonly substitutes for Si^{4+} (ionic radius, 0.42 Å), creating a deficit of positive charge which is manifested by a negative surface charge.

The adsorption of specific ions onto the particle surface occurs in natural systems, as well as synthetic ones. For example, fulvic acid, a natural polyelectrolyte, can adsorb onto the surface of calcite particles (Montgomery, 1985). Upon ionization, the adsorbed fulvic acid becomes anionic, imparting a negative charge to the particle surface. In synthetic systems, surfactants adsorb onto mineral surfaces. Depending on whether the ionized surfactant is anionic or cationic, the mineral surface manifests a negative or positive charge, respectively. Specific adsorption or chemisorption, like non-specific or physical adsorption, is pH-dependent. In contrast, however, non-specific adsorption does not occur at the point of zero charge (p.z.c.), the pH at which the particle surface has a zero net charge. The p.z.c. is to be distinguished from the isoelectric point (i.e.p.) which is the pH at which the zeta potential (defined in Section 1.2.3.2) of the particle is zero.

Many particulate materials contain ionisable surface groups, such as hydroxyl and carboxyl groups. Depending on pH, the groups ionize and impart their charge to the host particle surface. Hence, upon ionization of the hydroxyl group, OH^- enters the bulk solution and leaves a positive charge behind. Upon ionization of the carboxyl group, H^+ enters the bulk solution, leaving COO^- behind

to impart a negative charge to the particle surface. Metal oxides are examples of the first type, while bacteria exemplify the second (Montgomery, 1985). Surface group ionization is suppressed at the p.z.c.

The acquisition of a surface charge by differential dissolution is exemplified by silver iodide whose K_{SP} is 8.5×10^{-17} (Mortimer, 1986). If the salt were to dissolve symmetrically in water, it would do so to the limit of its solubility product, yielding equal concentrations of Ag^+ and I^-, and the surface of the residual, undissolved solid would be uncharged. In practice, however, silver is observed (Everett, 1988) to dissolve preferentially from the AgI lattice, leaving a negatively charged solid. The addition of another silver salt to the solution would suppress the preferential dissolution of silver from AgI. An equilibrium is attained at a certain Ag^+ concentration determined by the p.z.c. With further addition of Ag^+ to the solution, the undissolved solid acquires a positive charge, probably as a result of Ag^+ adsorption.

Regarding charged crystal surfaces, the different basal (or face) and edge surface charges existing in clays have been noted in Section 1.2.3, with kaolinite as the example. When a platelet is broken, Al–OH groups in the exposed edges adsorb H^+ to acquire a positive charge at low pH. Edge-to-face associations among the platelets could lead to destabilization of the dispersion.

It follows that, in natural systems, a variety of materials (*e.g.*, humic acids, fulvic acids, bacteria, algae) is available for adsorption onto particle surfaces, resulting in diverse modifications of particle surface properties. Hence, significantly different results are often obtained in identical tests involving a solid in its natural dispersion medium and the same solid dispersed in, say, de-ionized water in the laboratory.

1.2.3.2 Electrical Double Layer and DLVO Theory

Helmholtz originated the concept of the electrical double layer (Masliyah, 1994), which comprised a plane of charge within the solid surface and a parallel plane of counterions adsorbed at the solid-liquid interface. Gouy and Chapman independently arrived at the same modification of Helmholtz's concept. In the Gouy-Chapman model, Helmholtz's parallel plane of adsorbed counterions was replaced with a diffuse configuration. This conceptual configuration was developed to account for the ionic distribution created by Brownian motion

(engendered, in turn, by thermal gradients) and concentration gradients. Under the influence of electrostatic attraction, counterions move towards the charged surface. Accompanying the counterions in this migration are coions which, themselves, are electrostatically attracted to the counterions. The gross ionic migration from the bulk solution towards the charged surface creates a concentration gradient which opposes the electrostatically motivated migration. The opposing gradients, combined with Brownian motion, produce the diffuse layer of counterions and coions which can extend up to 300 nm into the bulk solution, depending on the ionic strength of the solution (Montgomery, 1985). An electrical potential, ψ_s, is assigned to the surface as a result of its electrical charge.

The Gouy-Chapman model holds for low ψ_s values (≤~25 mV) and modest levels of solution ionic strength (Masliyah, 1994). However, two major flaws are inherent in the model. The first arises from the perspective of ions as point charges which can approach the charged surface without limit; *i.e.*, the finite size of ions is ignored. The second flaw is the assumption that the dispersion medium has a constant dielectric value. Indeed, the dielectric constant of the medium in the double layer would be expected to differ from the dielectric constant of the bulk solution since, it was found (Gregory, 1993), that water close to a particle surface can be very different in nature from that in the bulk. Bockris *et al.* (1963) gave values for the dielectric constant of water at 298°K, as a function of location relative to the solid surface, as follows: $\varepsilon = 6$ in the inner Helmholtz layer, 32 in the outer Helmholtz layer, and 78.5 in the bulk. The Helmholtz layers will be defined presently. Similarly, the pH in the double layer can be quite different from that in the bulk solution. In addition, the higher ionic concentration in the double layer relative to the bulk solution can promote reactions, such as precipitation, ion exchange and adsorption, that are not normally predictable by equilibrium considerations (Montgomery, 1985).

The current conception of the electrical double layer is attributable to Graham (Majima and Peters, 1968) and Stern (Stumm, 1992), both of whom omitted the charged particle surface as a double layer component. Graham's and Stern's double layer models consisted of a compact layer (the Stern layer) of counterions at the charged particle surface and a diffuse layer (see Figure 1-2). The Stern layer was subdivided into two planes, namely, the inner and outer

Helmholtz planes. It is noteworthy that this subdivision is omitted from more recent literature.

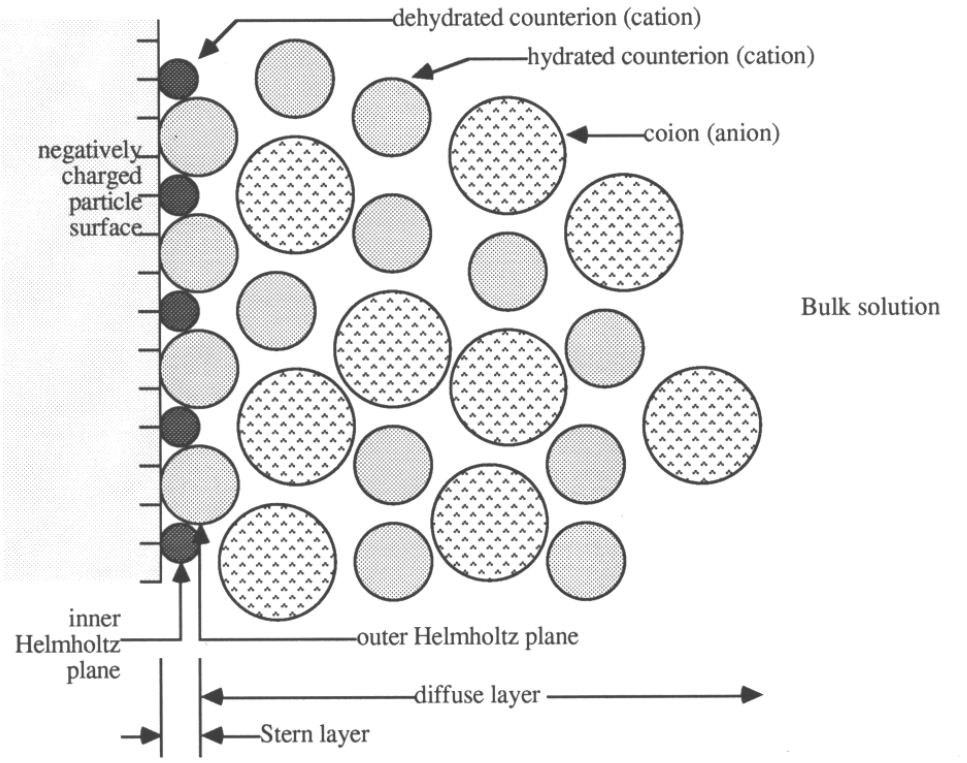

Figure 1-2. Current concept of the electrical double layer.

The inner Helmholtz plane is demarcated by the locus of the centres of a monolayer of dehydrated counterions which are adsorbed onto the particle surface. Dehydration (*i.e.*, loss of coordination water molecules) is prerequisite to their adsorption, either by covalent bond formation with the surface (specific adsorption or chemisorption), or by London-van der Waals attraction forces (non-specific or physical adsorption) (Gregory, 1993; Majima and Peters, 1968; Stumm and O'Melia, 1968). The outer Helmholtz plane is defined by the locus of the centres of hydrated counterions whose hydration sheaths contact the particle surface. Hence, the thickness of the Stern layer is the radius of a hydrated counterion. Since dehydration of the counterions requires energy (Gregory, 1993), it is deduced that the outer Helmholtz counterions were either crowded out from the particle surface by the inner Helmholtz counterions, or they did not acquire sufficient energy for dehydration.

The Debye length (κ^{-1}), which is a measure of the thickness of the electrical double layer, is calculated as shown by Equation 1-1 (Masliyah, 1994).

$$\kappa^{-1} = \left[\frac{\varepsilon\varepsilon_o kT}{2n_\infty e^2 z^2} \right]^{0.5} \qquad (1\text{-}1)$$

where ε = dielectric constant (dimensionless) of the dispersion medium at T°K

ε_o = permittivity of vacuum = 8.854×10^{-12} C/Vm

k = Boltzmann's constant = 1.381×10^{-23} J/°K

T = absolute temperature, °K

n_∞ = ionic number concentration in the dispersion medium (m^{-3})

e = elementary charge = 1.602×10^{-19} C

z = absolute value of valency for a dissolved symmetrical electrolyte.

Inspection of Equation 1-1 shows that, as the ionic strength of the dispersion medium (which determines n_∞) increases, the Debye length decreases; *i.e.*, the double layer or, more precisely, the diffuse layer, is compressed (Probstein, 1989). Compared to the effect of a 1:1 electrolyte like NaCl, a z:z (where z>1) electrolyte at the same concentration decreases the Debye length by a factor of 1/z. For a spherical particle of radius, a, in a dispersion medium of high ionic strength, $\kappa a >> 1$ (thin diffuse layer). Conversely, $\kappa a << 1$ (thick diffuse layer) in a medium of low ionic strength, such as de-ionized water.

Surrounding the particle is a layer of solution that is a little thicker than the Stern layer. It is immobile relative to the particle surface and remains intact during particle movement. The boundary of this layer is a slip surface called "the shear plane". The electrical potential difference between the shear plane and the bulk solution is called the zeta potential, ζ, which is calculated from the electrophoretic velocity of the particle. For $\kappa a << 1$, the Hückel equation applies (Equation 1-2), and for $\kappa a >> 1$, the Helmholtz-Smoluchowski equation is valid (Equation 1-3) (Masliyah, 1994). Implicit in these equations is the assumption that $\psi_s < 25$ mV.

$$\zeta = 1.5\mu U/\varepsilon\varepsilon_o E_\infty \qquad \text{for } \kappa a << 1 \qquad (1\text{-}2)$$

$$\zeta = \mu U/\varepsilon\varepsilon_o E_\infty \qquad \text{for } \kappa a >> 1 \qquad (1\text{-}3)$$

where μ = viscosity of the dispersion medium, Pa.s

U = particle electrophoretic velocity, m/s

E_∞ = electric field strength, V/m.

For intermediate values of κa (*i.e.*, intermediate ionic strengths), Henry's function, $f(\kappa a)$, is useful for calculating zeta potentials (Masliyah, 1994). Henry's function is written as Equation 1-4 and is incorporated in Equation 1-5 to calculate ζ. Equation 1-5 yields Equations 1-2 and 1-3 for the respective κa values.

$$f(\kappa a) = 1 + \frac{1}{16}(\kappa a)^2 - \frac{5}{48}(\kappa a)^3 - \frac{1}{96}(\kappa a)^4 + \frac{1}{96}(\kappa a)^5 - \frac{1}{8}(\kappa a)^4 e^{\kappa a}\left(1 - \frac{1}{12}(\kappa a)^2\right)\int_\infty^{\kappa a}\left(\frac{e^{-t}}{t}\right)dt \qquad (1\text{-}4)$$

where t is a dummy variable.

$$\zeta = 1.5\mu U/\varepsilon\varepsilon_o E_\infty f(\kappa a) \qquad (1\text{-}5)$$

In Equations 1-2, 1-3 and 1-5, ζ is assumed to equal ψ_s, which is not true, but the error this assumption introduces is acceptable. It is not possible to measure ψ_s, but ζ is a measure of ψ_s, as indicated in Figure 1-3 where ψ_d is the Stern potential. A significant interaction results when the diffuse layers of two approaching particles overlap. Whether the suspension remains stable will depend on the net interaction. The repulsion due to the electrical double layers and the attraction caused by the London-van der Waals forces are additive to give a net interaction as a function of separation distance (Gregory, 1993; Probstein, 1989). This is the essence of the theory of colloid stability, otherwise known as the DLVO theory after its formulators – Derjaguin, Landau, Verwey and Overbeek. The theory neglects forces not characterized as DLVO forces, such as those resulting from hydrophobic and hydration interactions (Gregory, 1993).

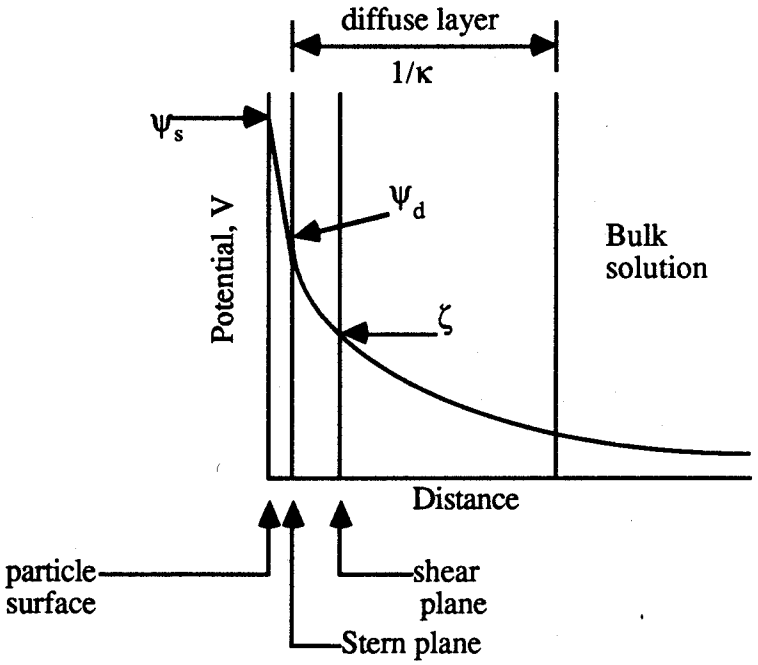

Figure 1-3. Potentials in the electrical double layer.

1.2.3.3 Colloidal Interactions

The electrical double layer derives its importance from the special conditions which promote chemical reactions, and from the physical interactions which influence the probability of particle collision. A suspension is destabilized (*i.e.*, coagulation occurs) by successful particle collisions. It follows that the collision frequency is important since, with increased frequency, the probability of successful collisions (*i.e.*, collisions resulting in permanent adhesion) increases. Once coagulation is achieved, floc growth proceeds by continued successful collisions which build the particulate unit to a size where the sedimentation behaviour, for example, is more strongly influenced by gravity. It should be emphasized that colloidal interactions are effective over distances that are small relative to the particle size. Hence, colloidal interactions influence collision frequency, floc structure and floc strength, among other parameters (Gregory, 1993).

The interaction between two approaching colloidal particles is experienced at a greater separation in a dispersion medium of low ionic strength than in one of high ionic strength. In the latter case, closer approach before

interaction is made possible by the thinner diffuse layers. In the case of two spherical particles of radii, a_1 and a_2, and surface electrical potentials, ψ_1 and ψ_2, the repulsive potential energy, V_R, at a separation of h is given by Equation 1-6 in joules (Masliyah, 1994).

$$V_R = \left(\frac{\pi\varepsilon\varepsilon_o a_1 a_2}{a_1 + a_2} \right) \left(2\psi_1\psi_2 \ell n \left[\frac{1 + e^{-\kappa h}}{1 - e^{-\kappa h}} \right] + (\psi_1^2 + \psi_2^2) \ell n (1 - e^{-2\kappa h}) \right) \qquad (1\text{-}6)$$

Equation 1-6 is valid for low Stern potentials (<25 mV). Also, a_1 and a_2 must be large relative to the Debye length, such that $\kappa a > 10$. Zeta potential values are normally substituted for ψ_1 and ψ_2. For particles of the same size, a, and zeta potential, ζ, Equation 1-6 reduces to Equation 1-7.

$$V_R = 2\pi\varepsilon\varepsilon_o a \zeta^2 e^{-\kappa h} \qquad (1\text{-}7)$$

Inspection of Equation 1-7 shows that V_R is always positive, even when ζ is negative. The force of repulsion, F_R, is calculated as shown in Equation 1-8 in newtons.

$$F_R = -\frac{dV_R}{dh} \qquad (1\text{-}8)$$

The general expression for F_R derived from Equation 1-6 is given in Equation 1-9.

$$F_R = \left[\frac{2\pi\varepsilon\varepsilon_o \kappa a_1 a_2 e^{-\kappa h}}{(a_1 + a_2)(1 - e^{-2\kappa h})} \right] \left[2\zeta_1\zeta_2 - (\zeta_1^2 + \zeta_2^2) e^{-\kappa h} \right] \qquad (1\text{-}9)$$

For two equal spherical particles, Equation 1-9 yields Equation 1-10, which is the same expression as would be obtained from Equations 1-7 and 1-8.

$$F_R = 2\pi\varepsilon\varepsilon_o \kappa a \zeta^2 e^{-\kappa h} \qquad (1\text{-}10)$$

Like the repulsive potential energy, the repulsive force is always positive. The magnitude of both quantities varies directly with particle size and with the square of the zeta potential.

The interaction energy of attraction among particles is quantified by Hamaker's expressions. For two spherical particles of radii, a_1 and a_2, separated by distance, h, the potential energy of attraction, V_A, is formulated according to Equation 1-11 and expressed in joules (Masliyah, 1994).

$$V_A = -\frac{Aa_1a_2}{6h(a_1 + a_2)} \qquad (1\text{-}11)$$

where A = Hamaker's constant, J, and both a_1 and a_2 are much larger than h.

Hamaker's constant was based on the interaction of two molecules in vacuum, and the relationship was integrated for all the molecules in two individual particles. It can be modified to compensate for the effect of an intervening medium (such as the dispersion medium), and for the effect of particles of different materials. For two spherical particles of equal radius, a, Equation 1-11 reduces to Equation 1-12.

$$V_A = -\frac{Aa}{12h} \qquad (1\text{-}12)$$

The force of attraction is given by: $$F_A = -\frac{Aa}{12h^2} \qquad (1\text{-}13)$$

Equations 1-11 to 1-13 reveal that the potential energy and force of attraction are always negative, depend on particle size, and decrease with increasing interparticle separation (h). With Equations 1-7 and 1-12, sample calculations were performed to compare the ranges of influence of V_R and V_A. It should be noted that the calculations were based on spherical crystalline quartz particles, 1 µm in diameter, dispersed in de-ionized water containing 200 mg/L NaCl at 298°K. This salt concentration decreased the Debye length from 188 nm to 5.2 nm. Hence, the thickness of the diffuse layer was compressed by 97%. The particles were assumed to have a zeta potential of -20 mV. In Figure 1-4, the

absolute values of V_A were plotted to facilitate the comparison of the magnitudes of the interaction potential energies. The repulsive energy exceeded the attractive energy in the interparticle separation range of 1 to 15 nm. Consequently, when the diffuse layers overlap, the interparticle separation would be about 10 nm which is within the range of repulsive energy predominance. Figure 1-4 also illustrates that the attractive energy predominates at small and large interparticle separations, while the repulsive energy predominates at intermediate separations (Probstein, 1989).

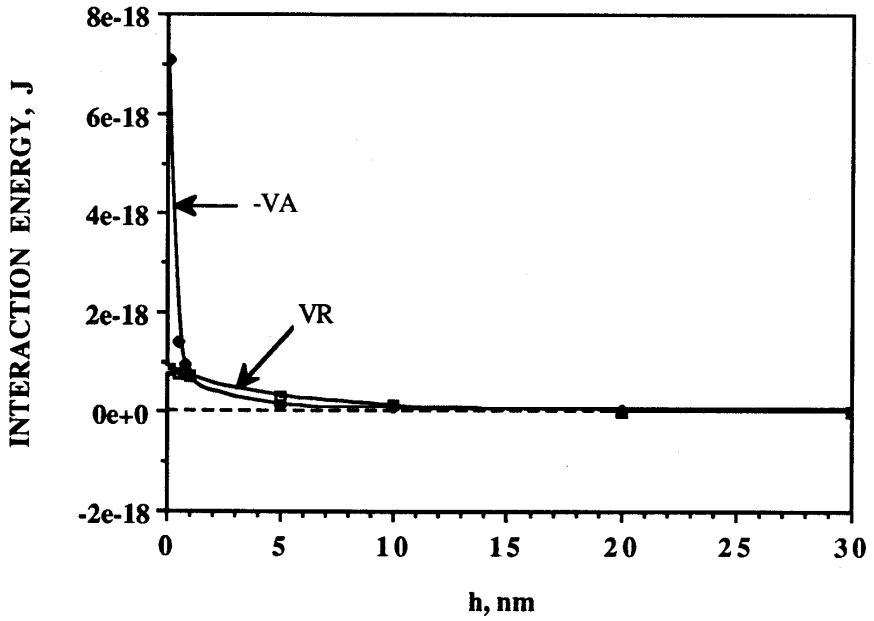

Figure 1-4. Comparison of magnitudes of V_R and V_A.

The DLVO theory makes it possible for the net interaction energy, V, to be obtained by the sum of V_R and V_A. A positive value indicates a net repulsive energy, while a negative value indicates a net attractive energy. Therefore, for two equal spherical particles, V is given by Equation 1-14.

$$V = 2\pi\varepsilon\varepsilon_o a\zeta^2 e^{-\kappa h} - \frac{Aa}{12h} \qquad (1\text{-}14)$$

Figure 1-5 depicts the variation of the net interaction energy with separation distance and κ^{-1}. For κ^{-1} of 5.2 nm, the graph illustrates the short- and long-range predominance of V_A ($V < 0$ at $h \leq 1$ nm and $h >$ ~15 nm), and the

intermediate-range predominance of V_R. Since the diffuse layers overlap within the range of V_R predominance (V>0), coagulation is not likely to occur without assistance to the system (Probstein, 1989).

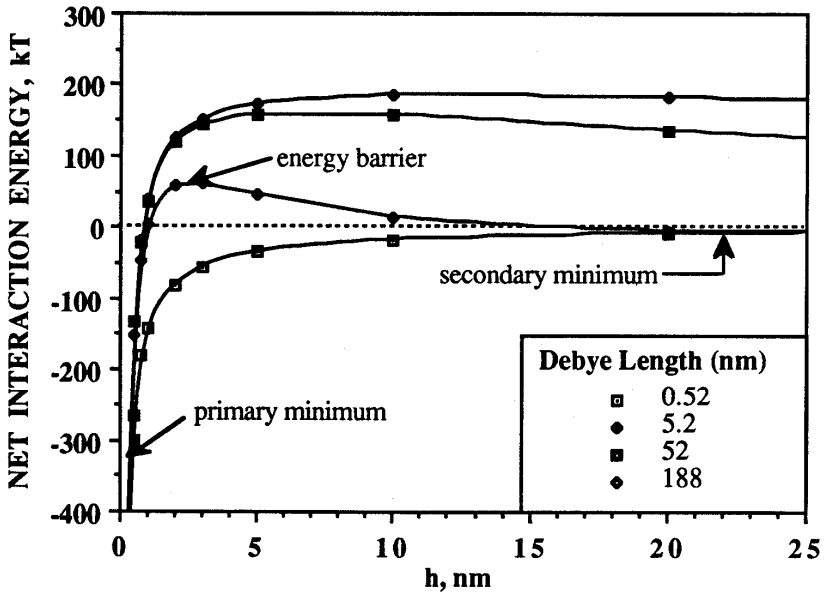

Figure 1-5. Variation of net interaction energy with interparticle separation and Debye length.

The maximum net interaction energy occurring at ~3 nm (Figure 1-5, κ^{-1} = 5.2 nm) is repulsive, and approaching particles must overcome this energy barrier for true interparticle contact to result. Once the barrier is surmounted, particles reside in permanent adhesion (*i.e.*, coagulation) in a deep primary minimum. London-van der Waals forces constitute the adhesive force. Re-dispersion of the coagulated particles is made improbable by the depth of the energy "well". The secondary minimum is a manifestation of the long-range influence of V_A. Owing to the weak interaction, however, only weak coagulation is achieved by colloidal particles. On the other hand, by virtue of their larger size, particles larger than 1 μm in diameter experience a stronger interaction in the secondary minimum. Moderately high ionic strength in the dispersion medium also intensifies the attractive interaction in the secondary minimum, consequent to the reduced magnitude and range of influence of V_R. This permits closer approach of the particles into the range of separations where V_A predominates. It follows that the reduction in V_R creates a deeper secondary minimum.

Equation 1-15 describes the relationship between molar concentration and n_∞.

$$n_\infty = 10^3 M N_a \qquad (!\text{-}15)$$

where M = molar concentration of electrolyte, mol/L

N_a = Avogadro's number = 6.02×10^{23}/mol.

Substitution for n_∞ in Equation 1-1 allows M to be expressed in terms of the inverse Debye length, as illustrated by Equation 1-16.

$$M = 9.26 \times 10^{-20} \kappa^2 \qquad (1\text{-}16)$$

Equation 1-16 facilitated calculation of the NaCl concentrations which would create Debye lengths of 0.52, 5.2, 52 and 188 nm. Table 1-5 shows that a NaCl concentration of 20 g/L would reduce the Debye length from 188 nm (de-ionized water) to 0.52 nm.

Table 1-5. Debye lengths and corresponding NaCl concentrations.

κ^{-1}, nm	κ, m^{-1}	NaCl Concentration	
		M, mol/L	mg/L
0.52	1.92×10^9	3.41×10^{-1}	20,000
5.2	1.92×10^8	3.41×10^{-3}	200
52	1.92×10^7	3.41×10^{-5}	2
188	5.32×10^6	2.62×10^{-6}	0.15

The calculation of net interaction energy performed for the Debye length of 5.2 nm was repeated for Debye lengths of 0.52, 52 and 188 nm. The results plotted in Figure 1-5 illustrate the influence of the ionic strength of the dispersion medium in intensifying the attractive interaction in the secondary minimum, as ionic strength increases. Indeed, for the Debye length of 0.52 nm, the net interaction is one of attraction over the interparticle separation range of 0 to 30 nm (see Appendix A). Consequently, it is reasonable to expect perikinetic coagulation to occur in the 20 g/L NaCl solution. In contrast, particles with Debye lengths of 52 nm and greater experience high repulsive energies of interaction over the separation range of 2 to 30 nm, close approach to where London-van

der Waals forces can predominate being effectively prohibited. Gregory (1993) states that an energy barrier of at least ~20 kT J defines a stable suspension. For the systems analyzed in Figure 1-5, 20 kT is equivalent to 8.2×10^{-20} J, which is below the net interaction energy values for κ^{-1} of 52 and 188 nm over the interparticle separation range of 1 to 30 nm (Appendix A). Hence, these two systems are expected to be too stable even for orthokinetic coagulation to occur.

1.2.3.4 Coagulation

Coagulation can be induced by several methods. In water treatment practice, high-energy agitation (flash mixing) is performed for less than a minute to promote coagulation. This is followed by a much longer period of less intense mixing to facilitate floc growth (Montgomery, 1985). Flash mixing promotes coagulation by establishing high interparticle collision frequencies. In other words, kinetic energy is used to overcome the repulsive energy barrier (see Figure 1-5) so that particles can make contact and adhere. The same principle is applied to churn cream into butter.

Chemists are familiar with the technique of boiling to induce coagulation of precipitates. Thermal energy input is converted, in part, to kinetic energy which increases the collision frequency of the dispersed particles, in a manner analogous to flash mixing. Coagulation by boiling has also been attributed to a reduction in the degree of hydration of particles, since stripping of hydration water is precursory to true interparticle contact (Gregory, 1993; Sawyer *et al.*, 1994).

At the other extreme, freezing has been reported (Sawyer *et al.*, 1994) to effect coagulation. With the progressive removal of water as ice, the electrolyte concentration in the residual water increases, compressing the electrical diffuse layer and permitting closer approach among the dispersed particles. Concomitantly, the removal of water causes the particulate concentration to increase in the residual water, effectively bringing the particles closer together. Coagulation results from the combined effects of diffuse layer contraction and closer interparticle proximity. Notably reduced, however, is the kinetic energy of the particles; hence, agitation is necessary.

Mixing one stable particulate dispersion with another, oppositely charged one leads to charge neutralization and coagulation. The floc growth kinetics are slow, however (Sawyer *et al.*, 1994).

The addition of electrolytes, such as alum and ferric sulphate, to particulate dispersions is widely practised in water treatment. Surface charge neutralization, complemented by diffuse layer compression, facilitates coagulation.

Coagulation mechanisms are:

(i) compression of the electrical diffuse layer,
(ii) surface charge neutralization,
(iii) interparticle bridging, and
(iv) sweep floc or enmeshment.

(i) Compression of the electrical diffuse layer.

The effect of NaCl addition to de-ionized water has been illustrated. The dependence of κ^{-1} on n_∞ implies dependence on the electrolyte concentration, as Equation 1-15 and Figure 1-5 have illustrated. In addition, κ^{-1} varies inversely with z, from which it follows that the decrease of κ^{-1} is greater for z_1 than for z_2, where $z_1>z_2$, at a given electrolyte concentration. This is the essence of the Schulze-Hardy rule, which states that the valence of the counterion exercises the principal effect on the stability of the colloidal particle, while the nature and valence of the coion are of subordinate importance (Everett, 1988; Masliyah, 1994). This leads to the concept of the critical coagulation concentration (c.c.c.) of an electrolyte (more precisely, the counterions it provides), defined as the ionic concentration which causes rapid coagulation (Everett, 1988; Masliyah, 1994; Montgomery, 1985). The proportionality existing between c.c.c. (expressed in meq/L) and counterion valence is stated by Equation 1-17.

$$\text{c.c.c.} \propto z^{-6} \qquad (1\text{-}17)$$

It is essential to note that, in addition to compressing the electrical diffuse layer, electrolytes decrease the zeta potential (depicted in Figure 1-6) and, hence, the range and magnitude of the double layer repulsion (Gregory, 1993). Rapid coagulation is promoted by $|\zeta| < 20$ mV (approx.), depending on the particulate

system (Montgomery, 1985). This upper ζ limit is interpreted by Riddick (1968) as representing the threshold of delicate dispersion. In other words, coagulation is easy to accomplish. With the diffuse layer sufficiently compressed, particles can approach close enough for the London-van der Waals forces to dominate, permitting coagulation (Probstein, 1989).

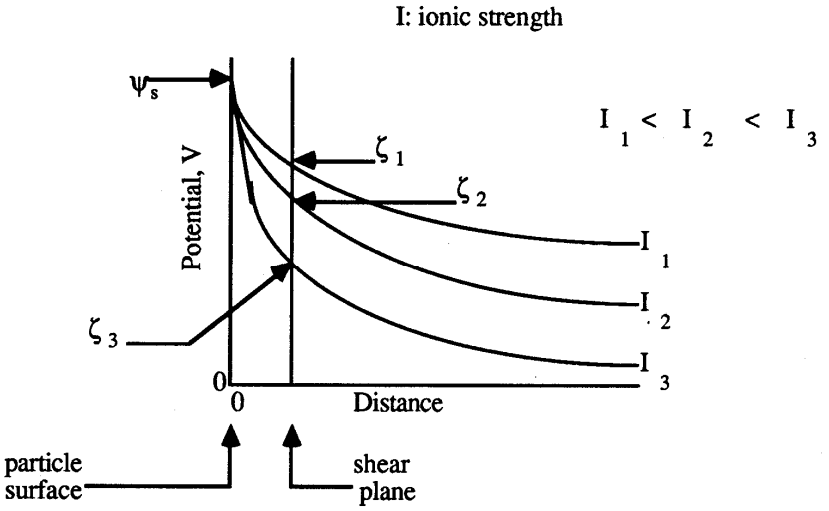

Figure 1-6. Effect of ionic strength on zeta potential.

Perikinetic coagulation, for which particle transport is by Brownian motion, predominates for colloidal particles, while orthokinetic coagulation (facilitated by forced hydrodynamic transport, namely, agitation) predominates for larger particles (Masliyah, 1994; Montgomery, 1985; Probstein, 1989).

(ii) Surface charge neutralization.

Part of the effectiveness of coagulants is ascribed to the neutralization of the particle surface charge by the counterions they release. This mechanism is also called “electrostatic attraction” to indicate the manner by which the counterions become adsorbed onto the particle surface. It should be pointed out that pH determines the nature of the surface charge: at pH < i.e.p., $\zeta > 0$; at pH > i.e.p., $\zeta < 0$. As the pH approaches the i.e.p., coagulation occurs. If the pH changes past the i.e.p. during coagulation, the particle surface would assume the opposite charge. Consequently, the ions that were originally coions, relative to the particle surface charge, now become counterions which are adsorbed onto the particle

surface. Now, the system is peptized again (*i.e.*, the particles are re-dispersed), but is oppositely charged (charge reversal) (van Olphen, 1977). It is worth pointing out that the addition of too much electrolyte causes charge reversal.

(iii) Interparticle bridging.

This mode of destabilization is the exclusive mechanistic domain of long-chain polymeric electrolytes or polyelectrolytes. The most effective of these are linear and are of high molecular weight (several million) so that extended loops and tails are present, increasing the probability of attachment to suspended particles. An individual polymer chain can bridge more than two particles and form a floc. Polyelectrolytes are designed to be anionic, cationic or non-ionic. Preferably, the anionic and cationic types are used to flocculate particles of opposite charge, mainly by charge neutralization (Montgomery, 1985). The polymer adsorbs strongly onto the particle surface as a result of the high charge density of the former, and facilitates interparticle bridging. As such, the length of the polymer chain (*i.e.*, the magnitude of its molecular weight) declines in importance as a selection criterion. However, interparticle bridging is a very effective flocculation mechanism, to the extent that the flocs formed are notably strong. Polyelectrolyte over-dosage causes steric re-stabilization of the particulate suspension. This phenomenon is attributed to the saturation of adsorption sites on particles, such that no sites are available for bridge formation. Consequently, the polymer coating on the particles prevents interparticle contact (Stumm and O'Melia, 1968). The coulombic character of non-ionic polyelectrolytes is defined by aqueous equilibrium. For example, polyacrylamide hydrolyzes in basic aqueous solution and becomes anionic (Montgomery, 1985).

(iv) Enmeshment or sweep floc.

This mechanism is exploited to a great extent in water treatment. Cations, such as Al^{3+} and Fe^{3+}, hydrolyze and form amorphous precipitates (*i.e.*, K_{S0} is exceeded) which entrap and sweep away suspended particles. It is not clear whether the precipitate nucleates heterogeneously or homogeneously (Dentel and Gossett, 1988). Heterogeneous nucleation seems more likely, but the solution chemistry would be expected to dictate whether one or both nucleation paths are followed.

1.2.3.5 Floc Growth and Fragmentation

As flocs grow, the solid volume fraction or floc density decreases (*i.e.*, porosity increases) and they weaken mechanically. Hence, floc density decreases with increasing interparticle collision frequency. On the other hand, slower growth rates produce denser flocs (Gregory, 1993). Large, dense flocs are desirable in thickening and filtration operations while small, low-density flocs are amenable to flotation.

Floc growth kinetics are determined by physical and chemical parameters. The physical parameters include pulp density, shear conditions and initial particle size. The chemical parameters include the molecular weight and structure of the coagulant, the pH of the suspension and the ionic species present in the dispersion medium (Ayyala *et al.*, 1995). These parameters influence the kinetics by modifying the floc shape, structure, density, strength and size.

Initially, floc growth is rapid, but then decreases as a limiting size is approached. Floc growth is defined in three regions (Ayyala *et al.*, 1995; Wang Y. *et al.*, 2009). In Region 1, primary particles aggregate to form microflocs of up to 50 µm in size. Microflocs are closely packed and, therefore, have the highest density (porosity below ~45% by volume). In Region 2, growth is by collision between primary particles and microflocs, as well as among microflocs, the latter growth mode being termed “multiple level aggregation”. In this growth region, porosity ranges from 45% to 95% by volume, with multiple level aggregation being responsible for flocs in the higher end of the porosity range. The range of floc sizes is wide, from 50 µm to about 500 µm. In Region 3, floc size exceeds 500 µm and the porosity can exceed 95% by volume, depending on the extent of multiple level aggregation (Ayyala *et al.*, 1995). If floc growth were by aggregation of only primary particles, the floc density would be virtually independent of size, due to the tightest packing of particles. In Region 3 and the latter part of Region 2, rearrangement of microflocs, and floc fragmentation and re-aggregation occur (Zbik *et al.*, 2008). The net of these processes determines how the floc morphology is modified with retention time (Ayyala *et al.*, 1995; Gregory, 1993). It is important to note that flocs can have several equilibrium size distributions that they can adopt during re-aggregation.

Two main modes of fragmentation have been observed in turbulent flow (Ayyala *et al.*, 1995). The first is massive fragmentation into two or more flocs, which would be expected for large parent flocs. A significant modification in dewatering behaviour is also anticipated. The second mode is small scale erosion or stripping of "fibre" components from the floc surface. This fragmentation mode would be expected to occur with strong or moderate size parent flocs.

1.2.4 Aqueous Chemistry of Aluminum

This section discusses the aqueous chemistry of aluminum, since it is the material of construction of the electrodes used in this project.

1.2.4.1 Hydroxoaluminum Complexation

The effectiveness of electrocoagulation in treating particulate suspensions is related to the ionic species it releases into solution from the electrode material. The anodic half-cell reaction is written in Equation 1-18. Equation 1-19 (Cañizares *et al.*, 2009; Trompette and Vergnes, 2009; Cañizares *et al.*, 2005b) and Equation 1-20 represent side reactions by which oxygen is evolved, depending on the pH conditions. Hydrogen is generally agreed to be evolved at the cathode (Cañizares *et al.*, 2005b; Harif *et al.*, 2006; Barkley *et al.*, 1993; Jenke and Diebold, 1984; Pretorius *et al.*, 1991; Vik *et al.*, 1984), as indicated by Equation 1-21 or 1-22, depending on the pH of the water.

Anode: $Al(s) \rightarrow Al^{3+} + 3e$ (1-18)

$2\ H_2O\ (\ell) \rightarrow 4\ H^+ + O_2(g) + 4e$ (neutral to acidic pH range) (1-19)

$4\ OH^- \rightarrow 2\ H_2O\ (\ell) + O_2(g) + 4e$ (basic pH range) (1-20)

Cathode: $2\ H_2O\ (\ell) + 2e \rightarrow H_2(g) + 2\ OH^-$ (neutral to basic pH range) (1-21)

$2\ H^+ + 2e \rightarrow H_2(g)$ (acidic pH range) (1-22)

Equations 1-21 and 1-22 imply that the water is oxygen-starved. In aerated water, however, oxygen is reduced, as represented by Equation 1-23 or 1-24, depending on the water pH.

Cathode: $2\ H_2O\ (\ell) + O_2(g) + 4e \rightarrow 4\ OH^-$ (neutral to basic pH range) (1-23)

$O_2(g) + 4\ H^+ + 4e \rightarrow 2\ H_2O\ (\ell)$ (acidic pH range) (1-24)

Al^{3+} enters complexation reactions with water to form a range of hydroxo species. Baes and Mesmer (1976) identified complex hydroxoaluminum ions, such as $AlOH^{2+}$, $Al(OH)_2^+$, $Al(OH)_4^-$, $Al_2(OH)_2^{4+}$ and $Al_3(OH)_4^{5+}$, as well as the neutral species, $Al(OH)_3^o$. The relative abundances of these species are determined mainly by pH and the total concentration of dissolved aluminum. Ageing and temperature also determine the distribution and identity of the species (Stumm and O'Melia, 1968). The oxyhydroxoaluminum species, $Al_{13}O_4(OH)_{24}^{7+}$, was also identified (Baes and Mesmer, 1976; Akitt and Farthing, 1978). Snoeyink and Jenkins (1980) mentioned $Al_7(OH)_{17}^{4+}$ and $Al_{13}(OH)_{34}^{5+}$ which, like other polynuclear species, are considered to be formed by the condensation of mononuclear hydrolysis products (Dentel and Gossett, 1988; Parthasarathy and Buffle, 1985; Snoeyink and Jenkins, 1980), as summarized by Equations 1-25 and 1-26, where the role of coordinated water molecules is evident.

$$Al(H_2O)_6^{3+} \leftrightarrow Al(H_2O)_5OH^{2+} + H^+ \qquad (1\text{-}25)$$

$$2\ Al(H_2O)_5OH^{2+} \leftrightarrow Al_2(H_2O)_8(OH)_2^{4+} + 2\ H_2O\ (\ell) \qquad (1\text{-}26)$$

Further, Black (1967) argued for the existence of $Al_6(OH)_{15}^{3+}$ and $Al_8(OH)_{20}^{4+}$, while Stumm and O'Melia (1968) added $Al_2(OH)_5^+$ and $Al_4(OH)_8^{4+}$ to the list.

Sarpola *et al.* (2004), by mass spectrometric analysis of $AlCl_3$ solutions (pH 3.27 to 4.20), identified over 80 univalent cations (Al_2 to Al_{13} cores) and 19 polyvalent cations (Al_{10} to Al_{27} cores). While it was well established (*e.g.*: Baes and Mesmer, 1976; Duan and Gregory, 2003) that the aluminate ion was the only known complex anion of aluminum, Sarpola *et al.* further identified 45 univalent anions (Al_1 to Al_{12} cores) and 9 polyvalent anions (Al_{10} to Al_{32} cores). Thus, the inference (Hunt, 1965; Stol *et al.*, 1976) that there might be a practically infinite range of hydrolytic aluminum complexes, was proven. The identity and distribution of the species change with pH, total dissolved aluminum concentration, and time (*i.e.*, age) (Sarpola *et al.*, 2006; Zhao *et al.*, 2009).

Many of the polynuclear hydroxo complexes are kinetic intermediates between Al^{3+} and $Al(OH)_3(s)$ such that, under conditions of supersaturation (*i.e.*,

$[Al^{3+}][OH^-]^3 > K_{S0}$), as is customary in water treatment practice, the intermediates ultimately precipitate as $Al(OH)_3(s)$ (Baes and Mesmer, 1976; Stumm and Morgan, 1970; Stumm and O'Melia, 1968). These thermodynamically metastable complexes can persist indefinitely (Baes and Mesmer, 1976; Parthasarathy and Buffle, 1985; Stumm and Morgan, 1970). On the other hand, the complexes can form transient metastable precipitates, as permitted by the prevailing conditions of hydrolysis (Baes and Mesmer, 1976). Conceivably, these transient precipitates could contribute to the coagulation kinetics, depending on their nature. The predominant intermediates are determined by solution pH: below the i.e.p. of $Al(OH)_3(s)$, cationic complexes predominate; above the i.e.p., anionic complexes and negatively-charged $Al(OH)_3(s)$ colloids predominate (Stumm and Morgan, 1970; Stumm and O'Melia, 1968). The presence of these charged colloids suggests specific OH^- adsorption onto the surface of the amorphous $Al(OH)_3(s)$ precipitate (pH > i.e.p.). It is possible that anionic complexes are also adsorbed.

The mononuclear species (*e.g.*, $AlOH^{2+}$) are formed rapidly and reversibly. The small polynuclear species (*e.g.*, $Al_2(OH)_2^{4+}$) are formed less rapidly than the mononuclear species. The large polynuclear ions (*e.g.*, $Al_{13}(OH)_{34}^{5+}$) are formed the slowest (Baes and Mesmer, 1976; Stumm and Morgan, 1970), considering that such species are formed by the condensation of mononuclear species. While the formation of polynuclear species by the dissolution of aluminum salts in water might be thermodynamically feasible, the kinetics of formation could be too slow (Baes and Mesmer, 1976) to be beneficial in water treatment practice. It is considered that the electrocoagulation technique supplies sufficient energy to accelerate the formation kinetics of polynuclear hydroxoaluminum species in the electrical double layer at the anode surface. For instance, the temperature at the anode surface is significantly higher than that in the bulk solution or suspension.

In expressing rules of hydrolysis speciation, Stumm and Morgan (1970) stated that metal ions hydrolyze more readily at low concentration and with increasing pH. Hence, as expected, hydroxoaluminum complexation kinetics decrease significantly in the acidic pH range. Another rule stated that the abundance of polynuclear complexes increases with the total dissolved aluminum concentration. It should be remembered that the concentrations under

consideration are of the order of 10^{-3} M or less. The hydrolysis speciation rules have been mentioned here because they are directly relevant to the conditions under which electrocoagulation has been examined in this project. Hence, the speciation of the hydroxoaluminum complexes changes with electrocoagulation retention time, current density and pH.

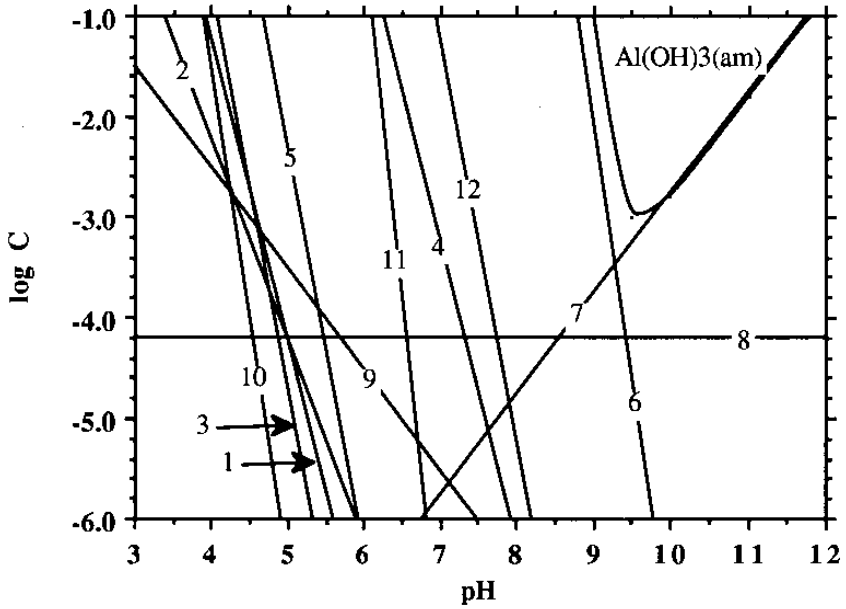

Figure 1-7. Equilibrium pC-pH diagram for Al-H_2O system (C = 10^{-3} M, T = 25°C).

Figure 1-7 illustrates the concentration variation with pH for a number of hydroxoaluminum complexes existing in equilibrium with amorphous aluminum hydroxide, $Al(OH)_3$(am). The complexes corresponding to the numbered lines are listed in Appendix A. Equations for these lines and for the aluminum solubility boundary ($C_{T,diss}$) are derived and plotted in Appendix B. Each numbered line has a slope which is numerically equal to the charge on the complex species it represents, but the sign is opposite to that of the charge. Line 9, for instance, represents $Al(OH)_2^+$ and has a slope of -1.

The $Al(OH)_3$(am) stability field, which is delimited by the solubility boundary indicated in Figure 1-7, occurs in a basic pH range which widens as the concentration of total aluminum (C) increases. Aluminum solubility reaches its minimum at the approximate pH of 9.6 at 25°C. Hence, at a total aluminum concentration of 10^{-1} M, $Al(OH)_3$(am) would be expected to precipitate within the

approximate pH range of 9 to 11.7. At total concentrations of $<10^{-3}$ M, however, $Al(OH)_3(am)$ is not expected to precipitate at any pH. It follows, then, that when C exceeds $C_{T,diss}$ in the pH range of $Al(OH)_3(am)$ precipitation, the dissolved Al concentration is reduced by $(C - C_{T,diss})$ at equilibrium.

1.2.4.2 Adsorption of Hydroxoaluminum Complexes

Hydroxoaluminum complexes, rather than Al^{3+}, have been identified as the effective coagulative species produced from alum (Beecroft *et al.*, 1995; Hahn and Stumm, 1968; Parthasarathy and Buffle, 1985; Stumm and Morgan, 1970). These complexes adsorb strongly, rapidly and specifically onto the particle surface, and the tendency towards adsorption is pronounced for the polynuclear polyhydroxo species (Dentel and Gossett, 1988; Stumm and Morgan, 1970). In fact, the adsorption tendency is so strong that Stumm and Morgan (1970) remarked, "Adsorption of hydrolysis species must be assumed to occur on most interfaces . . . ". The explanation they offered for this marked proclivity for adsorption was that hydrolyzed species are larger and less hydrated (fewer coordinated H_2O molecules; see Equations 1-25 and 1-26) than unhydrolyzed species ($Al(H_2O)_6^{3+}$). The presence of coordinated –OH appears to enhance adsorption when it is considered that –OH itself adsorbs strongly. In other words, the hydroxoaluminum complexes could be duplicating the adsorption behaviour of –OH, possibly possessing greater adsorptivity. In addition, the replacement of the aquo group (*i.e.*, H_2O) by the hydroxo group (*i.e.*, –OH) in the coordination sheath (around Al^{3+}) could be endowing the complex with hydrophobic character, thus enhancing the adsorption behaviour. As stated earlier, dehydration is prerequisite to adsorption. Since dehydration is being equated with increased hydrophobicity, Stumm and Morgan's explanation is consistent with the prerequisite. They further stated that the polynuclear species could be acting as short-chain polymers which adsorb at specific sites on the particle surface. The immediate implication is that interparticle bridging could be a mechanism by which the polynuclear hydroxoaluminum complexes destabilize particulate suspensions. In addition, the high ionic charge on many of these complexes is evident. Consequently, it is reasonable to conclude that the polynuclear complexes are the most efficient coagulative species (Dentel and

Gossett, 1988; Hahn and Stumm, 1968; Stumm and Morgan, 1970) by virtue of their high ionic charge and probable bridging capacity. It is appropriate to note that these complexes are effective in destabilizing sols at much lower concentrations than non-sorbable species (Hahn and Stumm, 1968; Stumm and O'Melia, 1968). Covalent bonding between the complexes and the adsorption surface could be enhanced (Stumm and O'Melia, 1968), and would be consistent with the strong adsorption reported. Hahn and Stumm (1968) suggested that the complexes are attached to the adsorption surface by –OH groups. It is important to note, also, that these complexes can adsorb onto surfaces of the same polarity as the complexes (Stumm and O'Melia, 1968).

It is worth emphasizing that the hydroxoaluminum complexes were studied under laboratory conditions that were closely controlled. This degree of control is not possible in industrial process facilities by virtue of scale. Consequently, it is safe to conclude that, given the slow formation kinetics of the more coagulation-effective complexes, they do not play a significant role on the industrial scale. In contrast, electrocoagulation is considered to provide the energy required to accelerate the formation kinetics of these complexes and is not sensitive to scale. It is quite probable, therefore, that the polynuclear hydroxoaluminum complexes play a significant role in the effectiveness of electrocoagulation. Parekh *et al.* (1992) and Barkley *et al.* (1993) attributed the electrocoagulation mechanism to electrostriction, which they described as the stripping of surface charge from the suspended particles. If this were true, carbon electrodes would have been able to destabilize particulate suspensions, but they are ineffective, as demonstrated in the current study.

1.2.4.3 Effects of Ageing

The ageing effects exhibited by metal ion solutions are endogenous to structural transformations of the isopolyions. A change in the solution composition accompanies ageing as precipitation results from the transformations (Stumm and Morgan, 1970). Beecroft *et al.* (1995) studied the ageing of partially neutralized alum solutions which were determined to contain mononuclear and polynuclear hydroxoaluminum species. The concentrated solution could be stored for several months, depending on the storage temperature. The dilute solution exhibited a shorter "shelf life" owing to

accelerated ageing, during which the concentrations of the polynuclear species decreased as a precipitate of basic aluminum sulphate was formed. The loss of these species was accompanied by diminished coagulative capacity of the aged solution. It is interesting to note that most of the precipitation of the polynuclear species occurred early in the ageing time. Hence, there was a rapid initial loss of coagulative capacity. In the latter stages of ageing, the mononuclear complexes were the principal species precipitated.

In the current program of study, electrocoagulated material was observed to possess coagulative capacity two years after electrocoagulation. This long "shelf life" makes electrocoagulation very attractive.

1.3 PROJECT DEFINITION

This research project was conceived from reports of the difficulty experienced by oil sands and coal processing plants in thickening fine solids (*e.g.*, MacKinnon, 1986; Parekh *et al.*, 1992). Clays are an example of natural materials which are commonly handled by mineral processing plants, and which possess notoriously poor thickening characteristics. The consequences of such characteristics to the plant have been summarized in Section 1.1.1. Hence, this research program was developed to study the enhancement of the settling behaviour of fine silica as the model material. The AC/EC technique was then extended to bentonite (a finely divided clay), as well as to two industrial discharges, namely, Syncrude mature fine tailings and Luscar Sterco coal tailings.

Enhancement of the dewatering characteristics of particulate solids is accomplished on the industrial scale solely through the use of chemical reagents, which serve as coagulants and flocculants in water and wastewater treatment, and in the mineral industry. The high and ever increasing cost of these reagents, together with their uncertain effectiveness on colloidal particles, argues strongly for a less expensive, more effective alternative dewatering treatment.

Thermal methods, such as boiling and freezing, demand enormous quantities of heat transfer because of the high thermal capacity of water. In addition, the freezing technique is limited to cold regions and, even so, would be seasonal in its application. The addition of a particulate suspension of opposite charge for charge neutralization would involve large quantities of water which, for

economic reasons, would be mill water taken from a river or lake. Such water will contain humic substances which are known (Chowdhury *et al.*, 1991; Montgomery, 1985) to interfere with coagulation processes. On the other hand, charge neutralization by the addition of oppositely charged, fine, dry solids could be a viable alternative.

Since the alternative process would be replacing an existing system, totally or partially, it must have the characteristic of being easily integrated into the existing plant without creating process upsets. If the alternative process equipment can be built by the plant operator on site, and if it is simple to maintain by the plant operator, these considerations would favour the adoption of the process. Alternating current electrocoagulation satisfies all of these requirements, except energy consumption, about which the literature is not consistent in its analysis. The literature review has made it clear, however, that optimization studies are greatly desirable. AC/EC systems can be made modular and portable without diminution of the technique's effectiveness (Brewster and Passmore, 1994; Woytowich *et al.*, 1993).

This thesis project embraces two principal areas of study, namely, colloidal interactions and aqueous chemistry. The electrocoagulation literature has revealed an inadequate understanding of the mechanisms by which AC/EC enhances the dewatering characteristics of particulate solids. The studies reported are restricted in scope, having been designed to address a particular objective. It is evident that a fundamental program of study is necessary. This project constitutes such a program which is expected to contribute significantly to the understanding of the mechanisms inherent in the application of AC/EC.

1.4 EXPERIMENTAL PLAN

A fundamental study of AC electrocoagulation has been conducted. It examines the influence of a wide range of process parameters on the effectiveness of electrocoagulation. Effectiveness is measured by the degree of enhancement of the settling behaviour of silica. The following parameters have been tested:

- agitation,
- retention time duration and mode (continuous and cumulative),
- current density,

- electrode area,
- conductivity of the dispersion medium,
- electrode separation,
- AC/EC mode (direct and indirect),
- ageing of the electrocoagulated solids,
- electrode material, and
- initial pH and temperature of the dispersion medium.

Identification of the predominant hydroxoaluminum complex species was attempted. Characterization of the floc morphology was performed on selected samples to provide information about the structure and its modification by electrocoagulation conditions.

No attempt was made to optimize process parameters or to generate data for scale-up since these endeavours were outside the scope of this work.

1.5 ORGANIZATION OF THE THESIS

This thesis has been prepared in paper format as prescribed in *FGSR Thesis Format Specifications*, University of Alberta, effective Fall 2009. Data, from which graphs have been plotted, are tabulated in Appendix A, while calculations yielding such data are derived and illustrated in Appendix B.

This thesis consists of seven chapters. Chapter 1 introduces the subject of this study by demonstrating the relevance of electrocoagulation to industrial processing and environmental control strategies. Published reports are summarized in a literature review and fundamental principles are presented. The influences of agitation, retention time, AC/EC mode, current density and quantity of electricity on the performance of AC/EC are discussed in Chapter 2. Jar test results with alum and aluminum chloride are presented, and the ageing behaviour of electrocoagulated silica is analyzed. Chapter 3 examines the influences of the feed water conditions of specific conductivity, temperature and pH on AC/EC performance. Aluminum speciation is attempted. In Chapter 4, the roles of electrode area, separation and material of construction in the electrocoagulation of silica are examined. The amenability to AC/EC treatment of fine natural solids of industrial importance is evaluated in Chapter 5. Chapter 6 presents a general discussion of the results obtained in the research project and

conclusions are derived. Finally, recommendations for further study are made in Chapter 7.

1.6 REFERENCES

Akitt J.W. and Farthing A. (1978), New ^{27}Al NMR studies of the hydrolysis of the aluminum(III) cation. *J. Mag. Reson.,* **32,** 345-352.

Ayyala S., Pugh R.J. and Forssberg E. (1995), Aggregate characteristics in coagulation and flocculation. *Miner. Process. Extrac. Metall. Rev.,* **12,** 165-184.

Baes C.F. and Mesmer R.E. (1976), The Hydrolysis of Cations. John Wiley & Sons, New York, pp. 112-123.

Barkley N.P., Farrell C.W. and Gardner-Clayson T.W. (1993), Alternating current electrocoagulation for Superfund site remediation. *J. Air Waste Management Assoc.,* **43,** 784-789.

Beck E.C., Giannini A.P. and Ramirez E.R. (1974), Electrocoagulation clarifies food wastewater. *Food Technol.,* **February,** 18-22.

Beecroft J.R.D., Koether M.C. and vanLoon G.W. (1995), The chemical nature of precipitates formed in solutions of partially neutralized aluminum sulfate. *Water Res.,* **29**, 1461-1464.

Bejankiwar R.S. (2002), Electrochemical treatment of cigarette industry wastewater: feasibility study. *Water Res*., **36**, 4386-4390.

Belongia B.M., Haworth P.D., Baygents J.C. and Raghavan S. (1999), Treatment of alumina and silica chemical mechanical polishing waste by electrodecantation and electrocoagulation. *J. Electrochem. Soc*., **146**, 4124-4130.

Black A.P. (1967), Electrokinetic characteristics of hydrous oxides of aluminum and iron. In Faust S.D. and Hunter J.V. (Eds.), Principles and Applications of Water Chemistry. John Wiley & Sons, Inc., New York, pp. 274-300.

Bockris J.O'M., Devanathan M.A.V. and Miller K. (1963), On the structure of charged interfaces. *Proc. Roy. Soc. London,* **A274,** 55-79.

Brewster M.D. and Passmore R.J. (1994), Use of electrochemical iron generation for removing heavy metals from contaminated groundwater. *Environ. Progress,* **13**, 143-148.

Briggs T.R. (1921), Emulsions with finely divided solids. *J. Ind. Eng. Chem.,* **13**, 1008-1010.

Cañizares P., Carmona M., Lobato J., Martínez F. and Rodrigo M.A. (2005a), Electrodissolution of aluminum electrodes in electrocoagulation processes. *Ind. Eng. Chem. Res.*, **44**, 4178-4185.

Cañizares P., Jiménez, C., Martínez F., Rodrigo M.A. and Sáez C. (2009), The pH as a key parameter in the choice between coagulation and electrocoagulation for the treatment of wastewaters. *J. Hazard. Mater.*, **163**, 158-164.

Cañizares P., Jiménez, C., Martínez F., Sáez C. and Rodrigo M.A. (2007), Study of the electrocoagulation process using aluminum and iron electrodes. *Ind. Eng. Chem. Res.*, **46**, 6189-6195.

Cañizares P., Martínez F., Carmona M., Lobato J. and Rodrigo M.A. (2005b), Continuous electrocoagulation of synthetic colloid-polluted wastes. *Ind. Eng. Chem. Res.*, **44**, 8171-8177.

Chowdhury Z.K., Amy G.L. and Bales R.C. (1991), Coagulation of submicron colloids in water treatment by incorporation into aluminum hydroxide floc. *Environ. Sci. Technol.,* **25**, 1766-1773.

Den W. and Huang C. (2006), Electrocoagulation of silica nanoparticles in wafer polishing wastewater by a multichannel flow reactor: a kinetic study. *J. Environ. Eng.*, **132**, 1651-1658.

Dentel S.K. and Gossett J.M. (1988), Mechanisms of coagulation with aluminum salts. *JAWWA,* **80**, 187-198.

Donini J.C., Kan J., Szynkarczuk J., Hassan T.A. and Kar K.L. (1994), The operating cost of electrocoagulation. *Can. J. Chem. Eng.*, **72**, 1007-1012.

Duan J. and Gregory J. (2003), Coagulation by hydrolysing metal salts. *Advances Colloid Interface Sci.*, **100-102**, 475-502.

Everett D.H. (1988), Basic Principles of Colloid Science. Royal Society of Chemistry, London, UK, pp. 30-53.

Gao B. and Yue Q. (2005), Effect of SO_4^{2-}:Al^{3+} ratio and OH^-:Al^{3+} value on the characterization of coagulant poly-aluminum-chloride-sulfate (PACS) and its coagulation performance in water treatment. *Chemosphere*, **61**, 579-584.

Gao B., Yue Q. and Wang B. (2002), The chemical species distribution and transformation of polyaluminum silicate chloride coagulant. *Chemosphere*, **46**, 809-813.

Gelot A., Friesen W. and Hamza H.A. (1984), Emulsification of oil and water in the presence of finely divided solids and surface-active agents. *Colloids Surfaces,* **12,** 271-303.

Ghernaout D., Ghernaout B. and Boucherit, A. (2008), Effect of pH on electrocoagulation of bentonite suspensions in batch using iron electrodes. *J. Dispersion Sci. Technol.*, **29**, 1272-1275.

Gregory J. (1993), The role of colloidal interactions in solid-liquid separation. *Water Sci. Technol.,* **27**, 1-17.

Gregory J. and Duan J. (2001), Hydrolyzing metal salts as coagulants. *Pure Appl. Chem.*, **73**, 2017-2026.

Grøterud O. and Smoczynski L. (1992), Purification of wastewater by electrolysis at continuous flow. *J. Water Management Res.-Sweden,* **48**, 36-40.

Hahn H.H. and Stumm W. (1968), Coagulation by Al(III). The role of adsorption of hydrolyzed aluminum in the kinetics of coagulation. In Gould R.F. (Ed.), Adsorption from Aqueous Solution, Advances in Chemistry Series 79. ACS, Washington, DC, pp. 91-111.

Harif T. and Adin A. (2007), Characteristics of aggregates formed by electroflocculation of a colloidal suspension. *Water Res.*, **41**, 2951-2961.

Harif T., Hai M. and Adin A. (2006), Electroflocculation as potential pretreatment in colloid ultrafiltration. *Water Sci. Technol.: Water Supply*, **6**, 69-78.

Holt P.K., Barton G.W. and Mitchell C.A. (2005), The future for electrocoagulation as a localised water treatment technology. *Chemosphere*, **59**, 355-367.

Holt P.K., Barton G.W., Wark M. and Mitchell C.A. (2002), A quantitative comparison between chemical dosing and electrocoagulation. *Colloids Surfaces A*, **211**, 233-248.

Hunt J.P. (1965), Metal Ions in Aqueous Solution. W.A. Benjamin, Inc., New York, pp. 45-54.

Ilhan F., Kurt U., Apaydin O. and Gonullu M.T. (2008), Treatment of leachate by electrocoagulation using aluminum and iron electrodes. *J. Hazard. Mater.*, **154**, 381-389.

Ivanishvili A.I., Przhegorlinskii V.I. and Kalinichenko T.D. (1987), A comparative evaluation of the efficiency of electrocoagulation and reagent methods of clarifying waste water. *Soviet J. Water Chem. Technol.,* **9**(5), 118-119.

Jenke D.R. and Diebold F.E. (1984), Electroprecipitation treatment of acid mine wastewater. *Water Res.,* **18**, 855-859.

Jiang J-Q., Graham N., André C., Kelsall G.H. and Brandon N. (2002), Laboratory study of electro-coagulation-flotation for water treatment. *Water Res.*, **36**, 4064-4078.

Kindzierski W. (1995). CIV E 620 Course Notes, Fall 1995. Department of Civil Engineering, University of Alberta.

Lai C.L. and Lin S.H. (2003), Electrocoagulation of chemical mechanical polishing (CMP) wastewater from semiconductor fabrication. *Chem. Eng. J.*, **95**, 205-211.

La Mer V.K. (1964), Coagulation symposium introduction. *J. Colloid Sci.,* **19,** 291-293.

MacKinnon M.D. (1986), Environmental aspects of waste water management at an oil sands development in northern Alberta. In Lewis M.L. (Ed.), Proceedings of SPIB Conference on Northern Hydrocarbon Development, Environmental Problem Solving. Banff, Alberta, pp. 191-208.

MacKinnon M.D. (1989), Development of the tailings pond at Syncrude's oil sands plant: 1978-1987. *AOSTRA J. Res.,* **5**, 109-133.

Majima H. and Peters E. (1968), Electrochemistry of sulphide dissolution in hydrometallurgical systems. VIII International Mineral Processing Congress, Leningrad, Paper E1, 13 p.

Makarov V.M., Yusova A.P., Babanin V.F., Vasil'ev S.V. and Ivanov A.V. (1987), Influence of the pH of electrocoagulation in reactors with iron anodes on the structure of deposits. *J. Appl. Chem. USSR,* **60**, Pt. 1, 21-25.

Masliyah J.H. (1994), Electrokinetic Transport Phenomena. AOSTRA Technical Publication Series #12, Edmonton, Canada, 363 p.

Matteson M.J., Dobson R.L., Glenn R.W., Kukunoor N.S., Waits W.H. and Clayfield E.J. (1995), Electrocoagulation and separation of aqueous suspensions of ultrafine particles. *Colloids Surfaces A,* **104,** 101-109.

Mollah M.Y.A., Morkovsky P., Gomes J.A.G., Kesmez M., Parga J. and Cocke D.L. (2004), Fundamentals, present and future perspectives of electrocoagulation. *J. Hazard. Mater.*, **B114**, 199-210.

Mollah M.Y.A., Schennach R., Parga J.R. and Cocke D.L. (2001), Electrocoagulation (EC) – science and applications. *J. Hazard. Mater.*, **B84**, 29-41.

Montgomery J.M., Consulting Engineers, Inc. (1985), Water Treatment Principles and Design. John Wiley & Sons, New York, pp. 116-134.

Moreno H.A., Cocke D.L., Gomes J.A.G., Morkovsky P., Parga J.R., Peterson E. and Garcia C. (2009), Electrochemical reactions for electrocoagulation using iron electrodes. *Ind. Eng. Chem. Res.*, **48**, 2275-2282.

Mortimer C.E. (1986), Chemistry, 6th Edition. Wadsworth Publishing Company, Belmont, California, p. 863.

Ofir E., Oren Y. and Adin A. (2007a), Electroflocculation: the effect of zeta-potential on particle size. *Desalination*, **204**, 33-38.

Ofir E., Oren Y. and Adin A. (2007b), Modified equilibrium-solubility domains and a kinetic model of iron oxide and hydroxide colloids for electroflocculation. *Desalination*, **204**, 79-86.

Parekh B.K., Groppo J.G. and Justice J.G. (1992), Removal of fine particulates and metal ions from process discharge waste water using AC electro-coagulation technique. In Chandler S. (Ed.), Emerging Process Technologies for a Cleaner Environment. AIME Proceedings, Phoenix, Arizona, pp. 99-105.

Parthasarathy N. and Buffle J. (1985), Study of polymeric aluminum (III) hydroxide solutions for application in waste water treatment. Properties of the polymer and optimal conditions of preparation. *Water Res.,* **19**, 25-36.

Perng Y-S., Wang E.I-C., Yu S-T., Chang A-Y. and Shih C-Y. (2007), Pilot treatment of OCC-based paper mill wastewater using pulsed electrocoagulation. *Water Qual. Res. J. Canada*, **42**, 63-71.

Pretorius W.A., Johannes W.G. and Lempert G.G. (1991), Electrolytic iron flocculant production with a bipolar electrode in series arrangement. *Water SA,* **17**, 133-138.

Probstein R.F. (1989), Physicochemical Hydrodynamics: An Introduction. Butterworth-Heinemann, London, pp. 227-263.

Przhegorlinskii V.I., Ivanishvili A.I. and Grebenyuk V.D. (1987), Dissolution of aluminum electrodes in the electrocoagulation treatment of water. *Soviet J. Water Chem. Technol.,* **9**, 118-119.

Putnis A. and McConnell J.D.C. (1980), Principles of Mineral Behaviour. Elsevier, New York, pp. 23-24.

Renk R.R. (1988), Electrocoagulation of tar sand and oil shale wastewaters. *Energy Progress,* **8**, 205-208.

Riddick T.M. (1968), Control of Colloid Stability Through Zeta Potential, Vol. I. Livingston Publishing Company, Pennsylvania, pp. 2-3.

Sanfan W. (1991), Studies on economic property of pretreatment process of brackish water using electrocoagulation (EC) method. *Desalination,* **82,** 365-373.

Sarpola A., Hietapelto V., Jalonen J., Jokela J. and Laitinen R.S. (2004), Identification of the hydrolysis products of $AlCl_3 \cdot 6H_2O$ by electrospray ionization mass spectrometry. *J. Mass Spectrom.*, **39**, 423-430.

Sarpola A.T., Hietapelto V.K., Jalonen J.E., Jokela J. and Rämö J.H. (2006), Comparison of hydrolysis products of $AlCl_3 \cdot 6H_2O$ in different concentrations by electrospray ionization time of flight mass spectrometer (ESI TOF MS). *Intern. J. Environ. Anal. Chem.*, **86**, 1007-1018.

Sauer J.E. and Davis E.J. (1994), Electrokinetically enhanced sedimentation of colloid contaminants. *Environ. Sci. Technol.,* **28,** 737-745.

Sawyer C.N., McCarty P.L. and Parkin G.F. (1994), Chemistry for Environmental Engineering, 4th Edition. McGraw-Hill, Inc., New York, pp. 327-341.

Snoeyink V.L. and Jenkins D. (1980), Water Chemistry. John Wiley & Sons, New York, p. 213.

Solomentseva I.M., Barany S. and Gregory J. (2004), Surface properties and aggregation of basic aluminum sulphate hydrolysis products: 1. Electrokinetic potential and hydration of BAS hydrolysis product particles. *Colloids Surfaces A*, **230**, 117-129.

Stol R.J., van Helden A.K. and de Bruyn P.L. (1976), Hydrolysis-precipitation studies of aluminum(III) solutions: 2. A kinetic study and model. *J. Colloid Interface Sci.*, **57**, 115-131.

Stumm W. (1992), Chemistry of the Solid-Water Interface. Wiley-Interscience, New York, pp. 47-51.

Stumm W. and Morgan J.J. (1970), Aquatic Chemistry. Wiley-Interscience, New York, pp. 244-258.

Stumm W. and Morgan J.J. (1981), Aquatic Chemistry: An Introduction Emphasizing Chemical Equilibria in Natural Waters. John Wiley & Sons, New York, pp. 241-242.

Stumm W. and O'Melia C.R. (1968), Stoichiometry of coagulation. *JAWWA,* **60**, 514-539.

Syncrude Canada Ltd. (2009), 2009 Annual Tailings Plan Submission, Syncrude Mildred Lake (Leases 17 and 21). Submitted September 30 to Energy Resources Conservation Board, 45 p.

Trompette J.L. and Vergnes H. (2009), On the crucial influence of some supporting electrolytes during electrocoagulation in the presence of aluminum electrodes. *J. Hazard. Mater.*, **163**, 1282-1288.

Un U.T., Koparal A.S. and Ogutveren U.B. (2009), Electrocoagulation of vegetable oil refinery wastewater using aluminum electrodes. *J. Environ. Manage.*, **90**, 428-433.

van Olphen H. (1977), An Introduction to Clay Colloid Chemistry, 2nd Edition. John Wiley & Sons, New York, pp. 1-5.

Vik E.A., Carlson D.A., Eikum A.S. and Gjessing E.T. (1984), Electrocoagulation of potable water. *Water Res.,* **18**, 1355-1360.

Wang C-T., Chou W-L., Chen L-S. and Chang S-Y. (2009), Silica particles settling characteristics and removal performances of oxide chemical mechanical polishing wastewater treated by electrocoagulation technology. *J. Hazard. Mater.*, **161**, 344-350.

Wang D., Tang H. and Gregory J. (2002), Relative importance of charge neutralization and precipitation on coagulation of kaolin with PACl: effect of sulfate ion. *Environ. Sci. Technol.*, **36**, 1815-1820.

Wang Y., Gao B-Y., Xu X-M., Xu W-Y. and Xu G-Y. (2009), Characterization of floc size, strength and structure in various aluminum coagulants treatment. *J. Colloid Interface Sci.*, **332**, 354-359.

Waters D.N. and Henty M.S. (1977), Raman spectra of aqueous solutions of hydrolysed aluminium (III) salts. *J. Chem. Soc., Dalton Trans.,* 243-245.

Weast R.C. (Ed.) (1989), CRC Handbook of Chemistry and Physics, 70th Edition. CRC Press, Inc., Boca Raton, Florida, p. F-146.

Woytowich D.L., Dalrymple C.W., Gilmore F.W. and Britton M.G. (1993), Electrocoagulation (CURE) treatment of ship bilgewater for the U.S. Coast Guard in Alaska. *Marine Technol. Soc. J.,* **27**, 62-67.

Yildiz Y.Ş., Koparal A.S. and Keskinler B. (2008), Effect of initial pH and supporting electrolyte on the treatment of water containing high concentration of humic substances by electrocoagulation. *Chem. Eng. J.*, **138**, 63-72.

Zbik M.S., Smart R.S. and Morris G.E. (2008), Kaolinite flocculation structure. *J. Colloid Interface Sci.*, **328**, 73-80.

Zhao H., Liu H. and Qu J. (2009), Effect of pH on the aluminum salts hydrolysis during coagulation process: formation and decomposition of polymeric aluminum species. *J. Colloid Interface Sci.*, **330**, 105-112.

Zongo I., Leclerc J-P., Maïga H.A., Wéthé J. and Lapicque F. (2009), Removal of hexavalent chromium from industrial wastewater by electrocoagulation: a comprehensive comparison of aluminium and iron electrodes. *Sep. Purif. Technol.*, **66**, 159-166.

CHAPTER 2

STUDY OF AGITATION AND ALUMINUM DOSAGE IN A.C. ELECTROCOAGULATION OF FINE SILICA

2.1 INTRODUCTION

This research project originated from consideration of the poor settling characteristics exhibited by Syncrude fine tailings. AC/EC would possibly solve this thickening problem if the technique could be shown to enhance the settling behaviour of the tailings. Therefore, an understanding of electrocoagulation was pursued through a fundamental study, with fine silica as the model tailings solid and aluminum as the material of electrode construction. Silica was used because, like Syncrude fine tailings, it exhibited poor settling behaviour (*i.e.*, formed a stable suspension in water). Success in enhancing the settling behaviour of silica would lead to a trial on Syncrude fine tailings.

Research was initiated with silica dispersed in Edmonton tap water. AC/EC was effective in enhancing the settling behaviour of silica in a manner similar to that observed when tap water was replaced with de-ionized water. Tap water had been a convenient dispersion medium because its specific conductivity, which typically varied between 250 and 300 µS/cm, supported the magnitude of current that was required for most tests. Its use was discontinued, however, because its quality varied unpredictably, to the extent that one or more unidentified constituents interfered with the AC/EC process from time to time. The quality of de-ionized water, on the other hand, was controllable and interference was not a concern. Because of the low specific conductivity (typically <1 µS/cm) of the de-ionized water, sodium chloride was added to increase the current-carrying capacity.

2.2 THEORY AND BACKGROUND

2.2.1 Agitation and Floc Growth

Two stages were identified in flocculation studies of Neosil A™ ground silica (d_{50} of 24 µm) under shear in the impeller tip speed range of 1.96 to 4.58 m/s (Spears and Stanley, 1994). The silica concentration in the feed suspension ranged from 0.1 to 1.0 wt %, and Armac C™ (a flotation collector) served as the

flocculant at a dosage of 1.5 kg/t and pH 6.5. Flocculation began with rapid floc growth, followed by attainment of a steady state between floc growth and fragmentation. The limiting floc size was determined by the hydrodynamic conditions and the flocculant dosage. At zero flocculant dosage, flocculation did not occur at any agitation rate. The agitation rate, which produced the largest flocs, decreased as the solids concentration was increased. This result indicated that the closer proximity of the silica particles, due to increasing concentration, enhanced the flocculation process, consequent to the higher collision frequency. The result also illustrated that the flocs would fragment when subjected to excessive shear rates. Once the limiting floc size was attained, however, no significant net fragmentation resulted from prolonged agitation. It is interesting to note that flocculation was achieved at a zeta potential of -26 mV. This is not unusual since coagulation and flocculation can be achieved well before charge neutralization occurs (*i.e.*, when $\zeta \neq 0$) (Cohen and Hannah, 1971; Xiao *et al.*, 2008).

In another study at pH 6.5 with Neosil A™ (but d_{50} of 28 µm) in a 1 wt % solids suspension, Percol 351™ was used as the flocculant (Sharma *et al.*, 1994), being a non-ionic polyacrylamide of high molecular weight. It was added continuously at two mass flow rates to give a fixed dosage. Agitation was continued after the required dosage had been met. The floc size and growth rate were observed to increase with the flocculant dosing rate. At both dosing rates studied, doubling the shear rate almost halved the maximum floc size attained. After attainment of the maximum floc size, further addition of flocculant to the slurry did not further increase the floc size. Hence, at the limiting size, floc growth and fragmentation proceeded in steady state.

Hogg *et al.* (1993) used an unidentified non-ionic polyacrylamide to flocculate a 3 wt % kaolin suspension. Their results agreed with those of Sharma *et al.* (1994) that the floc growth rate increased with the flocculant dosing rate. Concomitantly, the floc porosity increased.

2.2.2 Adsorption

Cation adsorption onto hydrous metal oxides is typically extremely rapid because of ready accessibility to the surface (Kinniburgh and Jackson, 1981). Consistent with the reports of Beecroft *et al.* (1995), Cohen and Hannah (1971)

and Stumm and Morgan (1970), among others, Kinniburgh and Jackson acknowledged that the hydroxometal complexes adsorb much more strongly than the simple metal ion. Brewster and Passmore (1994) demonstrated the strength of adsorption by conducting toxicity characteristic leaching procedures (TCLP), during which only the non-specifically adsorbed barium was leached. The adsorption behaviour of polynuclear metal ions is sensitive to pH, such that small pH changes can cause relatively large changes in adsorption (Kinniburgh and Jackson, 1981).

Adsorption can increase with temperature, as might be intuitively inferred, but this is not always the case. The relation between adsorption and temperature is complicated by temperature effects on hydrolysis and precipitation kinetics, as well as on K_W (hence, pH) (Kinniburgh and Jackson). Many cationic hydroxometal complexes adsorb so strongly that the point of charge neutralization is surpassed and the originally negatively-charged surface acquires a net positive charge (Lyklema, 1978). Furthermore, when specific adsorption dominates electrostatic repulsion, a complex will adsorb onto a surface of the same polarity (Lyklema, 1978; Stumm and O'Melia, 1968).

2.2.3 Ageing of Al Species

The slow attainment of equilibrium by aluminum aqueous solutions is well documented (Gregory and Duan, 2001; Tsai and Hsu, 1984; Hem and Roberson, 1967; Pokras, 1956). Consequently, samples have been studied as they aged for years (*e.g.*, Hsu, 1992; Smith, 1971). Of particular relevance to this research is Smith's report on the 1-day ageing of complex hydroxoaluminum species, which were characterized by the ferron method. By this method, mononuclear (Al_a), polynuclear (Al_b) and solid (Al_c) species can be detected; however, individual members of these groups cannot be identified (Cañizares *et al.*, 2006; Solomentseva *et al.*, 2004; Gao *et al.*, 2002). By ageing aluminum solutions, which had been partially neutralized with base to various degrees (*i.e.*, various OH:Al ratios), Smith observed that the mononuclear Al complexes decreased in concentration to a greater extent as the initial pH was increased from 4.5 to 7.2. The pH itself tended towards larger drops as the initial solution pH was raised in accordance with the OH:Al ratio. The quantity of precipitate increased with increasing initial pH, while the polynuclear species increased at the expense of

the mononuclear species at pH < 5. At higher pH, however, the precipitate increased at the expense of the polynuclear species. In contrast, Tsai and Hsu (1984) determined that polynuclear Al species can also transform to other polynuclear species during ageing, depending on the solution conditions.

Bertsch (1989) reported the redissolution of amorphous aluminum hydroxide precipitate accompanied by the release, during ageing, of $Al_{13}O_4(OH)_{24}(H_2O)_{12}^{7+}$, which is an efficient coagulative species (Beecroft *et al.*, 1995). A partially neutralized $AlCl_3$ solution (OH:Al ratio 2.5) was shown by Bottéro *et al.* (1980b) to contain another efficient coagulative species, $Al_{13}O_4(OH)_{28}(H_2O)_8^{3+}$, after 1 day's ageing. It was further reported that interstitial solution can be expelled from the structure of $Al(OH)_3$ gel during ageing (termed "syneresis" by ceramicists (Scott, 1993)), decreasing the porosity of the gel and causing its structure to collapse. Hence, ageing can involve considerable surface reorganization (Kinniburgh and Jackson, 1981).

In summary, therefore, "ageing" may be defined as aqueous chemical reaction, characterized by slow kinetics. Ageing is usually studied at ambient temperature and commonly involves pH change. Additionally, morphological changes occur in the flocs (Wang *et al.*, 2009).

2.2.4 Silica Surface Chemistry

Hunter (1981) placed the i.e.p. of aged α-SiO_2 at pH 2.0±0.3, while Lyklema (1978) quoted the value of the p.z.c. for silica at pH ~ 2, and Hunter estimated the p.z.c. for quartz to be pH 2 to 3.7. These values attest to the acidic nature of silica. Consequently, the following equations have been proposed as possible surface reactions (Huang, 1981; Lyklema, 1978; Amirtharajah and O'Melia, 1990), where ≡Si represents a silicon surface atom.

$$\equiv SiOH \leftrightarrow \equiv SiO^- + H^+$$

$$\equiv SiOH + OH^- \leftrightarrow \equiv Si(OH)_2^-$$

$$\equiv SiOH + H^+ \leftrightarrow \equiv SiOH_2^+$$

$$\equiv SiOH \leftrightarrow \equiv Si^+ + OH^-$$

The adsorption of alkali metal cations is usually non-specific and it depends directly on the surface charge, which changes with pH.

2.2.5 Mechanisms of Chemical Coagulation

Amirtharajah and O'Melia (1990) elucidated the mechanisms involved in chemical coagulation as it occurs in the jar test. The initial high-intensity agitation, which they called "flash mixing", is intended to distribute the coagulant among the suspended particles, while ensuring a high collision rate among them. At low Al dosage, Amirtharajah and O'Melia stated that mononuclear complexes form rapidly (within 10^{-4} to 1 s) and coagulate the particles by charge neutralization upon becoming adsorbed. They further reported that, at high Al dosage, aluminum hydroxide precipitates (within 1 to 7 s) and is adsorbed onto the suspended particles.

With the coagulant uniformly distributed, rapid mixing is no longer essential since collision is still achieved among particles. Hence, the slow-mixing regime has the objective of promoting floc growth by interparticle collision. At low Al dosage, aluminum hydroxide precipitates at the particle surface from complexes already adsorbed there. At high Al dosage, however, hydroxide precipitation is rapid in the bulk solution and sweep floc becomes the dominant mode of coagulation.

2.3 EXPERIMENTAL METHODS

2.3.1 Materials and Equipment

The silica was supplied under the trade name, Sil-Co-Sil Ground Silica, by the Ottawa Silica Company of Ottawa, Illinois, USA, and was tested as received. Edmonton tap water was de-ionized with a Barnstead D8902 cartridge of mixed resin. It was then used as wash water and as the dispersion medium for the silica. The sodium chloride was of reagent grade.

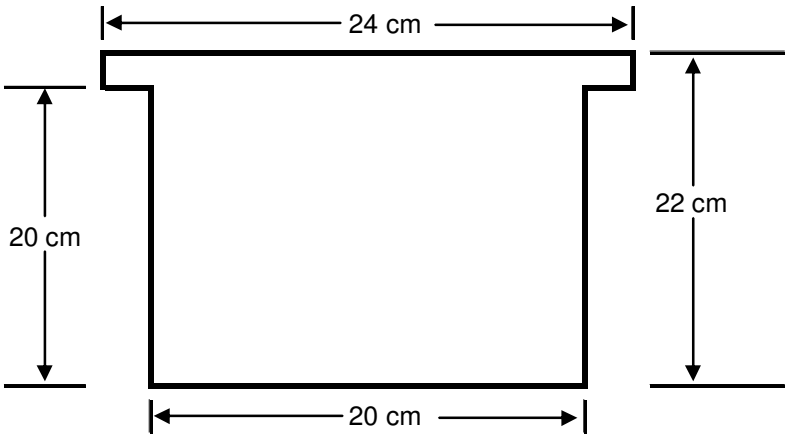

Figure 2-1. A plate electrode.

The electrodes were 0.7 mm-thick rectangular plates measuring 22 cm x 20 cm (Figure 2-1). They were fabricated from 6061-T6 aluminum alloy analyzing 91.8% Al, 1.0% Si, 1.6% Mg, 0.4% Fe, and the rest O.

Concentrated hydrochloric acid and sodium hydroxide pellets, both of reagent grade, were respectively diluted and dissolved in de-ionized water for use in pH adjustment. One drop of concentrated HCl was added to prevent precipitation in water samples that were designated for chemical analysis by atomic absorption spectrophotometry (AAS).

AAS was the analytical method preferred to ICP-ED (inductively coupled plasma with an emission detector) because the latter, which was outside the Department of Chemical Engineering, offered no greater accuracy in aluminum analysis. Analysis (predominantly of Al) was performed on a Perkin Elmer 4000 AAS double beam analyzer.

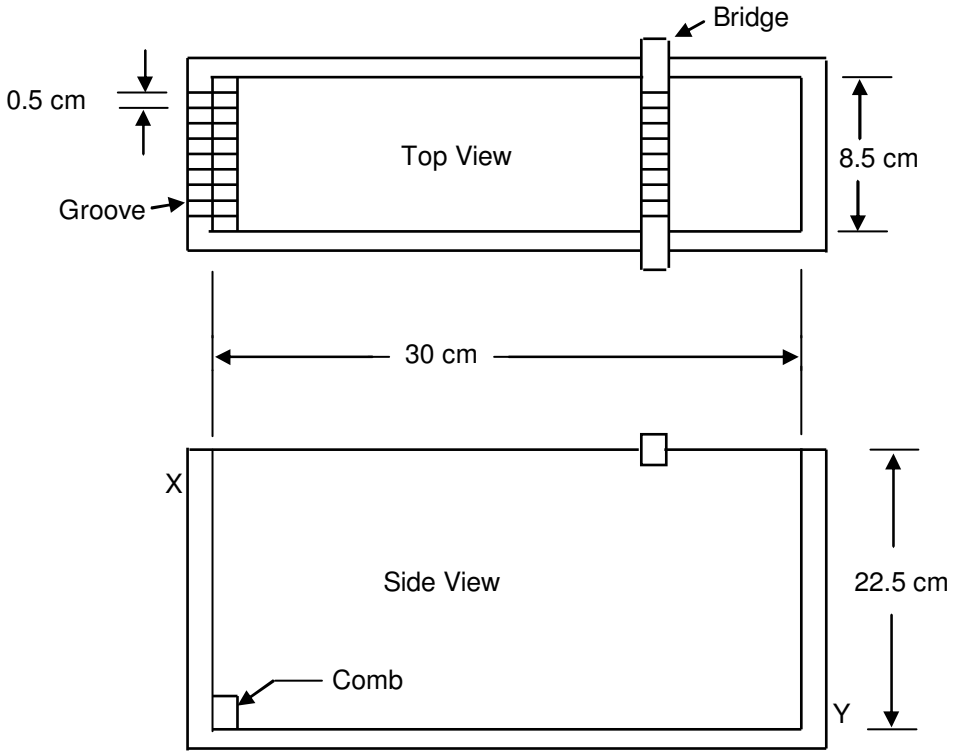

Figure 2-2. Sketch of the electrocoagulation cell.

Electrocoagulation was performed in the 5.7-L Plexiglas™ cell sketched in Figure 2-2. A spigot (not shown in the diagram), equipped with a sample cock, was fitted at X and at Y to facilitate sampling of the supernatant water and electrocoagulated slurry, respectively. The electrodes were held snugly in 1-mm wide grooves that were cut 0.5 cm apart along the top edge of one end-wall of the cell and along a removable Plexiglas™ bridge placed near the other end-wall. The bridge itself was slotted near its ends to ride the side walls of the cell snugly.

A Plexiglas™ comb, detailed in Figure 2-3, was placed on the base of the cell in contact with the left end-wall (see Figure 2-2). The bottom edges of the electrodes fitted snugly into the grooves of the comb to maintain a constant electrolytic area of 299.1 cm^2, as well as to prevent contact between electrodes when agitation was applied. An overhead motor powered a Teflon™-coated paddle assembly which incorporated an axial-flow impeller, 5 cm in diameter.

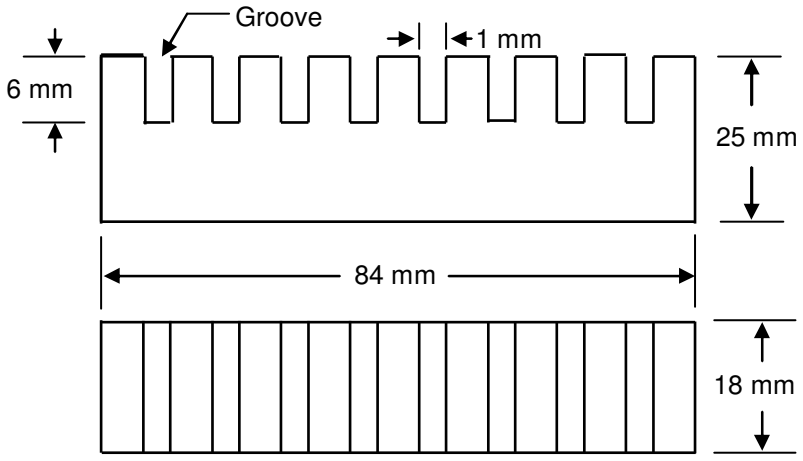

Figure 2-3. Diagram of the comb.

2.3.2 Characterization of As-received Silica

As-received silica was characterized by its moisture content, density, particle size distribution, by its natural settling behaviour in de-ionized water containing 0 and 200 mg/L of added NaCl, and by its zeta potential. Moisture content at 103°C and 180°C was determined as prescribed by Greenberg *et al.* (1992) in a vacuum oven. Density was determined with a 50-mL pyknometer.

The hydrometer method, set out in the 1995 MET E 331/MET E 533 laboratory manual and in Standard D 422 (ASTM, 1997), was used to establish the particle size distribution of as-received silica. This method is preferred to the Cyclosizer because it is simple and convenient, being capable of yielding a larger body of data for the size curve. In addition, it is not restricted to the sub-sieve sizes as is the Cyclosizer. De-ionized water was used instead of distilled water. The hydrometer had a cylindrical bulb and was graduated over a specific gravity range of 0.995 to 1.300. Treatment of the data is detailed in Appendix B.

The natural settling behaviour of as-received silica was established by the timed, downward movement of the solid-liquid interface in a graduated cylinder. The nature of the settling is described in Section 2.4.1.2. Zeta potential was measured in de-ionized water containing 0 and 200 mg/L added NaCl over the pH range of 3.0 to 9.3. A Rank Brothers micro-electrophoresis unit Mark II was used with a flat electrophoresis cell. At each stationary position, the time taken for each of 10 particles to traverse 100 µm was recorded. The particles were

timed successively in opposite directions of travel to minimize electrode polarization. The ratio of the cell dimensions (ℓ/d) was 9.64, where ℓ represents the internal height of the cell, and d the internal width of the cell. For the location of the stationary positions in the cell, the Komagata correction for ℓ/d < 20 was invoked, as instructed by Rank Brothers (1986) and as rationalized by Hunter (1981). Location of the stationary positions and calculation of the zeta potential are illustrated in Appendix B.

2.3.3 AC/EC Test Procedures

Electrocoagulation was studied in the direct and indirect modes. “Direct electrocoagulation” implies that silica was present as a suspension in the AC/EC cell during current flow, while “indirect electrocoagulation” connotes the absence of silica from the cell during current flow. Hence, in the indirect mode, the dispersion medium alone was subjected to AC/EC treatment and was then combined with silica. This AC/EC mode has the advantage of enabling study of the chemical changes occurring in the dispersion medium.

In preparation for electrocoagulation, 840 mg of NaCl was dissolved in 4.2 L of de-ionized water in the electrocoagulation cell. The temperature of the resulting solution was adjusted and noted, and a 100-mL sample was taken. The electrodes were installed and connected to the power supply, as sketched in Figure 2-4. The feed water pH was adjusted, if necessary, and noted. A 100-mL sample was taken.

Figure 2-4 shows a variable transformer by which the output voltage and, hence, the current to the electrocoagulation cell were controlled. The transformer was a Powerstat™ Model 136B from The Superior Electric Co. of Bristol, Connecticut, USA. A current transformer (not shown in Figure 2-4) enabled the magnitude of the current to be displayed digitally by a Novatron™ ammeter. A Novatron™ voltmeter indicated the AC voltage in digital readout.

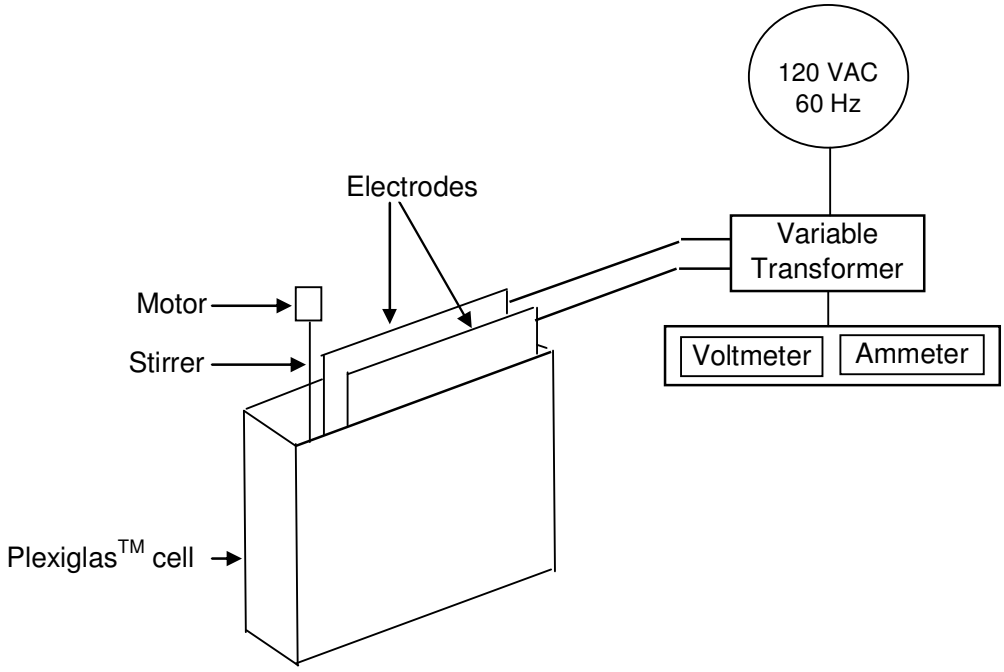

Figure 2-4. AC/EC apparatus.

For direct electrocoagulation, 210.5 g of as-received silica was slurried with about 800 mL feed water and dispersed in the cell at a concentration of 5.0 wt % solids. After the suspension temperature and pH had been recorded, the current flow and timing were started, the current being maintained by continual manual adjustment of the voltage. As electrocoagulation proceeded, the suspension temperature and the applied voltage were recorded every minute. Agitation was continuous at an impeller tip speed of 1.73 m/s. At the end of the electrocoagulation (or AC/EC retention) time, the current flow was stopped and the plates (electrodes), bridge and comb were removed. One litre of the electrocoagulated slurry was withdrawn, under continuous agitation, for a settling test and for the determination of the floc size distribution (see Section 2.3.5.2). A supernatant sample was taken from the cell for Al analysis, for zeta potential measurement of the contained particles, and for the measurement of absolute viscosity (after the solids had settled). A sample of the electrocoagulated slurry was retained for examination of the floc morphology.

In the case of indirect electrocoagulation, the current flow and timing were initiated with only the feed water in the cell. Agitation was continuous at an impeller tip speed of 1.75 m/s. At the end of the treatment time, the current flow

was stopped, and the plates, bridge and comb were removed. The treated water was sampled from the cell for Al analysis. For both the settling test and floc size determination, 1 L of indirectly electrocoagulated slurry was prepared with 51.56 g silica. A separate batch (5 wt % solids: 500 mL treated water and 26.32 g silica) of indirectly electrocoagulated slurry was prepared to provide supernatant and slurry samples, which were utilized in the same manner as described for direct electrocoagulation. Temperature and pH were measured in treated water, supernatant water and electrocoagulated slurry. After every test, the electrodes were cleaned with fine steel wool, washed with tap water, and rinsed with acetone for quick drying.

2.3.4 Water Sample Measurements

Temperature and pH were measured with a Cole Parmer Chemcadet Model 5986-60 combination pH/ORP (oxidation-reduction potential) meter. Temperature readings were occasionally checked against those of a mercury-in-glass thermometer. The pH meter was calibrated against standard buffers supplied by Fisher Scientific according to the range of pH measurement.

The absolute viscosity of de-ionized water and of de-ionized water containing 200 mg/L NaCl was measured to facilitate zeta potential calculation, as well as to facilitate determination of the particle size distribution of as-received silica. The viscosity was measured (at the same temperature as that of the particle or floc size determination) with a Cannon Fenske routine viscometer, No. 50-M309, immersed in a constant-temperature water-bath, as detailed in Standards D 445 and D 446 (ASTM, 1996). With the viscometer vertical in the water-bath, the gravity flow of a fixed volume of the liquid was timed to the nearest 0.1 s, and the average of three (closest) times was calculated. The result was multiplied by the temperature correction factor to give the kinematic viscosity which, when multiplied by the liquid density, in turn, yielded the absolute viscosity.

2.3.5 Characterization of Electrocoagulated Silica

2.3.5.1 Settling Test Procedure

After AC/EC treatment, 1 L of slurry was subjected to a 60-minute settling test at 24°C in a graduated cylinder. Enhancement in settling behaviour was evaluated by comparison of the initial settling rate with that for as-received silica. Similarly, the effect of a process parameter, such as retention time, was determined by comparison of the initial settling rates resulting from changes of the parameter value.

2.3.5.2 Determination of Floc Size Distribution

Another reason for preference of the hydrometer method to the Cyclosizer (see Section 2.3.2) is that high shear forces are absent; hence, the risk of floc degradation is reduced considerably. No dispersant was added. The slurry was homogenized by repeated inversion of the graduated cylinder. Immediately after the final inversion, the cylinder was set down and timing started. A hydrometer (SG range 0.995 to 1.300) was then carefully immersed in the slurry so as to minimize disturbance of the settling flocs. As soon as the SG was within the hydrometer range, SG and time readings were taken as frequently as possible to generate a good curve in the rapidly settling, coarse size range. It is recommended (MET E 331/MET E 533 laboratory manual, 1995) that, after the initial two minutes, the hydrometer should be carefully removed, rinsed, dried and re-immersed in the thickening slurry for each subsequent time-SG pair of readings. In a few instances, however, the solids settled so rapidly (within about 10 minutes) that it was not practical to remove, rinse, dry and re-immerse the hydrometer in time to generate a sufficiently large body of data. In such cases, the hydrometer was removed only after the SG began to change slowly. The supernatant SG and slurry temperature were measured.

The data treatment detailed in Appendix B is applicable to electrocoagulated silica, except for Equation B2-3 in which ρ_s must be replaced with $\rho_{s,bulk}$ (bulk density of electrocoagulated silica). Evidently, ρ_ℓ now denotes supernatant density in Equations B2-3 and B2-4. A sample calculation in Appendix B demonstrates the method of estimating the bulk density from the bulk volume of the sediment.

2.3.5.3 Examination of Floc Morphology

This work was performed in the Biological Sciences Department. One drop of a selected suspension or slurry sample was placed on a glass slide and covered gently with a small, thin glass cover-slip. The particles were viewed on a confocal SEM (Molecular Dynamics, Multipro 2001) which used an Ar/Kr laser as the light source with phase contrast imaging. Micrographs were prepared.

2.3.5.4 Zeta Potential Measurement

Zeta potentials of electrocoagulated particles were measured in the same way as for as-received silica particles, except that the sample pH was not adjusted.

2.4 ELECTROCOAGULATION STUDY

2.4.1 Characteristics of As-received Silica

2.4.1.1 Moisture Content, Density and Particle Size Distribution

Weight losses of <0.01% resulted when as-received silica was dried at 103°C and 180°C. Drying at 103°C removes all free water while minimizing the loss of water of crystallization (Sawyer *et al.*, 1994). However, it is possible that some mechanically occluded (*i.e.*, capillary) water could be retained (Greenberg *et al.*, 1992). Drying at 180°C is intended to remove all mechanically occluded water (Sawyer *et al.*, 1994), but it is possible that a very small proportion of this water could remain intact, and most of the water of crystallization could be removed (Greenberg *et al.*, 1992). The consistency of the insignificant weight losses observed at 103°C and 180°C indicates that the silica was thoroughly dry and contained no water of crystallization as received. Moreover, silica is not a porous or absorptive material like layered clays and, as such, has limited capacity for retaining capillary water. Hence, air-drying wet silica is a viable alternative to oven drying, since free water is the only form of moisture that can be associated with the silica. The density of as-received silica was determined to be 2534.8 kg/m^3.

Figure 2-5 shows the particle size distribution. The d_{50} was about 20 µm and the top size was about 65 µm. Approximately 28% of the silica was finer than 10 µm, while about 6% had an equivalent diameter of 1 µm or less. Depending

on the definition of “colloidal” chosen, 28% or 6% would constitute the colloidal fraction.

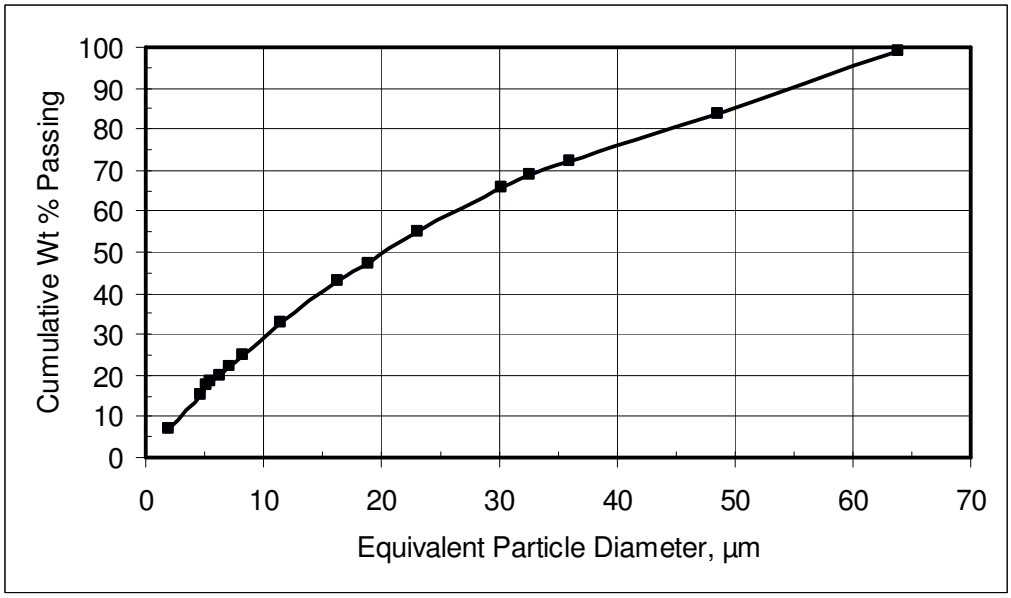

Figure 2-5. Particle size distribution of as-received silica.

2.4.1.2 Natural Settling Behaviour

As received, silica exhibited poor settling behaviour in de-ionized water (no NaCl addition), requiring 17.2 h to settle by 1.0 cm. This is equivalent to an initial settling rate of 9.7×10^{-4} cm/min. In de-ionized water containing 200 mg/L NaCl, the initial settling rate was practically the same at 1.6×10^{-3} cm/min. Hence, the 200 mg/L NaCl addition did not destabilize the suspension. Therefore, any significant enhancement in settling behaviour observed after electrocoagulation would be entirely attributable to the AC/EC process. At the time the natural settling behaviour of silica was observed, the supernatant was clear just below the meniscus, merging into a narrow region of pure colloidal dispersion which had a gelatinous appearance. Below this region, a stable suspension prevailed, such that the sludge line (*i.e.*, the interface between the settled solids and the suspension) was indistinguishable. Hence, the mode of settling was non-Stokesian.

2.4.1.3 Zeta Potential

The effects of pH and NaCl concentration on the zeta potential of silica are illustrated in Figure 2-6.

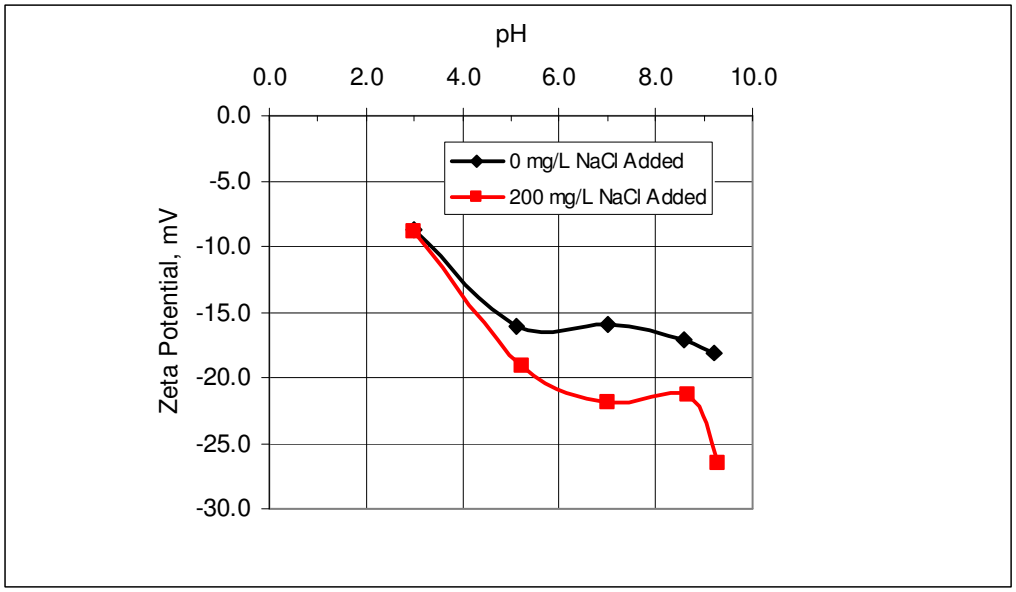

Figure 2-6. Variation of zeta potential of as-received silica with pH.

The zeta potential was negative over the pH range studied and increased negatively with rising pH. In the absence of NaCl, the zeta potential reached a plateau at -16 mV in the neutral pH range (approximately pH 5 to 7). With decreasing pH (<5), the physical adsorption of counterions (H^+) at the silica surface reduced the surface potential (hence, zeta potential). The magnitude of this reduction increased with [H^+] (*i.e.*, decreasing pH). Hence, at pH 3, the zeta potential was about -9 mV, and the i.e.p. would be expected to occur around pH 2. On the other side of the plateau (pH>7), the rate of zeta potential increase between pH 7 and 9 was slower (-1 mV/pH) than that between pH 3 and 5 (-3.5 mV/pH). This suggests that the mechanisms, by which H^+ and OH^- modified the zeta potential in their respective pH range of predominance, were different. In the basic pH range, OH^- is considered to have been specifically adsorbed at the silica surface, followed by a reaction which left an incremental negative charge on the surface, as suggested by Equation 2-1 (Stumm, 1992; Letterman *et al.*, 1982). The zeta potential increased to -18 mV at pH 9.

$$\equiv Si–OH + OH^- \leftrightarrow \equiv Si–O^- + H_2O \qquad (2\text{-}1)$$

Low concentrations of H^+ and OH^- in the neutral pH range are considered to have limited the adsorption of the ions, causing virtually zero net change in the zeta potential.

The addition of 200 mg/L (3.4 mM) NaCl to the silica suspension caused the zeta potentials to become more negative above pH 3.5 (Figure 2-6). Riddick (1968) showed that the zeta potential of colloidal silica (Minusil™) became more negative with NaCl additions to distilled water in the concentration range of 0 to 500 mg/L, after which the zeta potential became less negative. At 0 and 200 mg/L NaCl, the respective zeta potentials were -29 mV and -50 mV (Riddick, 1968). The pH at which these measurements were made was not stated. In the current study, however, as the pH decreased from 7 to 5, physical adsorption of Na^+ was more effective in reducing the zeta potential than that of H^+ because of the much higher concentration of Na^+ ($3.4x10^{-3}$ M vs. 10^{-7} to 10^{-5} M H^+). This is corroborated by comparison with the 0 mg/L NaCl curve. At pH < 5, the rate of zeta potential decrease with pH was augmented by the physical adsorption of both Na^+ and H^+: 200 mg/L NaCl, 5 mV/pH; 0 mg/L NaCl, 3.5 mV/pH. The i.e.p. still appears to occur close to pH 2. At the upper extreme of the pH range (> 8.7), the zeta potential increased sharply with pH, probably due to the surface reaction in Equation 2-1 combined with the participation of Cl^-, as suggested by Equation 2-2.

$$\equiv Si–OH + Cl^- + OH^- \leftrightarrow \equiv Si–OCl^{2-} + H_2O \qquad (2\text{-}2)$$

It is considered that the $HCO_3^-/CO_3^=$ equilibrium created by CO_2 absorbed from the atmosphere might have had some influence on the zeta potentials. Speculation suggests that the adsorption of HCO_3^- and, possibly, $CO_3^=$ onto silica would have contributed to making the zeta potentials more negative, as suggested by the following equations.

$$\equiv Si–OH + HCO_3^- \leftrightarrow \equiv Si–O^- + H_2O + CO_2$$

$$\equiv Si–OH + CO_3^= \leftrightarrow \equiv Si–O^- + HCO_3^-$$

2.4.2 Agitation

2.4.2.1 Agitation Test Procedure

The influence of agitation on the effectiveness of AC/EC treatment of silica was assessed in four tests. In each test, a 4-L batch of the suspension was electrocoagulated directly for 30 to 75 minutes, without or with agitation (impeller tip speed 1.73 m/s). The initial temperature and pH of the suspension were controlled in the ranges of 21.2 to 21.5℃ and 8.6 to 8.8, respectively. A current of 2.1 A (density 70.2 A/m^2) was passed between two electrodes positioned 3.0 cm apart.

2.4.2.2 Agitation Test Results and Discussion

Figure 2-7 depicts the enhanced settling behaviour of the electrocoagulated silica and the effect of agitation at two AC/EC retention times.

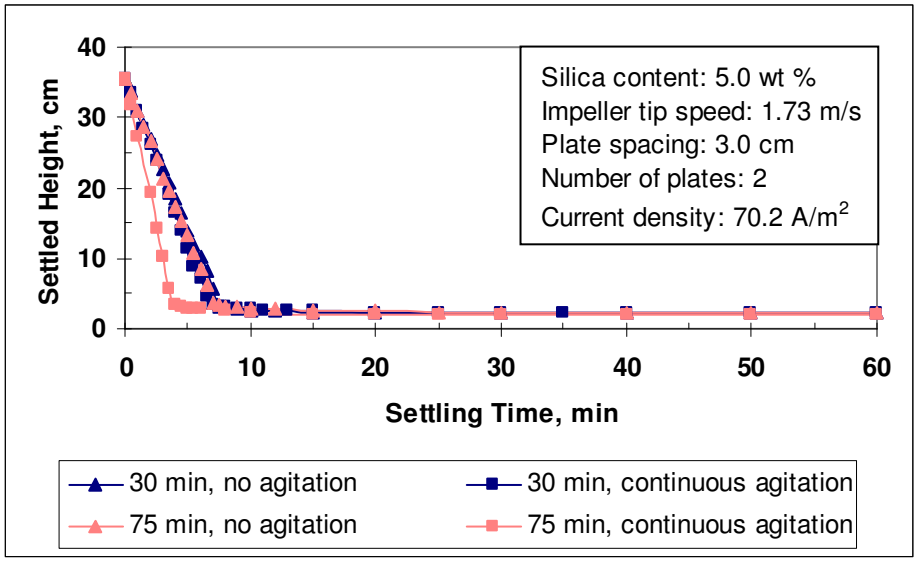

Figure 2-7. Enhanced settling behaviour of electrocoagulated silica.

Thirty minutes' electrocoagulation enhanced the settling behaviour of silica, such that initial settling was completed within 8 minutes, followed by about 20 minutes of compression. Agitation had a much greater effect on the degree of enhancement in 75 minutes of electrocoagulation than in 30 minutes. Initial settling ended within 4 minutes and was followed by about 10 minutes of compression. Hence, the silica electrocoagulated for 75 minutes under continuous agitation had finished settling within 15 minutes. The significance of

the relative displacement of the curves in Figure 2-7 can be assessed by inspection of the initial settling rates recorded in Table 2-1.

Table 2-1. Effect of agitation on electrocoagulation of silica.

Electrocoagulation Time, min	Agitation	Initial Settling Rate, cm/min
30	No	4.3
30	Yes	4.8
75	No	4.6
75	Yes	8.0

The table shows that the initial settling rates ranged from 4.3 to 8.0 cm/min, representing over 3 orders of magnitude enhancement relative to the natural settling rate (1.6×10^{-3} cm/min). The benefit of agitation is apparent, especially for the longer electrocoagulation time: agitation enhanced the initial settling rate further by 11.6% (30 minutes) and 73.9% (75 minutes). It is concluded, therefore, that agitation is desirable, but not essential, for AC/EC to be effective in enhancing the settling behaviour of silica. It is interesting to note that electrocoagulation for 30 minutes under continuous agitation and for 75 minutes without agitation produced the same degree of enhancement of the initial settling rate. Hence, agitation can shorten the electrocoagulation time required to achieve a given initial settling rate. Alternatively, it can be deduced that the initial settling rate of silica is enhanced more rapidly with increasing electrocoagulation time when agitation is applied than when it is not.

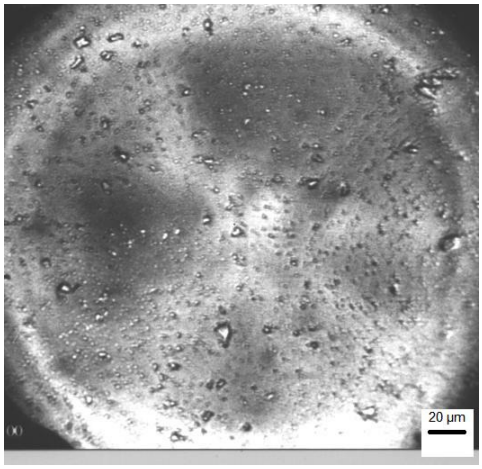

(a) As received.

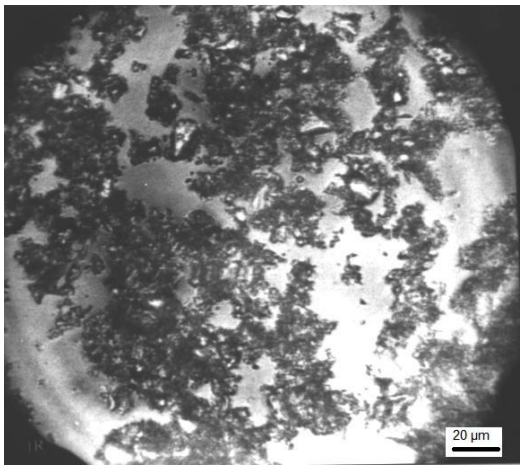

(b) AC/EC: 30 min, no agitation.

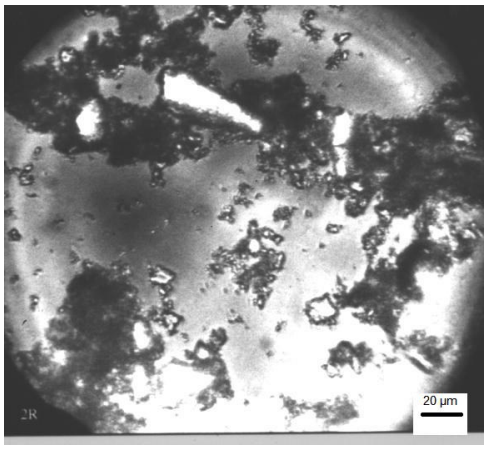

(c) AC/EC: 30 min, agitation.

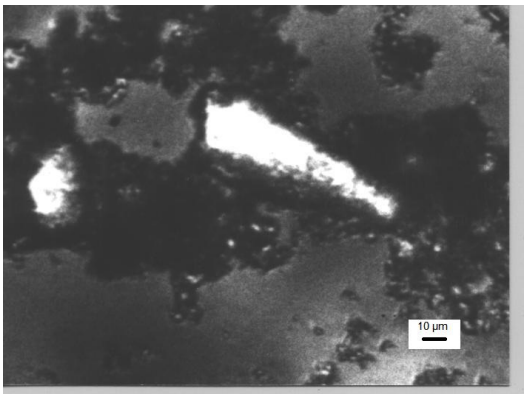

(d) Enlargement of (c).

Plate 2-1. Textures of as-received and electrocoagulated silica.

Plate 2-1 shows photomicrographs of: (a) discrete particles of as-received silica; (b) silica flocs formed in 30 minutes under quiescent conditions; and (c) silica flocs formed in 30 minutes under continuous agitation. The silica particles were angular, and the absence of any aggregation in the as-received silica is apparent in Plate 2-1a. Plates 2-1b and 2-1c illustrate the difference in character or texture of the flocs formed under different agitation conditions. In the absence of agitation (Plate 2-1b), the flocs adopted a fibrous, loose texture while, with agitation (Plate 2-1c), the flocs appear more compact. In addition to floc size, texture and morphology are expected to influence the settling behaviour of electrocoagulated silica. Bouyer *et al*. (2005) observed that the manner of floc development depended, in part, on the hydrodynamics (*e.g*., agitation rate). Further, Coufort *et al*. (2005) reported that shear stress caused the floc size to decrease, making the floc structure more compact. Plates 2-1b and 2-1c also show that the flocs were comprised of particles in a wide size range. The 55-µm particle in Plate 2-1c, enlarged in Plate 2-1d, shows small particles adsorbed onto its surfaces, even at the corners. Hence, the hydroxoaluminum complexes, which were formed during electrocoagulation, adsorbed onto the entire surface of the silica particles.

The quiescent conditions prevailing in two of the tests enabled observation of the onset of enhanced settling behaviour, which commenced after about 8 minutes of electrocoagulation. As the AC/EC treatment progressed, the

mud line (*i.e.*, the interface between the supernatant water and the electrocoagulated silica) became sharper.

Hydrogen was evolved (Jenke and Diebold, 1984; Pretorius *et al.*, 1991; Vik *et al.*, 1984) as tiny bubbles (≤ 0.5 mm in diameter) at the facing surfaces as the electrodes alternated duty as the cathode. These surfaces became pitted as the electrodes alternated duty as the anode. The pits, which were arrayed in the flow pattern of the suspension, developed as Al was oxidized to Al^{3+}, precursory to the formation of complex hydroxo species. Such species are capable of neutralizing the negative surface charge on the silica particles and of bridging the destabilized (*i.e.*, electrocoagulated) silica particles to form flocs (Black, 1967; Hahn and Stumm, 1968; Stumm and Morgan, 1970; Duan and Gregory, 2003; Trompette and Vergnes, 2009).

With increasing electrocoagulation time, the temperature of the suspension rose as a result of Joule heating. The water conductivity also increased, necessitating continual reduction of the applied voltage. Operating data are reported in Table 2-2.

Table 2-2. Operating data.

AC/EC Time, min	Agitation	Average Voltage Gradient, V/m	ΔT, ℃
30	No	1567	10.2
30	Yes	1542	8.9
75	No	1420	18.3
75	Yes	1432	17.1

For easy comparison, the electrocoagulated slurry and supernatant water samples were cooled to the initial temperature of the feed suspension before pH measurements were made. The pH of the electrocoagulated slurry tended to be slightly lower than that of the feed suspension, as Table 2-3 illustrates.

Table 2-3. Feed suspension and electrocoagulated slurry pH.

AC/EC Time (min)	Agitation	Temperature (°C)	pH	
			Feed Suspension	Electrocoagulated Slurry
30	No	21.2	8.63	8.57
30	Yes	21.4	8.79	8.57
75	No	21.4	8.70	8.70
75	Yes	21.5	8.62	8.54

In the 75-minute test (no agitation), the feed suspension and electrocoagulated slurry had the same pH of 8.70. Later in this thesis, data from other tests will illustrate how, during electrocoagulation, the pH first falls and then rises. Hence, the value of the terminal pH depends on the AC/EC retention time and on the reactions that occur.

Water pH data are reported in Table 2-4.

Table 2-4. Water pH data.

AC/EC Time (min)	Agitation	Temperature (°C)	pH	
			Feed Water	Supernatant
30	No	21.2	7.44	8.52
30	Yes	21.4	7.28	8.68
75	No	21.4	6.51	8.41
75	Yes	21.5	7.43	8.39

The dispersion of silica in the feed water resulted in a suspension whose pH was higher than that of the feed water (*cf.* Tables 2-4 and 2-3). Reactions occurring during electrocoagulation caused the pH of the supernatant to be higher than that of the feed water. This suggests net H^+ adsorption at the silica surface or net OH^- release from the silica surface, as the following reactions suggest.

$$\equiv SiO^- + H^+ \leftrightarrow \equiv SiOH$$

$$\equiv SiO^- + H_2O \leftrightarrow \equiv SiOH + OH^-$$

An important point arises from the enhancement of the initial settling rate achieved by direct electrocoagulation in the absence of agitation. Normally, colloidal particles are considered to be the size fraction that is amenable to

perikinetic coagulation (Masliyah, 1994; Montgomery, 1985; Tambo, 1991). In the as-received silica, colloidal particles constituted only a minor fraction (~6% ≤1 μm or ~32% <10 μm). Hence, in quiescent electrocoagulation, gas evolution from the electrodes, thermal convection currents, and sedimentation of silica flocs and coarse particles created hydrodynamic disturbances from which interparticle collision resulted. Yet, the entire mass of silica was electrocoagulated, as was evident from the sedimentation occurring in the cell, but the manner of electrocoagulation could be described neither as purely perikinetic nor as purely orthokinetic. Diffusion of the coagulative aluminum species is considered to have facilitated their specific adsorption onto the silica surface. Interparticle bridging is automatically implied. This leads to the postulation that, in the absence of applied agitation, the proximity of particles to one another facilitated collision for the achievement of electrocoagulation of silica dispersed at high concentration (51.56 g/L in this case). The average interparticle separation between as-received silica particles was estimated to be 54 μm (see Appendix B). Relative to its diameter, therefore, a particle would not have far to travel to become bridged to its nearest neighbour. The implication of this is that no externally applied shear is necessary, and incidental hydrodynamic disturbances (gas bubble movement, *etc*.) listed above would adequately facilitate floc formation. Test results in Table 2-1 show that interparticle collision induced by shear improved the effectiveness of electrocoagulation, particularly at extended retention times (*i.e.*, higher aluminum dosages). More importantly, however, the results demonstrate that, for the 2.1 A current flow in 30 minutes of electrocoagulation, externally applied agitation did not promote substantially superior electrocoagulation, as indicated by the initial settling rates.

Estimates of the collision rates, under quiescent and shear conditions, between aluminum ions and silica particles, and of interparticle collision rates under shear are presented in Appendix B. It will be shown later in this chapter that not all of the dissolved aluminum was adsorbed by silica. Hence, n_{Al} increased with electrocoagulation time, promoting higher frequency of complex aluminum ion collision with silica particles and flocs. Of course, n_s decreased as new flocs were formed and as existing flocs grew. The rate of floc growth by ion-particle and interparticle collisions is anticipated to be faster than the rate of formation of new flocs. The justification for this expectation is that the growing

flocs present a larger surface which, statistically, would experience a higher collision frequency. Hence, the effect of agitation in doubling the ion-particle collision rate became more productive with longer electrocoagulation time, as corroborated by the initial settling rates for 75 minutes' electrocoagulation (Table 2-1).

Since transport of the bulk of the silica particles was not caused by Brownian motion or by the AC electric field under quiescent conditions, electrostatic attraction between aluminum complexes and silica particles is expected to have played an important role in floc formation and growth. Such attraction would also facilitate collision between a particle bearing aluminum adsorbate and one without.

2.4.3 Agitation Rate

2.4.3.1 Agitation Rate Test Procedure

The influence of agitation on the efficacy of AC/EC was investigated further over a range of continuous agitation rates, which were defined by the impeller tip speed. Six tests were performed over the full range of agitator motor speed which gave a maximum impeller tip speed of 4.97 m/s. In these direct electrocoagulation tests, a current of 2.1 A (*i.e.*, density of 70.2 A/m^2) was passed for 30 minutes between two electrodes positioned 3.0 cm apart.

2.4.3.2 Agitation Rate Test Results and Discussion

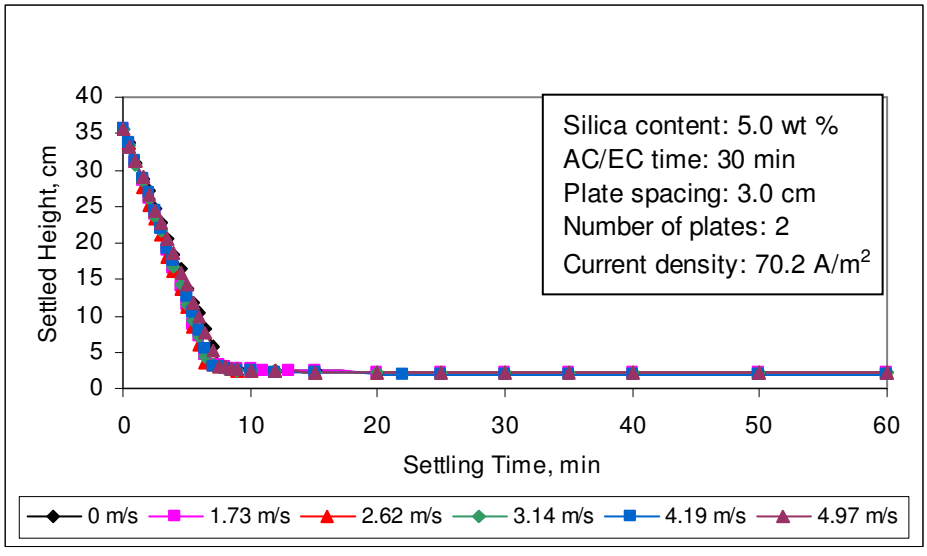

Figure 2-8. Effect of agitation rate during AC/EC on settling behaviour.

The settling curves for electrocoagulated silica are plotted in Figure 2-8 for impeller tip speeds of 0 to 4.97 m/s. The curves indicate that the settling behaviour of electrocoagulated silica did not change significantly over the full range of impeller tip speeds. In other words, the effectiveness of AC/EC in enhancing the settling behaviour of silica was not greatly sensitive to agitation rate. This modest sensitivity is quantified in Figure 2-9.

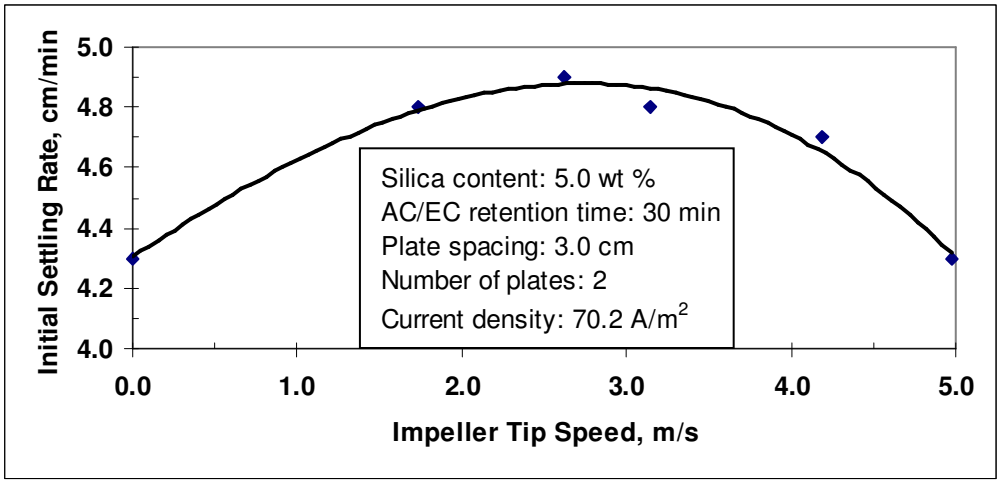

Figure 2-9. Effect of agitation rate during AC/EC on initial settling rate.

The maximum initial settling rate of about 4.9 cm/min occurred in the tip speed range of 2.0 to 3.0 m/s. Hence, at higher impeller tip speeds, agitation became counterproductive. It is inferred that such agitation rates limited floc size. The impeller tip speed of 1.73 m/s was selected for subsequent direct AC/EC tests because there was no risk of splattering and the effectiveness of electrocoagulation was virtually at its maximum. These results again indicate that agitation is desirable for, but not essential to, the effectiveness of AC/EC as a technique for enhancing the settling behaviour of silica. Consequently, in the practical application of the technique, the continuous flow of suspension through the cell would be expected to provide adequate agitation. The redundancy of an agitator, therefore, represents a capital cost saving, as well as operating cost savings arising from energy not used to drive the agitator and from maintenance that is not required.

2.4.4 AC/EC Retention Time

2.4.4.1 AC/EC Retention Time Test Procedure

Data generated in the agitation study (Section 2.4.2) alluded to the influence of AC/EC retention time (*i.e.*, electrocoagulation time) on the degree of enhancement of the settling behaviour of silica. Hence, a detailed study was conducted over the retention time range of 15 to 120 minutes in both the direct and indirect modes of electrocoagulation. This suite of tests also enabled study of the effect of the electrocoagulation mode on the degree of settling behaviour enhancement. The conditions, under which the electrocoagulation tests were performed, are as follows:

feed water temperature, 21.1 ° to 21.4 °C;
feed water pH, 8.45 to 8.50;
current density, 70.2 A/m^2;
number of electrodes, 2;
electrode separation, 3.0 cm; and
impeller tip speed, 1.75 m/s (indirect AC/EC) or 1.73 m/s (direct AC/EC).

Aluminum concentration in AC/EC-treated water samples and supernatant water samples was measured. When precipitation of aluminum hydroxide occurred in the treated water, the sample for analysis was taken while the water was agitated in the cell. The precipitate in the sample dissolved upon acidification. Treated water, with which silica was subsequently slurried, was similarly withdrawn from the cell. A settling test was performed and the floc size distribution determined on the freshly electrocoagulated silica. The settling test and floc size measurements were repeated a day (*i.e.*, 20 to 30 hours) later to evaluate the effect of ageing.

2.4.4.2 Indirect Electrocoagulation Test Results and Discussion

The response of the initial settling rate of silica, which was freshly electrocoagulated in the indirect mode, is depicted in Figure 2-10 for AC/EC retention times of 15 to 120 minutes. The maximum initial settling rate of 6.4 cm/min was attained after 45 minutes of electrocoagulation. Otherwise, the initial settling rate varied narrowly from 3.4 to 3.8 cm/min for the other retention times, trending towards a plateau for times exceeding 75 minutes.

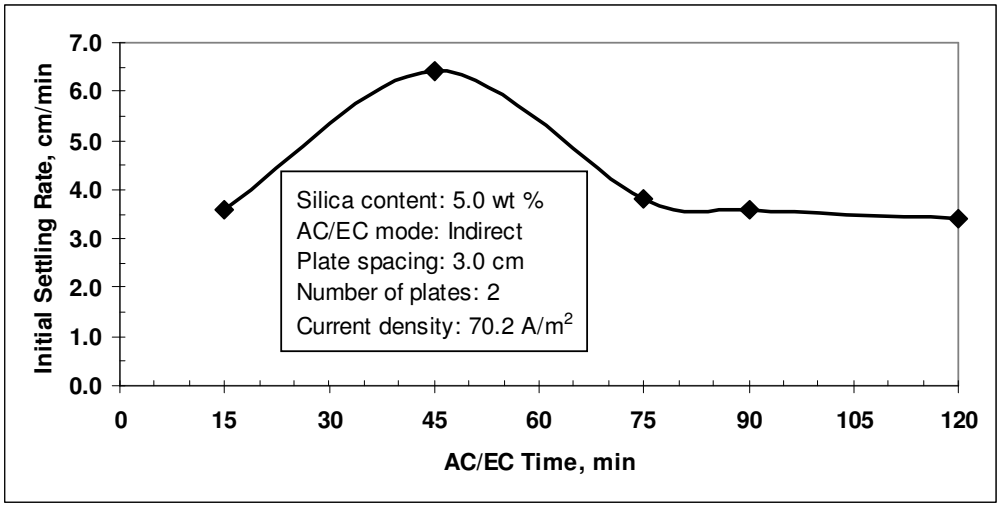

Figure 2-10. Variation of initial settling rate of freshly electrocoagulated silica with AC/EC time (indirect mode).

The variation of the initial settling rate with electrocoagulation time is reflected by the floc size distributions of the electrocoagulated silica in Figure 2-11, where the floc size distributions are compared with the particle size distribution of as-received silica.

The displacements of the “electrocoagulation” curves relative to the “as-received” curve attest to the size increases due to floc formation. As expected from Figure 2-10, 45 minutes of AC/EC engendered the coarsest flocs, the top size of which exceeded an equivalent diameter of 100 µm, in contrast to ~65 µm in the as-received material. More dramatic was the 80-fold growth in the bottom size, from approximately 0.5 µm in the as-received state to approximately 40 µm in the electrocoagulated condition. Figure 2-11 also shows the distributions for the 90- and 120-minute AC/EC treatments to be coincident. This is consistent with the measured respective initial settling rates of 3.6 and 3.4 cm/min which, within the limits of experimental error, are not substantially different. The distributions for 15 and 75 minutes of AC/EC, however, are more widely displaced along the size axis than would be anticipated from the respective initial settling rates of 3.6 and 3.8 cm/min. The 75-minute curve is just slightly offset to coarser sizes from the 90- and 120-minute curves.

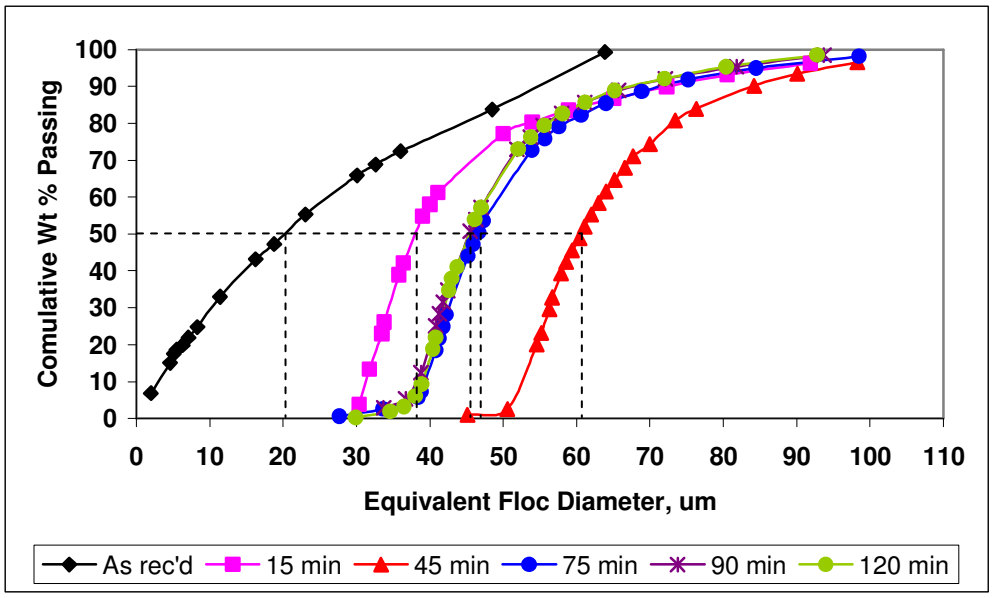

Figure 2-11. Floc size distributions of freshly electrocoagulated silica (indirect mode).

Demarcated on Figure 2-11 are the d_{50} sizes for the as-received and electrocoagulated silica samples. The d_{50} is one of the commonly used criteria in mineral beneficiation for characterizing particle size distribution. Qualitatively, the d_{50} values confirm to the curve displacements discussed above. As-received silica had a d_{50} of 20 µm which increased to 60 µm after 45 minutes of AC/EC. The d_{50} sizes for the electrocoagulated silica samples are plotted as a function of AC/EC time in Figure 2-12. The plot mirrors the shape of the initial settling rate curve in Figure 2-10, showing that the initial settling rate was controlled solely by floc size.

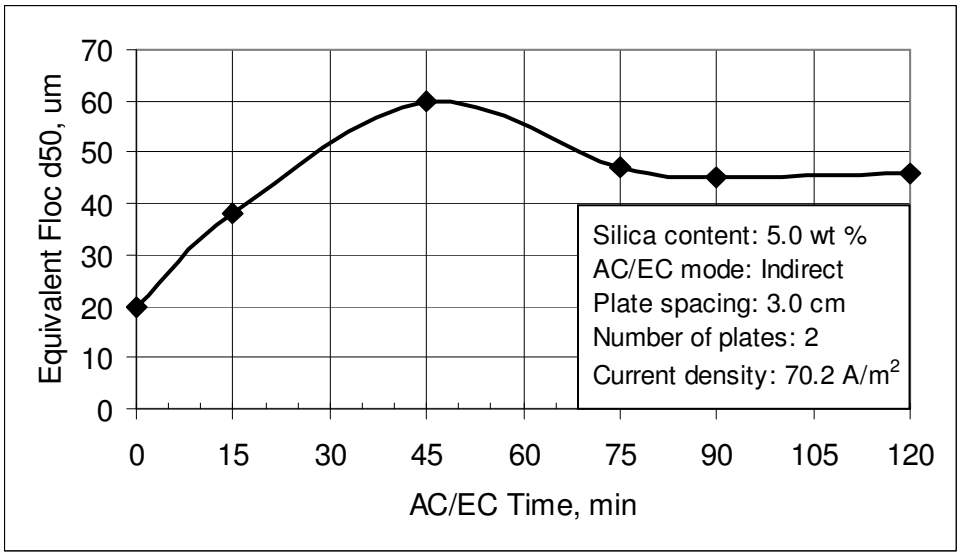

Figure 2-12. d_{50} sizes of freshly electrocoagulated silica (indirect mode).

The pH and temperature of the feed water, AC/EC-treated water, electrocoagulated slurry and supernatant water are reported in Appendix A for the AC/EC retention times studied. These pH values are plotted against AC/EC time in Figure 2-13.

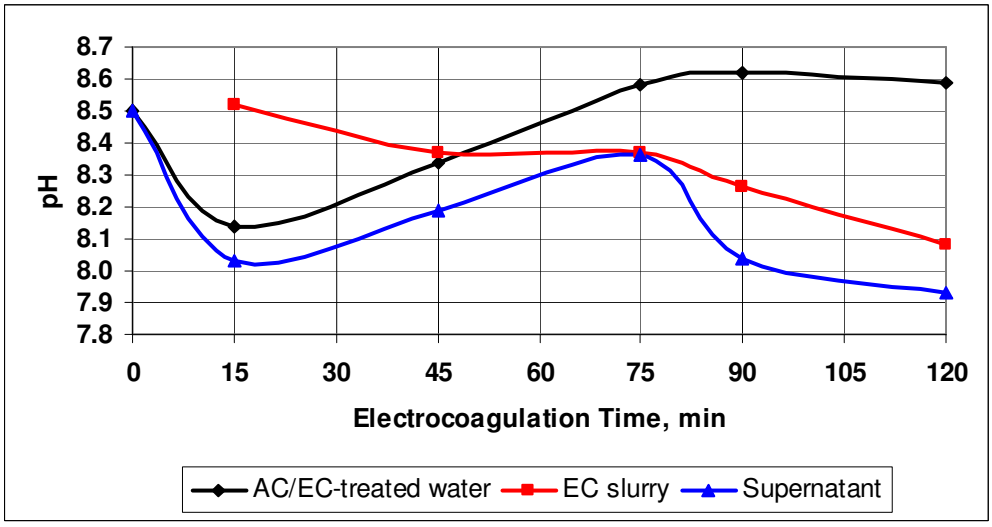

Figure 2-13. Variations of pH with time of indirect electrocoagulation.

From a value of 8.5 in the feed water, the pH decreased to 8.1 after 15 minutes' AC/EC treatment but rose to 8.6 after AC/EC times of 75 minutes and longer. As Figure 2-13 illustrates, negative net pH changes resulted for AC/EC retention times of up to approximately 60 minutes. The observed pH changes represent the net effects of aqueous reactions, examples of which are given

below: Equations 2-3a and 2-3b would contribute to pH increase, while Equation 2-3c would contribute to pH decrease.

$$2\ H_2O + 2e \rightarrow H_2(g) + 2\ OH^- \quad (2\text{-}3a)$$

$$2\ H_2O + O_2(g) + 4e \rightarrow 4\ OH^- \quad (2\text{-}3b)$$

$$Al(H_2O)_6^{3+} \rightarrow Al(H_2O)_5OH^{2+} + H^+ \quad (2\text{-}3c)$$

In indirect electrocoagulation, the effect was immediate upon contact between the silica and the AC/EC-treated water. To ensure homogeneous distribution of the hydroxoaluminum complexes, the slurry was agitated in a 1-L beaker for 2 to 3 minutes with an overhead stirrer. Two 13-mm wide polyethylene baffles were inserted to optimize the mixing. Figure 2-13 depicts the slurry pH decrease from 8.5 to 8.1 as AC/EC time was extended. AC/EC times of up to 45 minutes produced slurries with pH values higher than that of the treated water. This phenomenon is attributed to reactions between the hydroxoaluminum complexes and the silica surface, the net effect of which was elevation of the pH. After 45 minutes' AC/EC, however, the slurry pH was the same as the pH of the treated water and, at longer AC/EC times, the slurry pH became progressively lower than the pH of the treated water. This is attributed to surface reactions in which a net release of H^+ ions or a net adsorption of OH^- ions occurred. Examples of surface reactions, which would increase and decrease the slurry pH, are presented in Equations 2-4 to 2-6. The reactions involve silanol surface groups (Stumm, 1992).

$$\equiv Si–OH + Al(OH)_4^- \leftrightarrow \equiv Si–Al(OH)_4 + OH^- \quad \text{(pH increases)} \quad (2\text{-}4)$$

$$\equiv Si–OH + OH^- \leftrightarrow \equiv Si–O^- + H_2O \quad \text{(pH decreases)} \quad (2\text{-}5)$$

$$\equiv Si–OH + Al_2(OH)_2^{4+} \leftrightarrow \equiv Si–OAl_2(OH)_2^{3+} + H^+ \quad \text{(pH decreases)} \quad (2\text{-}6)$$

The zero net pH change in the slurry (observed alter 45 minutes of AC/EC) indicates that the OH^- ions released balanced the total of H^+ ions released and OH^- ions adsorbed. It is worth pointing out that different reactions occur at different electrocoagulation times because the combination of pH and total Al concentration (hence, speciation) changes with time (Xiao *et al.*, 2008; Harif and Adin, 2007).

As Figure 2-13 illustrates, the supernatant water pH was always lower than the pH of the AC/EC-treated water and electrocoagulated slurry. Under 75

minutes of AC/EC time, the supernatant pH increased with AC/EC time from 8.0 to 8.4, mimicking the trend of the treated water pH. Over 75 minutes of AC/EC time, the supernatant pH decreased to 7.9, following the slurry pH.

Concentrations of total aluminum in AC/EC-treated and supernatant water samples are plotted against AC/EC time in Figure 2-14 ("Poly.": polynomial curve fitting by Microsoft Excel™). Water treated for 90 minutes analyzed the highest at 28.5 mg/L Al, while the 120-minute sample analyzed at only 21.4 mg/L Al. The reason for the lower concentration occurring at 120 minutes is not clear, despite analytical checks.

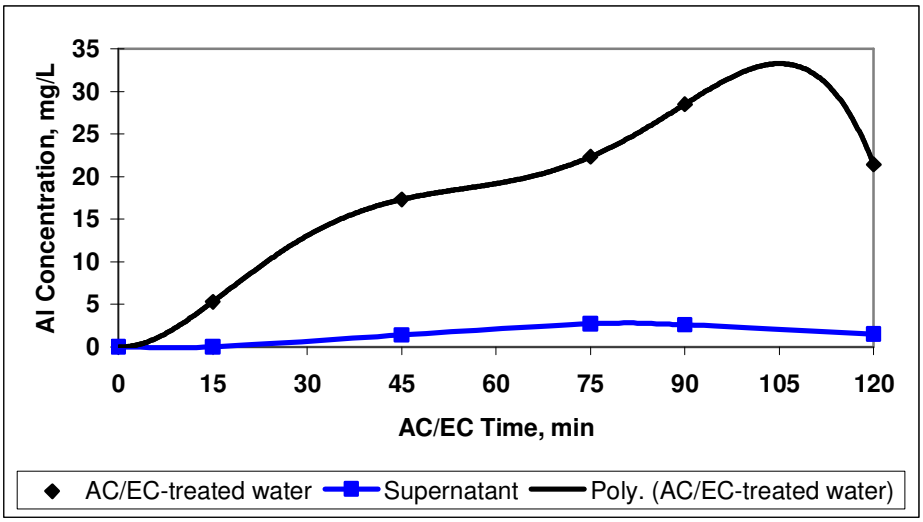

Figure 2-14. Variation of total aluminum concentration with AC/EC time (indirect mode).

Indirect electrocoagulation was accomplished by the adsorption of aluminum species from the treated water onto the silica surface. Adsorbed aluminum fractions (*i.e.*, ratios of adsorbed aluminum to aluminum in the treated water) are listed in Table 2-5 as a function of electrocoagulation time. The data suggest a relationship for electrocoagulation times exceeding 15 minutes, such that approximately 90% of the Al in the AC/EC-treated water was adsorbed by the silica. Clearly, this adsorbed fraction was independent of the Al concentration in the treated water, provided a threshold concentration was exceeded. Indirect electrocoagulation of silica was achieved with water that was treated for 15 minutes, even though the Al concentration attained in the treated water was probably below the threshold, as suggested by Figure 2-10. Evidently, the quantity of Al adsorbed per unit mass of silica varied with AC/EC retention time,

suggesting that multilayer adsorption may have occurred in proportion to the concentration gradient between the bulk treated water and the silica surface. The nature of the complex aluminum species present is also expected to have influenced adsorption in a currently unknown stoichiometry.

Table 2-5. Adsorbed aluminum fractions (indirect electrocoagulation).

Electrocoagulation Time, min	Adsorbed Al Fraction
0	0
15	> 0.81
45	0.92
75	0.88
90	0.91
120	0.93

Adsorption mass ratios (mg Al/g silica) are recorded in Table 2-6. For the 45- to 120-minute tests, the ratio ranged from 0.3 to 0.5 mg Al/g silica. In other words, the quantity of Al adsorbed was equivalent to the range of 0.03% to 0.05% of the silica mass. Adsorption mass ratios exceeding 0.3 mg Al/g silica did not engender higher initial settling rates (see Figure 2-10) or coarser d_{50} sizes (Figure 2-12) than those attained with 0.3 mg Al/g silica. This relative ineffectiveness of the ratios is attributed to exaggeration by precipitation. In other words, it is probable that the actual adsorption of aluminum did not exceed 0.3 mg/g of silica, but precipitation made it appear otherwise. It is also possible that multilayer adsorption occurred.

Table 2-6. Aluminum adsorption mass ratios (indirect electrocoagulation).

AC/EC Time, min	Al Adsorption Mass Ratios	
	mg Al/g Silica	% of Silica Mass
15	> 0.08	> 0.008
45	0.30	0.030
75	0.37	0.037
90	0.49	0.049
120	0.38	0.038

Appendix B shows the calculation of the theoretical aluminum concentration in AC/EC-treated water as a function of time. The theoretical and

actual concentrations (which include re-dissolved precipitate) are compared in Table 2-7, where the actual concentrations ranged from 6.1% to 13.1% of theoretical.

Table 2-7. Theoretical and actual Al concentrations in AC/EC-treated water.

AC/EC Time, min	Total Al in AC/EC-treated Water		
	Theoretical, mg/L	Actual, mg/L	% of Theoretical
15	44.0	5.3	12.0
45	132.1	17.3	13.1
75	220.2	22.3	10.1
90	264.2	28.5	10.8
120	352.3	21.4	6.1

Precipitation was observed in the 45- and 120-minute treated water samples, but not in the 15-minute sample. It must be noted that the total Al concentrations plotted in Figure 2-14 included the precipitate which dissolved upon acidification of the samples in preparation for analysis. Aluminum precipitation from treated water tended to increase with AC/EC time, (*i.e.*, with increasing dosage) as Table 2-8 demonstrates. As mentioned earlier, the reason for the inconsistent 120-minute results is not clear.

Table 2-8. Extents of aluminum precipitation from AC/EC-treated water.

AC/EC Time, min	Al Concentration, mg/L		Al Precipitation	
	Initial	Final	mg/L	%
15	5.3	5.3	0	0
45	17.3	7.3	10.0	57.8
75	22.3	9.1	13.2	59.2
90	28.5	8.5	20.0	70.2
120	21.4	9.2	12.2	57.0

When precipitation occurred, its extent was considerable, ranging from 57% to 70%. The extent of precipitation was minimal during the 45-minute retention time, most of the precipitation occurring after AC/EC treatment, as the water cooled. With longer retention times, however, much of the precipitation occurred during AC/EC treatment as a result of the delivery of larger quantities of Al into the water. Moreover, precipitation continued after AC/EC treatment. The

"final" analyses reported in Table 2-8 were derived from samples which were collected within 1 to 2 hours of treatment of the water. The precipitate was amorphous (detailed discussion in Chapter 3).

The pH and total aluminum concentration data recorded in Table 2-9 facilitated estimation of $[Al^{3+}][OH^-]^3$ product, Q. This is not to say that the dissolved aluminum existed only as Al^{3+} but, in the absence of speciation data, this was the approach used.

Table 2-9. Measured $[Al^{3+}][OH^-]^3$ products for AC/EC-treated water.

AC/EC Time, min	Before Precipitation			After Precipitation		
	pH	$[Al_T]$, M	Q	pH	$[Al_T]$, M	Q
15	8.1	$2.0x10^{-4}$	$4.0x10^{-22}$	8.1	$2.0x10^{-4}$	$4.0x10^{-22}$
45	8.3	$6.4x10^{-4}$	$5.1x10^{-21}$	8.6	$2.7x10^{-4}$	$1.7x10^{-20}$
75	8.6	$8.3x10^{-4}$	$5.2x10^{-20}$	8.6	$3.4x10^{-4}$	$2.1x10^{-20}$
90	8.6	$1.1x10^{-3}$	$6.9x10^{-20}$	8.6	$3.2x10^{-4}$	$2.0x10^{-20}$
120	8.6	$7.9x10^{-4}$	$5.0x10^{-20}$	8.5	$3.4x10^{-4}$	$1.1x10^{-20}$

Al_T: total aluminum

Precipitation was accompanied by appreciable pH change in only two samples. In the 45-minute sample, the pH increased from 8.3 to 8.6, while it decreased from 8.6 to 8.5 in the 120-minute sample. The observed pH changes are the net result of the precipitation and other reactions (*e.g.*, ageing) occurring. The pH changes were, therefore, characteristic of the hydroxoaluminum species existing in the AC/EC-treated water, and the speciation varied with pH and temperature. For example, hydrolytic precipitation of cationic metal species causes the pH to drop (Equation 2-7), while precipitation of anionic metal species by protonation causes the pH to rise (Equation 2-8).

$$Al(OH)_2^+ + H_2O \rightarrow Al(OH)_3(am) + H^+ \quad (2\text{-}7)$$

$$Al(OH)_4^- + H^+ \rightarrow Al(OH)_3(am) + H_2O \quad (2\text{-}8)$$

The ion products before precipitation (Table 2-9) exceeded the K_{SP} (or K_{S0}) of $Al(OH)_3(am)$, $6.3x10^{-32}$ (Stumm and Morgan, 1981), justifying precipitation. However, the ion products after precipitation still exceeded the K_{SP}, although they were lowered by precipitation. The 45-minute sample showed a higher ion product which tripled after precipitation because of the increase in pH.

Precipitation was kinetically controlled (Hayden and Rubin, 1974), and continued while the unacidified samples stood overnight. In this extended reaction time, precipitation also occurred in the 15-minute sample. It is probable that the dissolved aluminum concentration would not decrease enough for Q to equal K_{SP} because of complex speciation and slow kinetics. O'Melia (1986) reported, for example, that the oxyhydroxoaluminum complex, $Al_{13}O_4(OH)_{24}^{7+}$, is kinetically stable for long periods of time in solutions which are supersaturated with respect to $Al(OH)_3$(am). Reference to Figure 1-7 reveals that, at 25°C, the data in Table 2-9 (pH, 8.1 to 8.6; $[Al_T]$, $2.0x10^{-4}$ to $1.1x10^{-3}$ M; *i.e.*, log $[Al_T]$, -3.7 to -3.0) correspond to a region where precipitation would not have occurred, even though the ion product, Q, exceeded K_{SP}. Therefore, consider two cases, the first being hypothetical, while the other concerns the actual testwork. In the hypothetical case, consider electrocoagulation having been performed isothermally at 25°C, such that Figure 1-7 is an accurate representation of the aluminum speciation, including the absence of precipitation. If the "before precipitation" data for 90 minutes (Table 2-9) are used as the example, Figure 1-7 would indicate that the relevant aluminum species would be those represented by Lines 6, 7, 8 and 12; *i.e.*, $Al_{13}(OH)_{34}^{5+}$, $Al(OH)_4^-$, $Al(OH)_3^o$ and $Al_7(OH)_{17}^{4+}$. The mass balance for the total dissolved aluminum concentration is given by Equation 2-9.

$$[Al_T] = 1.1x10^{-3}\ M = 13\,[Al_{13}(OH)_{34}^{5+}] + [Al(OH)_4^-] + [Al(OH)_3^o] + 7\,[Al_7(OH)_{17}^{4+}] \quad (2\text{-}9)$$

From Figure 1-7, the maximum concentrations of the species attainable at pH 8.6 are: $Al_{13}(OH)_{34}^{5+}$, 1.02 M (calculated from the plotting equation given in Appendix A); $Al(OH)_4^-$, $7.9x10^{-5}$ M; $Al(OH)_3^o$, $6.3x10^{-5}$ M; $Al_7(OH)_{17}^{4+}$, $2.5x10^{-8}$ M. Evidently, $[Al_{13}(OH)_{34}^{5+}]$ is not known since, unlike the other three species, it is present in a concentration which is lower than the maximum. From Equation 2-9, $[Al_{13}(OH)_{34}^{5+}]$ was calculated to be $7.4x10^{-5}$ M. The aluminum distribution, α_i (where *i* represents the Line number), among the species is as follows: $\alpha_6 = 0.87$, $\alpha_7 = 0.07$, $\alpha_8 = 0.06$ and $\alpha_{12} \approx 0$. Hence, 87% of the aluminum would exist as $Al_{13}(OH)_{34}^{5+}$, 7% as $Al(OH)_4^-$ and 6% as $Al(OH)_3^o$. The fraction of $Al_7(OH)_{17}^{4+}$ is

negligible, its concentration being 3 orders of magnitude lower than those of the other species. Consequently, the predominant species would be $Al_{13}(OH)_{34}^{5+}$ which is one of the most efficient coagulative species.

In the actual test, the water temperature increased by 20°C as a result of Joule heating. Precipitation occurred, reducing $[Al_T]$ to $3.2x10^{-4}$ M (Table 2-9, 90 minutes "after precipitation"). These observations indicate that, during AC/EC treatment of the feed water, the pH increased, taking $[Al_T]$ into the $Al(OH)_3(am)$ stability field. The species forming the precipitate are expected to have been $Al_{13}(OH)_{34}^{5+}$ and $Al(OH)_4^-$ (Lines 6 and 7, Figure 1-7). At 25°C and pH 8.6, $[Al_{13}(OH)_{34}^{5+}]$ was estimated to be $1.4x10^{-5}$ M. This reduced concentration represents 81% precipitation of the species. The new aluminum distribution among the species is as follows: $\alpha_6 = 0.56$, $\alpha_7 = 0.24$, $\alpha_8 = 0.20$ and $\alpha_{12} \approx 0$.

Such loss of $Al_{13}(OH)_{34}^{5+}$ would represent significant diminution of coagulative capacity from the AC/EC-treated water, and would explain the decline in d_{50} size and initial settling rate shown in Figures 2-12 and 2-10, respectively. The pH increase was augmented by the large temperature rise, basic pH values being known to increase with temperature. It is expected that the ranges of pH and $[Al_T]$, over which the $Al(OH)_3(am)$ stability field extends, would be modified by temperature increases. Simultaneously, the pC-pH lines for individual species would shift to new pH values. For example, Duan and Gregory (2003) reported that the effect of temperature on coagulation performance derived from its effect on hydrolysis reactions and on the solubility of $Al(OH)_3$. It was calculated that a temperature change from 25°C to 1°C would cause:

- the pH of minimum $Al(OH)_3$ solubility to increase by 0.6 to 0.8 unit; and
- the minimum $Al(OH)_3$ solubility to decrease by 0.7 log unit.

In summary, therefore, while the actual aluminum speciation is not known, the foregoing discussion illustrates how $Al(OH)_3(am)$ precipitation can alter the speciation. The discussion also sheds some light on the effect of temperature on speciation.

In the supernatant samples, also, the ion product exceeded the K_{SP} (or K_{S0}) ($6.3x10^{-32}$) and precipitation was observed to have occurred overnight in the unacidified samples. The ion products are recorded in Table 2-10.

Table 2-10. Measured $[Al^{3+}][OH^-]^3$ products for supernatants (indirect AC/EC).

AC/EC Time (min)	pH	mg/L Al	$[Al_T]$, M	Q
15	8.0	< 1	$< 3.7x10^{-5}$	$< 3.7x10^{-23}$
45	8.2	1.4	$5.2x10^{-5}$	$2.1x10^{-22}$
75	8.4	2.7	$1.0x10^{-4}$	$1.6x10^{-21}$
90	8.0	2.6	$9.6x10^{-5}$	$9.6x10^{-23}$
120	7.9	1.5	$5.6x10^{-5}$	$2.8x10^{-23}$

Al_T: total aluminum

2.4.4.3 Direct Electrocoagulation Test Results and Discussion

The settling behaviour of silica, which had been freshly electrocoagulated in the direct mode, was enhanced progressively with electrocoagulation time, as illustrated by Figure 2-15. The initial settling rate improved linearly between 15 and 120 minutes of electrocoagulation time.

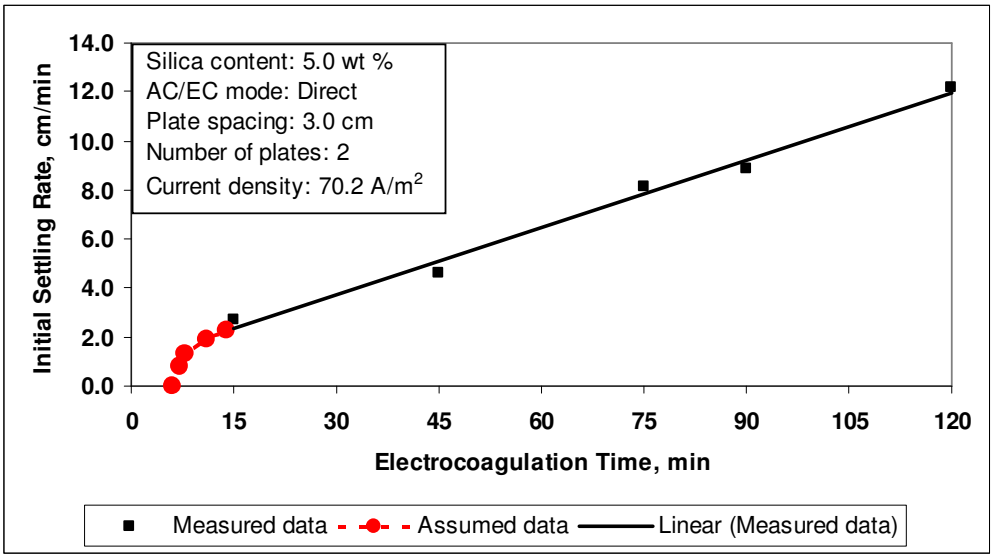

Figure 2-15. Variation of settling behaviour of freshly electrocoagulated silica with AC/EC time (direct mode).

The measured values of the initial settling rate increased from 2.7 cm/min after 15 minutes to 12.2 cm/min after 120 minutes. Hence, the maximum initial settling rate will occur at an electrocoagulation time that is greater than 120 minutes. The assumed data describe, in a general sense, how the settling

behaviour of the electrocoagulated silica is expected to change from 0 to 15 minutes of retention time.

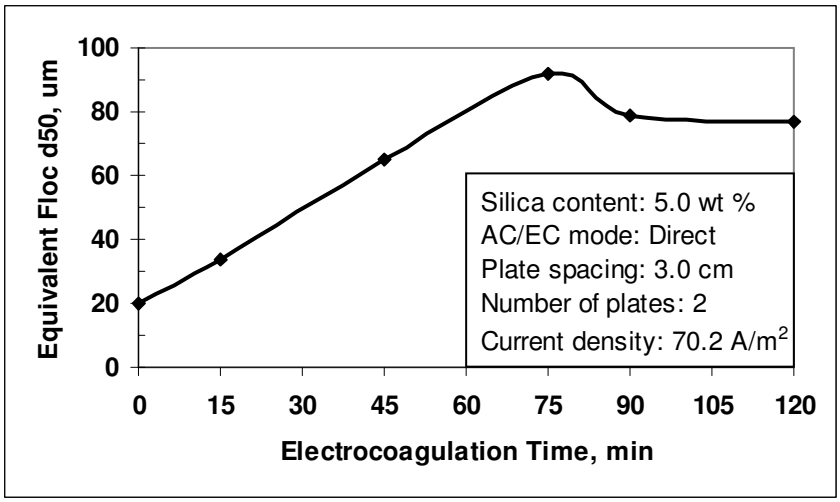

Figure 2-16. d_{50} sizes of freshly electrocoagulated silica (direct mode).

The mass median floc sizes (*i.e.*, d_{50}) of electrocoagulated silica samples are compared with that of as-received silica in Figure 2-16. From 15 to 75 minutes of electrocoagulation time, the d_{50} increased linearly from 34 to 92 µm. Longer electrocoagulation times resulted in decreased d_{50} sizes: 90 minutes, 79 µm; 120 minutes, 77 µm. Despite the decreased d_{50}, however, the initial settling rate increased (see Figure 2-15). This apparent contradiction will be resolved by examination of the bulk density and porosity (calculated in Appendix B) of the electrocoagulated sediments (Table 2-11). The sediment porosity is considered to provide a measure of floc porosity.

Table 2-11. Bulk density and porosity of electrocoagulated sediments.

Electrocoagulation Time, min	Bulk Density, kg/m^3	Porosity, vol %
15	1527 ± 1.2%	65.5 ± 1.8%
45	1526 ± 1.2%	65.6 ± 1.8%
75	1462 ± 1.0%	69.7 ± 1.3%
90	1461 ± 1.0%	69.8 ± 1.3%
120	1451 ± 1.0%	70.5 ± 1.3%

From 15 to 45 minutes of electrocoagulation, the porosity of the sediment (and, hence, of the flocs) was unchanged with floc growth (d_{50} increased from 34 to 65 µm). The porosities, which were ~66%, were too high for microfloc

formation from primary silica particles to constitute the predominant growth mode (refer to Section 1.2.3.5). Rather, the predominant growth mode appears to be Region 2 growth between primary particles and microflocs. Electrocoagulation times of 75 and 90 minutes engendered somewhat higher respective porosities of 69.7% and 69.8%. In this time domain, therefore, it is inferred that Region 2 growth proceeded predominantly by multiple level aggregation. It is evident from Figure 2-16 that floc fragmentation occurred when the electrocoagulation time exceeded ~75 minutes. It is known that flocs become mechanically weak as they grow and, beyond some limiting size, fragmentation becomes prominent (Ayyala *et al.*, 1995; Gregory, 1988). The limiting equivalent diameter was approximately 125 µm for silica that was freshly electrocoagulated in the direct mode. It is concluded that, for electrocoagulation times of up to about 75 minutes, the initial settling rate was controlled by floc size.

As indicated by the sediment bulk density, the floc density decreased as the floc size and, hence, the porosity increased – a well known phenomenon (Ayyala *et al.*, 1995; Gregory, 1993; Tambo and Watanabe, 1979). Between 75 and 90 minutes of electrocoagulation, floc fragmentation occurred (Figure 2-16) without significant change in porosity or bulk density (Table 2-11). At the same time, however, the initial settling rate increased (Figure 2-15). This body of evidence suggests that there may have been re-aggregation and rearrangement of floc fragments (Zbik *et al.*, 2008), marking a transition in growth mode from Region 2 to Region 3 (see Section 1.2.3.5). Extension of the electrocoagulation time to 120 minutes caused the median pore size to increase and the bulk density to decrease. With continued re-aggregation and rearrangement of the floc fragments and microflocs, the rate of drainage of water from the flocs was enhanced so as to enable further increase of the initial settling rate.

Variations of pH with electrocoagulation time are presented in Figure 2-17 for the feed suspension, electrocoagulated slurry and supernatant. The data are recorded in Appendix A.

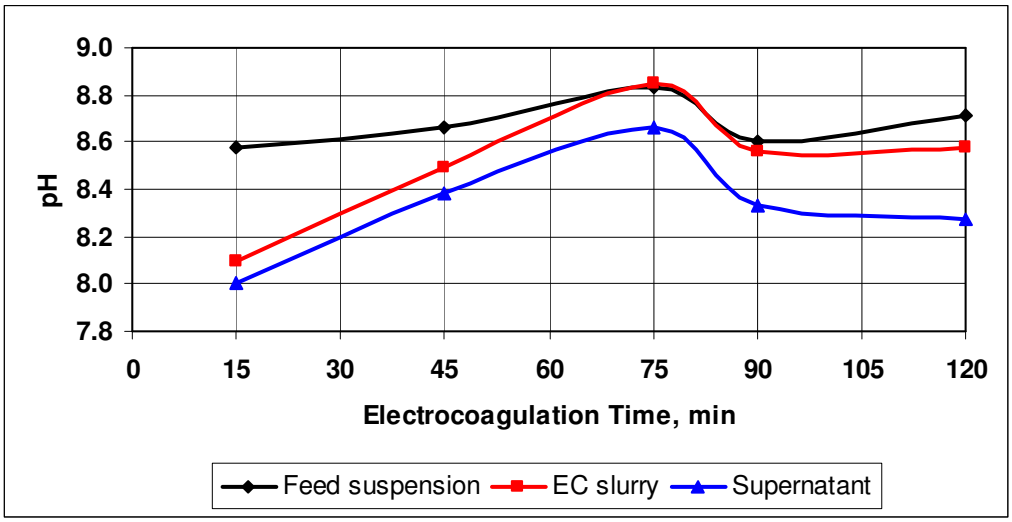

Figure 2-17. Variations of pH with direct electrocoagulation time.

Despite tight control of the feed water pH (8.47 to 8.50), the pH of the feed suspension varied unpredictably between 8.6 and 8.8. The pH always increased upon dispersion of the silica in the feed water. For electrocoagulation times ≤70 minutes and >85 minutes, the pH of the electrocoagulated slurry was below that of the feed suspension. Between 70 and 85 minutes of electrocoagulation, no net change in pH resulted. The pH trend exhibited by the electrocoagulated slurry was mimicked by the supernatant, the pH of which was always the lower.

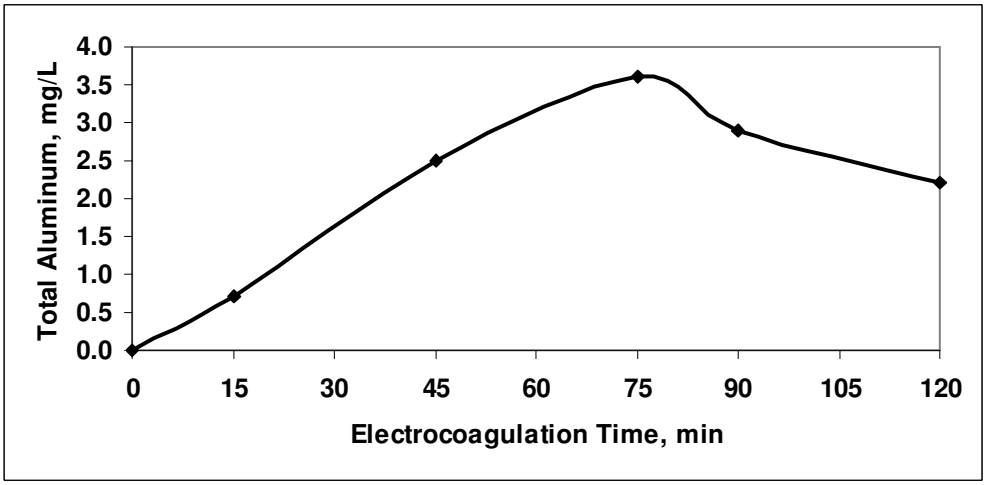

Figure 2-18. Total aluminum concentration in supernatants after direct electrocoagulation.

Figure 2-18 illustrates the variation of the concentration of total aluminum in the supernatants which resulted from direct electrocoagulation. The aluminum

concentration increased from 0.7 mg/L after 15 minutes' electrocoagulation to a maximum of 3.6 mg/L after 75 minutes' electrocoagulation, and declined to 2.2 mg/L after 120 minutes of electrocoagulation.

If it is assumed that the total aluminum released from the electrodes during direct electrocoagulation equals that released to the treated water in the indirect mode, Al adsorption mass ratios could be calculated. Such data are presented in Table 2-12.

Table 2-12. Aluminum adsorption mass ratios (direct electrocoagulation).

Electrocoagulation Time, min	Al Adsorption Mass Ratios	
	Fraction of Al Adsorbed, %	mg Al/g Silica
0	0	0
15	86.8	0.09
45	85.5	0.28
75	83.9	0.36
90	89.8	0.49
120	89.7	0.36

Between 80% and 90% of the total aluminum released from the electrodes was adsorbed by the silica. The adsorption mass ratio ranged from 0.09 to 0.49 mg Al/g silica (*i.e.*, 0.01% to 0.05% of the silica mass) during 15 to 90 minutes of electrocoagulation. Up to 75 minutes of electrocoagulation, the increase of the adsorption ratio with time corresponded to increasing floc size (Figure 2-16) and initial settling rate (Figure 2-15). Adsorption ratios are graphed in Figure 2-19.

It could be argued that the further increase of the adsorption ratio at 90 minutes was a consequence of the larger adsorption surface created by floc fragmentation. However, the ratio diminished from 0.50 mg Al/g silica at about 98 minutes to 0.36 mg Al/g silica at 120 minutes of electrocoagulation. Meanwhile, the initial settling rate was continually enhanced by electrocoagulation for 90 and 120 minutes. It is interesting to note that the curve in Figure 2-19 has the same shape as the curve for AC/EC-treated water in Figure 2-14. The implication is that the adsorption ratio is proportional to the total concentration of aluminum released from the electrodes. Hence, it may be inferred that multilayer adsorption

occurred in proportion to the aluminum concentration gradient established between the dispersion medium and the silica surface.

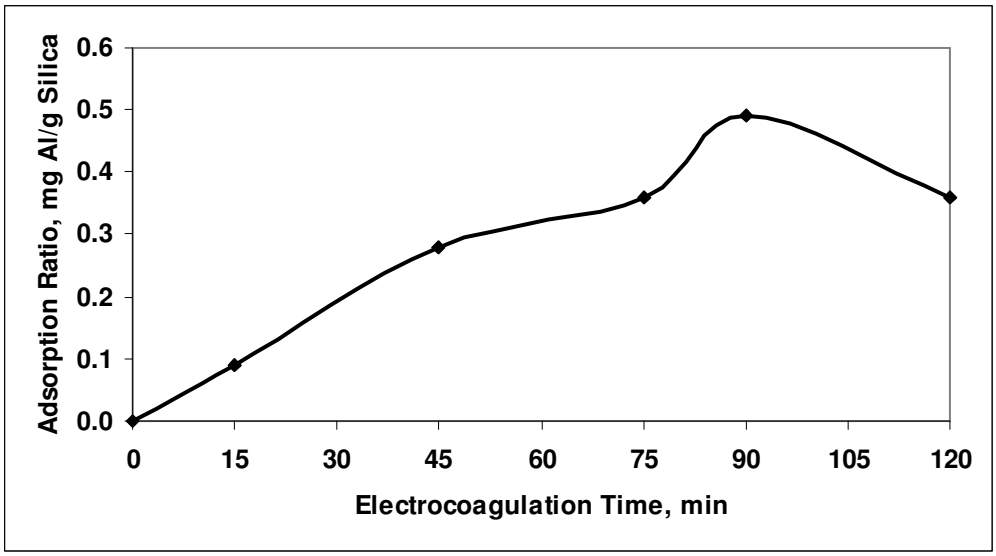

Figure 2-19. Variation of aluminum adsorption mass ratio with time of direct electrocoagulation.

The foregoing argument suggests the possibility that the decrease in aluminum concentration in the 90- and 120-minute supernatants resulted from precipitation. Such precipitation would not be indicated by Figure 1-7 which was constructed for 25°C, whereas temperatures exceeding 40°C were reached in the 90- and 120-minute tests. It has been reported (Ham and Christman, 1969; Tambo, 1991) that the aluminum hydroxide precipitate could effect floc growth by interparticle bridging. Ham and Christman arrived at this deduction from coagulation studies with silica suspensions, while Tambo was investigating clay suspensions. Interparticle bridging by the precipitate would promote a new growth mode of silica flocs, which could increase in density and, hence, in initial settling rate because of the adsorbing solid phase. Ion products have been calculated for the supernatants and are tabulated in Table 2-13. As before, the "Al^{3+}" is not intended as a comment on aluminum speciation in the supernatants.

Table 2-13. Measured $[Al^{3+}][OH^-]^3$ products for supernatants (direct AC/EC).

AC/EC Time (min)	pH	$[Al_T]$, M	log $[Al_T]$	Q
15	8.0	$2.6x10^{-5}$	-4.6	$2.6x10^{-23}$
45	8.4	$9.3x10^{-5}$	-4.0	$1.3x10^{-21}$
75	8.7	$1.3x10^{-4}$	-3.9	$1.3x10^{-20}$
90	8.3	$1.1x10^{-4}$	-4.0	$1.0x10^{-21}$
120	8.3	$8.2x10^{-5}$	-4.1	$5.6x10^{-22}$

Table 2-13 shows that the concentration of total aluminum increased with pH from 15 to 75 minutes of electrocoagulation. At 90 and 120 minutes, however, the pH dropped, as did $[Al_T]$. This behaviour is characteristic of metal precipitation reactions. In reaching the same final pH of 8.3, the supernatants appear to have attained an equilibrium, which is probably a reflection of equilibrium in the slurries after the long electrocoagulation times. However, precipitation was not observed in the supernatants after the electrocoagulated silica had settled. This, of course, does not preclude the formation and assimilation of precipitate among the silica particles. It is postulated, therefore, that aluminum precipitation occurred to a significant extent for electrocoagulation times exceeding 75 minutes. The decrease of pH and $[Al_T]$ constitutes corroborative evidence of precipitation.

Air-dried electrocoagulated silica was observed to settle quickly after it was re-slurried with water. This enhanced settling behaviour, engendered by electrocoagulation, was thus shown to remain intact in the dry solids. Hence, treated solids can be stored dry without loss of their ability to coagulate. The life of this retained ability was indicated by results from a similar test with silica that had been electrocoagulated for 90 minutes. The solids were air-dried and kept for over a year, yet settled quickly when re-slurried with water. Upon filtration, the cake was shown not to contain any lumps, indicating that the solids had been fully dispersed during the re-slurrying operation. Further, the cake successfully coagulated as-received silica. It is concluded, therefore, that not all of the silica particles subjected to AC/EC treatment have to be electrocoagulated for the bulk of the solids to acquire enhanced settling characteristics. However, the greater the fraction of the particles that is electrocoagulated, the greater is the enhancement of the settling behaviour of the bulk solids.

In another test, silica that had been electrocoagulated for 90 minutes and then air-dried two years previously, was used to successfully coagulate a mature fine tailings (MFT) sample obtained from Syncrude Ltd. It is noteworthy that the "sludge formers" (after MacKinnon, 1986), which are particles of equivalent diameter <22 µm, are predominantly silt and clay, with the clay particles being <2.8 µm in size (MacKinnon, 1986). A significant fraction of the clay particles would, therefore, be expected to be of colloidal size. This test result highlights the potential usefulness and flexibility of electrocoagulated silica as a coagulant for solids in various waste streams. Since silica is an inexpensive solid which does not introduce any toxic constituents, the electrocoagulated material would be convenient for use as an industrial coagulant. Inherent in the use of electrocoagulated silica is the flexibility it lends to an operation; that is, the option of either electrocoagulating a waste stream directly, or of adding electrocoagulated silica like a traditional coagulant.

2.4.4.4 Effects of Electrocoagulation Mode

The last two paragraphs of Section 2.4.4.3 described the long "shelf life" of directly electrocoagulated silica and the material's qualification as a coagulant. In contrast, a qualitative test demonstrated that the coagulating ability of AC/EC-treated water endured for only about 2 to 3 weeks. In this section, the results of the indirect and direct modes of electrocoagulation are compared, beginning with a review of the enhanced initial settling rates in Figure 2-20.

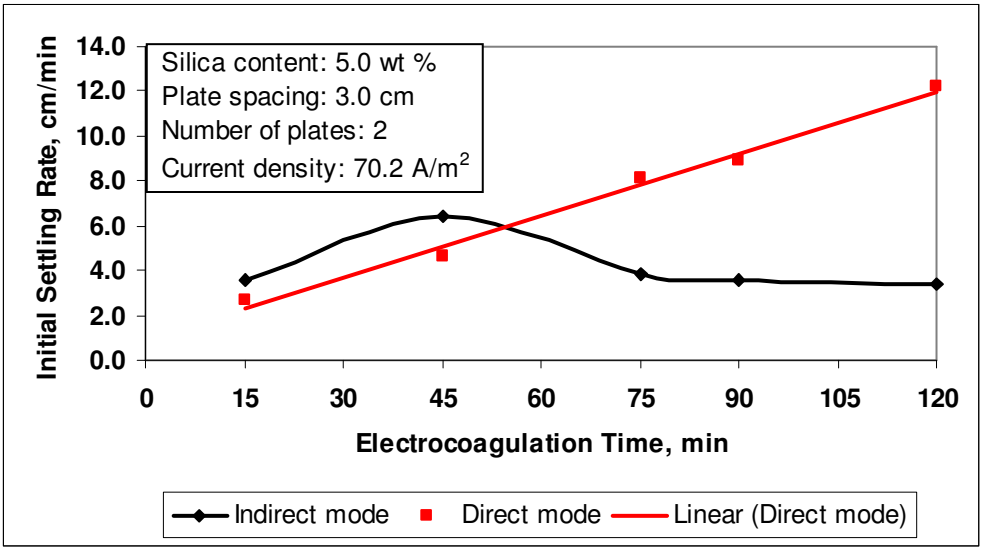

Figure 2-20. Initial settling rates of freshly electrocoagulated silica.

In the initial 55 minutes of AC/EC retention time, higher initial settling rates were achieved with indirect electrocoagulation because of the higher aluminum dosage in the AC/EC-treated water (hence, greater adsorption of aluminum species therefrom). With direct electrocoagulation, in contrast, the aluminum was not allowed to accumulate to high dosages because it was adsorbed as it was produced. At 55 minutes, the two modes of electrocoagulation are expected to engender the same initial settling rate of 6.0 cm/min. For retention times exceeding 55 minutes, the indirectly electrocoagulated silica attained a plateau of initial settling rates of 3.8 to 3.4 cm/min from 75 to 120 minutes. Meanwhile, the initial settling rate of directly electrocoagulated silica increased linearly to 12.2 cm/min at 120 minutes. Hence, indirect electrocoagulation yielded the greater enhancement of initial settling rate in the retention time range of 15 to 55 minutes. For extended retention times (>55 minutes), direct electrocoagulation was the superior treatment mode. It is inferred that the high concentrations of total aluminum, elevated temperatures (due to Joule heating) and increased pH in the AC/EC-treated water combined to promote aluminum precipitation, thus limiting the enhancement of the initial settling rate by indirect AC/EC at the longer retention times.

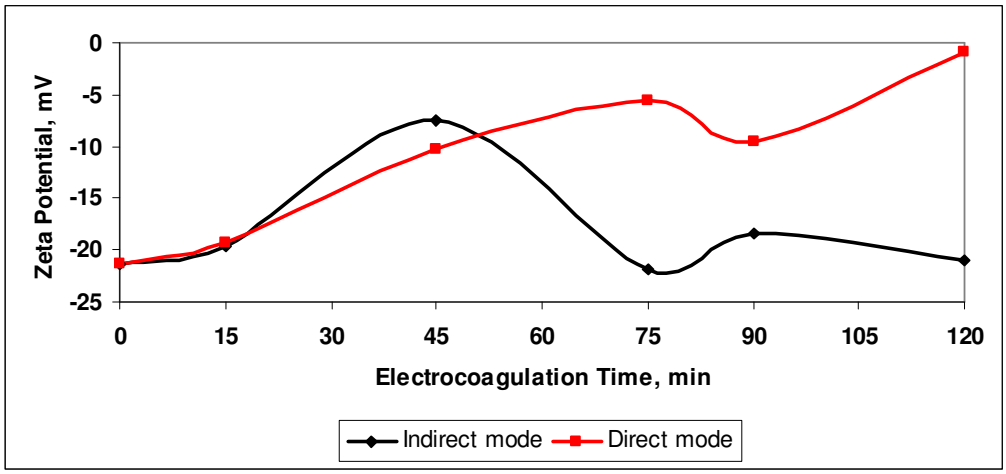

Figure 2-21. Zeta potentials of electrocoagulated silica.

The effect of electrocoagulation mode on initial settling rate is examined further with the aid of zeta potentials graphed in Figure 2-21. The zeta potential at zero electrocoagulation time was that of as-received silica in de-ionized water containing 200 mg/L NaCl at pH 8.5, the pH of feed water in the electrocoagulation tests. With the application of electrocoagulation in either

mode, the zeta potentials decreased (*i.e.*, became less negative) from -21.4 mV. After 15 minutes' electrocoagulation, the zeta potential decreased by only ~2 mV, although the initial settling rate was enhanced by over 3 orders of magnitude, from 1.6×10^{-3} cm/min (as received) to 3.6 cm/min (indirect mode) and to 2.7 cm/min (direct mode). These results show that the destabilization of suspended particles can occur with hardly any change in zeta potential, when destabilization is effected by specific adsorption (Xiao *et al.*, 2008; Ofir *et al.*, 2007). Further, it is reasonable to suggest that the DLVO theory, which pertains to particle destabilization by purely physical means, does not account for the 15-minute AC/EC results.

For indirect electrocoagulation, the minimum zeta potential of -7.5 mV (*i.e.*, the least negative value) and the maximum initial settling rate were both attained after 45 minutes' electrocoagulation. The 15- and 45-minute slurries settled well and the supernatants cleared up within five hours. However, longer periods of indirect electrocoagulation caused the zeta potential to revert to values of the order of -20 mV. The slurries gave rise to supernatants that were stable dispersions of fine (most likely, colloidal) silica. These supernatants required protracted settling times for clarification, as tabulated below for two days of settling in a 1-L graduated cylinder.

Electrocoagulation Time, min	Supernatant Description
75	~180 cm^3 clear water ~790 cm^3 gelatinous dispersion
90	~120 cm^3 clear water ~830 cm^3 gelatinous dispersion
120	~115 cm^3 clear water ~825 cm^3 gelatinous dispersion

The dispersion of fine silica upon indirect electrocoagulation was accompanied by increased zeta potentials (Figure 2-21). Nevertheless, electrocoagulation of a fraction of the silica particles was achieved. It must be recalled that aluminum hydroxide precipitated from the AC/EC-treated water. The evidence is strong that this precipitation contributed to the reduced indirect electrocoagulation of silica and, hence, to the initial settling rate. Indeed, when as-received silica was slurried with AC/EC-treated water from which the

precipitate had been removed, the same turbid supernatant resulted. If the hypothetical calculation performed with Equation 2-9 (Section 2.4.4.2) were to be repeated here, the estimated loss of $Al_{13}(OH)_{34}^{5+}$ would be 81%, with concomitant loss of coagulative capacity (see Figure 2-20). Residual $Al(OH)_4^-$ is not expected to have contributed greatly to the indirect electrocoagulation of silica, but might have aided in reversing the zeta potential.

Precipitate from a mass balance test was found to have a zeta potential of +9.3 mV, consistent with reports elsewhere (Amirtharajah and O'Melia, 1990; Letterman *et al.*, 1982; O'Melia, 1986; Tambo, 1991) that aluminum hydroxide precipitate particles carry a small positive charge in the pH range of this study. It would be expected that these particles would be adsorbed onto the silica surface and, to some extent, mitigate the negative charge thereon, depending on their quantity. The quantity of precipitate might have been large enough to neutralize a portion of the charge (see Figure 2-21, 90 and 120 minutes). From Stumm's (1992) proposed models of surface complex formation, Equations 2-10 and 2-11 are proposed to illustrate the involvement of $Al(OH)_3$(am) in coagulation by interparticle bridging.

$$\equiv Al\text{–}OH + Al_2(OH)_2^{4+} \leftrightarrow \equiv Al\text{–}OAl_2(OH)_2^{3+} + H^+ \qquad (2\text{-}10)$$

$$\equiv Al\text{–}OAl_2(OH)_2^{3+} + HO\text{–}Si\equiv \leftrightarrow \equiv Al\text{–}OAl_2(OH)_2^{2+}\text{–}OSi\equiv + H^+ \qquad (2\text{-}11)$$

Equation 2-10 exemplifies the acquisition of a positive charge on $Al(OH)_3$(am) particles.

For direct electrocoagulation, Figure 2-21 shows that the zeta potential decreased (*i.e.*, became less negative) from -21.4 mV with electrocoagulation time. Apart from a small reversal of 4 mV between 75 and 90 minutes of electrocoagulation, the zeta potential decreased overall to -1 mV after 120 minutes of electrocoagulation.

Mass median sizes (d_{50}) of indirectly and directly electrocoagulated silica are compared in Figure 2-22. The d_{50} of indirectly electrocoagulated silica decreased from 60 µm after 45 minutes' AC/EC treatment to ~45 µm after 120 minutes, while that of directly electrocoagulated silica increased to a maximum of 92 µm after 75 minutes' treatment. Thereafter, a plateau was reached at ~80 µm. Hence, while the floc growth rate was, initially, slightly higher for indirect electrocoagulation, due mainly to a higher Al dosage in the AC/EC-treated water

(hence, greater adsorption of aluminum species therefrom), much larger flocs were formed by direct electrocoagulation at AC/EC retention times longer than 45 minutes. The arrested floc growth during indirect electrocoagulation is attributed to loss of the more efficient coagulative aluminum species by precipitation. In addition, aluminum hydroxide is known (Wang *et al.*, 2009) to form the weakest bridges in floc construction. For direct electrocoagulation, the situation is different: the largest flocs were formed after 75 minutes' electrocoagulation; yet, with extension of the retention time to 90 and 120 minutes, floc sizes decreased. The only explanation for this phenomenon is floc fragmentation.

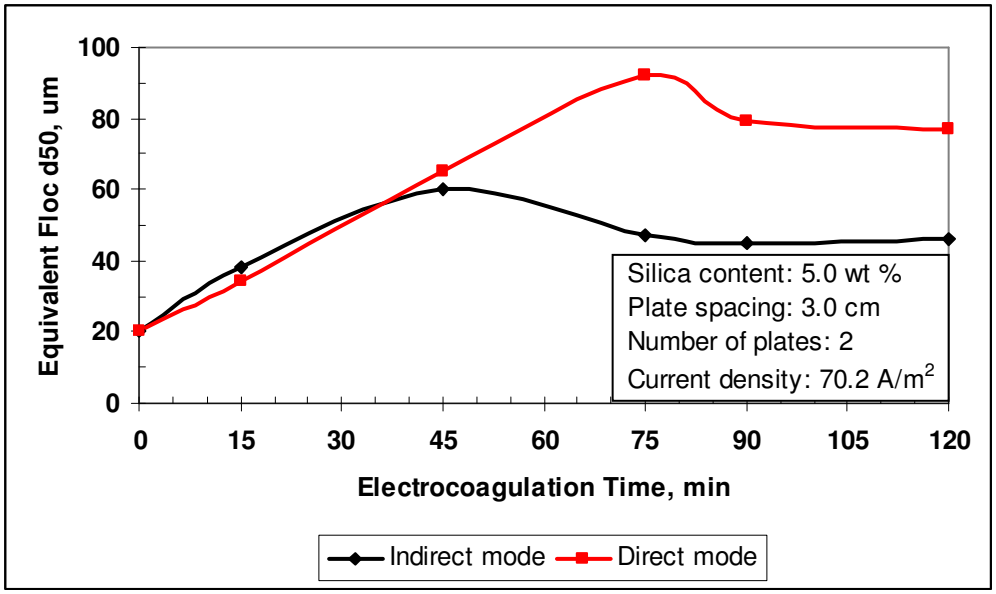

Figure 2-22. Effects of AC/EC mode and time on d_{50} of freshly electro-coagulated silica.

In the electrocoagulation tests, the initial temperature was controlled, but the temperature rise generated by Joule heating was not. Table 2-14 shows that temperature rises were similar for the two electrocoagulation modes, with slightly smaller increases (≤1.4℃) occurring in direct electrocoagulation owing to heat absorption by the silica.

The voltage required to maintain the current decreased with electrocoagulation time as the water warmed up and became more conductive. Time-averaged voltages, V_{avg}, decreased with time from 49 V for 15 minutes to 42 V for 120 minutes of electrocoagulation, and were similar for both electrocoagulation modes. From the average voltage, the current and the electrocoagulation time, the energy input was calculated. On the basis of a unit

mass of silica, it was termed the “specific energy input” (SEI). As expected, the SEI increased with time from 440 kJ/kg (0.12 kWh/kg) to 3040 kJ/kg (0.85 kWh/kg) silica over the range of electrocoagulation times studied.

Table 2-14. Comparison of AC/EC operating data.

AC/EC Time, min	AC/EC Mode	T_i, ℃	T_f, ℃	V_{avg}	SEI, kJ/kg Silica
15	Indirect	21.2	26.2	49.2	441
45		21.2	34.1	45.6	1228
75		21.2	38.8	44.2	1984
90		21.2	41.1	43.2	2325
120		21.3	44.2	42.1	3020
15	Direct	21.3	26.1	49.0	440
45		21.6	34.0	45.3	1219
75		21.5	39.0	43.3	1944
90		21.3	39.8	42.8	2306
120		21.3	42.8	42.3	3038

T_i: initial temperature T_f: final temperature SEI: specific energy input

Residual aluminum in the supernatants was higher for direct electrocoagulation over the range of AC/EC retention times studied, as demonstrated in Figure 2-23.

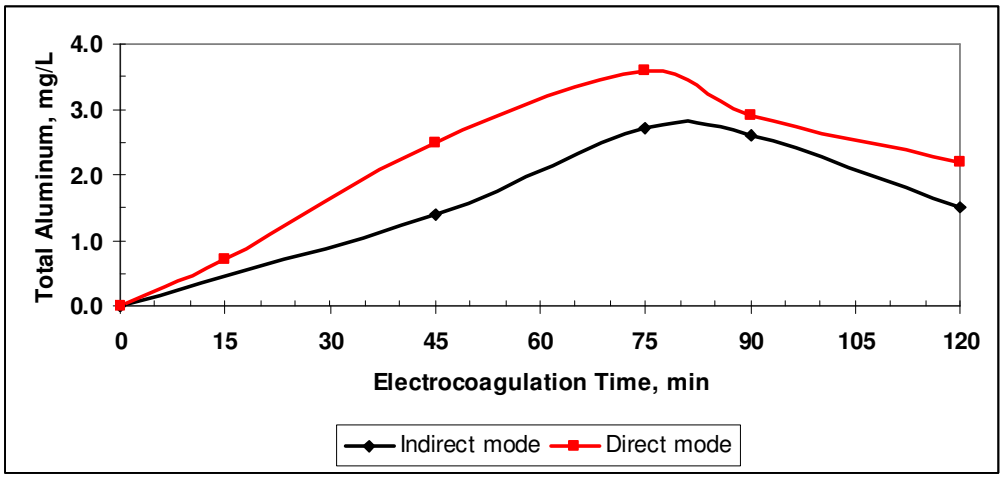

Figure 2-23. Effect of electrocoagulation mode on residual aluminum in supernatants.

It is clear from Figure 2-23 that the utilization of aluminum by silica was lower in direct electrocoagulation. In addition, direct electrocoagulation always

produced supernatants which clarified within <1 to 5 hours. No colloidal dispersions were formed, as was the case with indirect electrocoagulation. Hence, electrocoagulation engendered higher mass settling rates in the direct mode than it did in the indirect mode for times exceeding 45 minutes. A major phenomenological difference between the two modes of electrocoagulation was that the silica encountered the entire aluminum dosage immediately in indirect electrocoagulation whereas, for direct electrocoagulation, the aluminum dosage can be regarded as having been metered into the silica suspension continuously. It is reasonable to suggest that this metering process allowed more time for the floc fragments to rearrange themselves and to re-aggregate (Wang et al., 2009; Zbik et al., 2008) into morphologies of enhanced settling characteristics. In this way, adsorption proceeded on an as-needed basis.

It is probable that aluminum hydroxide precipitated during lengthy direct electrocoagulation times. In such cases, the precipitate would be expected to adsorb onto the silica flocs and infill voids, and so increase the floc density. It should be noted that the concentration of dissolved silicon in all water samples from both electrocoagulation modes was consistently below the detection limit of 2 mg/L.

Major fractions of the total aluminum were adsorbed by silica in both modes of electrocoagulation. During indirect electrocoagulation, between 81 and 93% of the total aluminum was adsorbed from the AC/EC-treated water. In direct electrocoagulation, the range was 84 to 90%, the assumption being that the total aluminum released from the electrodes in a given time was the same for both electrocoagulation modes. It is considered that a portion of the aluminum was adsorbed as hydroxide precipitate. The adsorption mass ratios did not differ markedly with electrocoagulation mode, as is evident from Table 2-15.

Table 2-15. Adsorption of total aluminum.

AC/EC Time (min)	Indirect Electrocoagulation		Direct Electrocoagulation	
	Fraction, %	mg Al/g Silica	Fraction, %	mg Al/g Silica
0	0	0	0	0
15	> 81.1	> 0.08	86.8	0.09
45	91.9	0.30	85.5	0.28
75	87.9	0.37	83.9	0.36
90	90.9	0.49	89.8	0.49
120	93.0	0.38	89.7	0.36

Values of pH, which were extracted from the data used to construct Figures 2-13 and 2-17, are plotted against electrocoagulation time in Figure 2-24 to illustrate the variation during electrocoagulation. Values of pH for the AC/EC-treated water were obtained during treatment of the feed water before the indirect electrocoagulation of as-received silica. At zero AC/EC time, the pH was that of the feed water, and was determined by the $HCO_3^-/CO_3^=$ equilibrium established from absorption of atmospheric CO_2. On the other hand, pH values for electrocoagulated slurry were measured in slurries that were electrocoagulated directly. At zero AC/EC time, the pH was that of the feed suspension.

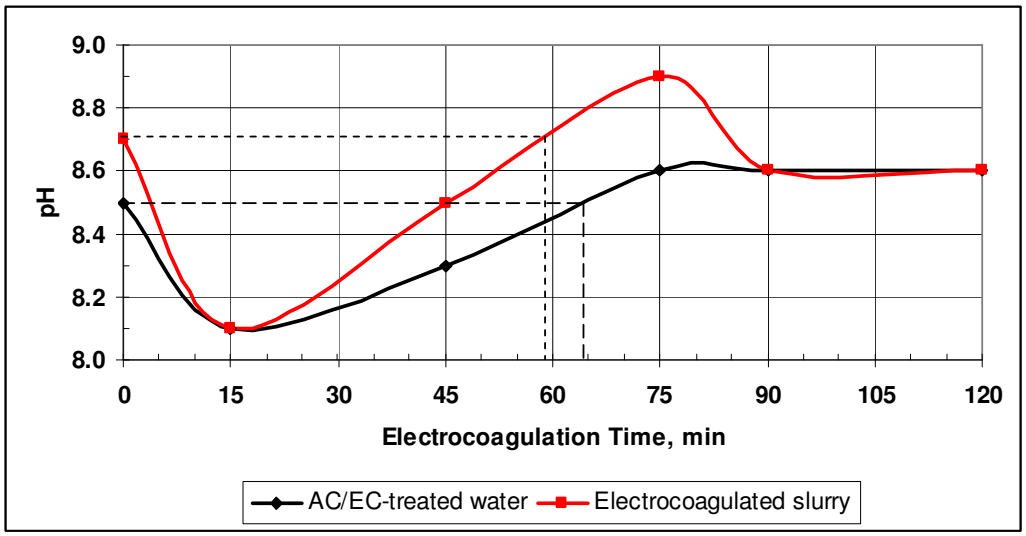

Figure 2-24. The variation of pH during electrocoagulation.

For both modes, 15 minutes of electrocoagulation produced the lowest measured final pH of 8.1. It is quite possible that a lower pH was attained

between 0 and 15 minutes, such that the pH could have been on the rebound at the end of 15 minutes. However, the curves illustrate the initial pH drop which is attributed mainly to the consumption of OH^- in aluminum complexation reactions. Speculation suggests that the minimum pH (during direct electrocoagulation) was attained at the end of the destabilization of the dispersion because, within two minutes thereafter, enhanced settling could be observed. This aspect will be discussed in more detail in Chapter 4.

In Figure 2-24, pH increased with time of electrocoagulation beyond 15 minutes. AC/EC treatment of the feed water caused the pH to return to its original value (*i.e.*, zero net change) after ~65 minutes. The pH reached a plateau of 8.6 after 75 minutes, indicating that an equilibrium (*i.e.*, steady state) had been established between aluminum complexation and aluminum hydroxide precipitation during electrocoagulation. In Section 2.4.4.2, precipitation was reported to have been observed during AC/EC treatment of the water in tests longer than 45 minutes, whereas precipitation occurred in the 45-minute AC/EC-treated water during cooling (after the test was concluded).

During direct electrocoagulation, the pH value for zero net change was reached after approximately 60 minutes and the pH continued to increase to a maximum of 8.9 after 75 minutes. Further extension of the electrocoagulation time produced a drop in the pH to a plateau at 8.6 after 90 minutes. The behaviour of the pH is consistent with the precipitation of metal hydroxides. It is significant that, in both modes of electrocoagulation, the equilibrium was established at the same pH (8.6), which indicates that the reaction chemistry became the same for both modes. It can now be concluded from Figure 2-24 that precipitation did occur during direct electrocoagulation in the 90- and 120-minute tests. The equilibrium was established earlier in the AC/EC-treated water (indirect mode) because aluminum accumulated. In contrast, equilibrium was delayed in direct AC/EC because aluminum was adsorbed continuously, and could not accumulate as rapidly as in indirect AC/EC until the adsorption rate decayed. Although the precipitation did not impair the initial settling rate of silica, it is considered to have increased the floc density, especially since aluminum hydroxide has a specific gravity of 2.42 (Weast, 1989), compared to ~1.0 for the pore fluid it was displacing. Being very fine, the precipitate could infill voids in the silica flocs, reducing the floc porosity.

It is possible that silica floc fragmentation occurred during direct AC/EC because the limiting size had been attained between 75 and 90 minutes of electrocoagulation time. It is also possible that the concurrence of fragmentation and substantial precipitation was not coincidental. In consideration of this second possibility, it is most likely that precipitation began before 75 minutes of electrocoagulation time, but became substantial between 75 and 90 minutes. It is postulated that, from the time precipitation began, precipitate particles adsorbed onto the silica flocs and participated in interfloc bridging. With continued AC/EC past 75 minutes, the flocs reached sizes which could not be maintained in the prevailing hydrodynamic regime, the precipitate bridges conceivably being weaker than those formed by soluble aluminum complexes. It is postulated, therefore, that fragmentation occurred primarily at precipitate-bridged sites.

Changes in pH with time and mode of electrocoagulation are compared in Figure 2-25. The supernatants produced by both modes of electrocoagulation displayed the same pH trend from 75 minutes and beyond because the water chemistry was identical. However, from 15 to 75 minutes, the pH rates of increase were governed by the continuous removal of aluminum from solution by adsorption (direct electrocoagulation) and by the accumulation of aluminum in solution (indirect electrocoagulation). The directly electrocoagulated slurry, and the supernatant it yielded, displayed the same pH trend. In contrast, the indirectly electrocoagulated slurry displayed an almost linear mode of decrease with increasing electrocoagulation time.

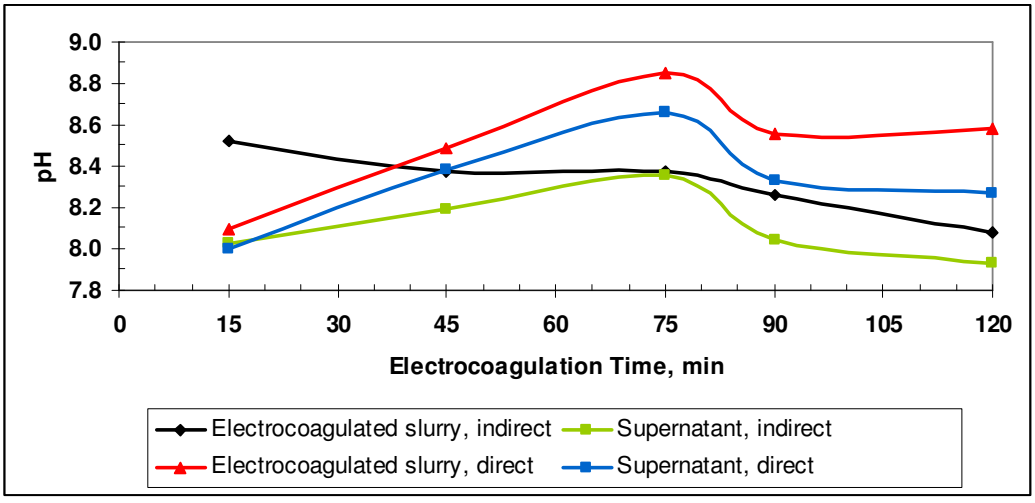

Figure 2-25. Variation of pH with time and mode of electrocoagulation.

2.4.4.5 Ageing of Electrocoagulated Silica

In this section, the effect of one day's ageing on indirectly and directly electrocoagulated silica is examined with respect to settling behaviour and floc size distribution. It should be noted that this is ageing that occurred in the retention time test slurries (refer to Figures 2-10 and 2-15) while they sat at room temperature (22℃). Figure 2-26 depicts the settling behaviour of 1-day old, indirectly electrocoagulated silica.

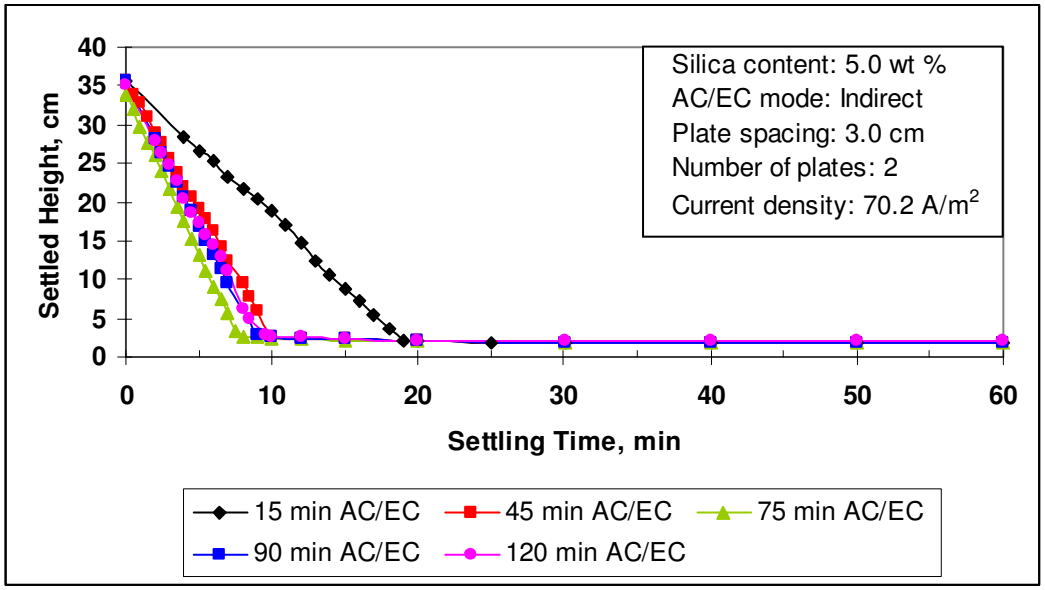

Figure 2-26. Settling behaviour of indirectly electrocoagulated silica, aged 1 day.

The settling behaviour was still differentiated with respect to electrocoagulation time, such that settling improved with electrocoagulation time of up to 75 minutes. The initial settling rates are compared in Figure 2-27. One day's ageing was detrimental to the enhanced initial settling rates engendered by indirect electrocoagulation for times under 75 minutes. The initial settling rate of the aged electrocoagulate was greatest (4.1 cm/min) for 75 minutes of electrocoagulation. As it was for the fresh electrocoagulate, initial settling rate was virtually unchanged by age for electrocoagulation times of 75 minutes and longer. However, the initial settling rates of aged 15- and 45-minute electrocoagulates contrast sharply with those of the fresh electrocoagulates. Ageing caused substantial diminutions in initial settling rate of 50% (15 minutes) and 48% (45 minutes). Hence, the 75-minute initial settling rate emerged as the maximum.

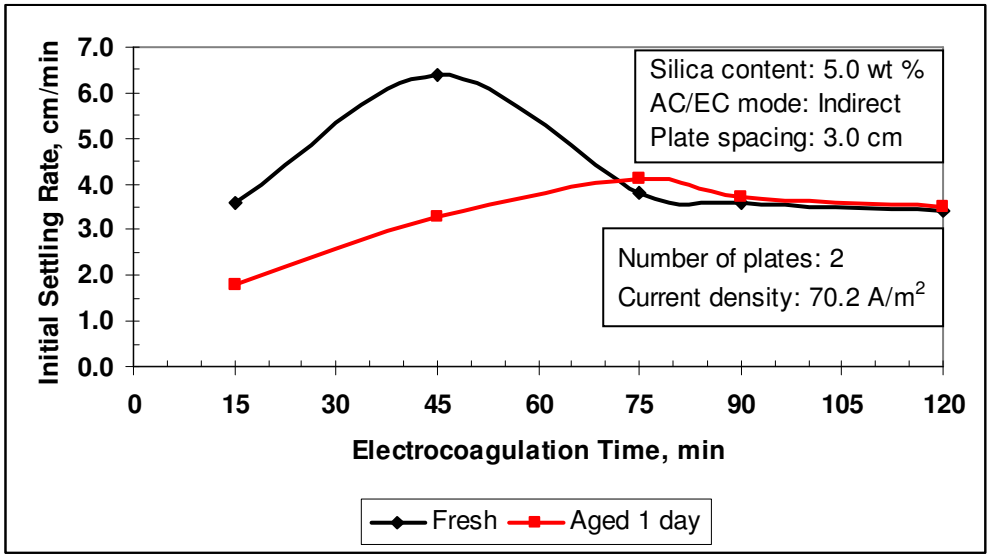

Figure 2-27. Effect of ageing on the settling behaviour of indirectly electrocoagulated silica.

Initial settling rates for the fresh and aged electrocoagulates were the same for electrocoagulation times of 75 minutes and longer because the efficient coagulative aluminum species had been precipitated. For electrocoagulation times shorter than 75 minutes, on the other hand, efficient coagulative species were present in the fresh electrocoagulates, to which the initial settling rates attest. Upon ageing, the electrocoagulates of less than 75 minutes' treatment exhibited drastically reduced initial settling rates. It is clear, therefore, that the effect of ageing on settling behaviour, for electrocoagulation times of under 75 minutes, resulted from its effect on the efficient coagulative species. It is reasonable to deduce that these species degraded with age, with accompanying loss of coagulative capacity, in agreement with the observations of Baes and Mesmer (1976) and Beecroft *et al.* (1995), among others.

Floc size distributions of the aged electrocoagulates are presented in Figure 2-28 which shows that the floc sizes shifted to smaller equivalent diameters, with less relative displacement among the curves than is evident in Figure 2-11. Consistent with Figure 2-27, the coarsest flocs were now to be found in the 75-minute, aged electrocoagulate.

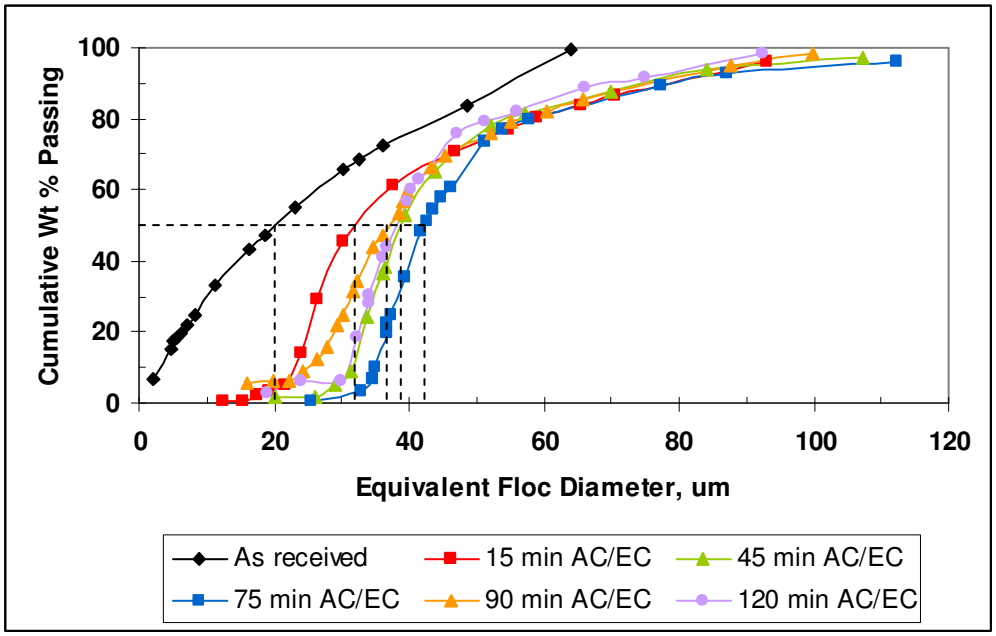

Figure 2-28. Floc size distributions of indirectly electrocoagulated silica, aged 1 day.

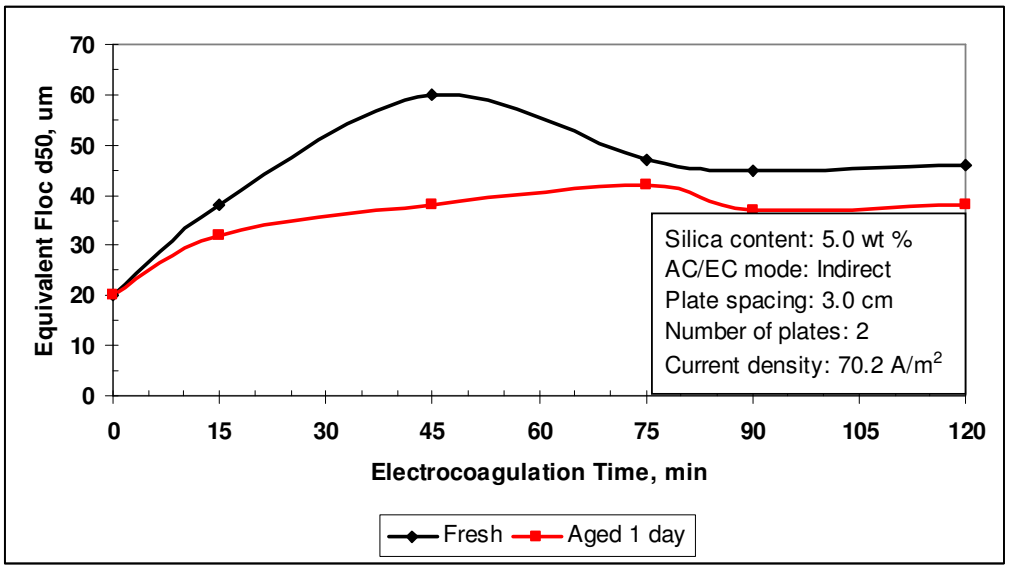

Figure 2-29. Effect of ageing on d_{50} of indirectly electrocoagulated silica.

A clearer comparison is provided by Figure 2-29 in which the d_{50} sizes are graphed. Whereas, floc d_{50} sizes of the fresh electrocoagulates ranged from 38 to 60 µm, floc d_{50} sizes of the aged electrocoagulates ranged from 32 to 42 µm, consistent with the narrow displacements of the distributions (Figure 2-28). It is

noteworthy that the porosities of the electrocoagulate sediments and, hence, the porosities of the flocs decreased during ageing (Table 2-16).

Table 2-16. Porosity decreases in sediments during ageing (indirect AC/EC).

Electrocoagulation Time (min)	Sediment Porosity, vol %	
	Fresh	Aged 1 Day
15	59.4	58.6
45	66.2	61.7
75	66.2	61.3
90	64.4	62.4
120	64.4	60.2

The decreases in sediment porosity were not caused by the normal compression that accompanies sedimentation (and which has purely physical origins) for two reasons:

- electrocoagulated silica characteristically completed the compression stage before the settling test ended; and
- the floc sizes would not have changed.

Hence, the flocs collapsed during ageing (under quiescent conditions). This collapse is attributed to chemical reaction, namely, degradation of coagulative aluminum species. “Degradation” is defined as the conversion of larger hydroxoaluminum complexes to smaller ones of lower coagulative capacity. Evidence of degradation is offered in the discussion of the photomicrographs which follows shortly.

From Figures 2-29 and 2-27, the close similarity between the d_{50} and initial settling rate curves for aged electrocoagulate is apparent. Hence, the settling behaviour of the aged, indirectly electrocoagulated silica was controlled by floc size.

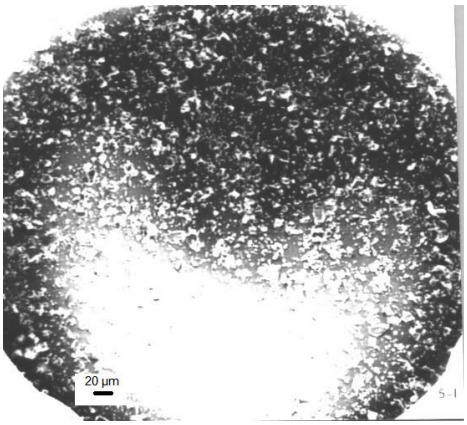

(a) 15 min

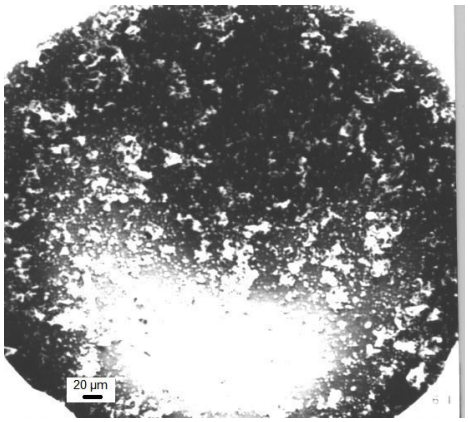

(b) 45 min

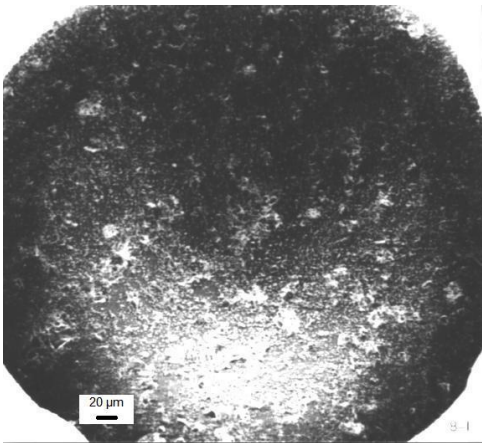

(c) 75 min

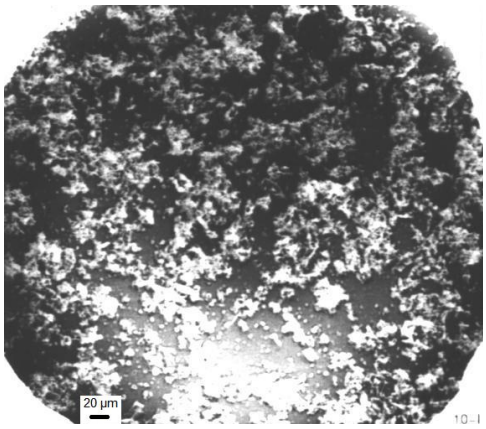

(d) 90 min

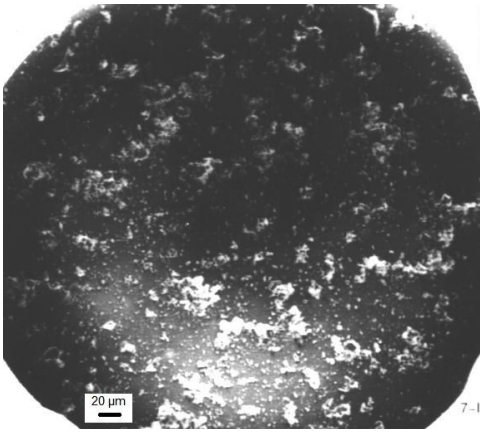

(e) 120 min

Plate 2-2. Indirectly electrocoagulated silica, aged several days.

Photomicrographs of silica, which was indirectly electrocoagulated for 15 to 120 minutes and then aged for several days, are introduced as Plate 2-2. Plate 2-2a shows that the 15-minute electrocoagulate consisted of:

- single, coarse, transparent particles;
- fine particles appearing as dots; and
- sparse, small flocs of silica.

The free particles and microflocs appear to constitute a large proportion of the silica. Flocs are less sparse in the 45-minute electrocoagulate (Plate 2-2b), but a significant fraction of the solids appears to be discrete particles or microflocs. Flocs in the 75-minute sample (Plate 2-2c) have a tattered appearance that is suggestive of degradation. In freshly electrocoagulated silica, the flocs would be expected to be well developed, similar in appearance to those in Plate 2-1c. The 90-minute electrocoagulate (Plate 2-2d) contained larger and more plentiful flocs while, by comparison, the 120-minute sample shows smaller flocs and an increase in the proportion of microflocs. In summary, therefore, Plate 2-2 indicates that flocs degraded with age, particularly for the shorter electrocoagulation times. Consequently, the proportion of discrete particles and microflocs increased. Evidently, Plate 2-2 should not be compared with the results obtained for one day's ageing. Aluminum hydroxide precipitates could not be distinguished from the silica masses.

Directly electrocoagulated silica, aged one day, showed differentiation of settling behaviour enhancement with electrocoagulation time. As Figure 2-30 shows, the degree of enhancement increased with electrocoagulation time, and the settling behaviour of the 45- to 120-minute electrocoagulates showed marginal differentiation.

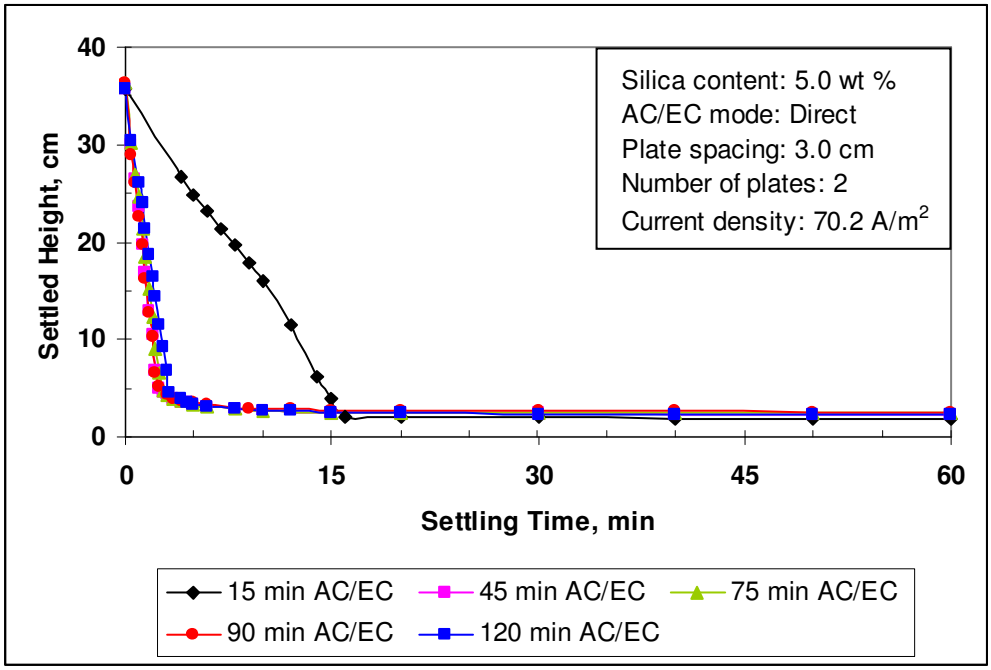

Figure 2-30. Settling behaviour of directly electrocoagulated silica, aged 1 day.

The initial settling rates of aged and fresh, directly electrocoagulated silica are plotted in Figure 2-31.

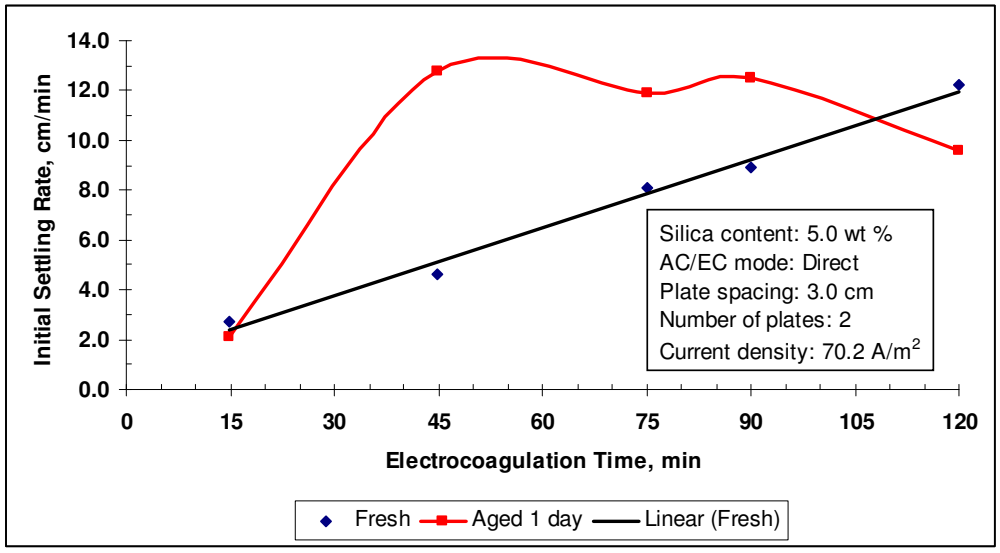

Figure 2-31. Effect of ageing on the settling behaviour of directly electrocoagulated silica.

In sharp contrast to the settling behaviour of aged, indirectly electrocoagulated silica, directly electrocoagulated silica (16 to 110 minutes of electrocoagulation) displayed further enhancement of settling behaviour upon

ageing. This further enhancement was dramatic (178%) for silica that had been electrocoagulated for 45 minutes. For electrocoagulation times of 15 minutes and >110 minutes, however, settling behaviour deteriorated, especially for the longer times.

The floc size distributions are shown in Figure 2-32. Silica flocs created in 90 minutes of electrocoagulation grew to become the coarsest as the electrocoagulate aged. Meanwhile, the 75-minute flocs decreased in size. Clearly, hydroxoaluminum complexes underwent modification in a manner that was unlike that which occurred in indirectly electrocoagulated silica, for the most part. Thus, it might then be inferred that the proportion of the more effective coagulative species in the 90-minute supernatant increased during the ageing process. This could well include redissolution of some portion of the precipitate in the production of the more highly coagulative species. In the case of the 75-minute sample, the reverse is inferable; *i.e.*, the proportion of the more efficient coagulative species decreased, perhaps by precipitation to some extent.

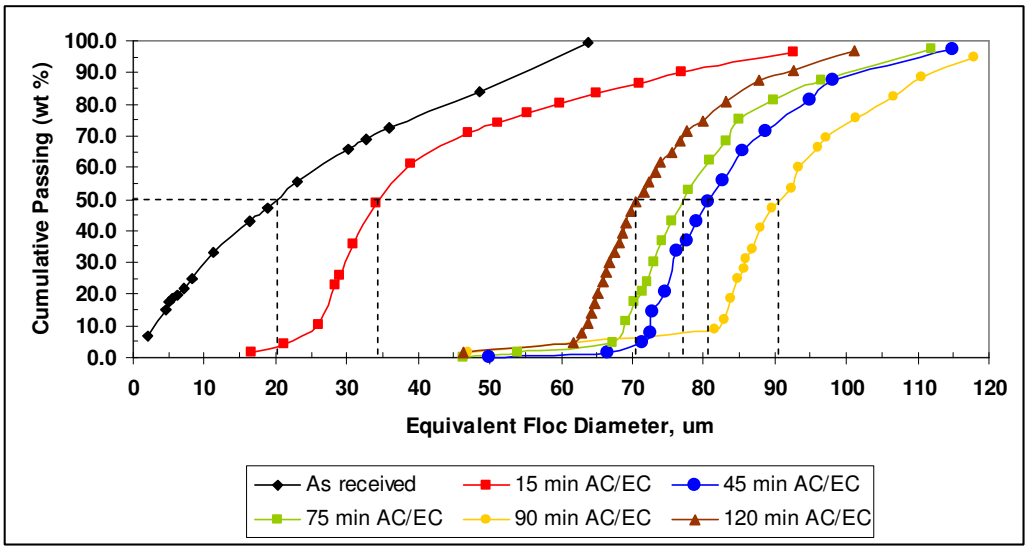

Figure 2-32. Floc size distributions of directly electrocoagulated silica, aged 1 day.

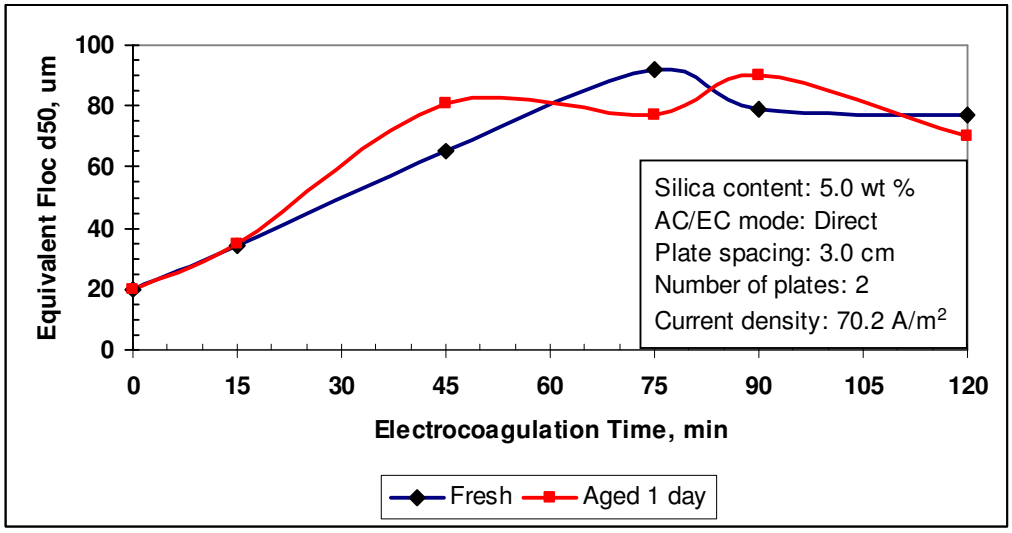

Figure 2-33. Effect of ageing on d_{50} of directly electrocoagulated silica.

An important feature of Figure 2-33 is the similarity of the d_{50} curve (aged) to the initial settling rate curve (aged) in Figure 2-31. In addition to the reproducibility of the data, these graphs together verify that the 75- and 90-minute data points were not spurious, and that settling behaviour was dictated by floc size. Figure 2-33 indicates that the d_{50} of the fresh 15-minute flocs was not changed by ageing for a day. Flocs produced by longer periods of electrocoagulation, however, either coarsened or degenerated through ageing. Floc degeneration has been addressed in the discussion of aged, indirectly electrocoagulated silica. On the other hand, floc coarsening or growth (45 and 90 minutes of direct electrocoagulation) with age evidently indicates that incremental coagulation occurred, representing a special case of indirect electrocoagulation. It is interesting to note from Table 2-17 that, like the sediments of aged, indirectly electrocoagulated silica, the sediments of directly electrocoagulated silica underwent reduction of porosity, except for the 90- and 120-minute electrocoagulates (more so the former).

Table 2-17. Porosity changes in sediments during ageing (direct AC/EC).

Electrocoagulation Time (min)	Sediment Porosity, vol %	
	Fresh	Aged 1 Day
15	66.2	60.2
45	66.1	63.8
75	69.7	63.8
90	70.1	71.0
120	67.3	67.8

In the study of floc growth by electrocoagulation, it has been usual to find that the bulk density of the sediment decreases with increasing floc size and, hence, initial settling rate. Contrary to this trend was the aged 45-minute electrocoagulate which increased both in floc size and bulk density (fresh, 1521 kg/m^3; aged, 1556 kg/m^3), while the 90-minute electrocoagulate conformed to the trend (fresh, 1458 kg/m^3; aged, 1444 kg/m^3). Yet, both of these electrocoagulates exhibited floc growth, the mechanisms of which must have been different. It is postulated that the increased porosity in the 90-minute electrocoagulate resulted from redissolution of aluminum hydroxide precipitate (wt % solids in sediment decreased from 52.0 to 51.0) to form efficient coagulative species. It is further postulated that the reduced porosity in the aged, 45-minute electrocoagulate resulted from re-aggregation, which means that the flocs rearranged themselves into a denser configuration (bulk density increased from 1521 to 1556 kg/m^3), with a new, larger limiting size (Ayyala *et al.*, 1995; Gregory, 1993) (see Section 1.2.3.5).

Photomicrographs, which contrast those in Plate 2-2, are presented in Plate 2-3. They show silica that was directly electrocoagulated for 15 to 120 minutes and aged several days. The flocs consistently appear to be more robust than those of Plate 2-2. In Plate 2-3a, the flocs appear as dark masses owing to the adjustment of the SEM optics. With lengthening electrocoagulation time, floc size increased, particularly in the 15- to 75-minute range (Plates 2-3a to 2-3c). The photomicrographs for longer retention times suggest some degree of floc degradation (Plates 2-3d and 2-3e). Plate 2-3 cannot be compared with the results obtained for one day's ageing.

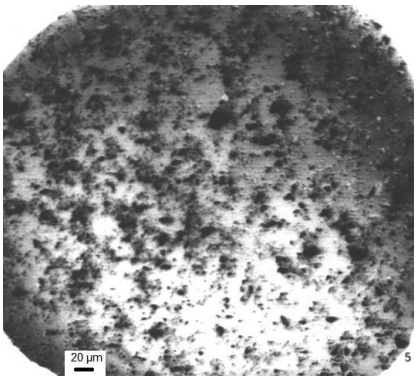

(a) 15 min.

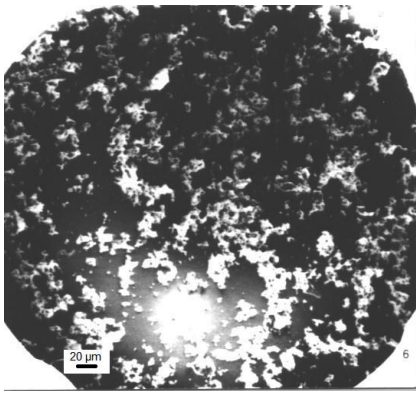

(b) 45 min.

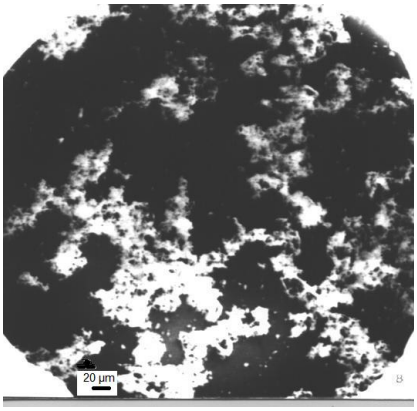

(c) 75 min.

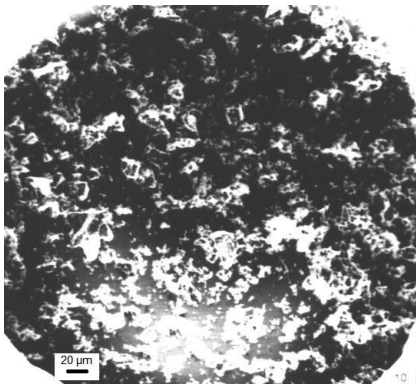

(d) 90 min.

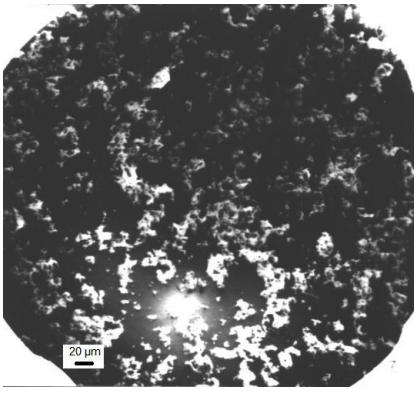

(e) 120 min.

Plate 2-3. Directly electrocoagulated silica, aged several days.

In Figure 2-34, the effects of ageing on the settling behaviour of indirectly and directly electrocoagulated silica are compared.

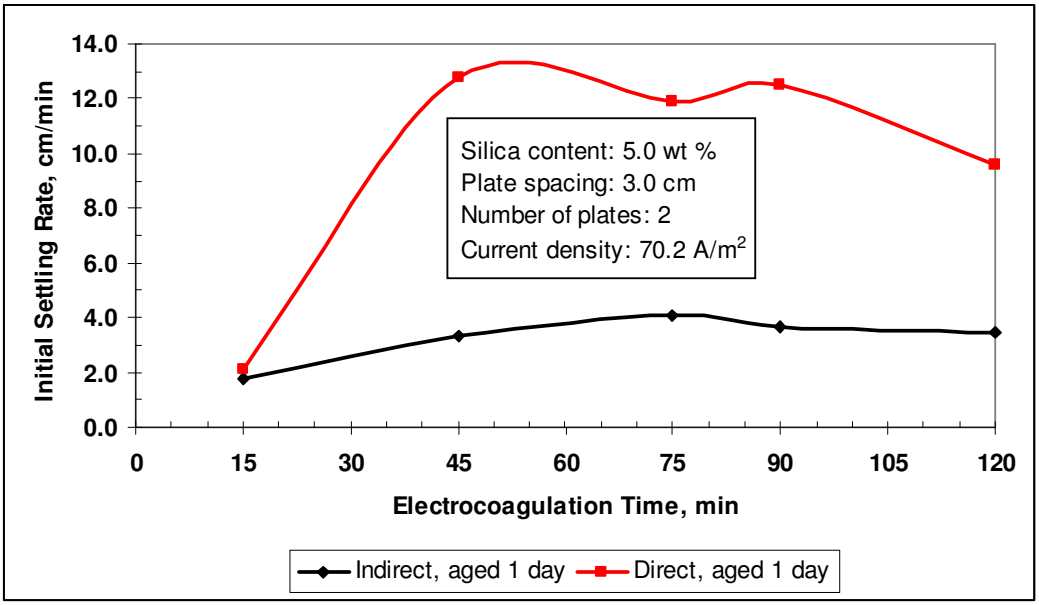

Figure 2-34. Effect of electrocoagulation mode on settling behaviour after ageing.

The responses of settling behaviour of the electrocoagulates to ageing were radically different for electrocoagulation times greater than 15 minutes. Aged, directly electrocoagulated silica displayed consistently superior initial settling rates to those of aged, indirectly electrocoagulated silica. The values of the former ranged from 2.1 to 12.8 cm/min, in contrast to the 1.8 to 4.1 cm/min range of the latter. While the settling behaviour of directly electrocoagulated silica was generally enhanced by ageing, no such benefit accrued to indirectly electrocoagulated silica (Figure 2-27). In fact, the settling behaviour of the latter material deteriorated with ageing. Figure 2-35 shows that the settling behaviour of both types of aged electrocoagulates was determined by floc size.

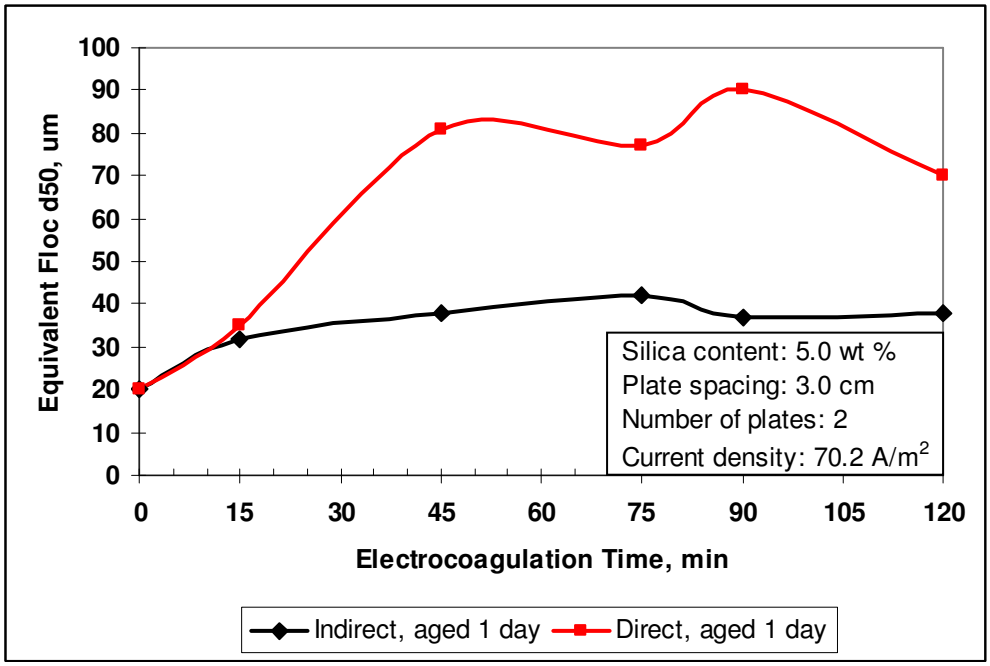

Figure 2-35. Effect of electrocoagulation mode on d_{50} after ageing.

Modifications of floc characteristics, which were observed with changes in the mode and time of electrocoagulation, and with ageing, were reflected in the characteristics of the sediments. Variations in the sediment characteristics are depicted in Figure 2-36. The bulk density (B.D.) and solids content curves are similar, due to the direct relationship between bulk density and wt % solids on one hand, and solids mass on the other. The porosity curves are inverted versions of the previous two because of the inverse relationship between porosity and solids volume, the latter varying directly with solids mass. Relative to the fresh electrocoagulates, the bulk density and wt % solids of indirectly electrocoagulated silica increased during ageing and the floc porosity decreased (data in Appendix A). It is inferred that the bulk density and solids content increases, and the accompanying porosity decrease, resulted from aluminum hydroxide precipitation onto the silica flocs during ageing. Silica, which had been directly electrocoagulated for 15 to 90 minutes, increased in bulk density and solids content during ageing, while the porosity decreased. This is generally similar to the behaviour of aged, indirectly electrocoagulated material. The sharp decrease in bulk density and wt % solids, shown in Figure 2-36 for aged, directly electrocoagulated silica (75 to 90 minutes), was accompanied by a sharp increase in porosity, as would be expected.

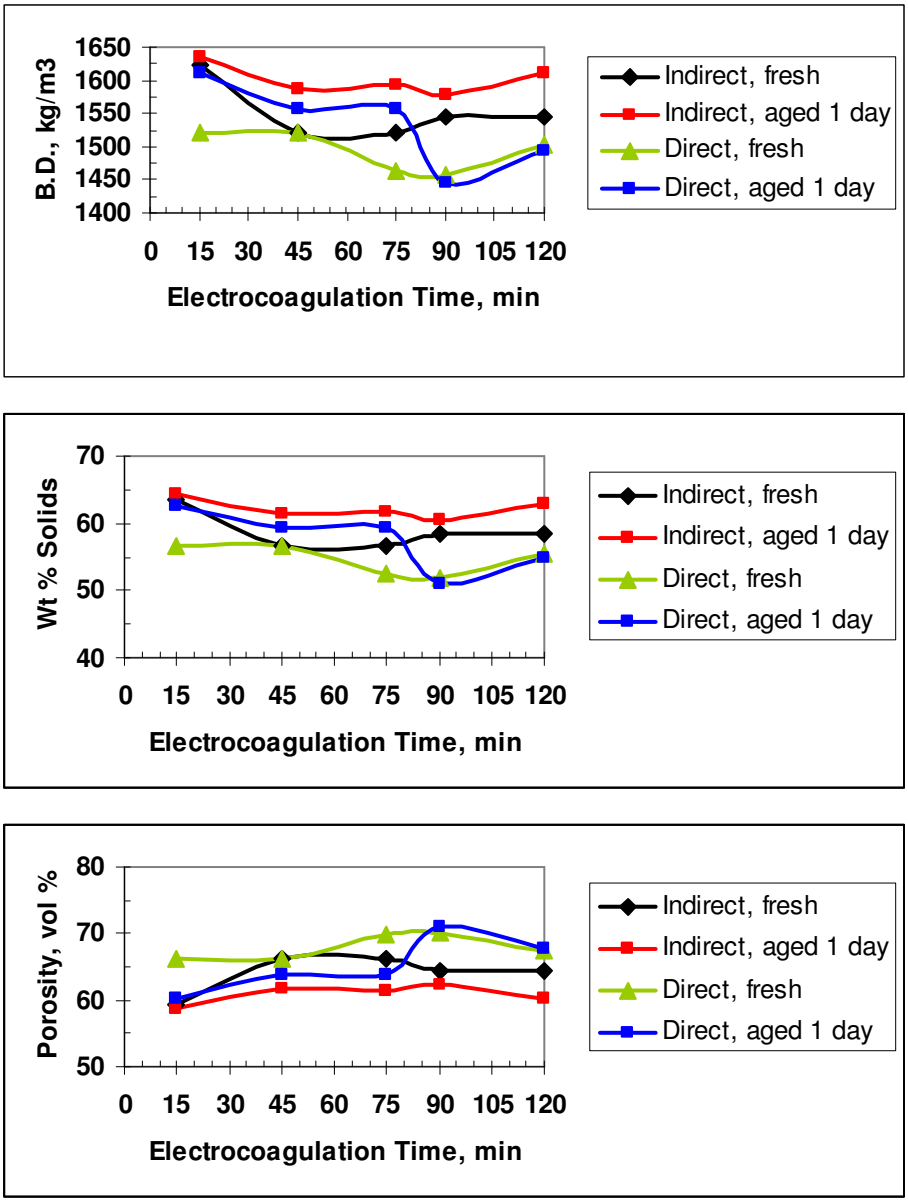

Figure 2-36. Effects of ageing and electrocoagulation mode on sediment characteristics.

2.4.5 AC/EC Retention Time Mode

2.4.5.1 Retention Time Mode Test Procedure

The influence of AC/EC retention time mode, *i.e.*, whether continuous or cumulative, on the settling behaviour of silica was studied during 15 minutes of direct electrocoagulation. In both tests, continuous agitation was imposed at an impeller tip speed of 1.73 m/s. In the cumulative retention time test, however,

electrocoagulation was applied for an initial period of 10 minutes and a final period of five minutes, with a 5-minute intermission. Agitation was suspended during the intermission. Two electrodes were immersed 3.0 cm apart in the feed suspension and current was passed at a density of 70.2 A/m^2.

2.4.5.2 Retention Time Mode Test Results and Discussion

Initial settling rates of 2.6 and 3.9 cm/min were achieved for the continuous and cumulative treatments, respectively. These results illustrate that interruption of the electrocoagulation process is not detrimental to the enhancement of settling behaviour and it might even be beneficial. Indeed, the results demonstrate that electrocoagulation is flexible and its enhancing effect cumulative, facilitating re-treatment of under-coagulated solids to achieve the desired settling characteristics. It is noteworthy that the silica showed enhanced settling behaviour after the initial 10-minute treatment period in the cumulative test. The settling curves are shown in Figure 2-37.

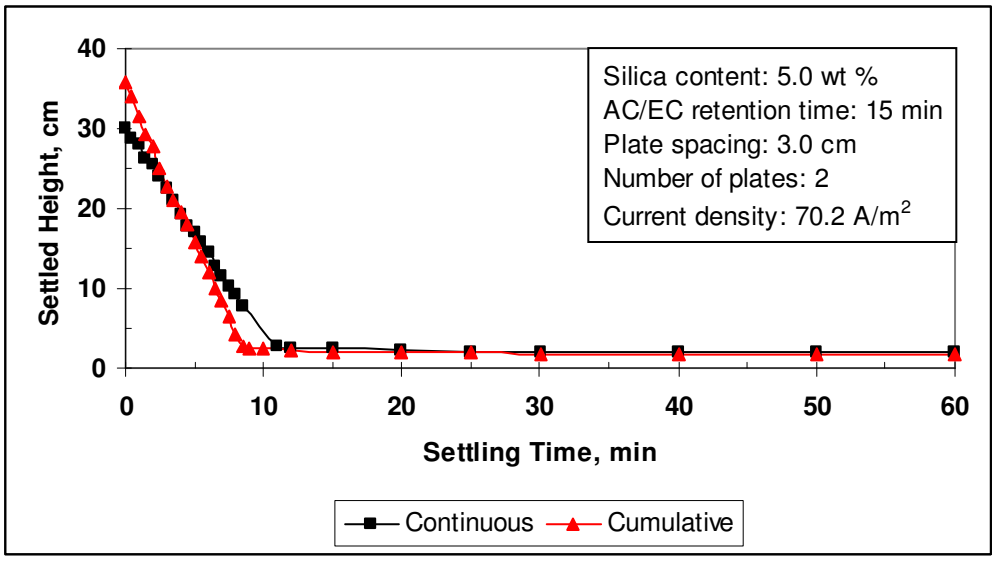

Figure 2-37. Effects of AC/EC retention time mode on the settling behaviour of silica.

The 50% higher initial settling rate achieved by cumulative electrocoagulation deserves discussion. Table 2-18 is presented for this purpose.

Table 2-18. Retention time mode – pH values.

AC/EC Time Mode	T, ℃	pH		
		Feed Suspension	EC* Slurry	Supernatant
Continuous	20.7	8.81	8.68	8.52
Cumulative	20.5	8.83	8.15	8.01

*Electrocoagulated

From an initial value of 8.8, the pH of the feed suspensions decreased during electrocoagulation, such that the electrocoagulated slurries registered the following values: continuous, 8.7; cumulative, 8.2. This pH difference of 0.5 between the electrocoagulated slurries persisted to the supernatants which gave pH values of 8.5 (continuous) and 8.0 (cumulative). It appears that the difference in pH values was attributable to the quiescent period (intermission) during cumulative treatment. The intermission could have facilitated the progress of Al^{3+} complexation as exemplified by Equation 2-12, the hydrolysis product of which would have promoted floc growth, with further enhancement of the settling behaviour. In addition, the deprotonation of water in the hydrolysis reactions (*e.g.*, Equation 2-12) would have contributed to the incremental pH drop observed.

$$Al^{3+} + H_2O \leftrightarrow Al(OH)^{2+} + H^+ \qquad (2\text{-}12)$$

Table 2-19. Operating data from retention time mode tests.

AC/EC Time Mode	T_i, ℃	T_f, ℃	V_{avg}, V	SEI, kJ/kg Silica
Continuous	20.7	25.9	49.9	448
Cumulative	20.5	25.3	48.7	437

Operating data from the tests are recorded in Table 2-19. The marginally lower T_f for the cumulative test resulted from cooling during the intermission, giving a ΔT of 4.8℃, compared to 5.2℃ for the continuous test. The average voltage was slightly lower for cumulative electrocoagulation. The specific energy inputs were calculated at 448 and 437 kJ/kg silica for continuous and cumulative electrocoagulation, respectively.

2.4.6 Current Density

2.4.6.1 Current Density Test Procedure

Six direct electrocoagulation tests were performed to examine the influence of current density on the direct electrocoagulation and resulting settling behaviour of silica. The current densities ranged from 3.3 to 167.2 A/m^2. In the 3.3 A/m^2 test, no NaCl was added to the water and the electrocoagulation time was extended to 30 minutes. In the other tests, the time was fixed at 15 minutes. In all tests, two electrodes were installed 3.0 cm apart and agitation was applied continuously at an impeller tip speed of 1.73 m/s. The feed suspension pH was adjusted to 8.8 at 21.3°C to 21.5°C.

2.4.6.2 Current Density Test Results and Discussion

Figure 2-38 depicts the enhanced settling behaviour of silica achieved over the current density range of 70.2 to 167.2 A/m^2 in 15 minutes of electrocoagulation.

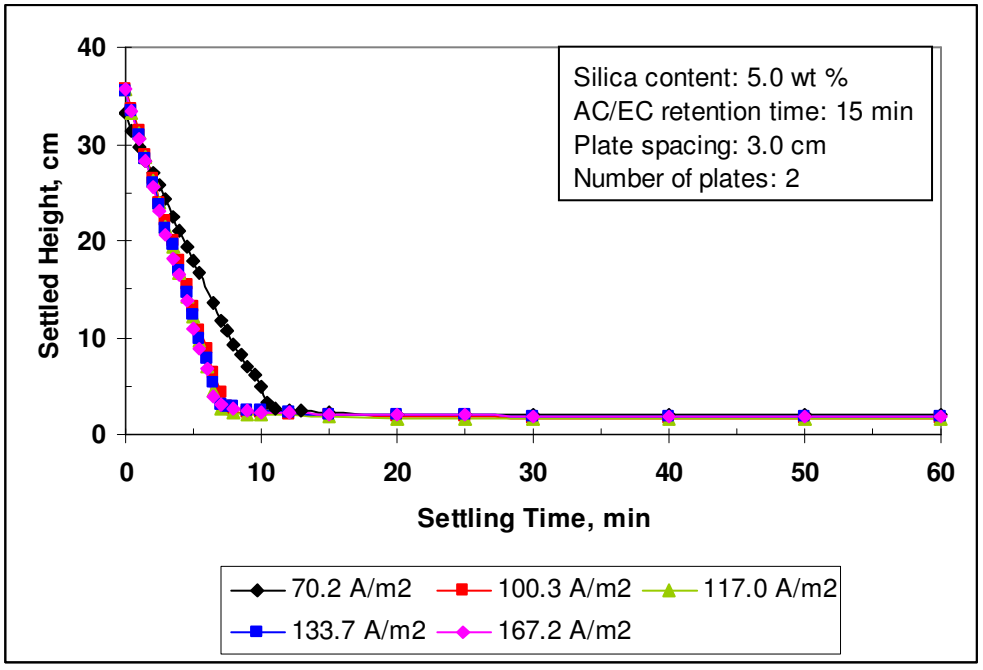

Figure 2-38. Enhanced settling behaviour of silica electrocoagulated at various current densities.

The omission of NaCl from the suspension in the 3.3 A/m^2 test kept the conductivity low. A maximum current of only 0.1 A was attained, despite a potential of 100 V across the electrodes. After 30 minutes, the suspension

remained intact and no appreciable settling was observed over 24 hours. The theoretical concentration of aluminum was calculated at 4.2 mg/L. From the analysis of AC/EC-treated water prepared specifically for aluminum analysis, 14.8% of the theoretical aluminum was oxidized at the current density of 70.2 A/m^2. If this fraction were applied to the 3.3 A/m^2 current density, the aluminum concentration would be 0.6 mg/L. However, since the fraction of theoretical tends to diminish with current density, it was assumed to be 5% for 3.3 A/m^2, giving an aluminum concentration of 0.2 mg/L. At <0.01 mg Al/g silica, this concentration would be insufficient to coagulate 210.5 g silica. Even 0.6 mg/L is considered too low at 0.01 mg Al/g silica, as will later be demonstrated by Figure 2-42.

The initial settling rate of electrocoagulated silica increased from 2.8 to 4.7 cm/min as the current density was raised from 70.2 to 117.0 A/m^2. Further increase of the current density did not increase the initial settling rate further, as Figure 2-39 illustrates.

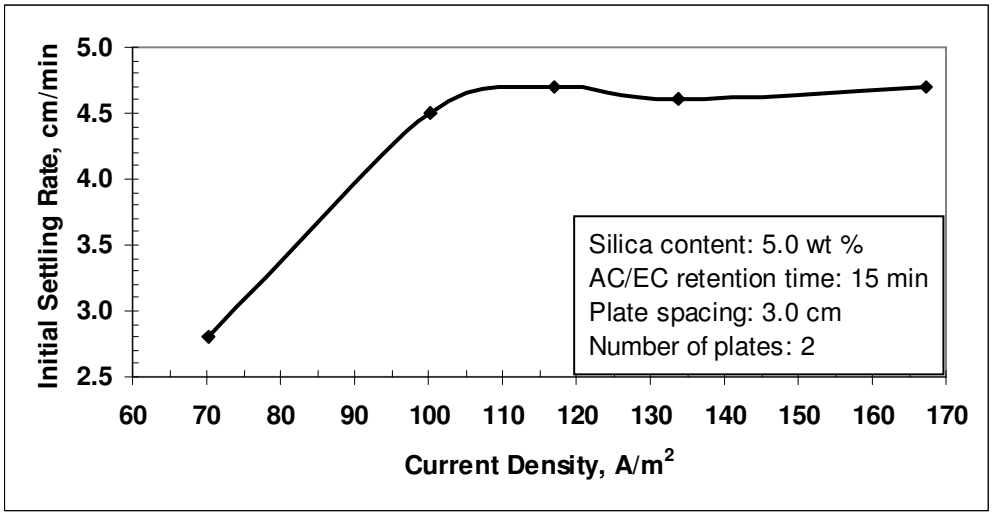

Figure 2-39. Effect of current density on settling behaviour of electro-coagulated silica.

"Onset" of enhanced settling is defined as the first appearance of the meniscus due to solids settling. With current density increase, the time for the onset of enhanced settling, denoted elsewhere (Holt *et al.*, 2002) as the "lag stage", decreased as follows: 70.2 A/m^2, 8 minutes; 117.0 A/m^2, 5 minutes; 167.2 A/m^2, 3 minutes. These data, which are plotted in Figure 2-40, indicate that the kinetics of electrocoagulation were accelerated by increased current density (more specifically, increased current), due to the more rapid oxidation of

aluminum from the electrodes. By interpolation of Figure 2-40, the onset times for current densities of 100.3 and 133.7 A/m^2 were deduced to be 6 minutes and 4.3 minutes, respectively.

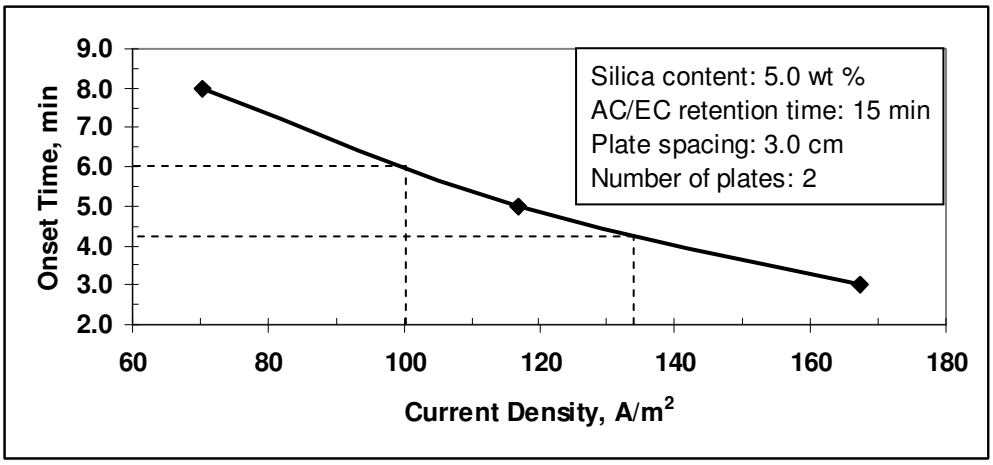

Figure 2-40. Variation of time of onset of enhanced settling with current density.

In qualitative tests conducted at low current densities (<70.2 A/m^2), the electrocoagulation process exhibited induction periods, the duration of which depended on the magnitude of the current density. During the induction period, the current decreased, necessitating positive adjustment of the voltage. At sufficiently high current densities (*e.g.*, 70.2 A/m^2), however, the induction period disappeared. Speculation on the rate-determining step responsible for the induction period suggests two possibilities:

- the nucleation and growth of gas bubbles on the electrode surfaces, and
- anodization of the electrodes.

These would account for the initial current decrease. The current density of 3.3 A/m^2 can be considered to be an extreme case where the system never emerged from the induction state (≥30 minutes) because of the very slow kinetics. This is consistent with the observation of Grøterud and Smoczynski (1992) that there exists a lower current density limit, below which electrocoagulation is not possible. Hence, the induction period was shortened and ultimately eliminated by increasing current density. As expected, the rate of gas evolution increased with current density.

Indirect electrocoagulation tests were performed at current densities of 70.2, 100.3 and 167.2 A/m^2 to prepare AC/EC-treated water for analysis of total

aluminum, the results of which are reported in Table 2-20. The aluminum dosage increased linearly with current density, as expected, and amounted to 14.8% of the theoretical concentrations. Average dosing rates (mg Al/L/min) were calculated for the current densities listed.

Table 2-20. Total aluminum concentrations in AC/EC-treated water.

Current Density (A/m^2)	Current (A)	Total Al in AC/EC-treated Water		
		Theoretical, mg/L	Actual, mg/L	% of Theoretical
70.2	2.1	44.0	6.5	14.8
100.3	3.0	62.9	9.3	14.8
167.2	5.0	104.9	15.5	14.8

On the basis of the 6.5 mg/L total aluminum, which produced the initial settling rate of 2.8 cm/min at current density 70.2 A/m^2 in 15 minutes, electrocoagulation times required at current densities 100.3 and 167.2 A/m^2 to give the same initial settling rate were estimated. From the time estimates, the average voltages and SEI values were calculated. These data are all given in Table 2-21. A record of voltage readings from the direct electrocoagulation tests has been placed in Appendix A.

Table 2-21. Energy requirements to achieve the initial settling rate of 2.8 cm/min.

Current Density (A/m^2)	Average Dosing Rate (mg/L/min)	AC/EC Time (min)	V_{avg} (V)	SEI (kJ/kg Silica)
70.2	0.4	15.0	49.1	440
100.3	0.6	10.8	66.7	616
167.2	1.0	6.5	104.6	969

With increasing current density (70.2 to 167.2 A/m^2), the average dosing rate increased from 0.4 to 1.0 mg/L/min. Consequently, the required electrocoagulation time decreased from 15 to an estimated 6.5 minutes for the same initial settling rate (2.8 cm/min). Owing to the higher currents (3.0 and 5.0 A), the average voltage increased from 49.1 V at 2.1 A to 104.6 V at 5.0 A.

Inspection of the specific energy inputs reveals that operation at 100.3 and 167.2 A/m^2 would require, respectively, 1.4 times and 2.2 times as much SEI as at 70.2 A/m^2. It is evident, therefore, that the time economy accruing to the use of higher current densities did not offset the accompanying energy increases. Hence, the selection of conditions for electrocoagulation as a unit process must be based on considerations that include energy consumption analysis.

It is instructive to estimate the aluminum concentrations that would accumulate in AC/EC-treated water at the times of onset of enhanced settling. In terms of direct electrocoagulation, this would be the total quantity of aluminum released into the solution up to the onset of enhanced settling. These concentrations, from which adsorption mass ratios may be calculated, would represent critical values for electrocoagulation. From the average dosing rates (Table 2-21) and onset times (Figure 2-40), the critical values were estimated and they are listed in Table 2-22. Average dosing rates at 117.0 and 133.7 A/m^2 were evaluated at 0.7 and 0.8 mg/L/min, respectively, by interpolation of Figure 2-41.

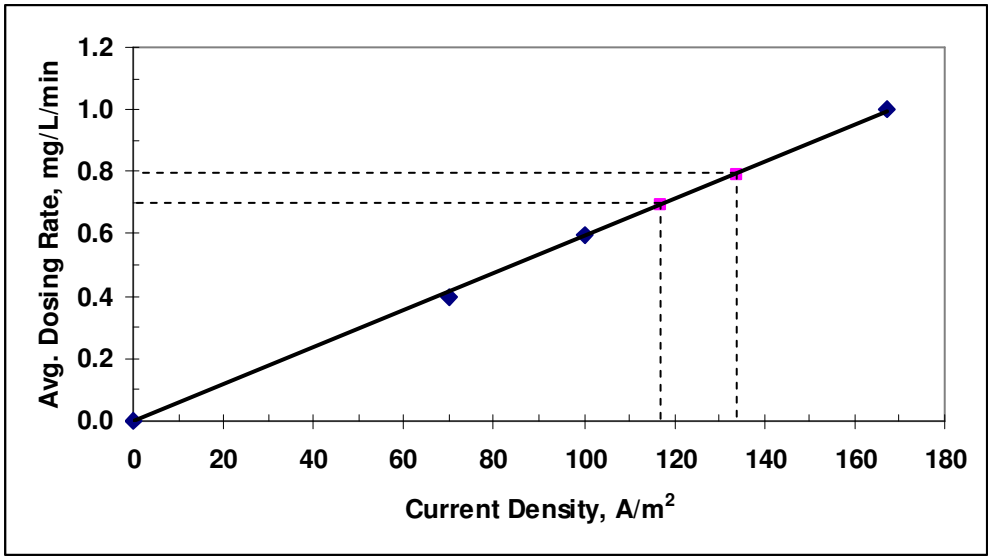

Figure 2-41. Variation of average Al dosing rate with current density.

Table 2-22. Critical aluminum concentrations and adsorption mass ratios.

Current Density (A/m^2)	Critical Total Al (mg/L)	Critical Adsorption Mass Ratio (mg Al/g Silica)
70.2	3.2	0.06
100.3	3.6	0.07
117.0	3.5	0.07
133.7	3.4	0.06
167.2	3.0	0.06

From Table 2-22, the average critical aluminum concentration at which the onset of enhanced settling occurred was 3.3 mg/L, and the average critical adsorption mass ratio was 0.06 mg Al/g silica. It is assumed that the critical quantity of aluminum in solution would be adsorbed completely by the silica. The onset of enhanced settling could be considered to signify the end of suspension destabilization. The variation of initial settling rate with total aluminum concentration is illustrated in Figure 2-42. Under the test conditions imposed, aluminum concentrations exceeding 10 mg/L did not increase the initial settling rate further.

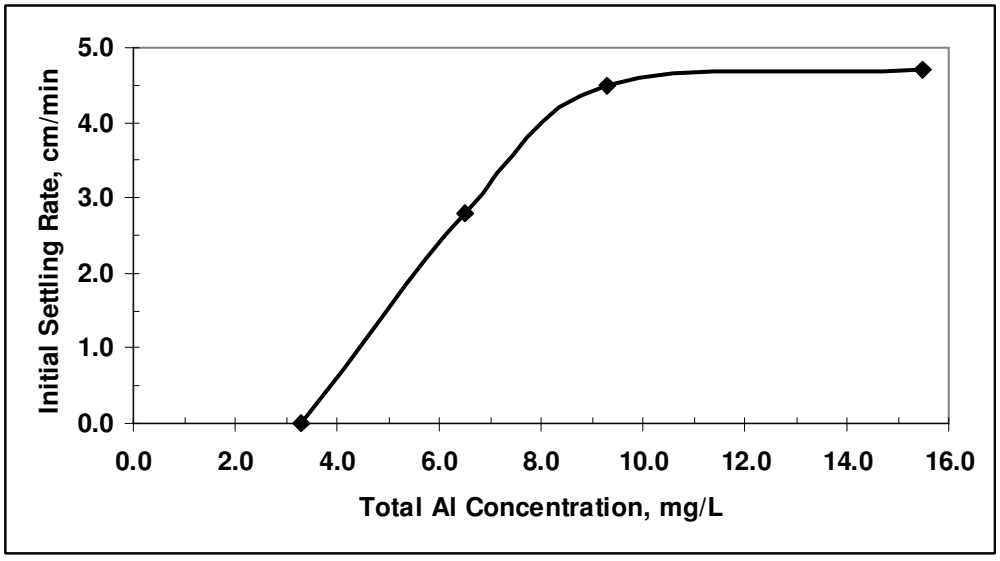

Figure 2-42. Response of initial settling rate to total dissolved aluminum concentration.

Table 2-23. Critical energy requirements.

Current Density (A/m^2)	Onset Time (min)	Onset Charge (C)	V_{avg} (V)	Critical SEI (kJ/kg Silica)
70.2	8	1008	50.2	240
100.3	6	1080	68.1	349
117.0	5	1050	79.2	395
133.7	4.3	1032	89.1	437
167.2	3	900	109.2	467

In Table 2-23, the electrical charge passed in the onset time ranged from 900 C to 1080 C. These are only estimates since the exact times could not be determined. Also listed in Table 2-23 are the critical SEI values, which increased from 240 to 467 kJ/kg (*i.e.*, 0.07 to 0.13 kWh/kg) silica as current density was increased from 70.2 to 167.2 A/m^2. These SEI values again show that energy requirements increase with current density and the increases are not offset by the time saved.

A record of the pH values for the feed suspension, electrocoagulated slurry, feed water and supernatant can be found in Appendix A. These measurements are graphed in Figure 2-43.

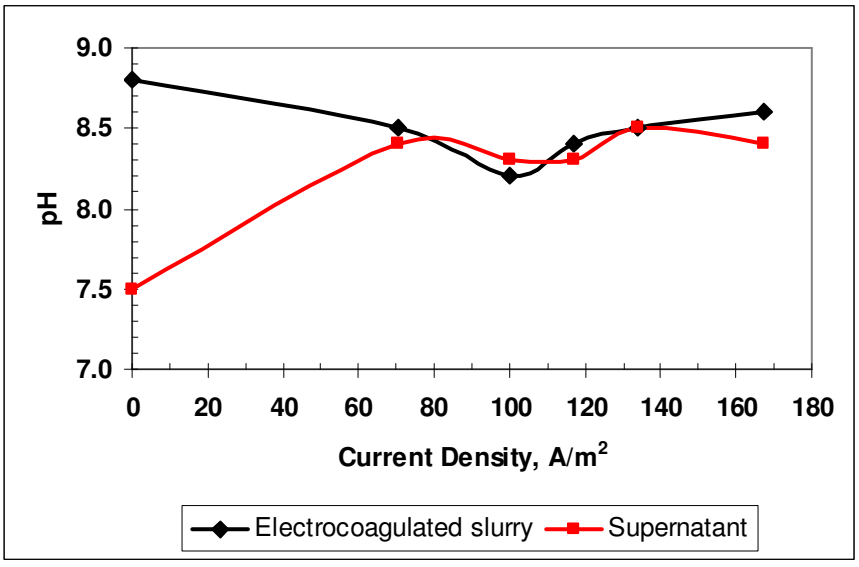

Figure 2-43. Variation of pH with current density.

The pH values plotted at zero current density on the slurry and water curves were those of the feed suspension and feed water, respectively. The

terminal pH of the supernatant was always considerably higher than the feed water pH, ranging from 8.3 to 8.5. Meanwhile, the terminal pH of the electrocoagulated slurry was appreciably lower than the pH of the feed suspension at all current densities tested, and ranged from 8.2 to 8.6. Thus, it may be readily inferred that ionic reactions in the pulp involved a net consumption of OH^- ions or a net production of H^+ ions.

While the pH of the feed slurry was 8.8 and that of the feed water was 7.5, the terminal pH values of the electrocoagulated slurry and the supernatant, at any given current density, were almost identical, differing by a maximum of only 0.2. At the current density of 117.0 A/m^2, the maximum initial settling rate was achieved, and the terminal pH values of the electrocoagulated slurry and the supernatant were 8.4 and 8.3, respectively.

Zeta potentials of electrocoagulated silica are presented in Figure 2-44 as a function of current density.

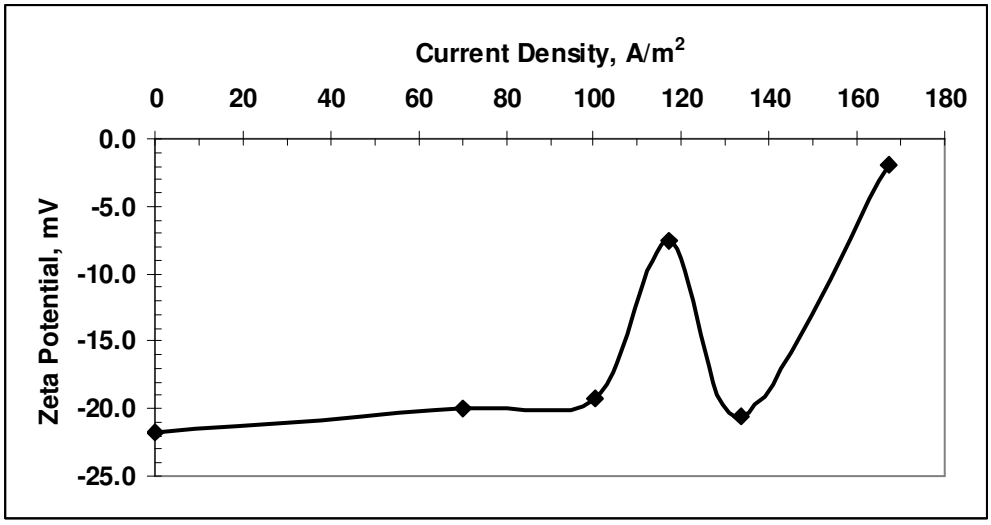

Figure 2-44. Effect of current density on zeta potential of electrocoagulated silica.

As-received silica had a zeta potential of -21.7 mV at the feed suspension pH of 8.8. The zeta potential of electrocoagulated silica slowly became less negative to -19.3 mV at current density 100.3 A/m^2. At 117.0 A/m^2, where the maximum initial settling rate was achieved, the zeta potential decreased sharply to -7.6 mV. Silica electrocoagulated at 133.7 A/m^2, however, showed a zeta potential which was close to that of the as-received material at -20.6 mV. There followed a sharp decrease to -1.9 mV for silica treated at 167.2 A/m^2. The curve

is considered to be expressing, in a general way, the effect of adsorbed complex cationic hydroxoaluminum species on the zeta potential of as-received silica.

It is interesting to note that, although the zeta potential of -7.6 mV coincided with the maximum initial settling rate, it decreased further to -1.9 mV, following electrocoagulation at 167.2 A/m^2. The initial settling rate at this current density equalled the maximum, the implication being that the maximum initial settling rate was attained in less than 15 minutes of electrocoagulation. From this observation, two inferences may be drawn. The first is that adsorption continued beyond the attainment of the maximum initial settling rate to reduce the zeta potential from -7.6 mV (at 117.0 A/m^2) to -1.9 mV (at 167.2 A/m^2). The second inference is that more-highly-charged cationic aluminum complexes, or a higher proportion of such complexes, were formed in the more energetic, higher-temperature environment created by the 167.2 A/m^2 current density. Operating data from the current density suite of tests are summarized in Table 2-24.

Table 2-24. Current density test operating data.

Current Density (A/m^2)	Suspension Temperature (°C)		V_{avg} (V)	SEI (kJ/kg Silica)
	T_i	T_f		
70.2	21.4	26.4	49.1	440
100.3	21.3	30.6	64.9	832
117.0	21.4	33.5	73.7	1102
133.7	21.5	36.7	81.7	1397
167.2	21.3	43.2	96.8	2068

T_i: initial temperature T_f: final temperature

Temperature rises caused by Joule heating increased with current density from 5.0° to 21.9°C, such that the final temperatures of the electrocoagulated slurries ranged from 26.4° to 43.2°C. It is suggested that aluminum speciation (*i.e.*, species identity and distribution) was influenced by these temperatures, as well as by pH. Both temperature and pH in the electrical double layers of the electrodes are expected to have been quite different from the readings obtained in the bulk suspension (Moreno *et al.*, 2009). At any given instant during electrocoagulation, the electrode temperature, for example, would have been higher than that of the suspension.

Table 2-24 also shows that the average voltage and, hence, the SEI increased with current density for 15 minutes of electrocoagulation. V_{avg} ranged from 49.1 to 96.8 V, while SEI ranged from 440 to 2068 kJ/kg silica. With 70.2 A/m^2 and 440 kJ/kg as the basis for comparison, 100.3 A/m^2 and its SEI were, respectively, 1.4 and 1.9 times as large. Corresponding ratios at 167.2 A/m^2 were 2.4 and 4.7. Hence, the energy input increased at a faster rate than the current density, and at an increasingly faster rate as the current density was raised.

2.4.7 Quantity of Electricity

2.4.7.1 Quantity of Electricity Test Procedure

In two direct electrocoagulation tests, a fixed quantity of charge, 3150 C, was passed between two electrodes separated by 3.0 cm. The objective was to determine whether any difference in enhancement of the settling behaviour of silica would result. The currents and times were as follows: 3.5 A for 15 minutes; 5.0 A for 10.5 minutes.

2.4.7.2 Quantity of Electricity Test Results and Discussion

Silica displayed enhanced settling behaviour after direct electrocoagulation by the passage of 3150 C of electricity (Figure 2-45).

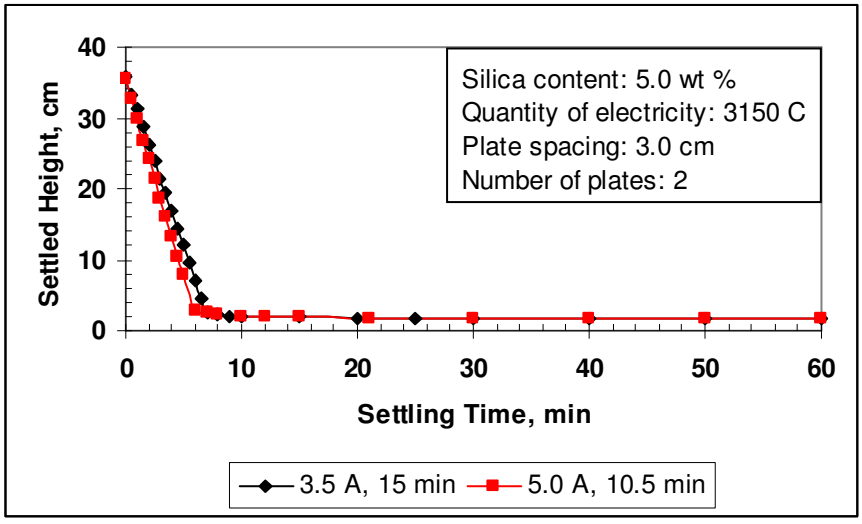

Figure 2-45. Enhanced settling behaviour of silica by electrocoagulation with 3150 coulombs of electricity.

Settling was fast in both cases, with initial settling being completed within about 7 minutes. However, the greater enhancement of settling behaviour was

achieved by 5.0 A flowing for 10.5 minutes. This treatment engendered an initial settling rate of 5.5 cm/min, compared to 4.7 cm/min for 3.5 A passed for 15 minutes. The 17% difference is attributed to the higher current which promoted faster aluminum oxidation, from which higher aluminum dosages resulted. In this way, floc growth at 5.0 A exceeded that at 3.5 A.

Changes in the pH of the pulp and supernatant are reported in Table 2-25.

Table 2-25. Suspension, electrocoagulated slurry and supernatant pH values.

Current (A)	AC/EC Time (min)	Temperature (℃)	pH		
			Suspension	EC* Slurry	Supernatant
3.5	15	21.4	8.8	8.4	8.3
5.0	10.5	21.5	8.6	8.8	8.7

*Electrocoagulated

Changes in pH provide evidence of the progress of electrocoagulation (Moreno *et al.*, 2009; Cañizares *et al.*, 2009), and the rate of pH change is related to the electrocoagulation rate. This was clearly established in Section 2.4.6. Table 2-25 shows that the pH of the electrocoagulated slurry in the first test (3.5 A, 15 min) indicated a net decrease of 0.4 unit from the feed suspension pH. The electrocoagulated slurry from the second test represented a net pH rise of 0.2 unit, indicating that electrocoagulation proceeded at a rate that was rapid enough for the pH to attain its minimum and then overtake the initial value. In the first test, however, the pH was still rebounding from its minimum, despite the longer electrocoagulation time of 15 minutes, when the test was concluded. Consequently, the supernatants registered pH values of 8.7 (5.0 A, 10.5 min) and 8.3 (3.5 A, 15 min).

In Section 2.4.6, the initial pH drop during AC/EC treatment was purported to reflect destabilization of the suspension, while the pH rise from the minimum indicated floc growth. It is tentatively suggested that destabilization of the silica suspension is characterized by substantial (depending on conditions) pH decrease which indicates net hydroxyl ion consumption and/or hydrogen ion release. Destabilization is deemed to be completed when the pH attains a minimum. Silica floc growth, on the other hand, is tentatively characterized by a

pH rise (which could be substantial) from the minimum. Hence, it can be inferred that, for a given set of conditions, routine operation of direct electrocoagulation as a unit process can be monitored through the suspension pH changes. These pH changes might also indicate when it is time to take a cell off line for electrode cleaning.

Table 2-26. Operating data from coulomb tests.

Current (A)	AC/EC Time (min)	Suspension Temperature, °C		V_{avg} (V)	SEI (kJ/kg Silica)
		T_i	T_f		
3.5	15	21.4	33.5	73.7	1102
5.0	10.5	21.5	38.4	99.8	1493

Operating data from the coulomb tests are given in Table 2-26. Greater Joule heating was generated by the 5.0 A current which elevated the suspension temperature by 16.9°C, compared to a 12.1°C rise generated by the 3.5 A current. Voltages averaging 99.8 V were required to maintain the 5.0 A current; for 3.5 A, the average voltage was 73.7 V. Hence, the SEI for the larger current was 35.5% higher at 1493 kJ/kg silica.

2.5 CHEMICAL COAGULATION STUDY

2.5.1 Jar Test Procedure

As-received silica was coagulated with alum, $Al_2(SO_4)_3 \cdot 18H_2O$, and with aluminum chloride, $AlCl_3 \cdot 6H_2O$, in jar tests for comparison with electrocoagulation. Since a 5.0 wt % silica suspension is much denser than raw water, the agitator speeds suggested by the American Water Works Association (AWWA) procedure (1977) had to be increased considerably.

The silica was dispersed in 800 to 900 mL of de-ionized water at 22°C in a 1-L beaker under continuous agitation at 800 r.p.m. (tip speed 2.09 m/s). The paddle assembly was the same as that used in the electrocoagulation studies. Two 13-mm wide polyethylene baffles were installed in the beaker to ensure good mixing while preventing splashing. The baffles were positioned diametrically opposite each other, with a space of about 2 mm from the beaker wall and bottom to prevent accumulation of the solids. After the temperature and pH of the suspension had been measured, a quantity of sodium carbonate was

dissolved in de-ionized water and added to the beaker. The mass of Na_2CO_3 was calculated to neutralize the acid that would be formed by hydrolysis of the aluminum salt, which would be added subsequently. Instead of NaOH, the AWWA procedure preferred Na_2CO_3 for its buffering action. After the suspension pH had stabilized, it was measured together with the suspension temperature.

A mass of the aluminum salt, which was calculated for a predetermined dosage (ranging from 10 to 100 mg/L Al), was dissolved in a volume of de-ionized water that complemented the 1.00 L required for the 52.63 g of silica dispersed at the beginning. The aluminum salt solution was added quickly to the suspension and timing started. After one minute, the impeller speed was reduced to 650 r.p.m. (tip speed 1.70 m/s) and maintained for an additional 20 minutes. These times were the same as those employed by Dentel and Gossett (1988) to coagulate silica. The coagulated slurry was subjected to a settling test in a 250-mL graduated cylinder at 24°C, after which the supernatant was sampled for Al analysis. A coagulated slurry sample was retained for morphological study.

2.5.2 Jar Test Results and Discussion

The settling behaviour of silica was enhanced over the entire range of dosages, as shown in Figures 2-46 and 2-47. Both coagulants engendered rapid settling, such that the time of initial settling did not exceed 5 minutes. The thickness of the sediments increased with aluminum dosage, *i.e.*, with the quantity of $Al(OH)_3$ precipitated. For instance, at an initial settling rate of 5.6 cm/min, the sediments produced by alum and aluminum chloride were 2.7 cm and 2.6 cm thick, respectively. These thicknesses are to be compared with 2.1 cm for direct AC/EC for the same initial settling rate. That chemical coagulation produces more voluminous sediments than does electrocoagulation was highlighted by Un *et al.* (2009), Yildiz *et al.* (2008), Barkley *et al.* (1993) and Vik *et al.* (1984). The explanation for the greater bulk of the chemical coagulation sediments is that the technique depends, virtually exclusively, on the precipitation of the hydroxide in the sweep floc mechanism. In contrast, electrocoagulation derives its efficacy mainly from the formation of hydroxoaluminum species, obviating the need for hydroxide precipitation. Hence, chemical coagulation requires a greater capacity (*i.e.*, more or larger thickeners, filters, *etc.*) in the solid-liquid separation plant than does electrocoagulation, for the same duty. It

should be noted that this comparison of sediment quantities is made on the basis that the silica was treated *in situ* in both chemical coagulation and electrocoagulation.

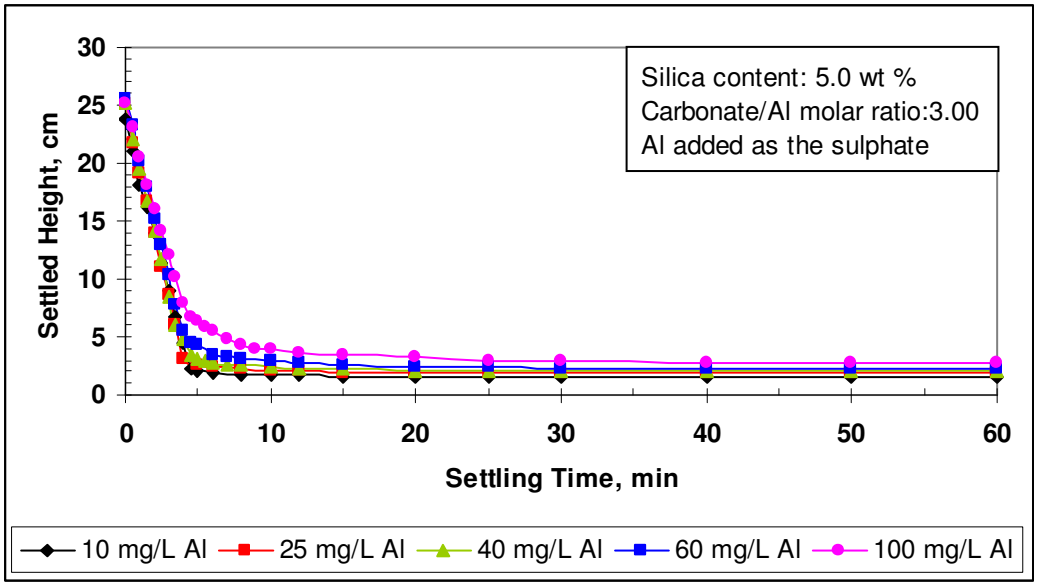

Figure 2-46. Coagulation of silica with alum.

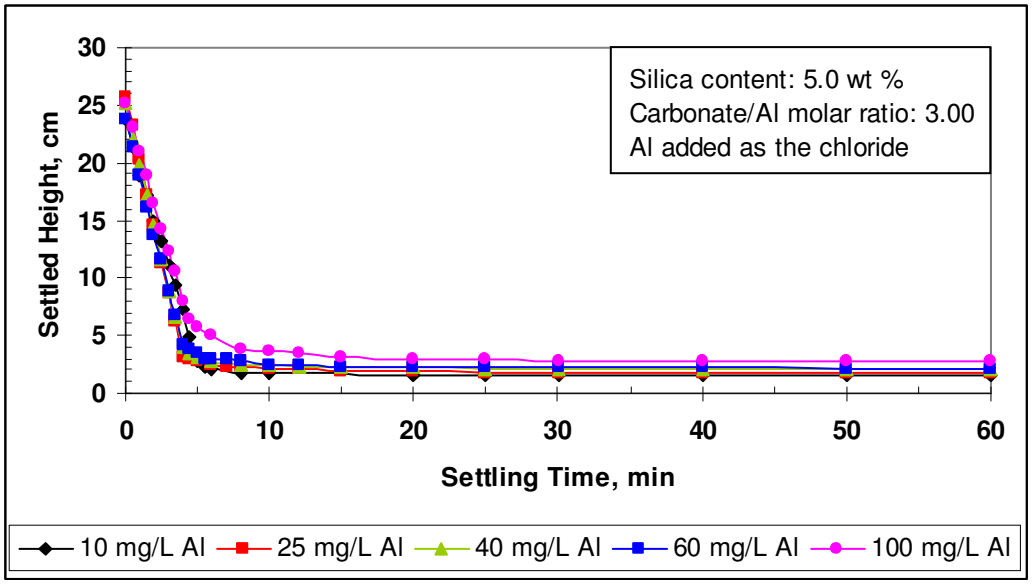

Figure 2-47. Coagulation of silica with aluminum chloride.

The initial settling rates produced by chemical coagulation are plotted in Figure 2-48. Both coagulants produced a maximum initial settling rate of 5.6 cm/min, but aluminum chloride achieved it at a slightly lower dosage of ~25 mg/L Al, while ~30 mg/L sufficed for alum. Alum, however, was more effective (*i.e.*,

produced a higher initial settling rate at a given dosage) than aluminum chloride in the dosage ranges of 10 to 20 mg/L Al and 30 to 75 mg/L Al; in other words, over most of the range studied. At dosages exceeding that at which the maximum initial settling rate was achieved, the initial settling rate diminished linearly and at similar rates for the coagulants (*i.e.*, 0.023 and 0.019 cm/min per mg/L Al dosage increase for alum and aluminum chloride, respectively).

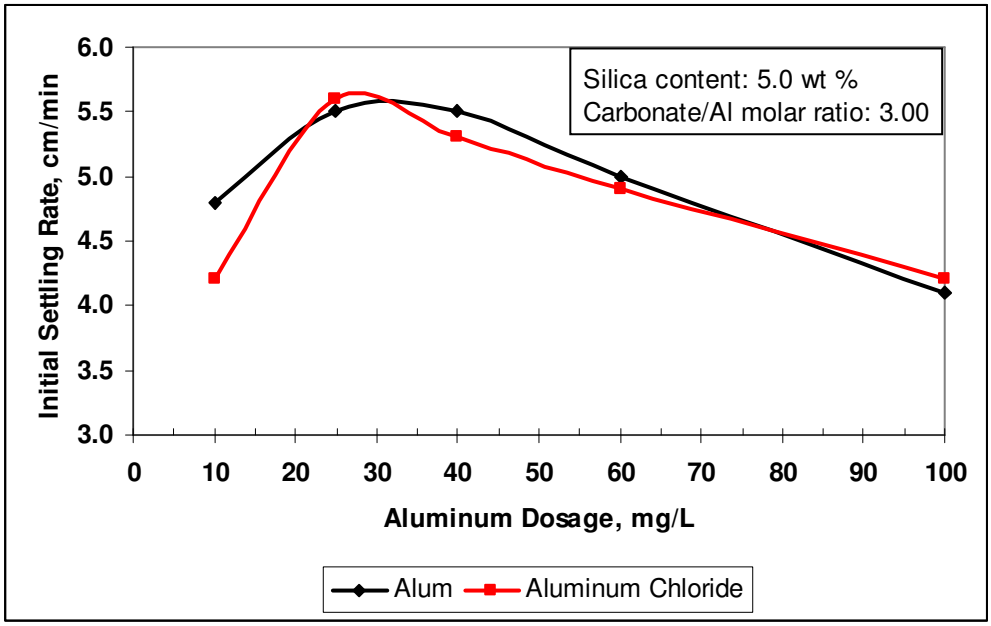

Figure 2-48. Settling behaviour of silica as a function of aluminum dosage and coagulant type.

It is to be noted that hydrolysis is facilitated by low concentrations of metal salts (Stumm and Morgan, 1970). For both coagulants, then, the increase of initial settling rate at low Al dosage is attributed to aluminum hydroxide precipitation at the silica surface from adsorbed mononuclear complexes, such as $Al(OH)^{2+}$ (Amirtharajah and O'Melia, 1990). With increasing Al dosage, enmeshment of the microflocs of silica by aluminum hydroxide precipitate is proposed to have become more prominent until the maximum initial settling rate was achieved. Further increase in the Al dosage resulted in rapid aluminum hydroxide precipitation, probably too rapid for the formation of mononuclear complexes to occur significantly (see Section 2.2.5). In such a case, microfloc aggregation would be suppressed. Thus, it is considered that enmeshment dominated, but now primarily individual silica particles, rather than microflocs, were enmeshed. Consequently, the initial settling rate diminished with the

smaller floc size. This hypothesis is supported by Duan and Gregory's (2003) four zones or levels of coagulation dosage for the settling of negatively-charged, dispersed particles.

Flocs produced at Al dosages of 25 and 100 mg/L are compared in Plate 2-4. The flocs formed with alum (Plates 2-4a and b) suggest greater cohesiveness at 25 mg/L Al dosage. Those formed with $AlCl_3$ (Plates 2-4c and d) show less porosity at 25 mg/L Al dosage.

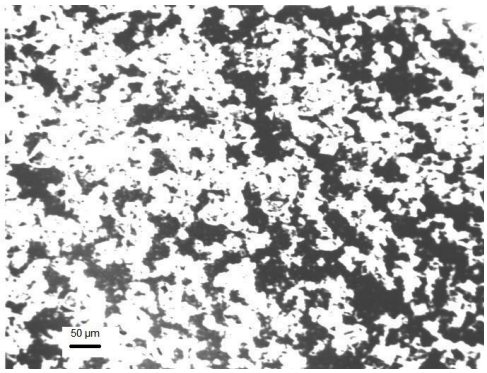

(a) Alum, 25 mg/L Al.

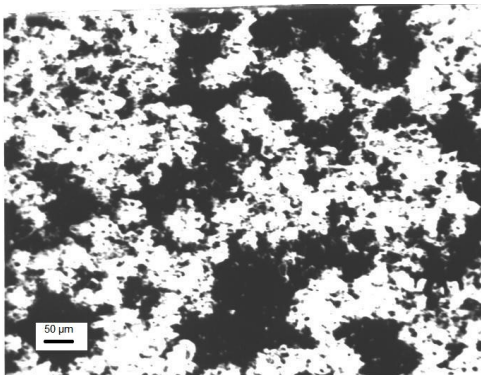

(b) Alum, 100 mg/L Al.

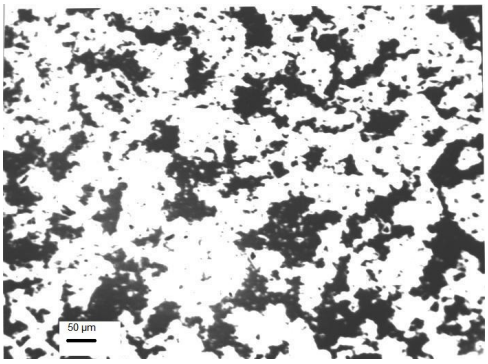

(c) $AlCl_3$, 25 mg/L Al.

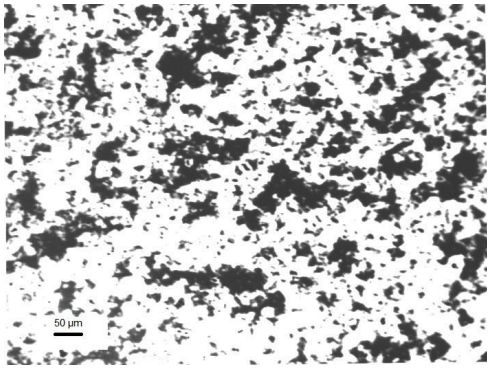

(d) $AlCl_3$, 100 mg/L Al.

Plate 2-4. Textures of chemically coagulated silica.

In separate tests, aluminum hydroxide was precipitated from solutions of alum and aluminum chloride by the addition of Na_2CO_3 (CO_3^{2-}:Al^{3+} molar ratio 3.00). The fresh precipitates were amorphous and still had not crystallized five months later. One reason given for the formation and persistence of the amorphous state is substitution of Cl^- for OH^- (Turner and Ross, 1970). The precipitate that was prepared from aluminum chloride solution analyzed 26.9% Al, 8.7% Na, 2.0% Cl, and the rest assumed to be OH. Hence, Na was

incorporated from Na_2CO_3. The precipitate that was prepared from alum analyzed 27.8% Al, 6.3% Na, 0.6% S, and the rest assumed to be OH. The S represents SO_4^{2-} substituting for OH^-, while Na was again incorporated from Na_2CO_3. Both precipitates were, therefore, deficient in Al (34.6% Al in $Al(OH)_3$) owing to replacement by Na.

The quantity of Na_2CO_3 added in each test was calculated to neutralize the acid produced by Al^{3+} hydrolysis. The pertinent reactions are summarized by Equations 2-13 to 2-15.

$$Al^{3+} + 3\ H_2O \rightarrow Al(OH)_3(am) + 3\ H^+ \qquad (Al^{3+}\ \text{hydrolysis}) \qquad (2\text{-}13)$$

$$3\ H^+ + 3\ CO_3^{2-} \rightarrow 3\ HCO_3^- \qquad (\text{acid neutralization}) \qquad (2\text{-}14)$$

$$Al^{3+} + 3\ H_2O + 3\ CO_3^{2-} \rightarrow Al(OH)_3(am) + 3\ HCO_3^- \qquad (\text{overall reaction}) \qquad (2\text{-}15)$$

Table 2-27. pH values in chemical coagulation.

Coagulant	Measurement	Dosage, mg/L Al				
		10	25	40	60	100
Alum	Temperature, ℃	22.2	22.1	22.2	22.4	22.2
	Feed suspension pH before Na_2CO_3 addition	8.62	8.68	8.52	8.40	8.56
	Feed suspension pH after Na_2CO_3 addition	10.00	10.34	10.44	10.46	10.64
	Coagulated slurry pH	7.16	7.27	7.25	7.54	7.37
	Supernatant pH	7.46	7.48	7.40	7.40	7.59
Aluminum chloride	Temperature, ℃	22.3	22.1	22.2	22.2	22.0
	Feed suspension pH before Na_2CO_3 addition	8.60	8.64	8.75	8.44	8.60
	Feed suspension pH after Na_2CO_3 addition	10.03	10.33	10.49	10.53	10.58
	Coagulated slurry pH	7.34	7.56	7.61	7.69	7.58
	Supernatant pH	7.74	7.79	7.83	7.90	7.88

Bicarbonate is shown as the reaction product from carbonate because the final pH of the coagulated slurries varied between 7 and 8. This pH range falls within the domain of HCO_3^- predominance ($pK_{a,1}$ = 6.4 and $pK_{a,2}$ = 10.4 at the test temperature) (Snoeyink and Jenkins, 1980). The pH measurements are recorded in Table 2-27. The feed suspension pH varied from 8.4 to 8.8 before Na_2CO_3 addition. Addition of Na_2CO_3 raised the suspension pH to 10.0 and higher, according to the quantity added. Immediately upon addition of the coagulant, coagulation occurred. The final pH of the coagulated slurries varied from 7.2 to 7.7. The supernatant pH, which ranged from 7.4 to 7.9, was generally higher than that of the coagulated slurry.

In the basic range (pH≥10), all of the added aluminum precipitated at all dosage levels studied, such that the supernatants analyzed below the detection limit at <1 mg/L Al. As Figures 2-46 and 2-47 clearly show, the precipitate bulked up the sediment volume.

Reference to Figure 2-15 reveals that the electrocoagulation time of 55 minutes at 70.2 A/m^2 current density would give the maximum initial settling rate (5.6 cm/min) that was produced by chemical coagulation. About 3 mg/L total Al would remain in the supernatant (Figure 2-18), and the mass ratio of adsorbed aluminum to silica would be about 0.3 mg Al/g silica (Figure 2-19). Since, in chemical coagulation, all of the aluminum reported to the solids as a precipitate, the corresponding mass ratio giving the maximum initial settling rate was calculated to be 0.6 and 0.5 mg Al/g silica for alum and aluminum chloride, respectively. Hence, electrocoagulation utilized a significantly smaller quantity of aluminum species to achieve the same initial settling rate of silica as chemical coagulation achieved. The difference may be attributed jointly to the aluminum speciations engendered by the two systems and to the coagulation mechanisms (interparticle bridging by Al complexes in AC/EC and sweep floc in chemical coagulation).

Alum and aluminum chloride were tested in the absence of Na_2CO_3 at the dosage level of 100 mg/L Al. Table 2-28 shows that alum was effective over a wider pH range than was aluminum chloride. In fact, the initial settling rate of silica (1.7×10^{-3} cm/min for aluminum chloride) was identical to that of as-received silica (1.6×10^{-3} cm/min) in de-ionized water containing 200 mg/L NaCl. Hence, aluminum chloride did not enhance the settling behaviour of silica in the working

pH range of 8.4 to 4.4, while alum achieved an initial settling rate of 1.1 cm/min. The absence of Na_2CO_3 caused the pH to dive out of the effective range of $AlCl_3$ (Duan and Gregory, 2003).

Table 2-28. Coagulant performance in the absence of Na_2CO_3.

Measurement	Coagulant	
	Alum	Aluminum Chloride
Dosage, mg/L Al	100	100
Temperature, °C	22.1	21.8
Feed suspension pH	8.7	8.4
Coagulated slurry pH	4.3	4.4
Supernatant pH	4.4	no data*
Initial settling rate, cm/min	1.1	$1.7x10^{-3}$
Residual Al in supernatant, mg/L	90.5	no data*

*No supernatant formed; stable suspension persisted.

The supernatant, that was created by alum coagulation, analyzed 90.5 mg/L Al. This was the residual concentration when Al^{3+} hydrolysis was curtailed by the decreasing pH.

2.6 CHAPTER SUMMARY

Agitation has been demonstrated to be beneficial, but not essential, to the electrocoagulation process. Interparticle proximity in suspensions of high solids concentration facilitated collision in promoting electrocoagulation within certain limits of AC/EC retention time. The benefit from agitation increased with retention time as larger dosages of aluminum were released from the electrodes for distribution amongst the silica particles. Agitation was also shown to be capable of reducing the electrocoagulation time for achieving a given initial settling rate. In practical application, the continuous flow of suspension through the cell is expected to provide adequate agitation, obviating the need for a separate mixer.

Electrocoagulation offers the flexibility of operating in either the indirect or direct mode. In the indirect mode, the aqueous dispersion medium is subjected to AC/EC treatment and is then slurried with the solids, inside or outside the cell. The indirect mode facilitates the study of chemical changes occurring in the dispersion medium, and it gave the faster initial settling rates for AC/EC retention

times of up to 55 minutes. In the direct mode, on the other hand, the suspension is electrocoagulated in the cell. For retention times exceeding 55 minutes, this mode was much superior to the indirect mode in enhancing the settling behaviour of silica.

In the absence of aluminum hydroxide precipitation, floc growth by indirect electrocoagulation was more rapid than by the direct mode because of the contact between the silica and the higher aluminum dosage in the AC/EC-treated water. The initial settling rate increased with electrocoagulation time. However, when precipitation occurred, the floc growth was limited in accordance with the fraction of efficient coagulative species removed from solution. Charge reversal was observed to accompany precipitation.

In the absence of precipitation, the initial settling rate of directly electrocoagulated silica was controlled by floc size, both of which increased with electrocoagulation time. The precipitation of aluminum hydroxide, however, did not adversely affect settling behaviour, but the mechanism controlling the settling behaviour changed. Although floc size decreased, inferably the result of fragmentation at sites bridged by precipitate particles, the flocs became less porous as precipitate particles were adsorbed in the pores. As a result of the general adsorption of precipitate particles onto the flocs, the increased floc density negated the effect of fragmentation on settling behaviour. Indeed, the settling behaviour was enhanced, perhaps with assistance from enmeshment by the precipitate. Hence, of the two electrocoagulation modes, the direct mode facilitated settling behaviour enhancement at longer electrocoagulation times. The zeta potential decreased with electrocoagulation time. For both modes of electrocoagulation, the changes in zeta potential are considered to be indicative of the charge of the adsorbed complexes.

Air-dried electrocoagulated silica, which had been stored for more than a year, was observed to coagulate as-received silica. This observation leads to the following conclusions.

1. Electrocoagulated silica is, itself, a practical coagulant. As such, it could possibly be used to coagulate particles of suspended materials other than silica.
2. The coagulative property of electrocoagulated silica has a long “shelf life”.

3. Not all of the as-received material needs to be electrocoagulated for enhanced settling behaviour to be achieved in the bulk. Treated and untreated material can be blended for enhanced settling of the whole.

Electrocoagulated silica has the advantage that, as a coagulant, it does not introduce any noxious constituents into the process stream it is meant to treat.

Energy requirements were similar for the two modes of electrocoagulation.

Adsorption of dissolved aluminum species was higher in indirect electrocoagulation. Higher initial settling rates also resulted, provided aluminum hydroxide did not precipitate. Hence, lower concentrations of residual aluminum were found in supernatants derived from indirect electrocoagulation. In both modes of electrocoagulation, it may be inferred that multilayer adsorption occurred in proportion to the aluminum concentration gradient between the bulk solution and the particle surface.

In AC/EC treatment of the feed water (*i.e.*, indirect mode) and feed suspension (*i.e.*, direct mode), the net pH change was negative for some initial period. As the electrocoagulation time was extended, zero and positive net pH changes were registered. At sufficiently long electrocoagulation times, the system attained an equilibrium or steady state between aluminum complexation and aluminum hydroxide precipitation at pH 8.6. Equilibrium was attained earlier in indirect electrocoagulation because dissolved aluminum accumulated in the water. In direct electrocoagulation, however, aluminum was adsorbed continuously as it entered solution, and accumulation occurred only when the adsorption rate decayed sufficiently.

One day's ageing was detrimental to the settling behaviour of silica that was electrocoagulated indirectly in the absence of precipitation. Initial settling rate deterioration, which was as high as 50%, is attributed to degradation of the efficient coagulative aluminum species to species of lower molecular weight and, hence, lower coagulative capacity. Consequently, the flocs are considered to have collapsed, as indicated by reduced porosity. Ageing did not seriously affect the settling behaviour of silica that was indirectly electrocoagulated with water from which substantial quantities of aluminum had precipitated. Smaller decreases of porosity resulted.

Ageing for one day effected dramatic enhancement of the initial settling rate of up to 178% in silica that had been electrocoagulated directly for periods between 15 and 110 minutes. Either growth or degeneration of flocs occurred, despite reduced porosity. Floc growth is ascribed to re-aggregation to a denser configuration possessing a larger limiting floc size. Floc degeneration has already been addressed for aged, indirectly electrocoagulated silica. Porosity increase, observed in the 90- and 120-minute electrocoagulates, is imputed to redissolution of aluminum hydroxide precipitates. Floc growth in the 90-minute electrocoagulate is considered to have resulted from the formation of new, efficient coagulative species. The settling behaviour of silica, electrocoagulated for 15 minutes and for more than 110 minutes, declined upon ageing.

Interruption of the electrocoagulation process proved not to be detrimental to the enhancement of settling behaviour. Indeed, the initial settling rate was higher for cumulatively treated silica than for the continuously treated material after 15 minutes' electrocoagulation. The difference in settling rate probably resulted from different rates of pH change during electrocoagulation. Nevertheless, the results show that under-coagulated material can be re-treated to achieve a higher initial settling rate or larger floc size.

Initial settling rate increased with current density up to 117.0 A/m^2, beyond which further current density increase to 167.2 A/m^2 did not engender further enhancement. The onset of enhanced settling behaviour was attained at progressively shorter electrocoagulation times as current density was increased. Hence, the electrocoagulation time required to achieve a given initial settling rate shortened with increasing current density, but the benefit of the time savings was negated by the increased energy demand. Therefore, in the design of an electrocoagulation unit process, an energy audit would play an instrumental role in the selection of the process parameters.

At low current densities, the system entered an induction period, the duration of which shortened with increasing current density. At one extreme, the system failed to emerge from the induction stage when a current density of 3.3 A/m^2 was employed. At the other extreme, the induction stage was eliminated at sufficiently high current density.

The critical Al dosage, at which the onset of enhanced settling behaviour occurred, was estimated to be 3.3 mg/L, giving a critical absorption mass ratio of

0.06 mg Al/g silica. In the dosage range studied, a dosage exceeding 10 mg/L did not enhance the initial settling rate further.

In electrocoagulation with equal quantities of electricity, the larger current produced the greater enhancement of settling behaviour.

Destabilization of the suspension is considered to be characterized by a pH decrease. With AC/EC time, the pH reaches a minimum which signifies the end of the destabilization process. Therefore, the net pH change for the process is always negative. Floc growth, on the other hand, is considered to be characterized by a pH increase from the minimum, and could involve either a negative or positive net change.

Compared to aluminum chloride, alum was effective over a wider pH range in enhancing settling behaviour, but aluminum chloride achieved the maximum initial settling rate at a lower Al dosage (~25 mg/L *vs*. ~30 mg/L for alum).

Chemical coagulants, such as alum and aluminum chloride, are routinely used at ambient temperature for water treatment. AC/EC, on the other hand, would be more appropriately applied to suspensions than to raw water, and especially to tailings. Such waste streams are normally above ambient temperature. Consequently, the chemical coagulation tests were performed at room temperature, while the temperature in the electrocoagulation tests was allowed to rise by Joule heating. The effectiveness of both chemical coagulation and electrocoagulation depends on the aluminum dosage. In addition to the dosage, pH and temperature influence the effectiveness of coagulation, mainly by determining the speciation (*i.e.*, the identity and distribution of ionic species) of the aluminum dose.

Chemical coagulation produced bulkier sediments than did direct AC/EC in achieving the same initial settling rate. The bulkier sediments require a greater capacity for solid-liquid separation (*i.e.*, a larger number or size of thickeners, filters, *etc.*) than that required by an electrocoagulation process for treating the same solids feed rate to achieve the same enhancement in settling behaviour. Electrocoagulation, however, requires high energy input which would represent a major portion of the operating cost. On the other hand, the cost of chemical coagulants is a major fraction of the operating cost of a water treatment plant.

Chemical coagulation and direct electrocoagulation are conducted *in situ* but utilize the aluminum dose differently. For example, for the maximum initial settling rate achieved by chemical coagulation in this study, the mass adsorption ratios were calculated to be 0.6 and 0.5 mg Al/g silica for alum and aluminum chloride, respectively, compared to 0.3 mg Al/g silica for electrocoagulation. These data demonstrate that electrocoagulation utilized dissolved aluminum more sparingly than did chemical coagulation in achieving the same initial settling rate.

2.7 REFERENCES

American Water Works Association (1977), Simplified Procedures for Water Examination: AWWA Manual M12. AWWA, pp. 68-78.

Amirtharajah A. and O'Melia C.R. (1990), Coagulation processes: destabilization, mixing, and flocculation. In Pontius F.W. (Ed.), Water Quality and Treatment, Fourth Edition. McGraw-Hill, Inc., New York, pp. 269-365.

ASTM (1996), Annual Book of ASTM Standards, Volume 05.01. American Society for Testing and Materials, Philadelphia, PA, pp. 162-191.

ASTM (1997), Annual Book of ASTM Standards, Volume 04.08. American Society for Testing and Materials, Philadelphia, PA, pp. 10-16.

Ayyala S., Pugh R.J. and Forssberg E. (1995), Aggregate characteristics in coagulation and flocculation. *Miner. Process. Extrac. Metall. Rev.*, **12**, 165-184.

Baes C.F. and Mesmer R.E. (1976), The Hydrolysis of Cations. John Wiley & Sons, New York, pp. 112-123.

Barkley N.P., Farrell C.W. and Gardner-Clayson T.W. (1993), Alternating current electrocoagulation for Superfund site remediation. *J. Air Waste Management Assoc.*, **43**, 784-789.

Beecroft J.R.D., Koether M.C. and vanLoon G.W. (1995), The chemical nature of precipitates formed in solutions of partially neutralized aluminum sulphate. *Wat. Res.*, **29**, 1461-1464.

Bertsch P.M. (1989), Aqueous polynuclear aluminum species. In Sposito G. (Ed.), The Environmental Chemistry of Aluminum. CRC Press, Inc., Boca Raton, FL, pp. 87-115.

Black A.P. (1967), Electrokinetic characteristics of hydrous oxides of aluminum and iron. In Principles and Applications of Water Chemistry (Edited by Faust S.D. and Hunter J.V.). John Wiley & Sons, Inc., New York, pp. 274-300.

Bottéro J.Y., Poirier J.E. and Fiessinger F. (1980b), Study of partially neutralized aqueous aluminium chloride solutions: identification of aluminium species and relation between the composition of the solutions and their efficiency as a coagulant. *Prog. Wat. Tech.*, **12**, 601-612.

Bouyer D., Coufort C., Liné, A. and Zdravka D-Q. (2005), Experimental analysis of floc size distributions in a 1-L jar under different hydrodynamics and physicochemical conditions. *J. Colloid Interface Sci.*, **292**, 413-428.

Brewster M.D. and Passmore R.J. (1994), Use of electrochemical iron generation for removing heavy metals from contaminated groundwater. *Environ. Progress*, **13**, 143-148.

Cañizares P., Jiménez, C., Martínez F., Rodrigo M.A. and Sáez C. (2009), The pH as a key parameter in the choice between coagulation and electrocoagulation for the treatment of wastewaters. *J. Hazard. Mater.*, **163**, 158-164.

Cañizares P., Martínez F., Jiménez, C., Lobato J. and Rodrigo M.A. (2006), Comparison of the aluminum speciation in chemical and electrochemical dosing processes. *Ind. Eng. Chem. Res.*, **45**, 8749-8756.

Cohen J.M. and Hannah S.A. (1971), Coagulation and flocculation. In Water Quality and Treatment – A Handbook of Public Water Supplies, Third Edition. McGraw-Hill Book Company, New York, pp. 66-122.

Coufort C., Bouyer D. and Liné, A. (2005), Flocculation related to local hydrodynamics in a Taylor-Couette reactor and in a jar. *Chem. Eng. Sci.*, **60**, 2179-2192.

Dentel S.K. and Gossett J.M. (1988), Mechanisms of coagulation with aluminum salts. *JAWWA*, **80**, 187-198.

Duan J. and Gregory J. (2003), Coagulation by hydrolysing metal salts. *Advances Colloid Interface Sci.*, **100-102**, 475-502.

Gao B., Yue Q. and Wang B. (2002), The chemical species distribution and transformation of polyaluminum silicate chloride coagulant. *Chemosphere*, **46**, 809-813.

Greenberg A.E., Clesceri L.S. and Eaton A.D. (Eds.) (1992), Standard Methods for the Examination of Water and Wastewater, 18th Edition. Published jointly by American Public Health Association, American Water Works Association and Water Environment Federation, Washington, DC, pp. 2-53 to 2-55.

Gregory J. (1988), Polymer adsorption and flocculation in sheared suspensions. *Colloids Surfaces*, **31**, 231-253.

Gregory J. (1993), The role of colloidal interactions in solid-liquid separation. *Water Sci. Technol.*, **27**, 1-17.

Gregory J. and Duan J. (2001), Hydrolyzing metal salts as coagulants. *Pure Appl. Chem.*, **73**, 2017-2026.

Grøterud O. and Smoczynski L. (1992), Purification of wastewater by electrolysis at continuous flow. *J. Wat. Manage. Res.-Sweden*, **48**, 36-40.

Hahn H.H. and Stumm W. (1968), Coagulation of Al(III). The role of adsorption of hydrolyzed aluminum in the kinetics of coagulation. In Adsorption from Aqueous Solution (Edited by Gould R.F.). Advances in Chemistry Series 79, ACS, Washington, DC, pp. 91-111.

Ham R.K. and Christman R.F. (1969), Agglomerate size changes in coagulation. *J. San. Eng. Div., Proc. ASCE*, **95**(SA3), 481-502.

Harif T. and Adin A. (2007), Characteristics of aggregates formed by electroflocculation of a colloidal suspension. *Water Res.*, **41**, 2951-2961.

Hayden P.L. and Rubin A.J. (1974), Systematic investigation of the hydrolysis and precipitation of aluminum(III). In Rubin A.J. (Ed.), Aqueous-Environmental Chemistry of Metals. Ann Arbor Science Publishers, Inc., Ann Arbor, MI.

Hem J.D. and Roberson C.E. (1967), Form and stability of aluminum hydroxide complexes in dilute solution. Geological Survey Water-Supply Paper 1827-A, US Government Printing Office, Washington, 55 p.

Hogg R., Bunnaul P. and Suharyono H. (1993), Chemical and physical variables in polymer-induced flocculation. *Miner. Metall. Process.*, **10**, 81-85.

Holt P.K., Barton G.W., Wark M. and Mitchell C.A. (2002), A quantitative comparison between chemical dosing and electrocoagulation. *Colloids Surfaces A*, **211**, 233-248.

Hsu P.H. (1992), Reaction of OH-Al polymers with smectites and vermiculites. *Clays and Clay Minerals*, **40**, 300-305.

Huang C.P. (1981), The surface acidity of hydrous solids. In Anderson M.A. and Rubin A.J. (Eds.), Adsorption of Inorganics at Solid-Liquid Interfaces. Ann Arbor Science Publishers Inc., Ann Arbor, MI, pp. 183-218.

Hunter R.J. (1981), Zeta Potential in Colloid Science. Academic Press, London, pp. 132-344.

Jenke D.R. and Diebold F.E. (1984), Electroprecipitation treatment of acid mine wastewater. *Wat. Res.*, **18**, 855-859.

Kinniburgh D.G. and Jackson M.L. (1981), Cation adsorption by hydrous metal oxides and clay. In Anderson M.A. and Rubin A.J. (Eds.), Adsorption of Inorganics at Solid-Liquid Interfaces. Ann Arbor Science Publishers Inc., Ann Arbor, MI, pp. 91-160.

Letterman R.D., Vanderbrook S.G. and Sricharoenchaikit P. (1982), Electrophoretic mobility measurements in coagulation with aluminum salts. *JAWWA*, **74**, 44-51.

Lyklema J. (1978), Surface chemistry of colloids in connection with stability. In Ives K.J. (Ed.), The Scientific Basis of Flocculation. Sijthoff & Noordhoff, The Netherlands, pp. 1-36.

MacKinnon M.D. (1986), Environmental aspects of waste water management at an oil sands development in northern Alberta. In Proceedings of SPIB Conference on "Northern Hydrocarbon Development, Environmental Problem Solving" (Edited by Lewis M.L.). Banff, Alberta, pp. 191-208.

Masliyah J.H. (1994), Electrokinetic Transport Phenomena. AOSTRA Technical Publication Series #12, Edmonton, Canada, 363 p.

Montgomery J.M., Consulting Engineers, Inc. (1985), Water Treatment Principles and Design. John Wiley & Sons, New York, pp. 124-125.

Moreno H.A., Cocke D.L., Gomes J.A.G., Morkovsky P., Parga J.R., Peterson E. and Garcia C. (2009), Electrochemical reactions for electrocoagulation using iron electrodes. *Ind. Eng. Chem. Res.*, **48**, 2275-2282.

Ofir E., Oren Y. and Adin A. (2007), Electroflocculation: the effect of zeta-potential on particle size. *Desalination*, **204**, 33-38.

O'Melia C.R. (1986), Polymeric inorganic flocculants. In Moudgil B.M. and Somasundaran P. (Eds.), Flocculation, Sedimentation and Consolidation.

Proceedings of the Engineering Foundation Conference, Georgia, AIChE, pp. 159-169.

Orvig C. (1993), The aqueous coordination chemistry of aluminum. In Robinson G.H. (Ed.), Coordination Chemistry of Aluminum. VCH, New York, pp. 85-121.

Pokras L. (1956), On the species present in aqueous solutions of "salts" of polyvalent metals. *J. Chem. Educ.*, **33**, 152-161.

Pretorius W.A., Johannes W.G. and Lempert G.G. (1991), Electrolytic iron flocculant production with a bipolar electrode in series arrangement. *Water SA*, **17**, 133-138.

Rank Brothers (1986), Operating Instructions and Manual for the Particle Micro-electrophoresis Apparatus Mark II. Rank Brothers, Cambridge, England, 27 p.

Riddick T.M. (1968), Control of Colloid Stability through Zeta Potential, Vol. I. Livingston Publishing Company, Pennsylvania, pp. 21-24.

Sawyer C.N., McCarty P.L. and Parkin G.F. (1994), Chemistry for Environmental Engineering, 4th Edition. McGraw-Hill, Inc., New York, pp. 327-341.

Scott R.P.W. (1993), Silica Gel and Bonded Phases: Their Production, Properties and Use in LC. John Wiley & Sons, New York, pp. 3-80.

Sharma S.K., Stanley D.A. and Harris J. (1994), Determining the effect of physicochemical parameters on floc size using a population balance model. *Miner. Metall. Process.*, **11**, 168-173.

Smith R.W. (1971), Relations among equilibrium and nonequilibrium aqueous species of aluminum hydroxyl complexes. In Gould R.F. (Ed.), Nonequilibrium Systems in Natural Water Chemistry. Advances in Chemistry Series 106. ACS, Washington, DC, pp. 250-279.

Snoeyink V.L. and Jenkins D. (1980), Water Chemistry. John Wiley & Sons, New York, pp. 197-241.

Solomentseva I.M., Barany S. and Gregory J. (2004), Surface properties and aggregation of basic aluminum sulphate hydrolysis products: 1. Electrokinetic potential and hydration of BAS hydrolysis product particles. *Colloids Surfaces A*, **230**, 117-129.

Spears D.R. and Stanley D.A. (1994), Study of shear-flocculation of silica. *Miner. Metall. Process.*, **11**, 5-11.

Stumm W. (1992), Chemistry of the Solid-Water Interface. Wiley-Interscience, New York, pp. 13-38.

Stumm W. and Morgan J.J. (1970), Aquatic Chemistry. Wiley-Interscience, New York, pp. 238-262.

Stumm W. and Morgan J.J. (1981), Aquatic Chemistry: An Introduction Emphasizing Chemical Equilibria in Natural Waters. John Wiley & Sons, New York, pp. 241-242.

Stumm W. and O'Melia C.R. (1968), Stoichiometry of coagulation. *JAWWA*, **60**, 514-539.

Tambo N. (1991), Basic concepts and innovative turn of coagulation/flocculation. *Water Supply*, **9**, Jönköping, 1-10.

Tambo N. and Watanabe Y. (1979), Physical characteristics of flocs – I. The floc density function and aluminum floc. *Wat. Res.*, **13**, 409-419.

Trompette J.L. and Vergnes H. (2009), On the crucial influence of some supporting electrolytes during electrocoagulation in the presence of aluminum electrodes. *J. Hazard. Mater.*, **163**, 1282-1288.

Tsai P.P. and Hsu P.H. (1984), Studies of aged OH-Al solutions using kinetics of Al-ferron reactions and sulfate precipitation. *Soil Sci. Soc. Am. J.*, **48**, 59-65.

Turner R.C. and Ross G.J. (1970), Conditions in solution during the formation of gibbsite in dilute Al salt solutions. 4. Effect of Cl concentration and temperature and a proposed mechanism for gibbsite formation. *Can. J. Chem.*, **48**, 723-729.

Un U.T., Koparal A.S. and Ogutveren U.B. (2009), Electrocoagulation of vegetable oil refinery wastewater using aluminum electrodes. *J. Environ. Manage.*, **90**, 428-433.

Vik E.A., Carlson D.A., Eikum A.S. and Gjessing E.T. (1984), Electrocoagulation of potable water. *Wat. Res.*, **18**, 1355-1360.

Wang Y., Gao B-Y., Xu X-M., Xu W-Y. and Xu G-Y. (2009), Characterization of floc size, strength and structure in various aluminum coagulants treatment. *J. Colloid Interface Sci.*, **332**, 354-359.

Weast R.C. (Ed.) (1989), CRC Handbook of Chemistry and Physics, 70th Edition. CRC Press, Inc., Boca Raton, Florida, p. F-146.

— (1995), MET E 331/MET E 533 Laboratory Experiments, Mineral Processing, Winter 1995. Department of Mining, Metallurgical and Petroleum Engineering, The University of Alberta, pp. L2-1 to L2-18.

Xiao F., Zhang X. and Lee C. (2008), Is electrophoretic mobility determination meaningful for aluminum(III) coagulation of kaolinite suspension? *J. Colloid Interface Sci.*, **327**, 348-353.

Yildiz Y.Ş., Koparal A.S. and Keskinler B. (2008), Effect of initial pH and supporting electrolyte on the treatment of water containing high concentration of humic substances by electrocoagulation. *Chem. Eng. J.*, **138**, 63-72.

Zbik M.S., Smart R.S. and Morris G.E. (2008), Kaolinite flocculation structure. *J. Colloid Interface Sci.*, **328**, 73-80.

CHAPTER 3

INFLUENCE OF WATER CONDITIONS ON A.C. ELECTROCOAGULATION OF FINE SILICA

3.1 INTRODUCTION

It is well established that aluminum speciation, specifically hydroxyl complexes, governs coagulation (*e.g.*, Bottéro *et al.*, 1980a; Brinker and Scherer, 1990; Buffle, 1988; Jiang and Graham, 1996), to the extent that pre-polymerized coagulants, such as polyaluminum chloride (alternatively designated PAC or PACl), are widely used in Japan, many European Community countries and China for potable and waste water treatment (Wang *et al.*, 2002; Gao *et al.*, 2002; Jiang and Graham, 1996; O'Melia, 1986; Tambo, 1991). Polyaluminum chloride contains complex aluminum species, such as $Al(OH)_4^-$ and $Al_{13}O_4(OH)_{24}^{7+}$, and is prepared by the careful neutralization of acidic aluminum chloride solution with base to a predetermined OH:Al molar ratio. Such partially neutralized aluminum solutions have been studied extensively (Gao and Yue, 2005; Wang *et al.*, 2009; Akitt and Mann, 1981; Bertsch, 1987; Sullivan and Singley, 1968; Stol *et al.*, 1976; Waters and Henty, 1977). The large hydroxoaluminum complex, $Al_{13}O_4(OH)_{24}^{7+}$ (also connoted by "Al_{13}") is considered to be the most effective coagulative aluminum species (Jiang and Graham, 1996).

In the case of stable particulate suspensions, any condition of the dispersion medium which affects aluminum speciation, affects the coagulation process. Similarly, the effectiveness of AC/EC would be influenced by conditions prevailing in the dispersion medium. Hence, a study was undertaken to evaluate the extents of the influences exercised on the electrocoagulation of fine silica by three feed water conditions: specific conductivity, pH and temperature. Analysis of the test results constitutes the subject of this chapter.

3.2 THEORY AND BACKGROUND

The application of electrospray ionization mass spectrometry to the identification of aluminum species in aqueous solution has generated results that have shed considerable light on aluminum speciation (Sarpola *et al.*, 2004a; Sarpola *et al.*, 2004b; Sarpola *et al.*, 2006; Zhao *et al.*, 2009). It is agreed that dissolved aluminum exists as $Al(H_2O)_6^{3+}$ at pH < 3 (Baes and Mesmer, 1976; Orvig, 1993; Zelazny and Jardine, 1989). With increasing pH, hydrolysis of $Al(H_2O)_6^{3+}$ occurs in an apparently stepwise manner to form the following mononuclear species: $AlOH(H_2O)_5^{2+}$, $Al(OH)_2(H_2O)_4^{+}$, $Al(OH)_3(H_2O)_3^{o}$ and $Al(OH)_4(H_2O)_2^{-}$, the last of which, until relatively recently, was known to be the only verified anion (Baes and Mesmer, 1976; Duan and Gregory, 2003). Sarpola *et al.* (2004a) have since identified 45 univalent anions (Al_1 to Al_{12}) and 9 polyvalent anions (Al_{10} to Al_{32}) in the pH range of 3.27 to 4.20.

There is doubt about the existence of the neutral mononuclear species (Bertsch, 1989), although Baes and Mesmer (1976), Bottéro *et al.* (1980b) and Zelazny and Jardine (1989) among others, accepted its existence. Until the work of Sarpola *et al.* (2004a) was published, however, much controversy surrounded the identities of the polynuclear species. The complexes, $Al_{13}O_4(OH)_{24}(H_2O)_{12}^{7+}$ and $Al_2(OH)_2(H_2O)_8^{4+}$, were positively identified (*e.g.*, Waters and Henty, 1977; Akitt and Farthing, 1978; Akitt and Mann, 1981). In addition, $Al_3(OH)_4(H_2O)_{10}^{5+}$ had been identified (Orvig, 1993). Considerable doubt, however, was still attached to the existence of complexes like (coordinated water omitted for simplicity) $Al_6(OH)_{15}^{3+}$, $Al_7(OH)_{17}^{4+}$ and $Al_8(OH)_{20}^{4+}$ (Bertsch, 1989). Indeed, Hunt (1965) inferred that Al polymerization could continue indefinitely by –O– and $-\overset{H}{O}-$ bridging, enabling the visualization of a large number of complex species. Consistent with this idea, Stol *et al.* (1976) listed 24 possible complexes that may be formed. In addition to the anions mentioned above, Sarpola *et al.* identified over 80 univalent cations (Al_2 to Al_{13}) and 19 polyvalent cations (Al_{10} to Al_{27}). They further highlighted the competition existing between the OH^- and Cl^- ligands

for constitution of the complexes. With increasing concentration in the solution, chloride replaced hydroxyl more successfully. Examples of the competition are:

$$Al_2(OH)_4Cl^+ \text{ and } Al_2(OH)_3Cl_2^+, \text{ and}$$

$$Al_3O_4(OH)Na^+ \text{ and } Al_3O_4NaCl^+.$$

In further work, Sarpola *et al.* (2006) demonstrated that the speciation changed with pH, age, and total concentration of dissolved aluminum.

In light of the foregoing discussion, therefore, no possible species is discarded out of hand in the current study. Furthermore, reports on aluminum speciation are based on neutralization studies, the conditions of which make for slow kinetics of polymer and other polynuclear Al species formation. AC/EC, on the other hand, is considered to accelerate the formation kinetics and, as such, can reasonably be expected to produce complexes whose existence was disputed. In addition, no report on aluminum speciation generated electrolytically has been found in the published literature. It is also an entirely feasible notion that some Al species are transient, lasting long enough to coagulate silica in either mode of electrocoagulation, for example.

Since reports on the variation of aluminum speciation with temperature are rare, discussion of the subject is open to conjecture. From their study of the effect of temperature (10° to 40°C) on ageing of partially neutralized $AlCl_3$ solutions, Turner and Ross (1970) found that polynuclear Al species persisted longer at low temperature. Otherwise, they formed mononuclear species and aluminum hydroxide precipitates, the latter representing the bulk of the transformed polynuclear species. The precipitation rate increased with temperature.

The influence of ionic strength (5.85×10^{-2} to 1.95×10^{-1} M Al_T and 6.2 to 20.8 g/L Cl^-) was also studied by Turner and Ross (1970) who showed that Al polynuclear species survived longer at the higher concentrations of total Al and Cl^- at 26°C. They concluded that the Cl^- ligand competed with the OH^- ligand in the formation of aluminum hydroxide precipitate. When Cl^- replaced OH^- partially, the precipitate was amorphous, but crystallized to gibbsite after Cl^- removal from the solids. Low Cl^- concentration in the mother liquor facilitated crystallization of the precipitate upon ageing (Turner, 1968). Hsu (1966) demonstrated that aluminum hydroxide precipitation was effected immediately by high NaCl concentrations (0.6 and 1.2 M) while, at low concentration (0.12 M NaCl),

precipitation did not occur for a year. The hydroxide that was precipitated at high NaCl concentrations was amorphous for over a year, but two weeks after removal of NaCl by dialysis, crystallization occurred.

Consultation with faculty members of the Chemistry Departments at the University of Alberta and Queen's University, Kingston, Ontario, has revealed that no satisfactory, single method exists for the unambiguous identification of all aluminum species present in a water sample. Ion chromatography was dropped from consideration because withdrawal of aluminum species from the sample disturbs the equilibrium distribution of the species. The ferron method and its modifications (Turner, 1969; Smith and Hem, 1972; Tsai and Hsu, 1984; Cañizares *et al.*, 2006; Gao *et al.*, 2002) are capable only of distinguishing between mononuclear and polynuclear species and, in the latter group, between fast- and slow-reacting polynuclear species. Analysis of the fast-reacting species by ^{27}Al nuclear magnetic resonance (NMR) showed Al_{13} to be present, but the members of the slow-reacting species could not be detected by NMR (Hsu, 1992). It seems reasonable, therefore, to suggest that Al_{13} might not have been the only member of the fast-reacting species. Indeed, there might be at least two members (Tsai and Hsu, 1984). Identification of individual Al species by the ferron method is, therefore, not advantageous to the objectives of the current work. ^{27}Al NMR is unable to distinguish between the hydroxyl ligand and coordinated water, being best suited for systems in which the constituent of interest is very different from the solvent. In addition, the low concentrations of total Al encountered in this study and the inherent, low sensitivity of NMR to aluminum in aqueous solution, seriously limit the usefulness of this analytical method to the purpose at hand. Raman spectroscopy and Fourier transform infrared (FTIR) analysis also proved unsuitable. Mass spectroscopy appears to offer the best chance for Al species identification because it measures the molecular mass and ion charge, expressing the m/z ratio in daltons. Species in a wide range of molecular mass can be analyzed and the sensitivity is at the µM level of concentration. Hence, the 10^{-5} to 10^{-3} M range of total aluminum concentrations generated in this study is within the analytical capability of mass spectroscopy.

Equilibrium aluminum speciation at 25°C varies with pH and concentration of total Al as is clearly shown in Figure 1-7. In addition to

determining Al speciation, pH also influences adsorption, to the extent that Schindler (1981) described pH as " . . . the master variable that governs the extent of adsorption . . . ". This description implies that the extent to which a metal ion is adsorbed depends upon the metal species, as supported by Kinniburgh and Jackson (1981) who stated further that small pH changes can effect relatively large changes in the adsorption of polynuclear ions. These authors concur with Stumm and Morgan (1970) and with Dentel and Gossett (1988) that hydroxymetal complexes adsorb much more strongly than the simple metal ion. Adsorption of complex metal cations onto hydrous metal oxides is regularly observed to be rapid because it is a surface phenomenon; *i.e.*, the surface is readily accessible to the adsorbing species.

3.3 EXPERIMENTAL METHODS

3.3.1 Mass Balance Test

An indirect electrocoagulation test was performed to establish an aluminum mass balance and to prepare water samples for the identification of aluminum species by mass spectrometry. A current of 3.2 A was passed for 30 minutes between two electrodes immersed in 4.0 L of de-ionized water containing 20 mg/L NaCl. This concentration was employed, instead of 200 mg/L, because the latter obscured the aluminum species. As has been observed in earlier discussion (Chapter 2), the total dissolved aluminum concentration was of the order of 10 mg/L (see Table 2-9). As such, the concentrations of individual species would be <10 mg/L, necessitating reduction of the background NaCl concentration.

During AC/EC treatment of the feed water, agitation was maintained continuously at 1.75 m/s impeller tip speed. At the end of the test, 52.63 g of as-received silica was slurried with 1.0 L of AC/EC-treated water, which included aluminum hydroxide precipitate that had been formed. Samples of feed water, AC/EC-treated water (minus precipitate) and supernatant water were submitted fresh for identification of aluminum species. Duplicate water samples were acidified with a drop of concentrated hydrochloric acid and submitted for analysis of total Al by AAS. Samples of the electrode material, as-received and indirectly electrocoagulated silica, precipitate, and solids recovered from the electrode

surfaces were analyzed by AAS and EDX (energy dispersive x-ray analysis). A settling test was performed on the electrocoagulated silica.

The precipitate and solids recovered from the electrode surfaces were subjected to XRD (x-ray diffraction) analysis for identification. Photomicrographs were taken of the precipitate and indirectly electrocoagulated silica, as described in Section 2.3.5.3.

3.3.2 Identification of Dissolved Aluminum Species

Freshly AC/EC-treated water and supernatant samples from the mass balance test (Section 3.3.1), together with a blank sample of de-ionized water containing 20 mg/L NaCl, were submitted to the Chemistry Department for identification of the dissolved aluminum species. Mass spectrometric analysis was performed in positive mode (to identify cations) of electrospray ionization on a Micromass ZabSpec Hybrid Sector-TOF. The samples were infused into the electrospray source with a Harvard syringe pump at a flow rate of 10 µL/min. Prepurified nitrogen served as a spray pneumatic aid and bath gas at approximately 80°C (to evaporate water from the atomized samples). The mass spectrum was acquired by full magnetic scan over the range of 10 to 1000 daltons (*i.e.*, ionic mass-to-charge ratios, m/z, of 10 to 1000) at a rate of 10 seconds/decade. It must be noted that 1 decade is 1 order of magnitude of daltons or, more precisely, the logarithm of 10 daltons. Data acquisition and processing were achieved by an OPUS software package on a Digital Alpha station with VMS operating system.

Owing to constant heavy use of the mass spectrometer by the Chemistry Department, the samples were analyzed four days after submission. Hence, the analysis that will be discussed in this chapter describes aluminum speciation in samples that had aged four days. A request was submitted for the analysis to be performed on fresh samples in both positive and negative modes. Continued heavy demand on the instrument, in addition to extended downtime for repairs, resulted in several months of waiting. That the analysis of fresh samples could not be done in the end is considered to represent an acute loss to this thesis, especially since it would have been a novel method of identifying complex aluminum species. Besides, it would have facilitated a study of the ageing of the species by comparison with the species in the 4-day old samples.

3.3.3 Specific Conductivity Tests

The specific conductivity series involved seven 15-minute direct electrocoagulation tests with two electrodes separated by 3 cm. A 2.1-A current was passed between the electrodes while continuous agitation was imposed at an impeller tip speed of 1.73 m/s. As-received silica was dispersed at a concentration of 5.0 wt % in de-ionized water to which NaCl had been added. The NaCl concentration ranged from 200 to 3400 mg/L, giving respective specific conductivities of 420 to 6320 μS/cm (microsiemens/cm). Feed and supernatant water conductivities were measured with a Sprite Industries 6000 digital conductivity/TDS meter. Immediately before measurement, the meter was calibrated against a standard supplied by either Cole Parmer or Fisher Scientific. The feed suspension temperature and pH varied as follows: 22.2° to 22.6°C and 8.6 to 8.8.

Settling tests and zeta potential measurements were performed on both the electrocoagulated and as-received silica. Zeta potential was measured as described in Chapter 2 and Appendix B. Settling tests on electrocoagulated silica were conducted as described in Chapter 2, while those on the as-received material lasted about 17 h.

3.3.4 Feed Water pH Tests

In this suite of five tests, indirect electrocoagulation was conducted with de-ionized water containing 200 mg/L NaCl. The initial pH was varied over the range of 3.0 to 9.1 and the initial temperature was controlled at 23.3° to 23.7°C. AC/EC treatment of the feed water was achieved with two electrodes positioned 6 cm apart. Over the 15-minute retention time, the current was held constant at 2.1 A while continuous agitation was maintained at an impeller tip speed of 1.75 m/s.

For feed water of pH 3.0, 5.4 and 9.1, as-received silica was slurried with the AC/EC-treated water in various proportions, as listed in Table 3-1, for a study of the adsorption behaviour of aluminum.

Table 3-1. Proportions of as-received silica and AC/EC-treated water.

As-received Silica, g	AC/EC-treated Water, L	Wt % Solids in Slurry
52.63	1.00	5.0
26.32	0.50	5.0
15.46	0.50	3.0
10.20	0.50	2.0
5.05	0.50	1.0
2.51	0.50	0.5

Acidified samples of the feed water, AC/EC-treated water and supernatant water were analyzed for total Al concentration by AAS. The supernatant samples were derived from the 0.5-L slurries, while the 1-L slurry served in settling and floc size distribution tests. As in Chapter 2, floc size distribution was determined by the hydrometer method. Zeta potentials of the indirectly electrocoagulated silica samples were measured.

3.3.5 Feed Water Temperature Tests

Six indirect electrocoagulation tests comprised this series. From an initial pH of 6.2 at 23°C, the feed water temperature was adjusted and the pH at that temperature was recorded. Having been previously found to be inert, carbon electrodes were used to preheat the feed water, the temperatures of which were varied from 23.2° to 85.0°C.

For indirect electrocoagulation, a current of 2.1 A was passed for 15 minutes between two aluminum electrodes inserted 6 cm apart. Continuous agitation was applied at an impeller tip speed of 1.88 m/s. As-received silica (52.63 g) was slurried with the AC/EC-treated water (1.00 L) to yield a solids concentration of 5.0 wt %. Settling tests were conducted on the electrocoagulated slurry.

3.4 RESULTS AND DISCUSSION

3.4.1 Mass Balance

Mass balance calculations for Al in the AC/EC treatment of water are described in Appendix B and the results are presented in Table 3-2.

Table 3-2. Aluminum distribution in AC/EC-treated water.

Al Input			Al Output		
Source	mg	%	Source	mg	%
Electrodes (wt. loss)	202.0	100.0	AC/EC-treated water	12.0	4.1
			Precipitate	191.3	65.8
			Solids from electrodes	87.4	30.1
Total input	202.0	100.0	Total output	290.7	100.0

The 43.9% discrepancy between the input and outputs is jointly attributed to difficulty in recovering adsorbed solids from the electrode surfaces, precipitate losses and analytical inaccuracy. The adsorbed solids were scraped with a rubber spatula from the electrodes. The residual solids were then spray-washed from the electrodes with de-ionized water into a collector. The total theoretical Al output was calculated at 536.8 mg, of which the total measured output accounted for 54.2%. Of the total measured Al output, only 4.1% was in solution while 65.8% precipitated. Analyses of the solids are summarized in Table 3-3.

Table 3-3. EDX analyses.

Sample	Wt %						
	Al	Si	Mg	Fe	Cl	O	Total
Electrode material	91.8	1.0	1.6	0.4	n.d.	5.2	100.0
Precipitate	36.5	n.d.	0.3	n.d.	n.d.	63.2*	100.0
Solids from the electrodes	34.8	0.3	0.5	0.2	0.5	63.7*	100.0

n.d.: not detected * Includes H

The aluminum alloy, from which the electrodes were fabricated, analyzed 91.8% Al and 1.0% Si, along with the other elements shown in Table 3-3. Mg was incorporated into both the precipitate and the solids recovered from the electrodes. Si and Fe were not detected in the precipitate but were found in the solids recovered from the electrodes. The discrepancy between the Si analyses of the electrode material and the solids recovered from the electrodes is attributed to unrepresentative sampling and to analytical inaccuracy. Cl was not detected in the precipitate but was incorporated into the solids recovered from

the electrodes. Since Na was not detected, it is to be inferred that Cl formed an association with Mg, Fe or Al itself.

The precipitate analyzed 36.5% Al and 63.2% (O + H). If O were attributed to Mg as MgO (the state in which Mg is assumed to have resided in the alloy), 63.0% would account for the remaining (O + H), which is taken to be OH. As such, the empirical formula for the precipitate (normalized to 36.7% Al, 63.3% OH) would be $Al(OH)_{2.74}$. The precipitate was amorphous and still had not crystallized several weeks later when analyzed by XRD. Since its composition falls between $Al(OH)_3$ (34.6% Al) and AlOOH (45.0% Al), it is equivalent to a mixture of 18% AlOOH and 82% $Al(OH)_3$.

Solids recovered from the electrodes analyzed 34.8% Al, 0.3% Si, 0.5% Mg, 0.2% Fe, 0.5% Cl and 63.7% (O + H). An intermetallic compound, $Al_{3.21}Si_{0.47}$, was identified by XRD analysis. Since the EDX analysis of the solids does not support the composition of the intermetallic compound (86.8% Al, 13.2% Si), it is deduced that the solids were a mixture of $Al_{3.21}Si_{0.47}$ and aluminum hydroxide, the latter not being identifiable by XRD because of its amorphous state. If all the Si in the solids were attributed to the intermetallic compound, 2.0% Al would be associated with the Si. If oxygen were attributed to Mg as MgO and to Fe as Fe_2O_3, the remaining (O + H) would amount to 63.3%. From their neutralization studies, Turner and Ross (1970) concurred with other researchers that Cl^- replaced OH^- in aluminum hydroxide which, consequently, precipitated in the amorphous state. This state persisted if the Cl^- was not removed. It is assumed, therefore, that the Cl^- content analyzed in the solids recovered from the electrodes replaced OH^-, and its presence is ascribed to reactions which occurred in the electrical double layer at the electrodes. It is interesting to recall that, in contrast, Cl^- was not detected in the precipitate that was formed in the bulk solution. Hence, the solids recovered from the electrodes consisted of $Al_{3.21}Si_{0.47}$ and the hydroxide to which the following proportions are attributed: 32.8% Al, 63.3% OH and 0.5% Cl. These proportions yield the empirical formula, $Al(OH)_{3.06}Cl_{0.01}$, for the aluminum hydroxide which was intermixed with $Al_{3.21}Si_{0.47}$. The intermetallic compound amounted to 2.3% of the solids recovered from the electrodes. Its presence on the electrode surface is probably the result of local cell activity in which isolated Si-rich micro-areas in the electrodes behaved cathodically.

As-received silica analyzed 0.59% Al by AAS. The aluminum concentration was expected to be somewhat higher in the electrocoagulated silica, depending on the quantity of aluminum species adsorbed. Instead, the indirectly electrocoagulated silica analyzed considerably lower at 0.34% Al. Whether this lower concentration resulted from dilution by increased –OH surface group density was resolved by moisture determinations at 103°C and 180°C, as described by Greenberg *et al.* (1992). After drying, the electrocoagulated silica showed a weight loss of only 0.005% at both temperatures. As-received silica, on the other hand, registered weight losses of the order of 0.001% at both 103° and 180°C. Hence, these results conclusively indicate that the lower Al analysis recorded for electrocoagulated silica did not result from dilution by –OH surface groups. Another possibility was that the 0.25% Al deficit resulted from leaching. This was not plausible, however, since a considerable increase in aluminum concentration of 131.6 mg/L would have resulted in the supernatant. In a previous analysis, a 0.33% Al deficit was recorded in the Al analysis of electrocoagulated silica. Hence, it is suggested that a systemic error might have occurred in both sets of analyses, perhaps arising from precipitation during dilution of the digested, electrocoagulated silica samples.

An Al mass balance on the indirect electrocoagulation of silica is detailed in Appendix B and is summarized in Table 3-4.

Table 3-4. Aluminum distribution in indirect electrocoagulation of silica.

Al Input			Al Output		
Source	mg	%	Source	mg	%
As-received silica	310.5	85.9	EC* silica	178.9	99.2
AC/EC-treated water	3.0	0.8	Supernatant	1.5	0.8
Precipitate	47.8	13.3			
Total input	361.3	100.0	Total output	180.4	100.0

*Electrocoagulated

The total output amounted to only 49.9% of the total input. It is noteworthy that silica, both in the as-received and electrocoagulated states, accounted for the bulk of the aluminum by virtue of the silica mass. Dissolved aluminum in the AC/EC-treated water and the supernatant was analyzed at 3.0 and 1.5 mg/L,

respectively. Hence, as-received and electrocoagulated silica should have shown the same Al analysis. Table 3-5 reports pH values.

Table 3-5. pH values.

Sample	T, ℃	pH
Feed water	21.4	6.17
AC/EC-treated water	21.4	8.40
Electrocoagulated slurry	21.4	8.74
Supernatant	21.4	8.17

The pH of the AC/EC-treated water rose with electrocoagulation time from 6.2 to 8.4. The pH rose further to 8.7 when as-received silica was slurried with the treated water. When decanted from the slurry, however, the supernatant registered a pH of 8.2, which was lower than the pH of both the treated water and the slurry. A possible cause of this pH drop in the supernatant was aluminum hydroxide precipitation.

Photomicrographs of the precipitate and electrocoagulated silica are shown in Plate 3-1. The precipitate particles (Plate 3-1a) were transparent when they adopted the plate morphology, and appeared as white subhedral bodies when they formed micro-flocs. While a proportion of the silica flocs (Plate 3-1b) was highly porous, flocs with minimal porosity can be observed. The flocs appear to form an extended, reticulate network in the quiescent conditions under which they were photographed.

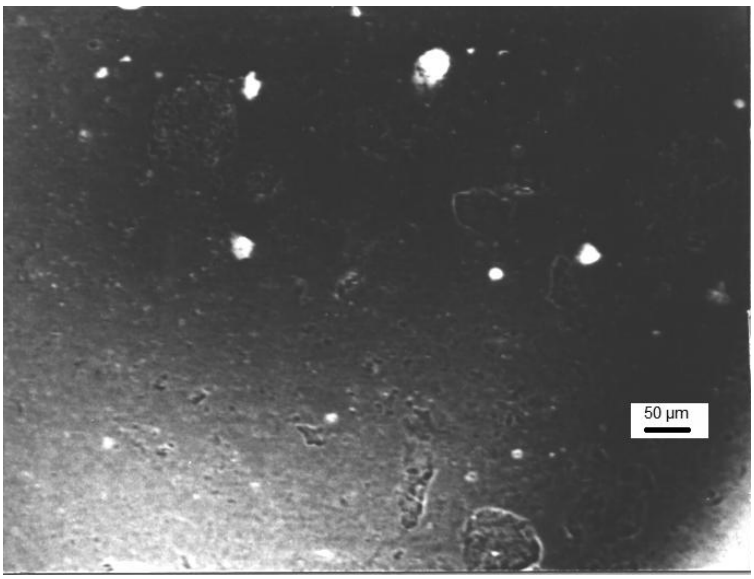

(a) Aluminum hydroxide precipitate.

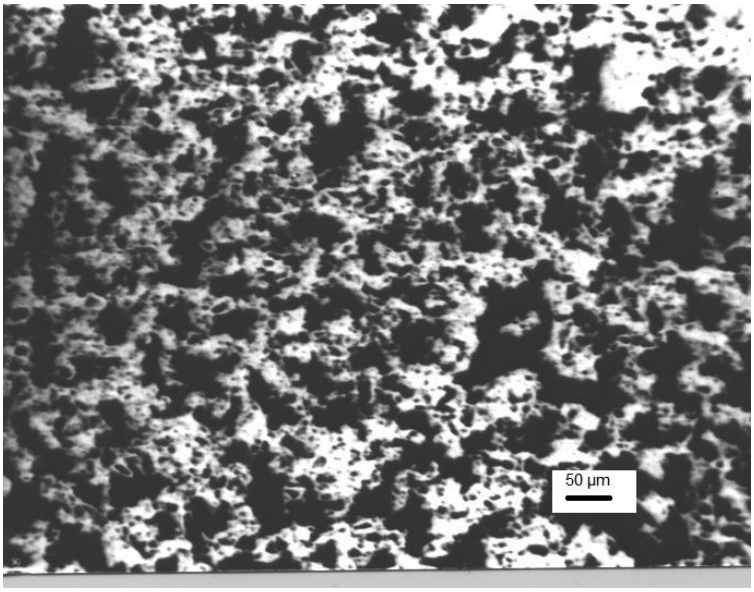

(b) Indirectly electrocoagulated silica.

Plate 3-1. Morphologies of aluminum hydroxide precipitate and indirectly electrocoagulated silica.

The electrocoagulated silica settled rapidly, such that initial settling was over within two minutes, as Figure 3-1 illustrates. The initial settling rate was 10.5 cm/min.

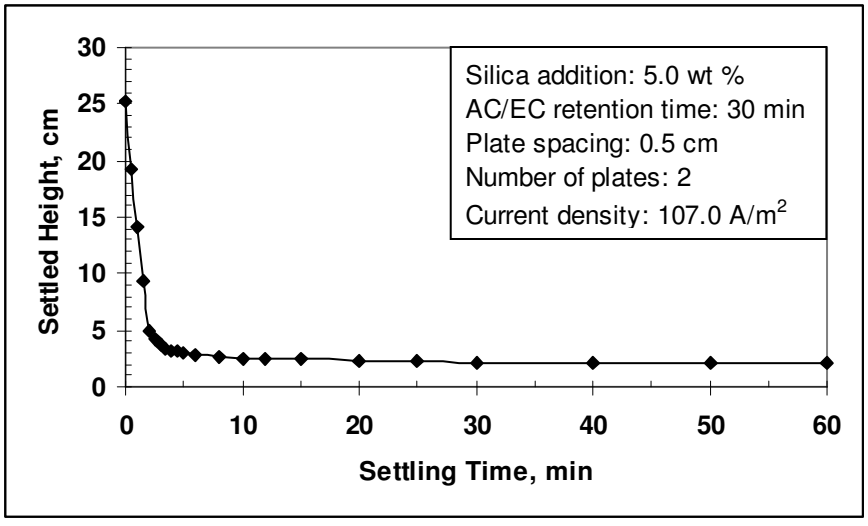

Figure 3-1. Settling behaviour of indirectly electrocoagulated silica.

Zeta potential measurements showed the aluminum hydroxide precipitate to be positively charged (+9.3 mV), while the electrocoagulated silica was negatively charged (-11.8 mV). It is interesting to note that, when the AC/EC-treated water (which contained 20 mg/L NaCl) was replaced with treated water containing 200 mg/L NaCl, the zeta potential of the precipitate reversed to -21.4 mV. In other words, the zeta potentials were compared (as the data show) for aluminum hydroxide precipitated in AC/EC-treated water containing 20 mg/L NaCl and 200 mg/L NaCl. The result is consistent with the increased negative zeta potential that was obtained for as-received silica when 200 mg/L NaCl was added to de-ionized water (see Figure 2-6). It should be stated that, in the treated 200 mg/L NaCl solution, the precipitate particles did not exhibit any tendency to disperse. This further suggests that the magnitude of the zeta potential is of subordinate importance when coagulation occurs by specific adsorption, rather than by purely physical means. Moreover, coagulation achieved by specific adsorption is not readily reversed by substantial change of the zeta potential.

Despite the close spacing of the electrodes (0.5 cm), the average voltage required to drive 3.2 A was high (95.8 V) owing to the reduced water conductivity (48 µS/cm for 20 mg/L NaCl vs. 420 µS/cm for 200 mg/L NaCl). A consequence of the high voltage was the 26.9°C rise from 21.4°C in 30 minutes of electrocoagulation. The specific energy input was evaluated at 138 kJ/L water or 2620 kJ/kg silica, another consequence of the high voltage.

3.4.2 Aluminum Speciation

Peaks in the spectrum obtained for the feed water blank sample were discounted from the spectra generated by the AC/EC-treated and supernatant water samples. Of the remaining peaks, those showing a minimum relative intensity of 10% were interpreted within the allowable ±0.55 dalton of the analyzed m/z ratio. All of the identified species were trivalent (as indicated by the triplet peaks) and contained NaCl in significant molar quantities. The presence of NaCl was indicated by lines for the two chlorine isotopes, $^{35}_{17}Cl$ and $^{37}_{17}Cl$. It is not known whether the inclusion of NaCl in the complexes was the result of ageing. The aluminum species that were identified are listed in Table 3-6. All species were identified by the mass spectroscopist.

Table 3-6. Aluminum species identified in AC/EC-treated and supernatant water samples, aged 4 days.

Water Sample	m/z (daltons)	Relative Peak Intensity (%)	Al Species
AC/EC-treated	75	55	$[Al(H_2O)_6 \cdot 1.54NaCl]^{3+}$
	84	100	$[Al(H_2O)_6 \cdot 2.00NaCl]^{3+}$
	93	60	$[Al_2(OH)_3(H_2O)_3 \cdot 2.05NaCl]^{3+}$ (1)
	148	11	$[Al_3(OH)_6(H_2O)_8 \cdot 2.00NaCl]^{3+}$ (1)
Supernatant	74	48	$[Al(H_2O)_6 \cdot 1.49NaCl]^{3+}$
	83	100	$[Al(H_2O)_6 \cdot 1.95NaCl]^{3+}$
	92	85	$[Al_2(OH)_3(H_2O)_3 \cdot 2.00NaCl]^{3+}$ (1)
	101	11	$[Al_3(OH)_6 \cdot 2.05NaCl]^{3+}$ (1)
	129	10	$[Al_3O(OH)_4(H_2O)_2 \cdot 3.18NaCl]^{3+}$ (2)
	156	11	$[Al_4O(OH)_7(H_2O)_2 \cdot 3.23NaCl]^{3+}$ (2)
	212	12	$[Al_5O_2(OH)_8(H_2O)_7 \cdot 3.54NaCl]^{3+}$ (2)

(1) Al:OH ratio suggested in Stol *et al.* (1976).

(2) Pattern of m/z relative peak locations changed, suggesting change from Al-OH species to Al-O-OH species.

Table 3-6 shows a trend in which increasing molar quantities of NaCl were associated with oxyhydroxoaluminum complexes of increasing molar mass. In contrast, the molar ratio of NaCl:Al^{3+} decreased with increasing size of the oxyhydroxo complexes (*e.g.*, from 1.06 for $[Al_3O(OH)_4(H_2O)_2 \cdot 3.18NaCl]^{3+}$ to 0.71 for $[Al_5O_2(OH)_8(H_2O)_7 \cdot 3.54NaCl]^{3+}$). For the hydroxoaluminum complexes containing coordinated water molecules, the NaCl:Al^{3+} molar ratio decreased as the molar mass of the complexes increased. However, unlike the trend observed for the oxyhydroxo complexes, the relation of NaCl molar content to the size of the complex is not readily apparent. Oxyhydroxo and hydroxo complexes incorporating NaCl were among the species identified by Sarpola *et al.* (2004a).

It was unexpected to find "non-hydroxy" Al^{3+} present in AC/EC-treated water of pH 8.4 (see Table 3-6). The species must have been originally present in the freshly prepared sample. While it is possible that a proportion of it hydrolyzed during ageing, it was still the most abundant species in the aged

sample. It could not have been formed from hydrolyzed species because of the high pH. Typically, hydrolyzed species age either to other hydrolyzed species (Tsai and Hsu, 1984) or to hydroxide precipitates (Smith, 1971). Hence, the persistence of non-hydroxy Al^{3+} is consistent with this author's claim that conditions in electrocoagulation are different from those of neutralization studies, such that different speciation results.

Since the relative intensities were derived in each sample by comparison with the intensity of the most abundant species in the particular sample, species registering the same relative intensity in two different samples would not necessarily be present in the same concentration. As such, no conclusive comment can be made on the extent to which each species was adsorbed from the AC/EC-treated water by silica. The unknown effects of ageing also mitigate against any pronouncement on the relative extents of adsorption of various species. The trinuclear species (148 daltons) in the AC/EC-treated water was absent from the supernatant sample, while more complex, polynuclear oxyhydroxoaluminum species appeared in the supernatant. The appearance of these latter complexes can be safely imputed to ageing.

Originally, the samples submitted for mass spectrometric analysis were prepared from feed water containing 200 mg/L NaCl. The analyses revealed only NaCl species, such as $Na(NaCl)_4^+$, $Na(NaCl)_{13}^+$ and $Na(NaCl)_{22}^+$, which obscured the Al species. Consequently, new samples were prepared from feed water containing 20 mg/L NaCl which allowed the Al species to be detected. However, NaCl was so pervasive as to associate with the Al complexes, presumably as outer-sphere entities, while existing as Na^+Cl^- ion pairs. Species of the type, $Na(NaCl)_n^+$, were identified by Zhao *et al.* (2009).

3.4.3 Specific Conductivity of Water

The stability of as-received silica dispersed in de-ionized water remained unaffected by increasing electrolyte concentration in the range of 200 to 3400 mg/L NaCl. Data quantifying the natural settling behaviour of the material are reported in Table 3-7.

Table 3-7. Natural settling behaviour of as-received silica in various NaCl solutions.

Specific Conductivity, µS/cm	Initial Settling Rate, cm/min
420	1.6×10^{-3}
2040	9.7×10^{-4}
2860	9.6×10^{-4}
3840	2.3×10^{-3}
4620	1.1×10^{-3}
5650	1.2×10^{-3}
6320	1.2×10^{-3}

In contrast, direct electrocoagulation enhanced the settling behaviour of silica by over 3 orders of magnitude. The initial settling rate improved from 2.7 to 4.1 cm/min as the specific conductivity of the dispersion medium was increased from 420 to 3840 µS/cm. At higher conductivities, the initial settling rate diminished, reaching 2.7 cm/min at 6320 µS/cm. These results are graphed in Figure 3-2.

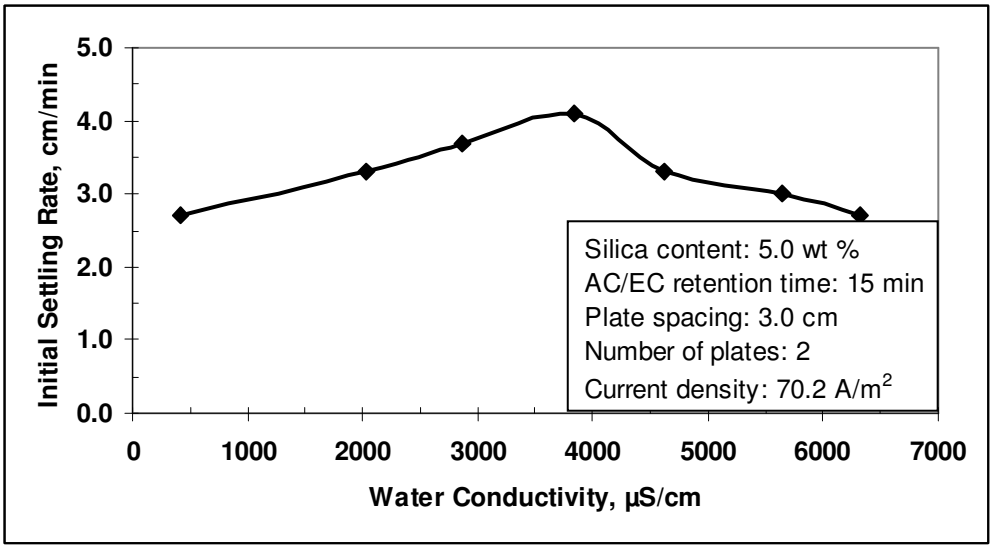

Figure 3-2. Effect of feed water conductivity on direct electrocoagulation of silica.

The observed increase of initial settling rate with water conductivity (420 to 3840 µS/cm) is attributed to increased aluminum dosing rate (discussed later in this Section). Consequently, the decline in initial settling rate at conductivities

exceeding 3840 µS/cm suggests that aluminum hydroxide was precipitated. In fact, an indirect electrocoagulation test was performed with feed water of specific conductivity 5650 µS/cm (3000 mg/L NaCl) to verify the occurrence of precipitation. Within five minutes of the 15-minute electrocoagulation time, precipitation commenced. In contrast, when feed water of conductivity 420 µS/cm (200 mg/L NaCl) was treated by AC/EC for 15 minutes, precipitation did not occur, although the current in both cases was controlled at 2.1 A. The feed water and supernatant conductivities are compared in Table 3-8.

Table 3-8. Specific conductivities of feed and supernatant water samples.

Feed Water Conductivity, µS/cm	Supernatant Conductivity, µS/cm
420	432
2040	2020
2860	2850
3840	3780
4620	4550
5650	5590
6320	6180

In the 420-µS/cm test, the water conductivity increased to 432 µS/cm in the supernatant owing to residual dissolved aluminum. In the other tests, however, the supernatant conductivity was lower than the feed water conductivity, indicating loss of dissolved solids (*i.e.*, the occurrence of precipitation). Figure 3-2 shows that the initial settling rate of electrocoagulated silica improved in the range of feed water conductivities of 420 to 3840 µS/cm, despite precipitation in the 2040 to 3840 µS/cm range. The diminution of initial settling rate at higher conductivities suggests that precipitation began earlier in the electrocoagulation process than it did at conductivities of 2040 to 3840 µS/cm. Precipitation is deduced to have commenced progressively sooner with increasing feed water conductivity as a result of the increasing aluminum dosing rate, which will be discussed shortly.

Hence, the previously observed effect of precipitation on the initial settling rate of silica (see Figures 2-10 and 2-39) is apparent here. However, the decline in initial settling rate was more dramatic (Figure 3-2) than that observed previously, and might be attributed to the higher background ionic strength of the

dispersion medium, which could have modified the aluminum speciation (both in identity and distribution). That background ionic strength influences aluminum solubility and speciation has been addressed elsewhere (Duan and Gregory, 2003; Bertsch, 1989; Stol *et al.*, 1976; Zelazny and Jardine, 1989). For example, Stol *et al.* (1976) have deduced that the degree of polymerization of aluminum species increases with background ionic strength. Further, Stumm and Morgan (1995) and O'Melia (1986) have reported that colloidal hydroxo polymers are formed, under conditions of aluminum supersaturation, from a series of olation (*i.e.*, $_{}^{H}{}_{O}{}_{}$ bridge formation) and oxolation (*i.e.*, –O– bridge formation) reactions. It follows, therefore, that increasing background ionic strength promotes aluminum precipitation. In addition, the chemistry of the water (*i.e.*, ionic strength) is known to influence aluminum speciation, altering the properties of the complexes by anion substitution for OH^- (Sarpola *et al.*, 2004a; Brinker and Scherer, 1990; Cohen and Hannah, 1971). This substitution creates species of different solubility, to the extent that the pH range in which aluminum hydroxide precipitation occurs is modified.

Aluminum dosing rate is considered to have increased with water conductivity (420 to 3840 µS/cm) because, as the conductivity was increased, less electrical energy was wasted as Joule heating and a larger proportion of the input energy became available for the anodic oxidation of aluminum. The voltage drop (V_{IR}) associated with the electrical resistance of the feed water was estimated as shown in Equation 3-1.

$$V_{IR} = \frac{ix}{\sigma} \qquad (3\text{-}1)$$

where i = current density, A/m^2
x = electrode separation, m
σ = water conductivity, S/m.

This and other operating data are entered in Table 3-9 to show the effect of conductivity on energy utilization. The data show that the temperature rise decreased from 4.9° to 0.3°C as the feed water conductivity was increased from 420 to 6320 µS/cm. The average applied voltage also decreased, from 47.7 to 4.9 V. Consequently, the SEI (specific energy input) dropped from 428 to 44

kJ/kg silica, and the electrolyte voltage drop diminished from 50.1 to 3.3 V. At the conductivity of 420 µS/cm, the electrocoagulation process kinetics was constrained by the relative magnitudes of V_{IR} and V_{avg}. In the other tests, V_{IR}/V_{avg} decreased with increasing conductivity, providing progressively increasing proportions of the input energy to anodic oxidation. It follows that the aluminum dosing rate increased with feed water conductivity. Figure 3-2 illustrates that AC/EC can be applied successfully to solids suspended in aqueous media of high conductivity to enhance the settling behaviour. Table 3-9 shows that aqueous dispersion media of high conductivity can reduce the energy consumption of the electrocoagulation process considerably.

Table 3-9. Effect of feed water conductivity on energy utilization.

σ, µS/cm	ΔT, ℃	V_{avg}, V	SEI, kJ/kg Silica	V_{IR}, V	V_{IR}/V_{avg}, %
420	4.9	47.7	428	50.1	105
2040	1.0	11.3	101	10.3	91.2
2860	0.8	8.4	75	7.4	88.1
3840	0.6	7.0	62	5.5	78.6
4620	0.4	6.1	55	4.6	75.4
5650	0.3	5.2	47	3.7	71.2
6320	0.3	4.9	44	3.3	67.3

Figure 3-3 shows that the mode of variation of pH values for the electrocoagulated slurry and supernatant samples was random. No trend, which can be related to Figure 3-2, is apparent.

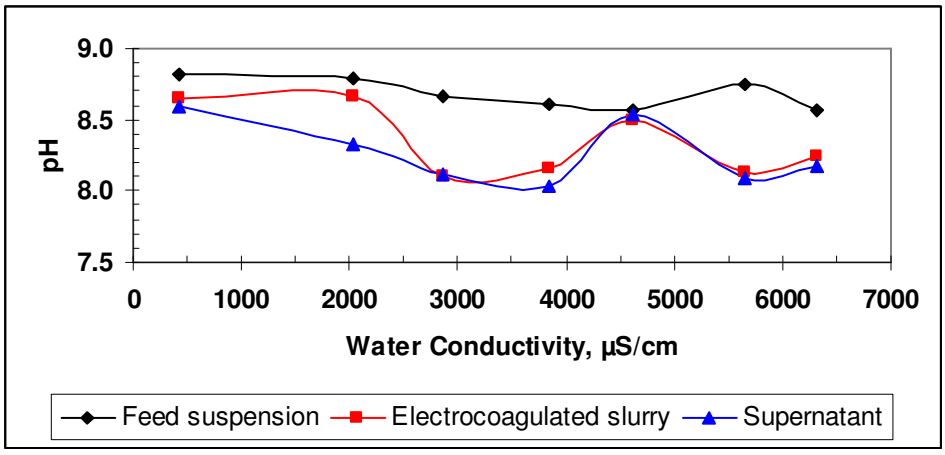

Figure 3-3. Variation of pH with water conductivity.

Zeta potentials for as-received and electrocoagulated silica were negative over the range of water conductivities tested, as is evident from Figure 3-4. For as-received silica, the zeta potential increased (*i.e.*, became more negative) from -16 mV and attained a maximum of -25 mV at 2860 µS/cm. Further increase of the conductivity resulted in lower (*i.e.*, less negative) zeta potentials. At 6320 µS/cm, the zeta potential was -22 mV.

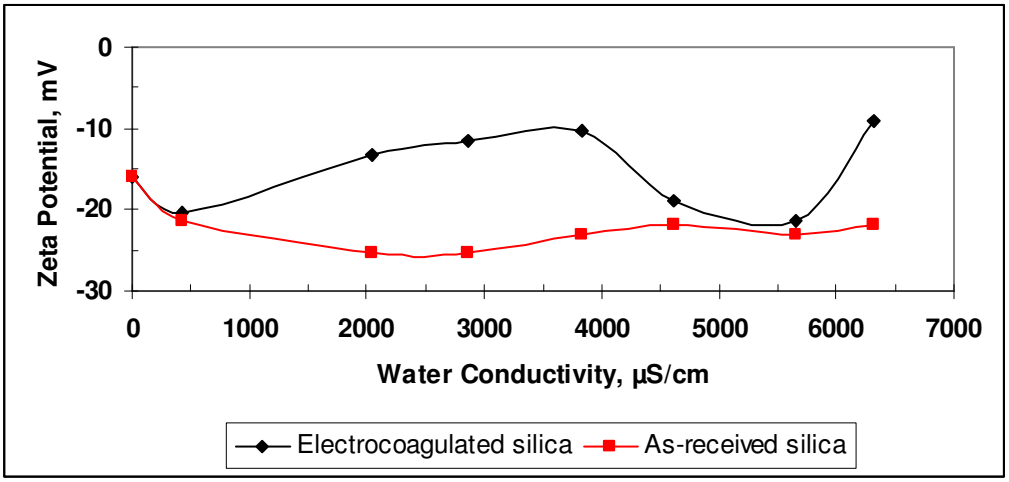

Figure 3-4. Effect of feed water conductivity on zeta potentials of as-received and electrocoagulated silica.

The Debye length (κ^{-1}), which is a measure of the thickness of the electrical double layer around a particle, was calculated for a d_{50} size particle (radius 10 µm) in feed water in the conductivity range of 0.3 µS/cm (de-ionized water with no added NaCl) to 6320 µS/cm. From the κ^{-1} and measured zeta potential (ζ) values, the net interaction energy existing between two d_{50} size silica particles was calculated from Equation 1-14 at 22.5°C, and then converted to kT units (1 kT = 4.081×10^{-21} J). Hamaker's constant, A, was taken as 1.70×10^{-20} J (Masliyah, 1994).

The resulting curves are shown in Figure 3-5, where positive and negative interaction energies connote repulsion and attraction, respectively. The graph indicates that the as-received silica particles would experience net attraction at progressively closer separations, as water conductivity increases. At conductivities exceeding 3840 µS/cm, the particles would experience net attraction over separations of 0.1 to 20 nm and should, therefore, coagulate spontaneously upon colliding. This, however, was not observed. Brinker and

Scherer (1990) have suggested that silica does not conform to the DLVO theory because it is stabilized by a layer of adsorbed water which prevents coagulation, even at zero zeta potential. This is an indication that destabilization of silica suspensions does not necessarily imply zero zeta potential, as this work and that of other researchers have demonstrated (Xiao *et al.*, 2008; Ching *et al.*, 1994; Letterman *et al.*, 1982; Van Benschoten and Edzwald, 1990). Brinker and Scherer attributed the water-stabilization of silica to the unusually low Hamaker's constant of silica. It follows, then, that dehydration of the particle surface is prerequisite to coagulation and floc growth. The incremental energy required for dehydration is expected to decrease with increasing water conductivity, due to the progressively thinner electrical double layer. Hence, electrocoagulation kinetics would be enhanced by increasing conductivity in agreement with the energy utilization analysis presented earlier in this Section.

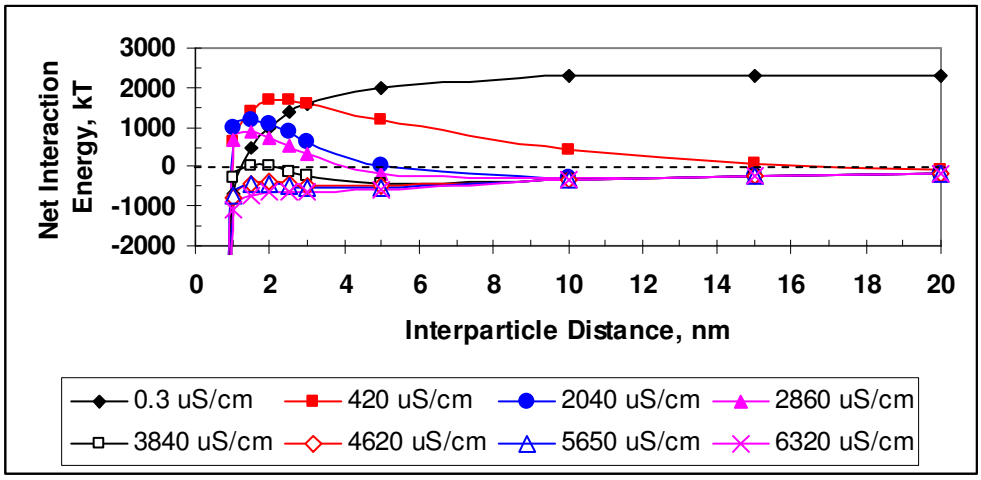

Figure 3-5. Variation of interaction energy between two d_{50} size particles of as-received silica as a function of water conductivity.

From the κ^{-1} values, estimates were made of the interparticle distance (h_{EDL}) where the diffuse layers of two approaching particles would touch (approximately $2\kappa^{-1}$). For these separations, the net interaction energy (V) values were deduced from Figure 3-5 and listed in Table 3-10.

Table 3-10. Net interaction energies at separation, h_{EDL}.

σ, μS/cm	κ^{-1}, nm	h_{EDL}, nm	V, kT
420	5.2	10	+400
2040	2.2	4	+250
2860	1.9	4	0
3840	1.6	3	-210
4620	1.5	3	-460
5650	1.3	3	-540
6320	1.3	3	-660

Table 3-10 shows that as-received silica particles, which are dispersed in water of conductivity 2860 μS/cm, would experience zero interaction energy when their diffuse layers touch. Figure 3-5, however, indicates that closer approach (such that the diffuse layers overlap) would cause the particles to encounter increasing repulsive energy. In water of conductivity ≥3840 μS/cm, the diffuse layers would overlap under net attraction. If values for V from Table 3-10 were assigned to the corresponding conductivities on the curve in Figure 3-4 for as-received silica, it would be observed that the repulsion energy decreases to zero (diffuse layers in contact) as the zeta potential increases. With further increase of the water conductivity, the attraction energy increases as the zeta potential decreases.

Electrocoagulation of silica in feed water of conductivity 420 μS/cm caused the zeta potential to increase by -4 mV (Figure 3-4). For 420<σ≤3840 μS/cm, the zeta potential decreased from -20 to -10 mV, as might be expected. At σ>3840 μS/cm, the zeta potential reversed twice, the second reversal probably reflecting the influence of the aluminum hydroxide precipitate which is normally positively charged.

3.4.4 Feed Water pH

Results are analyzed first for the 5.0 wt % solids suspension (Section 3.4.4.1) and then for the ≤5.0 wt % suspensions (Section 3.4.4.2).

3.4.4.1 5.0 Wt % Solids Suspension

Figure 3-6 illustrates the enhanced settling behaviour of the indirectly electrocoagulated silica, the concentration of which was 5.0 wt %.

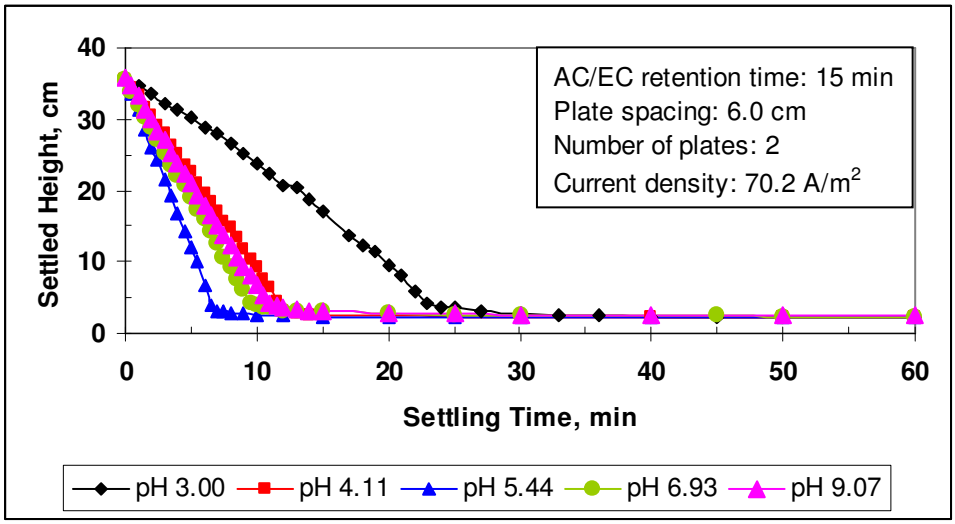

Figure 3-6. Effect of feed water pH on the settling behaviour of electro-coagulated silica.

From the graph, it is clear that electrocoagulation was effective in enhancing the settling behaviour of silica over the feed water pH range of 3.0 to 9.1. This pH range is wider than that in which alum and aluminum chloride function.

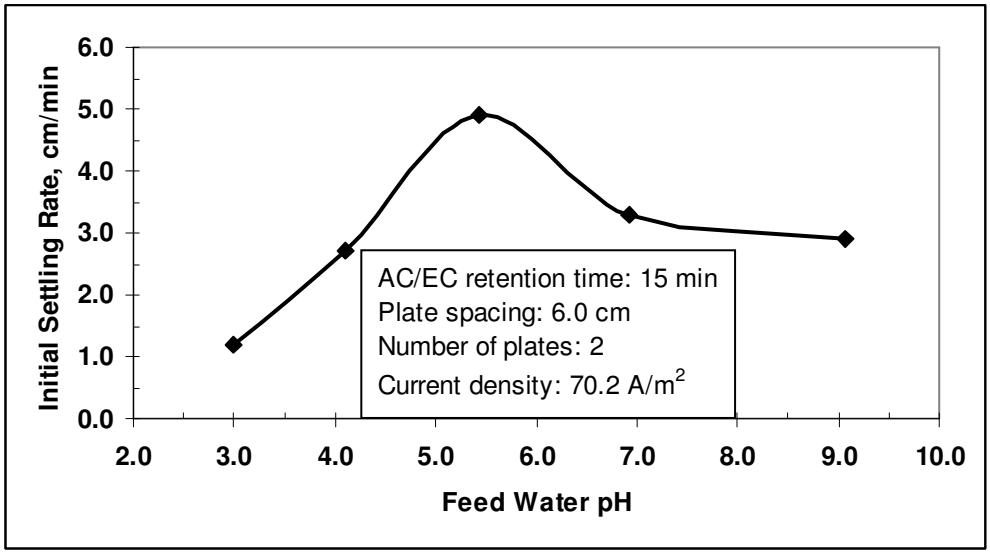

Figure 3-7. Variation of initial settling rate of electrocoagulated silica with feed water pH.

For feed water of pH 3.0, the initial settling of silica was slow, lasting for about 24 minutes. The fastest initial settling occurred for feed water electrocoagulated from pH 5.4, as shown in Figure 3-7.

The initial settling rate of the electrocoagulated silica increased from 1.2 cm/min for a feed water pH of 3.0 to a maximum of 4.9 cm/min for feed water of pH 5.4. Thereafter, the initial settling rate declined to 2.9 cm/min for feed water of pH 9.1. The settling rate variation was influenced by aluminum speciation, of which pH is a principal determinant. Precipitation did not occur during electrocoagulation in any of the tests.

Floc size distributions of silica, electrocoagulated indirectly with water treated from pH 3.0, 5.4 and 9.1, are compared with the particle size distribution of as-received silica in Figure 3-8. Compared to a d_{50} of 20 µm in the as-received state, the d_{50} sizes of electrocoagulated silica varied with feed water pH as follows: pH 3.0, 27 µm; pH 5.4, 48 µm; pH 9.1, 43 µm. These sizes are representative of the respective distributions in that they are consistent with the initial settling rates depicted in Figure 3-7. Silica, which had been electrocoagulated indirectly with water treated from pH 3.0, showed a relatively rapid floc size increase in the range exceeding the d_{50} size. However, Figure 3-8 suggests that silica, that was electrocoagulated with water treated from pH 5.4, attained the coarsest top size which probably exceeded 120 µm.

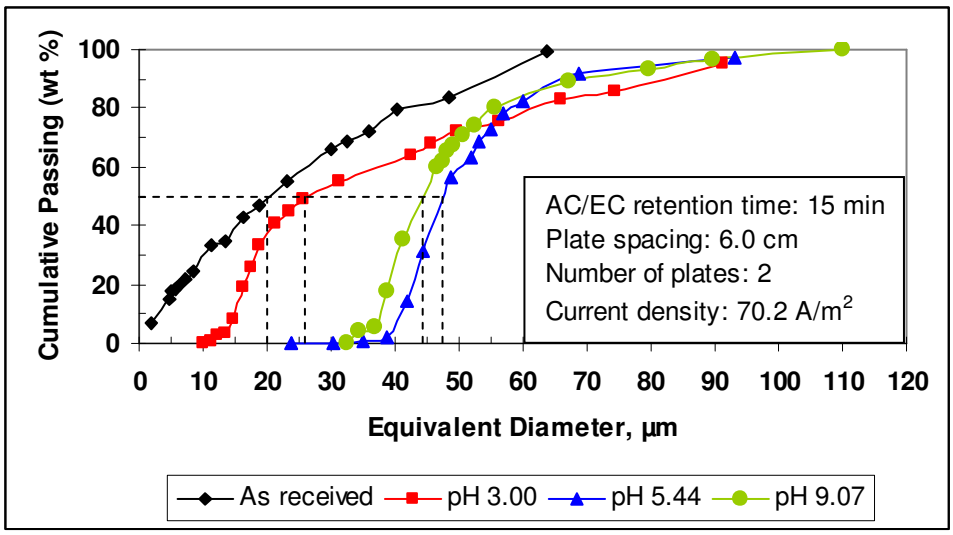

Figure 3-8. Variation of floc size distribution of electrocoagulated silica with feed water pH.

Figure 3-9 represents the zeta potential variation with feed water pH for as-received and electrocoagulated silica.

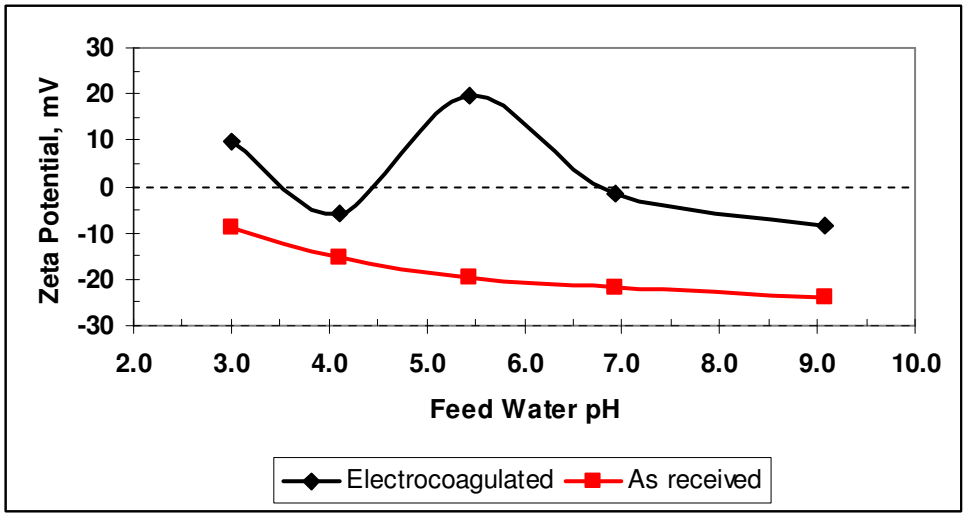

Figure 3-9. Variation of zeta potentials of as-received and electrocoagulated silica with feed water pH.

As expected, the zeta potential of the as-received silica increased steadily as the feed water pH was increased, from -9 mV at pH 3.0 to -24 mV at pH 9.1. The isoelectric point (i.e.p.) occurred at approximately pH 2. The zeta potential of electrocoagulated silica, on the other hand, did not manifest such a simple mode of variation. It reversed twice with increasing feed water pH: first, from -6 mV at pH 4.1 to +20 mV at pH 5.4; then to -1.5 mV at pH 6.9. It is noteworthy that the zeta potential of +20 mV (feed water pH 5.4) coincided with the achievement of the greatest enhancement in initial settling rate (Figure 3-7). From Figure 3-9, a zeta potential of 0 mV was deduced to have occurred at feed water pH values of approximately 3.5, 4.5 and 6.7. Relative to the zeta potentials of as-received silica, changes of considerable magnitude were engendered by the indirect electrocoagulation treatment, as Table 3-11 demonstrates. These changes, which made the zeta potentials less negative, are attributed to the adsorption of complex aluminum cations from the AC/EC-treated water.

Table 3-11. Magnitudes of zeta potential changes resulting from indirect electrocoagulation.

Feed Water pH	Zeta Potential Change, mV
3.00	18.7
4.11	9.6
5.44	39.2
6.93	20.3
9.07	15.4

Table 3-12 summarizes the pH values of the feed water and product streams.

Table 3-12. pH values for feed water and product streams.

Temperature (℃)	pH			
	Feed Water	Treated Water	EC* Slurry	Supernatant
23.5	3.00	4.27	4.25	4.12
23.6	4.11	5.56	6.16	6.00
23.3	5.44	8.16	8.03	8.22
23.5	6.93	8.00	7.96	7.74
23.7	9.07	8.21	7.97	7.84

*Electrocoagulated

Except for feed water of pH 9.1, AC/EC treatment of the feed water raised its pH. The maximum pH increase was coincident with the largest enhancement of silica settling rate. Principally, the net pH changes are considered to have resulted from the reactions by which the various types and relative proportions of complex aluminum species were formed. The pH values for the indirectly electrocoagulated slurries determined the equilibrium (*i.e.*, steady state) that existed between silica containing adsorbed aluminum species and the unadsorbed species (residual aluminum) in the supernatant.

Analyses of total aluminum in the AC/EC-treated and supernatant water samples are reported in Table 3-13.

Table 3-13. Effect of feed water pH on aluminum adsorption.

Feed Water pH	mg/L Al		Adsorption Mass Ratios	
	Treated Water	Supernatant	mg Al/g Silica	mg Al/ g Silica per cm/min
3.00	10.5	9.0	0.03	0.02
5.44	6.0	0.2	0.11	0.02
9.07	7.5	1.0	0.12	0.04

While the largest quantity of aluminum (10.5 mg/L) was solubilized in water treated from pH 3.0, only 14% of it was adsorbed by silica. Water treated from pH 9.1 contained 7.5 mg/L Al, of which 87% was adsorbed. Although water treated from pH 5.4 contained the smallest aluminum dosage (6 mg/L), 97% of it was adsorbed by silica. Hence, the adsorption mass ratios (mg Al/g silica) varied with feed water pH as follows: pH 3.0, 0.03; pH 5.4, 0.11; pH 9.1, 0.12. When the utilization of the adsorbed aluminum is expressed in terms of mg Al adsorbed/g silica per cm/min enhancement in initial settling rate, a value of 0.02 is obtained for water treated from pH 3.0 and 5.4, while a value of 0.04 results for water treated from pH 9.1. Although equal aluminum utilizations were calculated for water treated from pH 3.0 and 5.4, the respective initial settling rates were 1.2 and 4.9 cm/min. Hence, feed water treated from pH 5.4 gave the greatest economy of aluminum adsorbed. Clearly, this is directly related to aluminum speciation, which explains why the higher aluminum dosages in Table 3-13 did not achieve higher settling rates. For water treated from pH 3.0, it is inferred from the low fraction of aluminum adsorbed that Al^{3+} was the predominant species (Gregory and Duan, 2001; Beecroft *et al.*, 1995; Parthasarathy and Buffle, 1985; Stumm and O'Melia, 1968). In water treated from pH 9.1, complex aluminum anions (Sarpola *et al.*, 2004a) are expected to have constituted the major fraction of the complex species and, together with OH^-, would account for the observed effect on the zeta potential (Figure 3-9). Also, from the zeta potential of the indirectly electrocoagulated silica, water treated from pH 5.4 would be expected to contain a larger variety of cationic complexes than would the other water samples just discussed (see Figure 1-7 for a rough guide).

Operating data recorded during electrocoagulation of the feed water are reported in Table 3-14.

Table 3-14. Operating data from feed water pH tests.

Feed Water				V_{avg}	Specific Energy Input
pH	T_i* (°C)	ΔT (°C)	σ (µS/cm)	(V)	(kJ/kg Silica)
3.00	23.5	6.4	647	65.8	591
4.11	23.6	7.8	518	80.4	722
5.44	23.3	8.1	418	85.0	763
6.93	23.5	8.6	431	86.6	778
9.07	23.7	8.4	423	86.1	773

*Initial temperature

The HCl addition, that was required to lower the feed water pH to 3.0 from 7.1, increased the specific conductivity from ~420 µS/cm to 647 µS/cm (highest conductivity). Consequently, the temperature rise caused by Joule heating was the lowest at 6.4°C. The average voltage and the specific energy input (SEI) were calculated at 65.8 V and 591 kJ/kg silica. Lower feed water conductivities (after pH adjustment) in the other tests resulted in larger temperature rises (7.8° to 8.6°C), and in higher V_{avg} (80.4 to 86.6 V) and SEI (722 to 778 kJ/kg) values.

In Chapter 2 (Section 2.4.6), the induction phenomenon was observed at current densities below 70.2 A/m^2 for a feed suspension pH of 8.8 and an electrode separation of 3.0 cm. In the feed water pH tests, with a current density of 70.2 A/m^2 and electrode spacing of 6.0 cm, induction was observed at feed water pH of 3.0 and 4.1. To maintain the current at 2.1 A, positive adjustment of the applied voltage was required throughout the pH 3.0 test and for the first five minutes of the pH 4.1 test. Hence, in addition to current density, the feed water pH can render the system into an inductive state.

3.4.4.2 ≤5.0 Wt % Solids Suspensions

The effects of feed water pH (3.0, 5.4 and 9.1) and the solids concentration in the indirectly electrocoagulated slurry on the residual total aluminum concentration in the supernatant samples are depicted in Figure 3-10. The Al concentrations plotted at 0 wt % solids represent concentrations in the AC/EC-treated water samples. A maximum of only 1.5 mg/L Al was adsorbed from water that was treated by AC/EC from pH 3.0. This maximum adsorption, which was achieved with a minimum solids concentration of 1.0 wt %, did not

increase with increasing solids concentration. Hence, 86% of the aluminum species in the treated water is inferred to have been non-hydrolyzed (*i.e.*, Al^{3+}) because of the low pH (see Table 3-12). In contrast, for water treated from pH 5.4 and 9.1, aluminum adsorption increased with solids concentration, indicating the presence of an abundance of hydrolyzed species. In the case of water treated from pH 5.4, virtually all of the aluminum (97%) was adsorbed by the 5.0 wt % solids slurry. Adsorption mass ratios are presented in Table 3-15.

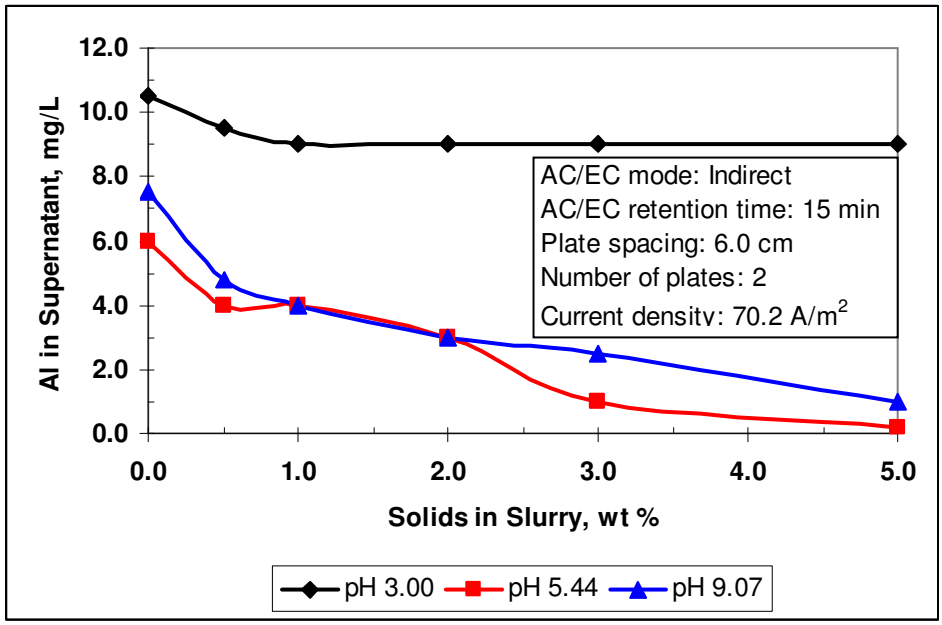

Figure 3-10. Effects of solids concentration and feed water pH on residual Al in supernatant.

Table 3-15. Variation of adsorption mass ratio with solids concentration.

Wt % Solids	Al Adsorption Mass Ratio, mg Al/g Silica		
	pH 3.00	pH 5.44	pH 9.07
0.5	0.20	0.40	0.54
1.0	0.15	0.20	0.35
2.0	0.07	0.15	0.22
3.0	0.05	0.16	0.16
5.0	0.03	0.11	0.12

The Al adsorption mass ratio varied with feed water pH for a given solids concentration because the aluminum speciation changed with changes in

temperature and pH during AC/EC treatment of the feed water. For water treated from pH 3.0, the Al adsorption mass ratio for >1.0% solids decreased only because the quantity of silica was increased (see Figure 3-10). Water treated from pH 5.4 and 9.1 gave higher ratios which decreased with increasing solids concentration. Although AC/EC-treated water, that was prepared from feed water of pH 9.1, showed the highest ratios, the aluminum speciation was not as efficient in facilitating silica floc growth as that in water that was treated from pH 5.4, based on the initial settling rates measured for the 5.0 wt % slurries (see Figure 3-7). That the ratios for feed water of pH 5.4 and 9.1 were not consistently inversely proportional to the solids concentration indicates that the aluminum complexes were not adsorbed stoichiometrically. Hence, adsorption was driven in part by the concentration gradient between the bulk solution and the silica surface. The other driver of adsorption, of course, was the affinity of the complex species for the silica surface. Table 3-15 and Figure 3-10 illustrate that the residual aluminum concentration can be controlled by the solids concentration in water treated by AC/EC from a given pH, as well as by feed water pH for a given solids concentration.

On the basis of the d_{50} particle size in as-received silica, aluminum adsorption per unit area (specific mass adsorption) was estimated (see Appendix B) and tabulated in Table 3-16.

Table 3-16. Specific mass adsorption of aluminum.

Wt % Solids	Specific Mass Adsorption, mg Al/m^2		
	pH 3.00	pH 5.44	pH 9.07
0.5	1.7	3.4	4.6
1.0	1.3	1.7	2.9
2.0	0.6	1.2	1.9
3.0	0.4	1.4	1.4
5.0	0.2	0.9	1.0

The specific mass adsorption data agree well with the adsorption mass ratios in Table 3-15 and reflect the same lack of stoichiometry. The ratio of the data in Table 3-15 to those in Table 3-16 gives the specific surface area of as-received silica. For a d_{50} particle, the specific surface area was 0.12 m^2/g (see Appendix B), which is in good agreement with the ratios calculated from Tables

3-15 and 3-16. As a corollary, the d_{50} basis was representative of the polydisperse mass.

Zeta potentials are plotted in Figure 3-11 as a function of feed water pH and solids concentration. For solids concentrations <5.0 wt %, only small changes in zeta potential were noted for each of the feed water pH values. However, at 5.0 wt % solids, the zeta potentials became less negative and, in the cases of feed water pH 3.0 and 5.4, they became positive.

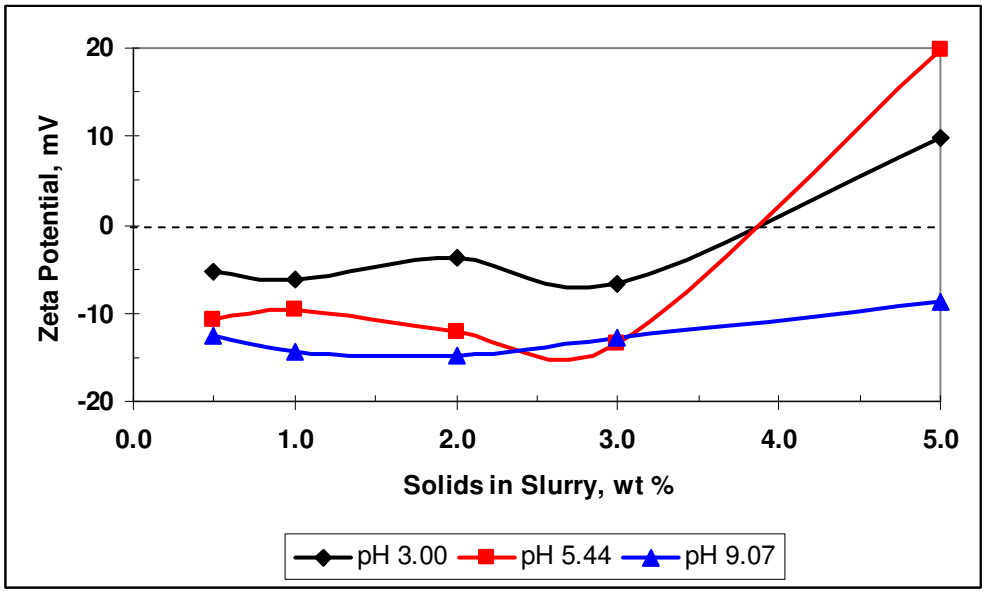

Figure 3-11. Effects of feed water pH and solids concentration on zeta potential of electrocoagulated silica.

3.4.5 Feed Water Temperature

Over the feed water temperature range of 23.2° to 85.0°C, the settling behaviour of silica was enhanced by electrocoagulation (Figure 3-12). Hence, AC/EC would be an effective treatment for effluents in a wide temperature range.

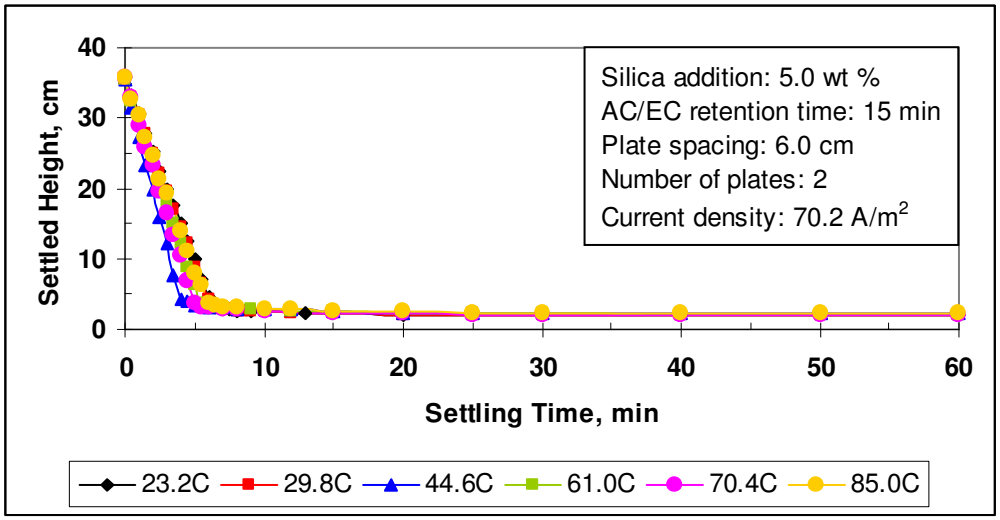

Figure 3-12. Effect of feed water temperature on the electrocoagulation of silica.

Figure 3-13 illustrates the effect of feed water temperature on the initial settling rate of electrocoagulated silica. Up to about 30℃, the feed water temperature exerted negligible influence on the initial settling rate. At higher temperatures, however, the initial settling rate changed quickly with feed water temperature. The maximum rate of 7.8 cm/min was achieved when the feed water temperature was adjusted to 44.6℃. The curve describes a second maximum of 6.4 cm/min for the feed water temperature of 70.4℃. It became apparent from test repeats that the initial settling rate of the indirectly electrocoagulated silica tended to improve as the temperature, at which the AC/EC-treated water was slurried with as-received silica, increased (in this case, the slurrying temperature was 60℃). This effect of the slurrying temperature is not unusual (Kinniburgh and Jackson, 1981), and is considered to result from aluminum speciation. Duan and Gregory (2003) have reported that the effect of temperature on coagulation performance arises from its influence on the kinetics of hydrolysis reactions (hence, on speciation) and on the solubility of $Al(OH)_3$ (see Section 2.4.4.2). That AC/EC was effective over a 62℃ range added flexibility to the process.

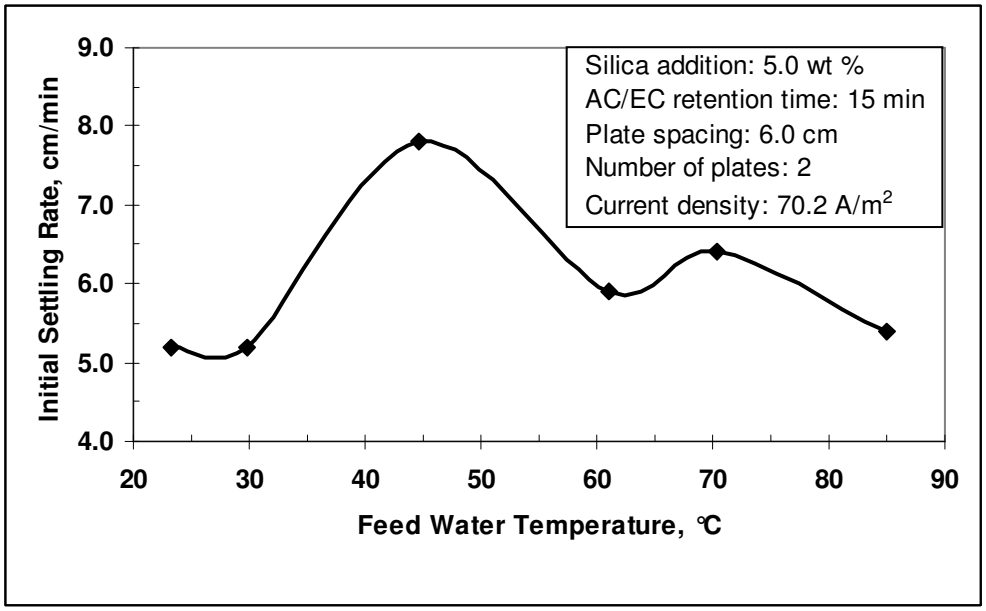

Figure 3-13. Effect of feed water temperature on the initial settling rate of electrocoagulated silica.

Table 3-17 reports operating data from the feed water temperature tests.

Table 3-17. Operating data from feed water temperature tests.

Feed Water Temperature (℃)	ΔT (℃)	V_{avg} (V)	Specific Energy Input (kJ/kg Silica)
23.2	8.8	87.1	782
29.8	6.9	77.6	697
44.6	3.2	61.3	550
61.0	-0.8	49.5	444
70.4	-3.0	46.4	427
85.0	-8.9	39.3	352

With increasing feed water temperature, the effect of Joule heating became less evident. At 23.2℃, the water temperature increased by 8.8℃ while, at 85.0℃, it fell by 8.9℃ owing to heat loss to the surroundings. The average applied voltage decreased from 87.1 V at 23.2℃ to 39.3 V at 85.0℃. Consequently, the specific energy input (SEI) declined from 782 to 352 kJ/kg silica. From these data, it may be inferred that the anode energy efficiency (for aluminum oxidation) increased with feed water temperature. This is similar to the conductivity tests, except that a stable precipitate was not observed. Therefore, it

is further inferred that the decline in initial settling rate for feed water temperatures exceeding 45°C was influenced by aluminum speciation. The reduction of the SEI with increasing temperature constitutes an advantage for treating hot industrial effluents.

3.5 CHAPTER SUMMARY

The composition of the aluminum hydroxide precipitate was OH-deficient, having the empirical formula, $Al(OH)_{2.74}$. This composition is equivalent to a mixture of 18% AlOOH and 82% $Al(OH)_3$. The precipitate was amorphous as prepared and had not crystallized several weeks later. Its zeta potential was +9.3 mV.

Solids recovered from the electrodes were a mixture of 2.3% $Al_{3.21}Si_{0.47}$ and $Al(OH)_{3.06}Cl_{0.01}$. The intermetallic compound is considered to indicate local cell activity in which isolated Si-rich micro-areas in the electrodes behaved cathodically.

Despite high specific conductivities (≤6320 µS/cm) of the water, as-received silica formed stable suspensions, but electrocoagulation enhanced the initial settling rate by over 3 orders of magnitude. At conductivities exceeding 3840 µS/cm, aluminum hydroxide precipitated, seriously impairing the settling behaviour of the electrocoagulated silica. The onset of precipitation is inferred to have occurred progressively earlier with increasing feed water conductivity. The explanation for this is that an increasing proportion of the input energy was utilized for anodic oxidation as conductivity was elevated. Thus, higher Al dosages resulted and aluminum solubility decreased with rising background ionic strength.

AC/EC was effective in enhancing the settling behaviour of silica in the feed water pH range of 3.0 to 9.1. This pH range of effectiveness far exceeds that of chemical coagulants. The greatest enhancement of the initial settling rate by indirect electrocoagulation was achieved at pH 5.4. Owing to its determinative influence on aluminum speciation, pH is a key control of electrocoagulation and, hence, of floc growth and settling rate enhancement.

The negative zeta potential of as-received silica was made less negative by electrocoagulation at all pH values studied. The greatest change of 39 mV was realized at pH 5.4 when the zeta potential reached +20 mV. The zeta

potential changes were responses to the charges carried by adsorbing complex aluminum ions.

Aluminum adsorption did not bear a stoichiometric relationship to the solids concentration or, therefore, to the silica surface area.

Settling behaviour enhancement increased with feed water temperature and attained its maximum at ~45°C. At higher feed water temperatures, settling behaviour was affected by the temperature at which the silica was slurried with the AC/EC-treated water, tending to increase with slurrying temperature. AC/EC was effective in enhancing the settling behaviour of silica over a wide range of temperatures (23° to 85°C). Hence, the technique is applicable to the treatment of hot waste streams.

Energy consumption by the AC/EC process was reduced by increased temperature and specific conductivity of the dispersion medium or feed water.

3.6 REFERENCES

Akitt J.W. and Farthing A. (1978), New ^{27}Al NMR studies of the hydrolysis of the aluminum(III) cation. *J. Mag. Reson.*, **32**, 345-352.

Akitt J.W. and Mann B.E. (1981), ^{27}Al NMR spectroscopy at 104.2 MHz. *J. Mag. Reson.*, **44**, 584-589.

Baes C.F. and Mesmer R.E. (1976), The Hydrolysis of Cations. John Wiley & Sons, New York, pp. 112-123.

Beecroft J.R.D., Koether M.C. and van Loon G.W. (1995), The chemical nature of precipitates formed in solutions of partially neutralized aluminum sulfate. *Water Res.*, **29**, 1461-1464.

Bertsch P.M. (1987), Conditions for Al_{13} polymer formation in partially neutralized aluminum solutions. *Soil Sci. Soc. Am. J.*, **51**, 825-828.

Bertsch P.M. (1989), Aqueous polynuclear aluminum species. In Sposito G. (Ed.), The Environmental Chemistry of Aluminum. CRC Press, Inc., Boca Raton, FL, pp. 87-115.

Bottéro J.Y., Cases J.M., Fiessinger F. and Poirier J.E. (1980a), Studies of hydrolyzed aluminum chloride solutions. 1. Nature of aluminum species and composition of aqueous solutions. *J. Phys. Chem.*, **84**, 2933-2939.

Bottéro J.Y., Poirier J.E. and Fiessinger F. (1980b), Study of partially neutralized aqueous aluminum chloride solutions: identification of aluminum species

and relation between the composition of the solutions and their efficiency as a coagulant. *Prog. Wat. Tech.*, **12**, 601-612.

Brinker C.J. and Scherer G.W. (1990), Sol-Gel Science: The Physics and Chemistry of Sol-Gel Processing. Academic Press, Inc., New York, pp. 2-262.

Buffle J. (1988), Complexation Reactions in Aquatic Systems: An Analytical Approach. Ellis Horwood Limited, Chichester, pp. 16-200.

Cañizares P., Martínez F., Jiménez, C., Lobato J. and Rodrigo M.A. (2006), Comparison of the aluminum speciation in chemical and electrochemical dosing processes. *Ind. Eng. Chem. Res.*, **45**, 8749-8756.

Ching H-W., Elimelech M. and Hering J.G. (1994), Dynamics of coagulation of clay particles with aluminum sulfate. *J. Environ. Engg.*, **120**, 169-189.

Cohen J.M. and Hannah S.A. (1971), Coagulation and flocculation. In Water Quality and Treatment – A Handbook of Public Water Supplies, Third Edition. McGraw-Hill Book Company, New York, pp. 66-122.

Dentel S.K. and Gossett J.M. (1988), Mechanisms of coagulation with aluminum salts. *JAWWA*, **80**, 187-198.

Duan J. and Gregory J. (2003), Coagulation by hydrolysing metal salts. *Advances Colloid Interface Sci.*, **100-102**, 475-502.

Gao B. and Yue Q. (2005), Effect of SO_4^{2-}:Al^{3+} ratio and OH^-:Al^{3+} value on the characterization of coagulant poly-aluminum-chloride-sulfate (PACS) and its coagulation performance in water treatment. *Chemosphere*, **61**, 579-584.

Gao B., Yue Q. and Wang B. (2002), The chemical species distribution and transformation of polyaluminum silicate chloride coagulant. *Chemosphere*, **46**, 809-813.

Greenberg A.E., Clesceri L.S. and Eaton A.D. (Eds.) (1992), Standard Methods for the Examination of Water and Wastewater, 18th Edition. Published jointly by American Public Health Association, American Water Works Association and Water Environment Federation, Washington, DC, pp. 2-53 to 2-55.

Gregory J. and Duan J. (2001), Hydrolyzing metal salts as coagulants. *Pure Appl. Chem.*, **73**, 2017-2026.

Hsu P.H. (1966), Formation of gibbsite from aging hydroxy-aluminum solutions. *Soil Sci. Soc. Am. Proc.*, **30**, 173-176.

Hsu P.H. (1992), Reaction of OH-Al polymers with smectites and vermiculites. *Clays and Clay Minerals*, **40**, 300-305.

Hunt J.P. (1965), Metal Ions in Aqueous Solution. W.A. Benjamin, Inc., New York, pp. 45-54.

Jiang J.Q. and Graham N.J.D. (1996), Enhanced coagulation using Al/Fe(III) coagulants: effect of coagulant chemistry on the removal of colour-causing NOM. *Environ. Technol.*, **17**, 937-950.

Kinniburgh D.G. and Jackson M.L. (1981), Cation adsorption by hydrous metal oxides and clay. In Anderson M.A. and Rubin A.J. (Eds.), Adsorption of Inorganics at Solid-Liquid Interfaces. Ann Arbor Science Publishers Inc., Ann Arbor, MI, pp. 91-160.

Letterman R.D., Vanderbrook S.G. and Sricharoenchaikit P. (1982), Electrophoretic mobility measurements in coagulation with aluminum salts. *JAWWA,* **74**, 44-51.

Masliyah J.H. (1994), Electrokinetic Transport Phenomena. AOSTRA Technical Publication Series #12, Edmonton, Canada, pp. 173-195.

O'Melia C.R. (1986), Polymeric inorganic flocculants. In Moudgil B.M. and Somasundaran P. (Eds.), Flocculation, Sedimentation and Consolidation. Proceedings of the Engineering Foundation Conference, Georgia, AIChE, pp. 159-169.

Orvig C. (1993), The aqueous coordination chemistry of aluminum. In Robinson G.H. (Ed.), Coordination Chemistry of Aluminum. VCH, New York, pp. 85-121.

Parthasarathy N. and Buffle J. (1985), Study of polymeric aluminum (III) hydroxide solutions for application in waste water treatment. Properties of the polymer and optimal conditions of preparation. *Water Res.*, **19**, 25-36.

Sarpola A., Hietapelto V., Jalonen J., Jokela J. and Laitinen R.S. (2004a), Identification of the hydrolysis products of $AlCl_3 \cdot 6H_2O$ by electrospray ionization mass spectrometry. *J. Mass Spectrom.*, **39**, 423-430.

Sarpola A., Hietapelto V., Jalonen J., Jokela J., Laitinen R.S. and Rämö J. (2004b), Identification and fragmentation of hydrolyzed aluminum species

by electrospray ionization tandem mass spectrometry. *J. Mass Spectrom.*, **39**, 1209-1218.

Sarpola A.T., Hietapelto V.K., Jalonen J.E., Jokela J. and Rämö J.H. (2006), Comparison of hydrolysis products of $AlCl_3 \cdot 6H_2O$ in different concentrations by electrospray ionization time of flight mass spectrometer (ESI TOF MS). *Intern. J. Environ. Anal. Chem.*, **86**, 1007-1018.

Schindler P.W. (1981), Surface complexes at oxide-water interfaces. In Anderson M.A. and Rubin A.J. (Eds.), Adsorption of Inorganics at Solid-Liquid Interfaces. Ann Arbor Science Publishers Inc., Ann Arbor, MI, pp. 1-50.

Smith R.W. (1971), Relations among equilibrium and nonequilibrium aqueous species of aluminum hydroxyl complexes. In Gould R.F. (Ed.), Nonequilibrium Systems in Natural Water Chemistry, Advances in Chemistry Series 106. ACS, Washington, DC, pp. 250-279.

Smith R.W. and Hem J.D. (1972), Effect of aging on aluminum hydroxide complexes in dilute aqueous solutions. Geological Survey Water-Supply Paper 1827-D, US Government Printing Office, Washington, 51 p.

Stol R.J., van Helden A.K. and de Bruyn P.L. (1976), Hydrolysis-precipitation studies of aluminum(III) solutions: 2. A kinetic study and model. *J. Colloid Interface Sci.*, **57**, 115-131.

Stumm W. and Morgan J.J. (1970), Aquatic Chemistry. Wiley-Interscience, New York, pp. 244-258.

Stumm W. and Morgan J.J. (1995), Aquatic Chemistry: Chemical Equilibria and Rates in Natural Waters, 3rd. Edition. John Wiley & Sons, New York, pp. 252-348.

Stumm W. and O'Melia C.R. (1968), Stoichiometry of coagulation. *JAWWA*, **60**, 514-539.

Sullivan J.H. and Singley J.E. (1968), Reactions of metal ions in dilute aqueous solution: hydrolysis of aluminum. *JAWWA*, **60**, 1280-1287.

Tambo N. (1991), Basic concepts and innovative turn of coagulation/flocculation. *Water Supply*, **9**, Jönköping, 1-10.

Tsai P.P. and Hsu P.H. (1984), Studies of aged OH-Al solutions using kinetics of Al-ferron reactions and sulfate precipitation. *Soil Sci. Soc. Am. J.*, **48**, 59-65.

Turner R.C. (1968), Conditions in solution during the formation of gibbsite in dilute Al salt solutions: 2. Effect of length of time of reaction on the formation of polynuclear hydroxyaluminum cations, the substitution of other anions for OH^- in amorphous $Al(OH)_3$ and the crystallization of gibbsite. *Soil Sci.*, **106**, 338-344.

Turner R.C. (1969), Three forms of aluminium in aqueous systems determined by 8-quinolinolate extraction methods. *Can. J. Chem.*, **47**, 2521-2527.

Turner R.C. and Ross G.J. (1970), Conditions in solution during the formation of gibbsite in dilute Al salt solutions: 4. Effect of Cl concentration and temperature and a proposed mechanism for gibbsite formation. *Can. J. Chem.*, **48**, 723-729.

Van Benschoten J.E. and Edzwald J.K. (1990), Chemical aspects of coagulation using aluminum salts – I. Hydrolysis reactions of alum and polyaluminum chloride. *Wat. Res.*, **24**, 1519-1526.

Wang D., Tang H. and Gregory J. (2002), Relative importance of charge neutralization and precipitation on coagulation of kaolin with PACl: effect of sulfate ion. *Environ. Sci. Technol.*, **36**, 1815-1820.

Wang Y., Gao B-Y., Xu X-M., Xu W-Y. and Xu G-Y. (2009), Characterization of floc size, strength and structure in various aluminum coagulants treatment. *J. Colloid Interface Sci.*, **332**, 354-359.

Waters D.N. and Henty M.S. (1977), Raman spectra of aqueous solutions of hydrolysed aluminium (III) salts. *J. Chem. Soc., Dalton Trans.*, 243-245.

Xiao F., Zhang X. and Lee C. (2008), Is electrophoretic mobility determination meaningful for aluminum(III) coagulation of kaolinite suspension? *J. Colloid Interface Sci.*, **327**, 348-353.

Zelazny L.W. and Jardine P.M. (1989), Surface reactions of aqueous aluminum species. In Sposito G. (Ed.), The Environmental Chemistry of Aluminum. CRC Press, Inc., Boca Raton, FL, pp. 147-184.

Zhao H., Liu H. and Qu J. (2009), Effect of pH on the aluminum salts hydrolysis during coagulation process: formation and decomposition of polymeric aluminum species. *J. Colloid Interface Sci.*, **330**, 105-112.

CHAPTER 4

INFLUENCE OF ELECTRODE PARAMETERS ON A.C. ELECTROCOAGULATION OF FINE SILICA

4.1 INTRODUCTION

In this chapter, attention is turned towards electrode parameters to examine their influences on the AC electrocoagulation process. The area, separation and material of construction of the electrodes were varied in direct electrocoagulation tests. As in testwork described previously in this thesis, the feed suspension consisted of 5.0 wt % silica dispersed in de-ionized water containing 200 mg/L NaCl. The response of the settling behaviour of silica to variations of the three electrode parameters was studied.

4.2 ELECTRODE AREA

4.2.1 Electrode Area Tests

In six direct electrocoagulation tests, current at a density of 70.2 A/m^2 was passed for 15 minutes between electrodes spaced 1.0 cm apart. This spacing was selected so that the cell could accommodate as many as 7 electrodes. Electrode area was increased from 299.1 to 1794.6 cm^2 by the addition of electrodes to the cell, and the current was increased proportionally. Continuous agitation was maintained with an impeller tip speed of 1.73 m/s. The temperature and pH of the feed suspension varied as follows: 22.3° to 22.7°C and 8.7 to 8.8. Settling tests were performed at 24°C on the electrocoagulated slurries.

4.2.2 Electrode Area Test Results and Discussion

Figure 4-1 describes the settling behaviour of electrocoagulated silica as it was affected by electrode area. Silica exhibited progressively enhanced settling behaviour with increasing electrode area. With the area increase from 299.1 to 1794.6 cm^2, the time of initial settling was curtailed from 11.5 to 5.5 minutes, and the slope of the initial portion of the settling curves increased. Hence, the initial settling rate increased with plate area, as depicted in Figure 4-2.

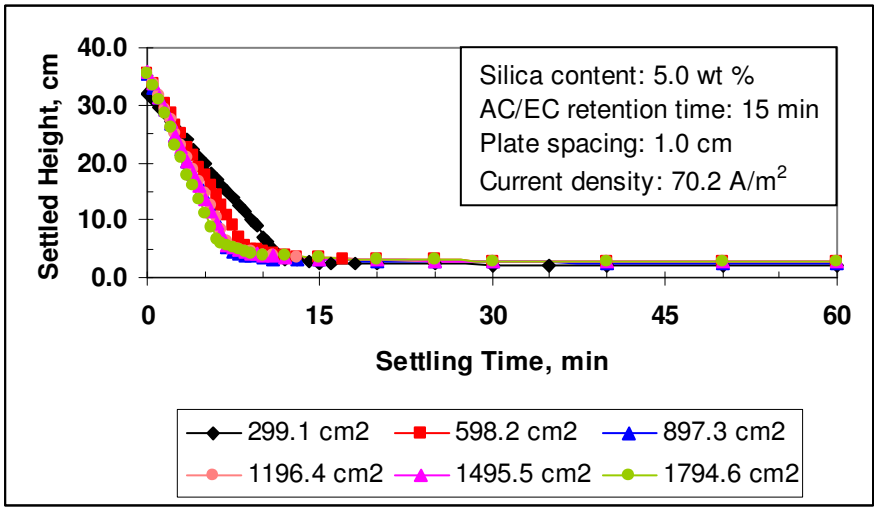

Figure 4-1. Progressive enhancement of silica settling behaviour with increasing electrode area.

As the electrode area was increased (Figure 4-2) from 299.1 to 897.3 cm^2 with current increase from 2.1 to 6.3 A, the initial settling rate increased linearly from 2.5 to 4.3 cm/min. Further area increases in the range of 1196.4 to 1794.6 cm^2 (current, I, raised from 8.4 to 12.6 A) caused the initial settling rate to adopt a different mode of improvement. From the discussion in Chapter 2, it is inferred that aluminum hydroxide precipitated when the electrode area was increased beyond 897.3 cm^2 (*i.e.*, I > 6.3 A).

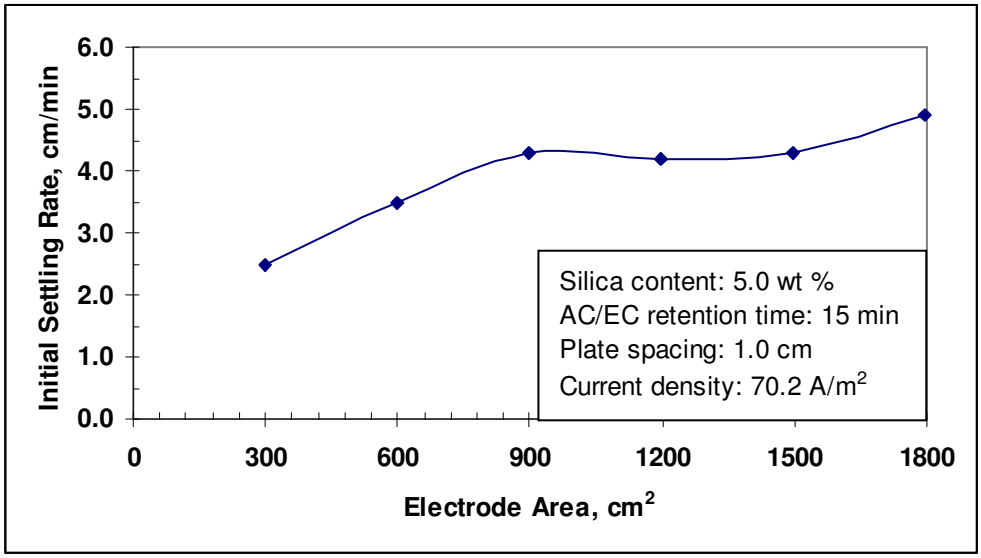

Figure 4-2. Effect of electrode area on the initial settling rate of electro-coagulated silica.

Between 900 and 1500 cm^2 of electrode area (6.3 A < I < 10.5 A), the initial settling rate reached a plateau which is attributed to floc fragmentation. It is proposed that aluminum hydroxide precipitate was adsorbed at bridging sites (see Chapter 2) on the silica flocs. The bridges so formed are considered to have been mechanically weaker than those formed by soluble aluminum complexes (Wang *et al.*, 2009).

As the electrode area was increased beyond 1500 cm^2 (I > 10.5 A), the precipitation rate increased to the extent that it enhanced the settling behaviour of the silica flocs by increasing their bulk density and, conceivably, by enmeshing the flocs. The range of sediment thicknesses in Figure 4-1 attest to the occurrence of precipitation. Hence, the interlude between 900 and 1200 cm^2 (6.3 A < I ≤ 8.4 A) constituted a transition in the mode by which the settling behaviour of silica was enhanced: from sole control by floc size to joint control by floc size, floc densification (*i.e.*, reduction of porosity) and, possibly, enmeshment. It is expected that the d_{50} for silica, which was electrocoagulated with currents exceeding 6.3 A (*i.e.*, electrode areas greater than 900 cm^2), would follow the trend depicted in Figure 2-16.

The variation of the pH of the silica slurry with electrocoagulation time is tracked in Figure 4-3. It should be noted that the pH values (tabulated in Appendix A) were measured at the instantaneous operating temperature which rose with time as a result of Joule heating. Initially, the pH tended to decrease more rapidly with increasing electrode area because of the accelerated reactions occurring at the higher current. In every case, the pH attained a minimum and the final slurry pH rose higher with increasing electrode area (hence, current) as floc growth progressed and/or settling behaviour improved.

In addition, Figure 4-3 shows that, for electrode areas in the range of 897.3 to 1495.5 cm^2 where the initial settling rates were practically the same (see Figure 4-2), the pH curves became almost indistinguishable from one another in the last third of electrocoagulation time. In general, therefore, the relative displacements of the curves connote the relative extents to which the settling behaviour of silica was enhanced.

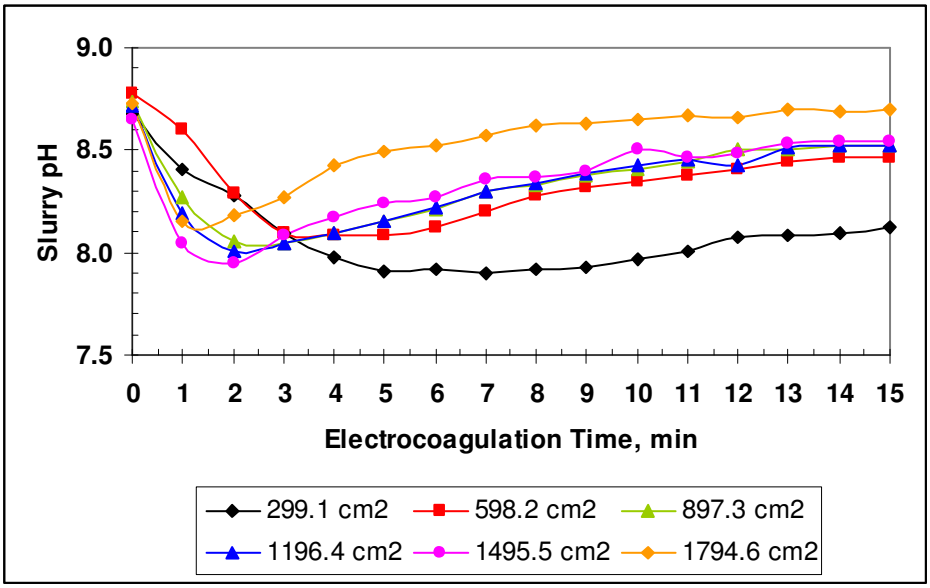

Figure 4-3. Variation of slurry pH with electrocoagulation time and electrode area.

Table 4-1. Effect of net change in slurry pH.

Electrode Area, cm^2	Slurry ΔpH	Initial Settling Rate, cm/min
299.1	0.56	2.5
598.2	0.32	3.5
897.3	0.22	4.3
1196.4	0.20	4.2
1495.5	0.11	4.3
1794.6	0.03	4.9

In Table 4-1, the net slurry pH change is recorded against electrode area and initial settling rate. The ΔpH value decreased with increasing area and, in general, with improvement in settling behaviour. The pH minima ranged narrowly, from 7.9 to 8.1 (Figure 4-3), but their values do not appear to hold special significance. However, the electrocoagulation times, at which the minima occurred, became shorter as the electrode area (hence, current) was increased, as would be expected. To be compared with these times are the observed times of the onset of enhanced settling, which were obtained by interrupting the current flow and agitation, and then observing the settling behaviour of the solids. Naturally, the times are not precise, but it can be stated that onset occurred within these times. The two sets of times are reported in Table 4-2.

Table 4-2. Comparison of onset times with times of pH minima.

Electrode Area, cm^2	Onset Time, min	Time of pH Minimum, min
299.1	< 8	7
598.2	< 6	4.5
897.3	< 4.5	2.8
1196.4	< 4	2
1495.5	< 3.5	1.8
1794.6	< 2	1

In the determination of the onset times, the settling behaviour of the solids was observed, on occasion, at the time at which the minimum suspension pH was recorded. On these occasions, enhanced settling was not perceptible, from which it is inferred that, having been only destabilized, the silica particles had not formed aggregates to any significant extent to demonstrate the enhanced settling that was expected. Microflocs are expected to have been formed at this stage and to have coexisted with discrete particles. As such, the particles and microflocs are considered to have been on the threshold of enhanced settling. Therefore, the times of minimum pH attainment are taken to be the times at which coagulation ended and floc growth began. The rise of the slurry pH from the minimum to the final value is interpreted to reflect floc growth.

Possible reactions, to which the initial pH drop might be ascribed, are represented by Equations 4-1 to 4-6.

$$2\ H_2O \rightarrow O_2(g) + 4\ H^+ + 4e \qquad \text{(anodic side reaction)} \qquad (4\text{-}1)$$

$$Al^{3+} + H_2O \leftrightarrow AlOH^{2+} + H^+ \qquad (4\text{-}2)$$

$$AlOH^{2+} + H_2O \leftrightarrow Al(OH)_2^+ + H^+ \qquad (4\text{-}3)$$

$$Al(OH)_2^+ + H_2O \leftrightarrow Al(OH)_3(am)^* + H^+ \qquad (4\text{-}4)$$

$$Al(OH)_3^o + H_2O \leftrightarrow Al(OH)_4^- + H^+ \qquad (4\text{-}5)$$

$$\equiv Si\text{–}OH + Al(OH)_x^{(3-x)+} \leftrightarrow \equiv Si\text{–}OAl(OH)_x^{(2-x)+} + H^+ \qquad (4\text{-}6)$$

*amorphous solid

Equation 4-6 represents electrocoagulation by the specific adsorption of aluminum complex species (formed in Equations 4-2 to 4-4) onto the silica surface, denoted by ≡Si–OH (Stumm, 1992). It also provides insight into the effect of specific adsorption on zeta potential. Equation 4-1 was reported by

Przhegorlinskii *et al.* (1987) not to occur during DC/EC treatment (0.45 A, 30 minutes) of water containing 1000 mg/L NaCl. This observation stems from the low current employed (Holt *et al.*, 2005).

In the absence of aluminum hydroxide precipitation, possible reactions, to which the final pH rise from the minimum might be attributed, are represented by Equations 4-7 to 4-9.

$$2H_2O + O_2(g) + 4e \rightarrow 4\ OH^- \qquad \text{(cathodic reaction)} \qquad (4\text{-}7)$$

$$2\ H_2O + 2e \rightarrow H_2(g) + 4\ OH^- \qquad \text{(cathodic reaction)} \qquad (4\text{-}8)$$

$$\equiv Si\text{–}OH + Al(OH)_4^- \leftrightarrow \equiv Si\text{–}Al(OH)_4 + OH^- \qquad (4\text{-}9)$$

Whether Equation 4-7 or 4-8 occurs is dictated by aeration. Owing to the continuous agitation applied in the current testwork, Equation 4-7 is expected to have assumed prominence.

Polynuclear hydroxoaluminum species are formed under conditions of supersaturation (*i.e.*, $[Al^{3+}][OH^-]^3 > K_{S0}$) (Stumm and Morgan, 1981; O'Melia, 1986). The K_{S0} was exceeded easily within 15 minutes' electrocoagulation as discussed in Chapter 2 (Table 2-13), but precipitation did not occur. The deferment of precipitation is attributed to the polynuclear species, which are capable of persisting indefinitely in supersaturated solution (Baes and Mesmer, 1976; Stumm and Morgan, 1981; Parthasarathy and Buffle, 1985). Surface reactions of the types exemplified by Equations 4-10 to 4-12 are proposed to have occurred.

$$\equiv Si\text{–}OH + OH^- \leftrightarrow \equiv Si\text{–}O^- + H_2O \qquad (4\text{-}10)$$

$$\equiv Si\text{–}O^- + Al_2(OH)_2^{4+} \leftrightarrow \equiv Si\text{–}OAl_2(OH)_2^{3+} \qquad (4\text{-}11)$$

$$\equiv Si\text{–}OH + Al_{13}O_4(OH)_{24}^{7+} \leftrightarrow \equiv Si\text{–}OAl_{13}O_4(OH)_{24}^{6+} + H^+ \qquad (4\text{-}12)$$

The surface reaction in Equation 4-10 would be favoured by basic pH. De-protonation reactions, like Equation 4-12, contribute to slowing the pH rise. The formation of silica aggregates is summarized by Equation 4-13.

$$\equiv Si\text{–}OAl_2(OH)_2^{3+} + \equiv Si\text{–}OH \leftrightarrow \equiv Si\text{–}OAl_2(OH)_2^{2+}\text{–}O\text{–}Si\equiv + H^+ \qquad (4\text{-}13)$$

It follows that a bridged pair of particles or microflocs would continue forming bridges with other bridged assemblages (multiple level aggregation), or with discrete particles, as long as adsorption sites and –OH surface groups were

available. The limiting floc size would be defined by hydrodynamic conditions alone (in the absence of precipitation).

The positive charge on aluminum hydroxide precipitate particles is attributable to either pH < i.e.p. or to adsorbed cationic aluminum complexes (*e.g.*, Equation 4-14).

$$\equiv Al–OH + Al(OH)^{2+} \leftrightarrow \equiv Al–OAl(OH)^{+} + H^{+} \qquad (4\text{-}14)$$

When precipitation occurred in AC/EC-treated water in Chapter 2 (indirect electrocoagulation), the precipitate particles formed flocs. In direct electrocoagulation, however, such floc growth is not likely to occur on an appreciable scale because of the miniscule proportion of precipitate (<1 mg Al/g silica or <3 mg $Al(OH)_3$/g silica) relative to silica. Instead, it is much more likely that the precipitate particles were adsorbed by the silica flocs, as exemplified by Equations 4-15 and 4-16.

$$\equiv Al–OAl(OH)^{+} + \equiv Si–OH \leftrightarrow \equiv Al–OAl(OH)–O– Si\equiv + H^{+} \qquad (4\text{-}15)$$

$$\equiv Si–OAl_2(OH)_2^{3+} + \equiv Al–OAl(OH)^{+} \leftrightarrow \equiv Si–OAl_2(OH)^{4+}–OAlO–Al\equiv + H_2O \qquad (4\text{-}16)$$

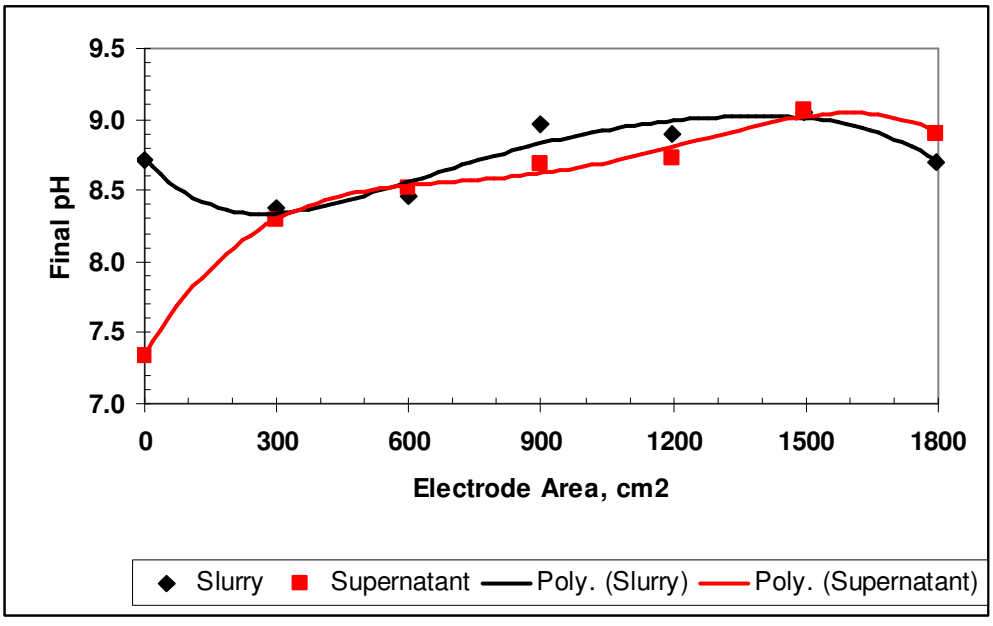

Figure 4-4. Variation of final pH with electrode area.

The final pH values of the electrocoagulated slurry and supernatant samples were measured at the temperature of the feed suspension for ready comparison. The data are reported in Appendix A and are graphed in Figure 4-4.

No relationship is apparent between the final slurry pH and the electrode area or current. The pH variation depended on the nature of the reactions that occurred. The supernatant pH, on the other hand, rose consistently with electrode area (*i.e.*, current).

Operating data from the tests are presented in Table 4-3 where T_i and T_f represent the temperatures of the feed suspension and electrocoagulated slurry, respectively.

Table 4-3. Operating data from electrode area tests.

Electrode Area (cm^2)	Current (A)	T_i (°C)	T_f (°C)	V_{avg} (V)	Specific Energy Input (kJ/kg Silica)
299.1	2.1	22.3	23.9	17.3	155
598.2	4.2	22.7	26.2	17.5	314
897.3	6.3	22.6	27.8	17.6	474
1196.4	8.4	22.7	29.4	17.4	623
1495.5	10.5	22.6	31.0	17.3	774
1794.6	12.6	22.5	32.5	16.5	889

As the current was increased from 2.1 A to 12.6 A at constant current density, the temperature increases in the slurry ranged from 1.6° to 10.0°C. The average voltage across two electrodes was the same as it was across seven because of the series arrangement. The specific energy input was influenced mainly by the magnitude of the current, and ranged from 155 to 889 kJ/kg silica.

4.3 ELECTRODE SEPARATION

4.3.1 Electrode Separation Tests

The effect of electrode separation on the electrocoagulation of silica was investigated with eight direct AC/EC tests. Current at a density of 70.2 A/m^2 was passed for 15 minutes between two electrodes at separations of 0.5 to 7 cm. Temperature and pH variations of the feed suspension were as follows: 20.5° to 20.9°C and 8.6 to 8.8. Agitation was maintained continuously at an impeller tip speed of 1.73 m/s. Settling tests were performed at 24°C on the electrocoagulated slurries.

4.3.2 Electrode Separation Test Results and Discussion

The initial settling rates of silica, after electrocoagulation at various electrode separations, are plotted in Figure 4-5. The experimental data were expected to give a line parallel to the Electrode Separation axis, since the same conditions were applied to each test. Instead, the result was the data scatter shown. In addition, the mode of variation of the initial settling rate with electrode separation was expected to reflect the influence of the hydrodynamics in the electrocoagulation cell. The hydrodynamics were expected to change with the cell geometry as the electrode separation was changed. However, the test results do not provide any clear evidence of hydrodynamic control of the electrocoagulation process, as measured by the initial settling rate.

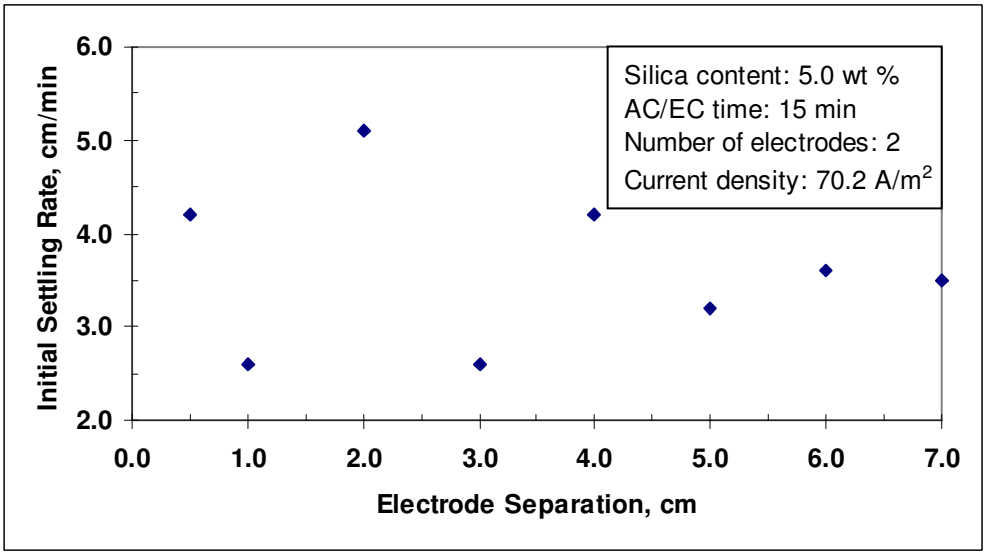

Figure 4-5. Effect of electrode separation on the initial settling rate of electrocoagulated silica.

4.4 MATERIAL OF ELECTRODE CONSTRUCTION

4.4.1 Test with Carbon Electrodes

In one direct electrocoagulation test, aluminum electrodes were replaced with carbon electrodes of the same length and width as the aluminum ones. Two carbon electrodes were positioned 2.5 cm apart and a current of 2.1 A (70.2 A/m^2 density) was passed for 15 minutes, with continuous agitation at 1.73 m/s impeller tip speed. After this treatment, agitation and current flow were stopped. When no enhancement of the settling behaviour of silica was observed, the test was resumed with the current increased to 3.5 A (117.0 A/m^2 density). After three

minutes, agitation and current flow were again stopped, but no enhanced settling could be observed. The test was concluded after a third treatment at 5.0 A (167.2 A/m^2 density) for 7 minutes.

4.4.2 Carbon Electrode Test Results and Discussion

After a total of 25 minutes' AC/EC treatment with carbon electrodes, the silica suspension remained stable. This result is consistent with the fact that metal ion hydrolysis species are the effective coagulants (Moreno *et al.*, 2009; Cañizares *et al.*, 2007; Jiang *et al.*, 2002; Beecroft *et al.*, 1995; Stumm and Morgan, 1981). The inert property of the carbon electrodes provided a convenient means of preheating feed water in the study of the effect of feed water temperature on AC/EC (Chapter 3, Section 3.3.5).

4.5 CHAPTER SUMMARY

Test results showed that, for a fixed current density, the initial settling rate of electrocoagulated silica increased with electrode area. Ultimately, the effect observed was really that of the current whose magnitude was increased proportionally with area to keep the current density constant.

For electrode areas in the approximate range of 300 to 900 cm^2 (2.1 A ≤ I ≤ 6.3 A), the initial settling rate was controlled by floc size. For areas ≥ 1500 cm^2 (I ≥ 10.5 A), the initial settling rate was controlled jointly by floc size, floc densification (*i.e.*, reduction of porosity) and, possibly, enmeshment by aluminum hydroxide precipitate. The intermediate range of 900 to 1500 cm^2 of electrode area represented transition in the mode of control of the initial settling rate as precipitation became more dominant. The transition range was also characterized by floc fragmentation, which is proposed to have occurred at sites where adsorbed precipitate formed mechanically weak inter-floc bridges, limiting the extent of multiple level aggregation.

Two stages of AC/EC treatment were defined by the behaviour of the suspension pH. The first stage was coagulation, during which the pH dropped dramatically. At the minimum pH attained, the coagulation stage was deemed to have ended. Within about two minutes afterwards, enhanced settling became evident. The time in which the minimum pH was attained was shortened by increased current, owing to acceleration of the kinetics of the electrode and other

reactions (see Section 4.2.2). In the second stage of AC/EC treatment, the slurry pH increased and silica floc growth progressed. As the current was raised with electrode area, the terminal pH of the electrocoagulated slurry increased.

No relationship could be defined between electrode separation and the enhanced settling behaviour of the electrocoagulated silica. It was anticipated that changes in electrode separation would alter the hydrodynamics in the electrocoagulation cell. However, the data obtained in these tests could not establish a clear dependence on the hydrodynamics.

Carbon electrodes, being inert in the aqueous environment, were incapable of undergoing anodic oxidation to form a hydrolyzable cation. Consequently, the stable silica suspension remained intact after AC/EC treatment.

4.6 REFERENCES

Baes C.F. and Mesmer R.E. (1976), The Hydrolysis of Cations. John Wiley & Sons, New York, pp. 112-123.

Beecroft J.R.D., Koether M.C. and van Loon G.W. (1995), The chemical nature of precipitates formed in solutions of partially neutralized aluminum sulfate. *Water Res.*, **29**, 1461-1464.

Cañizares P., Jiménez, C., Martínez F., Sáez C. and Rodrigo M.A. (2007), Study of the electrocoagulation process using aluminum and iron electrodes. *Ind. Eng. Chem. Res.*, **46**, 6189-6195.

Holt P.K., Barton G.W. and Mitchell C.A. (2005), The future for electrocoagulation as a localised water treatment technology. *Chemosphere*, **59**, 355-367.

Jiang J-Q., Graham N., André C., Kelsall G.H. and Brandon N. (2002), Laboratory study of electro-coagulation-flotation for water treatment. *Water Res.*, **36**, 4064-4078.

Moreno H.A., Cocke D.L., Gomes J.A.G., Morkovsky P., Parga J.R., Peterson E. and Garcia C. (2009), Electrochemical reactions for electrocoagulation using iron electrodes. *Ind. Eng. Chem. Res.*, **48**, 2275-2282.

O'Melia C.R. (1986), Polymeric inorganic flocculants. In Moudgil B.M. and Somasundaran P. (Eds.), Flocculation, Sedimentation and Consolidation. Proceedings of the Engineering Foundation Conference, Georgia, AIChE, pp. 159-169.

Parthasarathy N. and Buffle J. (1985), Study of polymeric aluminum (III) hydroxide solutions for application in waste water treatment. Properties of the polymer and optimal conditions of preparation. *Water Res.*, **19**, 25-36.

Przhegorlinskii V.I., Ivanishvili A.I. and Grebenyuk V.D. (1987), Dissolution of aluminum electrodes in the electrocoagulation treatment of water. *Soviet J. Water Chem. Technol.*, **9**, 118-119.

Stumm W. (1992), Chemistry of the Solid-Water Interface. Wiley-Interscience, New York, pp. 47-51.

Stumm W. and Morgan J.J. (1981), Aquatic Chemistry: An Introduction Emphasizing Chemical Equilibria in Natural Waters. John Wiley & Sons, New York, pp. 323-417.

Wang Y., Gao B-Y., Xu X-M., Xu W-Y. and Xu G-Y. (2009), Characterization of floc size, strength and structure in various aluminum coagulants treatment. *J. Colloid Interface Sci.*, **332**, 354-359.

CHAPTER 5

AMENABILITY OF FINE NATURAL AND INDUSTRIAL PARTICULATES TO A.C. ELECTROCOAGULATION

5.1 INTRODUCTION

After AC/EC was shown to be effective in enhancing the settling behaviour of silica, the question arose concerning the effectiveness of the technique on fine natural and industrial particulates. Hence, tests were conducted on bentonite, Syncrude mature fine tailings (MFT), and coal tailings from the former Luscar Sterco to assess their amenability to electrocoagulation.

In the U.S., the principal bentonite-producing area is the Black Hills region which includes Wyoming, South Dakota and Montana. Its fine particle size, very low permeability to water, and its swelling response to dispersion in water make bentonite an essential material for civil engineering applications in the construction of slurry trench cutoffs and of liners for tailings ponds, lagoons and canals (Buettner, 1985; Haug, 1985). One of the best known applications of bentonite is in oil field drilling mud. At a viscosity of approximately $1.5x10^{-3}$ Pa.s (1.5 cP), the mud lubricates the drill bit, suspends and aids removal of rock cuttings from the drill hole, and forms a water barrier on the wall of the drill hole (Grim and Güven, 1978). Bentonite is a constituent in paper, paints, pharmaceuticals, cosmetics and Portland cement. It serves as a coagulation aid in water treatment by providing surface for sweep floc formation and by increasing the floc density (Cohen and Hannah, 1971; Olin and Peterson, 1937; Olin and Gauler, 1938). In agriculture, bentonite improves water retention in soils. Catalysts are prepared from bentonite for use in petroleum cracking. Bentonite is either calcined to a glass or compacted to encase radioactive waste before emplacement in underground vaults (Grim and Güven, 1978).

Syncrude MFT is found at depths of over 17 m in the tailings ponds at Fort McMurray, Alberta. It contains 2 to 5 wt % bitumen and over 35 wt % solids. The solids have a top size of about 150 µm and consist of sand, silt and clay, as defined by particle size (Smart and Tovey, 1982). Over 60 wt % of the tailings is comprised of sludge formers, which are silt and clay particles <22 µm in size

(MacKinnon, 1989), and which confer on the tailings its poor settling characteristics. The clay particles (~10 wt %) have an equivalent diameter of <2.8 µm. It is expected (MacKinnon, 1989) that full compression of the solids in the ponds will be achieved in a matter of decades.

Luscar Sterco Ltd., Coal Valley, Alberta, used to mine sub-bituminous, high-volatile coal from which thermal grade coal was produced. Settling became problematic for coal from the Mynheer deposit because of the bentonite content, montmorillonite being the major clay mineral. Thickening difficulties created a bottle-neck in the operations, effectively limiting plant capacity and elevating the operating costs associated with chemical treatment, while increasing the demand for fresh water. The tailings, designated as “fines undersize”, had a top size of approximately 500 µm and contained up to 40 wt % ash when it was rejected to the tailings pond from the thickener.

5.2 THEORY AND BACKGROUND

5.2.1 Bentonite

Bentonite is well known for its ability to form stable suspensions in water (Kitchener, 1978; Olin and Pearson, 1937; van Olphen, 1987). It is a rock, the alteration product of volcanic ash, and is composed essentially of a crystalline clay mineral (Grim and Güven, 1978). The characteristic clay mineral is typically montmorillonite, but less often beidellite. Members of the montmorillonite-beidellite series constitute the smectites which commonly occur in bentonites (Ross and Shannon, 1926). Since the smectite mineral predominates in bentonite, the properties of the latter are dictated by those of the former (Grim and Güven, 1978). Montmorillonite accounts for 70 to 90 wt % of bentonite (van Veen, 1985). The general, ideal compositions of the end-members are described below (Grim and Güven, 1978):

$$\text{montmorillonite} \quad [(Al_x, Mg_z)Si_4O_{10}(OH)_2]M^+_z ,$$

where $x + z = 2.00$ and M^+ is an exchangeable cation; and

$$\text{beidellite} \quad [Al_{2x}(Si_{4.00-u}, Al_u)O_{10}(OH)_2]M^+_u ,$$

where M^+ is an exchangeable cation.

In montmorillonite, Mg^{2+} substitutes isomorphously for Al^{3+}. Total loss of Mg^{2+} and isomorphous substitution of Al^{3+} for Si^{4+} make beidellite the alteration product of

montmorillonite. M^+ is usually Na^+, Mg^{2+}, Ca^{2+} or K^+, or may be distributed among two or more of these cations, but one of which predominates. Na^+ and Ca^{2+} are the most commonly observed (Grim and Güven, 1978).

Montmorillonite is a 2:1 clay mineral, meaning that a layer of Al-6(OH) units in octahedral arrangement is sandwiched between two layers of Si-4(O) units in tetrahedral arrangement. Mg^{2+} (or Fe^{2+}, Zn^{2+} or Li^+) replaces Al^{3+} in the octahedral layer. These substitutions account for the negative basal surface charge on montmorillonite and, hence, bentonite particles. Exchangeable cations are adsorbed in compensation for the charge imbalance, and reside between layers, being too large for accommodation in the unit cell (van Olphen, 1977). The positive edge charge originates from exposed Al^{3+} and Si^{4+} sites. However, the negative charge on bentonite particles predominates because the basal area far exceeds the edge area. Characteristically, Wyoming bentonite is dominated by Na-montmorillonite which, upon dispersion in water, swells perpendicular to the basal plane. With gentle shearing, the platelets delaminate into very thin sheets which would contain one or two of the basic 2:1 units (Kitchener, 1978). Hence, Na-montmorillonite is weak in shear. Apart from this lamellar morphology, Na-montmorillonite can exist in bentonite as single crystallites or as aggregates thereof, with the crystallites adopting lath, fibrous or rhombic grain-forms (Grim and Güven, 1978).

In plant tests, Snyder and Gregory (1979) demonstrated the effectiveness of AC/EC in enhancing the settling behaviour of colloidal clay particles which, otherwise, created severe settling problems at a coal preparation plant. They also discovered that a quiescent period following AC/EC treatment was beneficial to the electrocoagulation effect.

From a study of the adsorption of hydroxoaluminum complexes onto montmorillonite, the data indicated that approximately 18% of the adsorbed aluminum resided at intercalation sites (Hsu, 1992). The exchangeable cations, which normally occupy these sites, were almost completely replaced by the adsorbing aluminum. Similar adsorption behaviour of aluminum complexes was observed by XRD studies on Wyoming bentonite, in which montmorillonite was the clay mineral (Oades, 1984). Hsu (1992) also determined that the monomeric species adsorbed only to a negligible extent. Indeed, Kinniburgh and Jackson (1981) characterized the adsorption of polynuclear Al species onto

montmorillonite as strong. It is interesting to note that, in the presence of montmorillonite (or another clay mineral), aluminum exhibits a tendency to hydrolyze and eventually precipitate (Kinniburgh and Jackson, 1981; Oades, 1984). The aluminum concentration was not given.

5.2.2 Coal

The surface hydroxyl group on lignite occurs in the carboxyl (–COOH) and phenolic –OH functional groups, and have the capacity for reaction with other chemical species (Cullen and Siviour, 1981). It has been established (Brinker and Scherer, 1990; Schindler, 1981; Stumm, 1992) that specific adsorption at a surface occurs at the hydroxyl groups which react chemically with the adsorbing species. Hence, the adsorption of complex hydroxoaluminum species onto coal is facilitated by high surface density of –OH-containing groups on the coal. Berkowitz (1994) has implied that coals containing more than 80% carbon appear to contain low surface densities of –COOH, from which it may be inferred that the surface density of –OH-containing groups on coal increases as the coal rank decreases. Surface group densities on lignite have been quantified variously as follows: 1.62 meq –COOH/g and 6.47 meq phenolic –OH/g lignite; 0.7 to 1.8 meq –COOH/g and 4.9 to 7.3 meq phenolic –OH/g lignite (Cullen and Siviour, 1981). These authors developed equilibrium models for the adsorption of Cu, Zn, Ni and Cd ammine complexes onto lignite, and found that the models were essentially identical to those developed by others for conventional cation exchange resins. Protons from the phenolic –OH, or from both the phenolic –OH and carboxyl –OH were exchanged for the metal cations. In addition, Parekh *et al.* (1992) showed AC/EC to be an effective technique for enhancing the settling behaviour of sub-bituminous coal (d_{50} = 1.8 μm). Hence, hydroxoaluminum complexes are effective coagulants for coal.

5.3 MATERIALS AND EQUIPMENT

Bentonite was supplied by Reef Mud of Calgary, Alberta, under the trade name, Reef Gel Wyoming Bentonite. It was tested as received.

A sample of MFT was obtained from the tailings pond at the Mildred Lake operations of Syncrude Canada Ltd. in Fort McMurray, Alberta. It was diluted with de-ionized water for testing.

A tailings slurry sample, designated as “fines undersize” in the plant, was obtained from the coal preparation plant of the former Luscar Sterco at Coal Valley, Alberta. It was tested as received.

The materials and equipment were as detailed in Section 2.3.1. No chemical analysis was performed since the intention was not to conduct detailed studies but, rather, to assess the amenability of the materials to AC/EC as a means of enhancing their settling behaviour.

5.4 BENTONITE STUDY

5.4.1 Characterization of As-received Bentonite

Bentonite was characterized by its density, particle size distribution, natural settling behaviour and zeta potential. The determination methods are described in Section 2.3.2. Bentonite had a density of 2344.6 kg/m^3. Its particle size distribution is plotted in Figure 5-1.

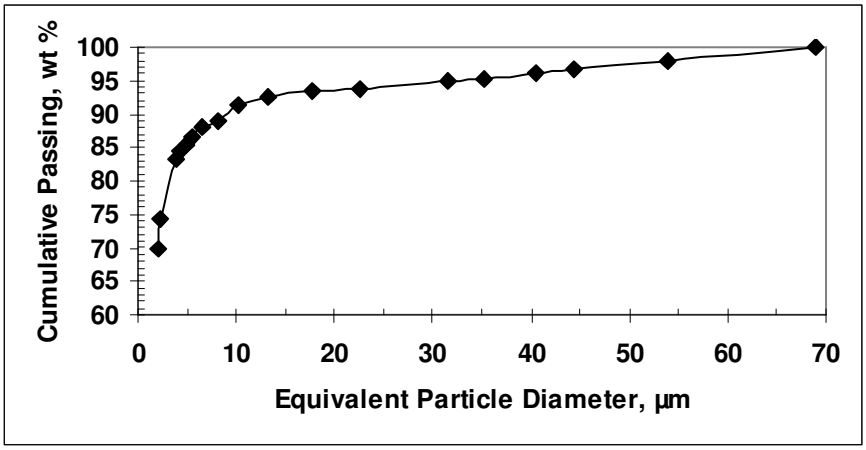

Figure 5-1. Particle size distribution of as-received bentonite.

As-received bentonite had a top size of about 70 µm. Approximately 90% was smaller than 10 µm and an estimated 60% passed 1 µm. Hence, the d_{50} size is estimated to be <1 µm. In de-ionized water containing 0 and 200 mg/L added NaCl, bentonite formed stable suspensions, with initial settling rates of 8.6×10^{-4} and 2.6×10^{-3} cm/min, respectively.

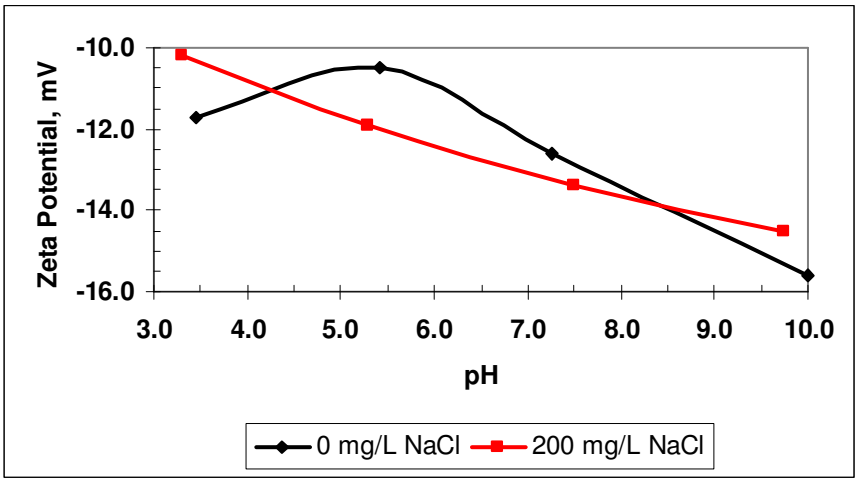

Figure 5-2. Effect of pH on zeta potential of as-received bentonite.

Zeta potentials are plotted against pH in Figure 5-2 for NaCl additions of 0 and 200 mg/L. When bentonite was dispersed in de-ionized water containing no NaCl, its zeta potential increased linearly with increasing pH, from -10.5 mV at pH 5.4 to -15.6 mV at pH 10. At pH < 5, the zeta potential increased as pH decreased. In de-ionized water containing 200 mg/L NaCl, bentonite showed an approximately linear increase in zeta potential with increasing pH, from -10.2 mV at pH 3.3 to -14.5 mV at pH 9.7. Over the pH range of 4.2 to 8.4, the zeta potential was higher in de-ionized water containing 200 mg/L NaCl.

5.4.2 Electrocoagulation of Bentonite

Electrocoagulation test procedures are detailed in Section 2.3.3. Bentonite was electrocoagulated at a concentration of 2.0 wt % solids, the concentration of drilling mud. The solids volume was so high that settling was hampered after electrocoagulation. The washings, however, exhibited enhanced settling, indicating that the solids content should be reduced to facilitate settling tests. Ultimately, after successive reductions of the solids concentration, 0.2 wt % solids proved practical for the testwork.

Unless noted otherwise, continuous agitation was applied at an impeller tip speed of 1.96 m/s and current was passed between two electrodes immersed 3.0 cm apart in 4.0 L of feed suspension. Settling tests were performed on the electrocoagulated materials at 24℃ (bentonite and coal) and at 22℃ (Syncrude

MFT). Zeta potential was measured for electrocoagulated bentonite samples from the retention time series.

5.4.2.1 Agitation

The effect of agitation was studied in two 15-minute direct electrocoagulation tests in which a current of 5.0 A was passed. Continuous agitation was employed in one test, but was omitted from the other. The feed suspension temperature and pH were 21.6℃ and 9.5.

Settling curves for bentonite after direct electrocoagulation, with and without agitation, are compared in Figure 5-3.

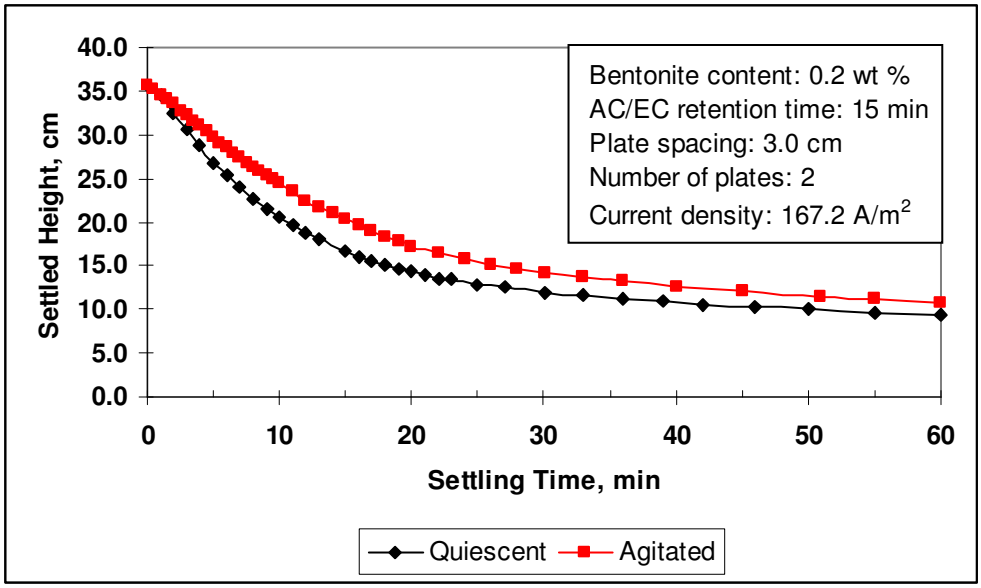

Figure 5-3. Effect of agitation during AC/EC on the settling behaviour of bentonite.

Owing to the viscosity changes with solids concentration in the slurries, and the slow rate of compression of the sediments, the settling curves assumed a rounded profile (Figure 5-3). They contrast with the more angular curves obtained for silica whose slurry viscosity did not change significantly with solids concentration, and whose sediments demonstrated faster compression rates.

Electrocoagulation in the absence of shear produced bentonite flocs with a higher initial settling rate (1.7 cm/min) than those produced in shear (1.2 cm/min), as a result of floc fragmentation (Kitchener, 1978). These initial settling rates represent more than two orders of magnitude enhancement in the initial

settling rate of as-received bentonite (2.6×10^{-3} cm/min). Flocs were observed after about 10 minutes of electrocoagulation.

Table 5-1. Pulp and water pH values from agitation tests.

Agitation	Pulp pH		Water pH	
	Feed	Electrocoagulated	Feed	Supernatant
No	9.50	9.41	6.50	8.89
Yes	9.49	9.52	6.59	9.03

Table 5-1 reports the pH values for the pulp, and for the feed and supernatant water. Dispersion of bentonite in the feed water increased the pH from 6.5 to 9.5 as exchangeable/leachable Na^+ and, possibly, Ca^{2+} were released from the solids in exchange for H^+ (Ghernaout *et al.*, 2008).

While the pH of the pulp registered only minor net change after 15 minutes of electrocoagulation, the pH of the water rose by 2.4 units. Operating data are presented in Table 5-2.

Table 5-2. Operating data from agitation tests.

Agitation	Pulp ΔT, ℃	V_{avg}, V	SEI, MJ/kg Bentonite
No	24.1	90.4	50.7
Yes	21.2	90.6	50.8

The net temperature change in the agitated pulp was ~3℃ lower owing to greater heat loss to the surroundings. The average applied voltages were the same. Consequently, the specific energy inputs (SEI) were the same but were high (50.8 MJ/kg bentonite). In sharp contrast, the SEI value for 5.0 wt % silica pulp was 2.1 MJ/kg (Table 2-24). It will be observed from these data that the silica concentration was 25 times as high as that of bentonite (0.2 wt %), but the SEI was approximately $\frac{1}{25}$ th that of bentonite. It appears, therefore, that SEI and solids concentration are inversely related, in which case the SEI for a 0.2 wt % silica pulp would be about 52.5 MJ/kg silica. Hence, the energy demands by the two types of pulp are comparable. It is apparent, therefore, that electrocoagulation of pulps of high solids content is advantageous with respect to

energy consumption. Thus, energy economics appear to argue against the application of AC/EC to water treatment on an industrial scale.

5.4.2.2 Retention Time

This series consisted of five direct electrocoagulation tests in which the AC/EC retention time ranged from 10 to 45 minutes and the current was fixed at 5.0 A. Feed suspension temperatures and pH varied from 21.5° to 21.7°C and from 9.3 to 9.5. A separate test was performed under the same conditions to determine the onset time of enhanced settling. In this test, agitation and current flow were interrupted every minute to allow observation of the settling behaviour.

The onset of enhanced settling was observed after four minutes of electrocoagulation. However, the supernatant was too cloudy for the settling test. Therefore, the electrocoagulation time was extended minute by minute to six minutes when the supernatant cleared up enough to give reliable settling data. The settling curves generated for AC/EC retention times of 6 to 45 minutes are shown in Figure 5-4.

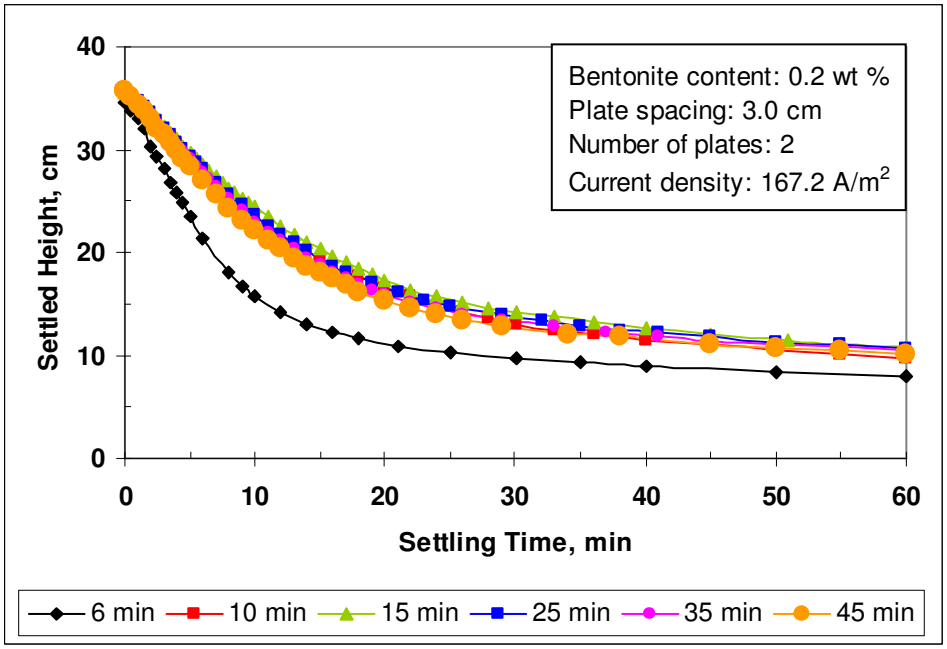

Figure 5-4. Effect of electrocoagulation time on the settling behaviour of bentonite.

The variation of initial settling rate with electrocoagulation time is plotted in Figure 5-5. A maximum rate of 2.2 cm/min was achieved after only 6 minutes'

electrocoagulation. Longer electrocoagulation times caused the rate to decline to about 1.3 cm/min.

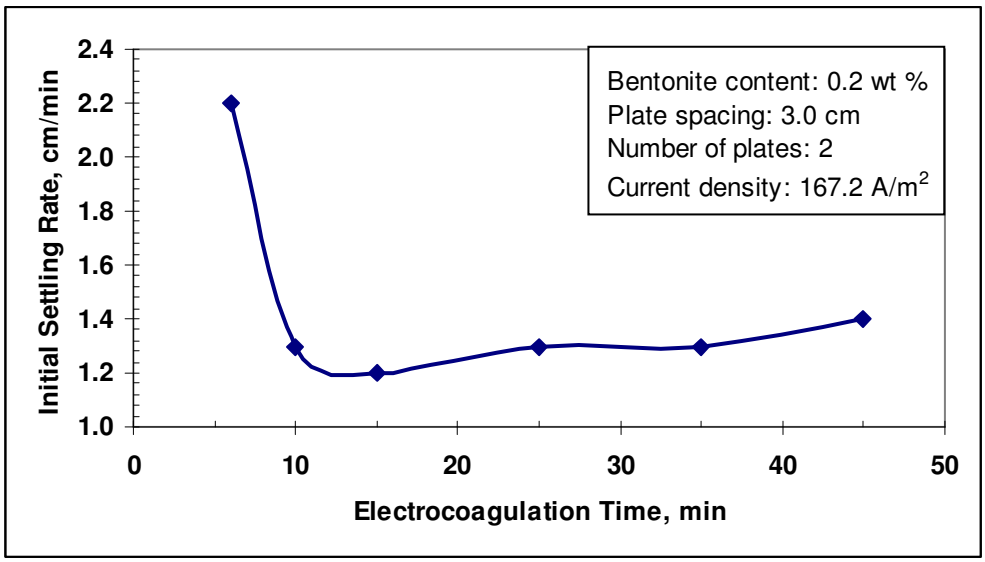

Figure 5-5. Variation of bentonite initial settling rate with electrocoagulation time.

From a value of -14.3 mV for the as-received bentonite (Figure 5-6), the zeta potential increased to a maximum of -16.1 mV after 25 minutes' electrocoagulation. With longer electrocoagulation times, the zeta potential decreased, reaching -14.5 mV at 45 minutes.

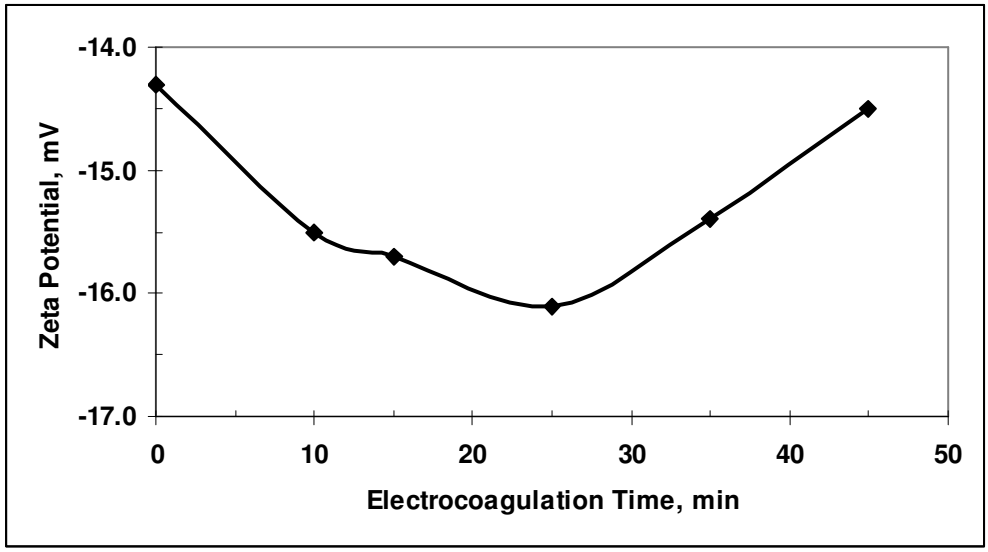

Figure 5-6. Effect of electrocoagulation time on the zeta potential of bentonite.

The zeta potentials (Figure 5-6) agree qualitatively with the conclusion of Tambo (1991), and with results reported from the silica study, that charge neutralization is not a prerequisite for the coagulation of clay particles. In further agreement with this work, Xiao *et al.* (2008) showed that zeta potential often does not determine or indicate the progress or likelihood of coagulation. Figure 5-6 illustrates that the zeta potential changed linearly from 25 to 45 minutes of electrocoagulation.

Table 5-3. Pulp and water pH values from retention time tests.

AC/EC Time (min)	Pulp pH		Water pH	
	Feed	Electrocoagulated	Feed	Supernatant
10	9.26	9.37	6.56	8.99
15	9.49	9.52	6.59	9.03
25	9.35	9.64	6.56	9.10
35	9.41	9.72	6.60	9.17
45	9.37	9.76	6.65	9.22

Pulp and water pH values are recorded in Table 5-3. As the electrocoagulation time was extended, the net pH elevations in the treated pulp increased; hence, from 10 to 45 minutes, ΔpH increased from <0.1 to 0.4. In the water, larger pH changes (2.4 to 2.6) occurred but appear not to have been influenced significantly by electrocoagulation time. Consideration of the variation of both the zeta potential and pulp pH with electrocoagulation time suggests that $Al(OH)_4^-$ was the predominant aluminum species, whose concentration increased with electrocoagulation time up to 25 minutes. At longer times, the effect of adsorbed $Al(OH)_4^-$ on zeta potential is proposed to have been ameliorated by aluminum hydroxide precipitate, whose particles were positively charged. The decrease in initial settling rate (Figure 5-5) at electrocoagulation times exceeding six minutes is imputed to low coagulative capacity of the $Al(OH)_4^-$ complex or to the formation of large, open flocs.

Operating data are summarized in Table 5-4.

Table 5-4. Operating data from retention time tests.

AC/EC Time, min	Pulp ΔT, ℃	V_{avg}, V	SEI, MJ/kg Bentonite
10	15.1	94.3	35.3
15	21.2	90.6	50.8
25	29.9	85.3	79.7
35	36.7	82.9	108.5
45	42.0	80.9	136.2

Pulp temperature increases of 15° to 42℃ accompanied electrocoagulation for periods of 10 to 45 minutes, respectively. The average applied voltage decreased with time, as was observed in the case of silica, as the water conductivity increased with temperature. However, the voltage decreases did not offset increases in energy demand owing to the time factor. Hence, SEI increased from 35.3 to 136.2 MJ/kg bentonite as AC/EC retention time was extended from 10 to 45 minutes.

The effect of cumulative AC/EC retention time mode was studied in a 15-minute test, thus: an initial 10 minutes of AC/EC, 5 minutes of intermission (no current or agitation), and a final 5 minutes of AC/EC. Settling curves generated from this test and the 15-minute continuous test are shown in Figure 5-7.

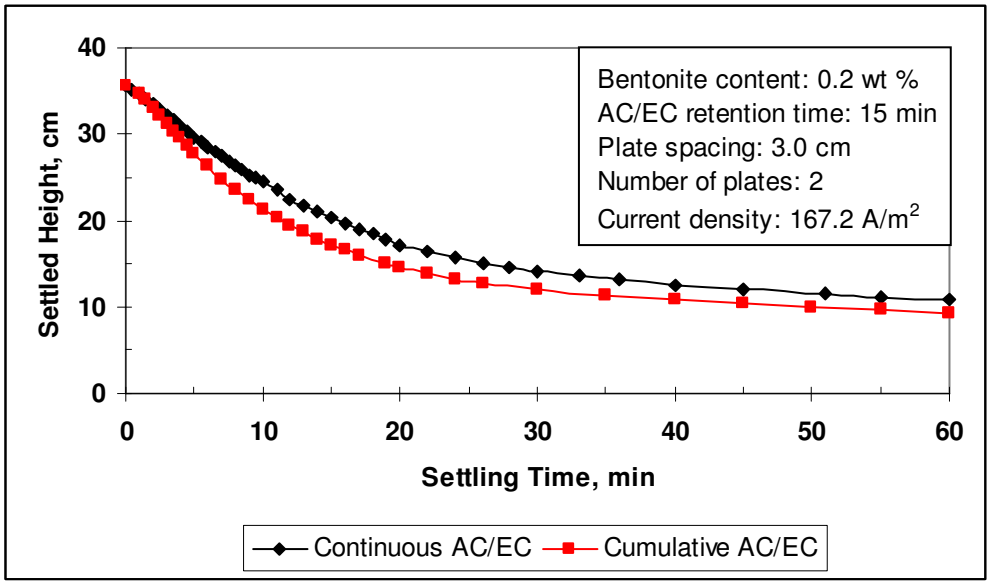

Figure 5-7. Influence of AC/EC retention time mode on settling behaviour of bentonite.

Initially, the cumulatively electrocoagulated bentonite behaved like the continuously treated material, which had an initial settling rate of 1.2 cm/min. After two minutes, however, the initial settling rate increased from 1.3 to 1.8 cm/min, giving an overall rate of 1.5 cm/min. These results indicate that under-electrocoagulated bentonite can be re-treated to improve its settling behaviour. The difference in settling behaviour for continuous and cumulative electrocoagulation is discussed further with the aid of Table 5-5.

Table 5-5. Comparison of settling behaviour engendered in bentonite by continuous and cumulative AC/EC.

AC/EC Time, min	AC/EC Time Mode	Initial Settling Rate, cm/min
10	Continuous	1.3
15	Cumulative	1.5
15	Continuous	1.2

While the initial settling rates in Table 5-5 are not greatly different, they illustrate the advantage of cumulative electrocoagulation. The initial 10 minutes of cumulative treatment gave an initial settling rate of 1.3 cm/min. A further five minutes of electrocoagulation improved the rate to 1.5 cm/min. Yet, continuous electrocoagulation for 15 minutes gave an initial settling rate of only 1.2 cm/min. From these results, it appears that the intermission during cumulative treatment allowed the flocs an opportunity for further growth. This is consistent with Snyder and Gregory (1979), and with Figure 5-3 which illustrated the benefit of quiescent conditions to the electrocoagulation process.

5.4.2.3 AC/EC Mode

The extents of enhancement of settling behaviour, achieved by the two modes of electrocoagulation (*i.e.*, direct and indirect), were compared in two tests. In the direct electrocoagulation test, the feed suspension temperature and pH were set at 21.5℃ and 9.4. In the indirect electrocoagulation test, the feed water temperature and pH were 21.6℃ and 6.6, this being the pH of the feed water in which bentonite was dispersed for the direct mode test. The pH rose considerably when bentonite was added to the water.

In both tests, a current of 5.0 A was passed for 45 minutes and agitation was applied continuously as follows: direct, 1.96 m/s; indirect, 1.75 m/s. The agitation rate was increased to 1.96 m/s to slurry bentonite with the AC/EC-treated water in the indirect mode test.

The enhanced settling behaviour of bentonite, after direct and indirect modes of electrocoagulation, is depicted in Figure 5-8.

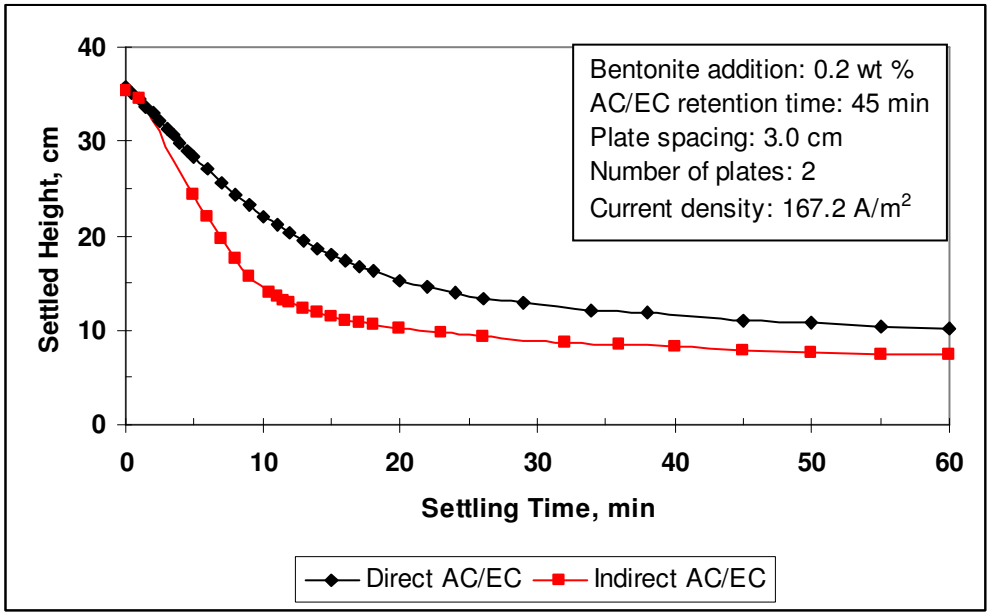

Figure 5-8. Effect of AC/EC mode on the settling behaviour of bentonite.

The indirectly electrocoagulated bentonite displayed the greater enhancement of settling behaviour. Compared to the initial settling rate of 1.4 cm/min for direct electrocoagulation, indirect electrocoagulation achieved an initial settling rate of 2.2 cm/min. Light precipitation of aluminum hydroxide was observed in the AC/EC-treated water, but it did not appear to hinder electrocoagulation of the bentonite. Hence, the greater enhancement of bentonite settling behaviour by indirect electrocoagulation represents similar behaviour to that of silica after 45 minutes' treatment (Figure 2-20). The pH values are presented in Table 5-6.

Table 5-6. Pulp and water pH variations with AC/EC mode.

AC/EC Mode	Pulp pH		Water pH		
	Feed	EC*	Feed	AC/EC-treated	Supernatant
Direct	9.37	9.76	6.65	-	9.22
Indirect	-	9.77	6.61	8.72	9.15

*Electrocoagulated

The pH values between the electrocoagulated pulps and between the supernatants were not appreciably different. This result suggests that the higher initial settling rate engendered by indirect electrocoagulation derived from the higher aluminum concentration in the AC/EC-treated water. The water pH increased from 6.6 to 8.7 during indirect electrocoagulation. In both electrocoagulation modes, the water pH increased from approximately 6.6 in the feed to 9.2 in the supernatant. Energy data are compared in Table 5-7 for the two modes of electrocoagulation.

Table 5-7. Operating data from AC/EC mode tests.

AC/EC Mode	ΔT, ℃	V_{avg}, V	SEI, MJ/kg Bentonite
Direct	42.0[1]	80.9	136.2
Indirect	46.1[2]	86.0	144.8

[1] Pulp [2] Water

In the case of silica, the average applied voltage and the temperature rise were the same for both modes of electrocoagulation. With bentonite, however, the temperature rise and average applied voltage were appreciably lower for direct electrocoagulation. This observation indicates that the water conductivity was increased by the presence of the bentonite from which leachable or exchangeable ions were released.

5.4.2.4 Current Density

In two direct electrocoagulation tests, currents of 2.5 and 5.0 A were passed for 15 minutes at densities of 83.6 and 167.2 A/m^2. The feed suspension temperature and pH were 21.6℃ and 9.5. The effect of current density on the settling behaviour of bentonite is illustrated in Figure 5-9.

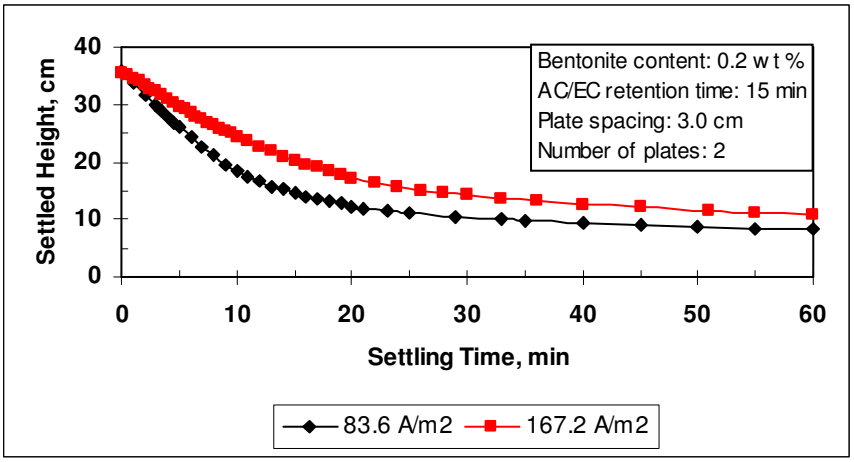

Figure 5-9. Effect of current density on the settling behaviour of bentonite.

A significantly higher initial settling rate (1.9 cm/min) was achieved by electrocoagulating bentonite at current density 83.6 A/m^2 than at 167.2 A/m^2 (1.2 cm/min). This result contrasts with that for silica, but it is consistent with the result obtained for bentonite in the retention time suite of tests (Section 5.4.2.2), where the possible formation of large open flocs was postulated. A review of the pH values is given in Table 5-8.

Table 5-8. Pulp and water pH values from current density tests.

Current Density (A/m^2)	Pulp pH		Water pH	
	Feed	Electrocoagulated	Feed	Supernatant
83.6	9.46	9.15	6.60	8.92
167.2	9.49	9.52	6.59	9.03

The water pH increased from 6.6 in the feed to 9.0 in the supernatants. In the pulps, the pH decreased from 9.5 to 9.2 at the lower current density, while showing virtually no net change at the higher density. Operating data are summarized in Table 5-9.

Table 5-9. Operating data from current density tests.

Current Density (A/m^2)	Current (A)	Pulp ΔT (°C)	V_{avg} (V)	SEI (MJ/kg Bentonite)
83.6	2.5	6.3	52.2	14.6
167.2	5.0	21.2	90.6	50.8

The pulp temperature rose by about 21°C during electrocoagulation at 167.2 A/m^2 and by approximately 6°C at 83.6 A/m^2. Respectively, the applied voltages averaged 52.2 V and 90.6 V, while the SEI values were 14.6 and 50.8 MJ/kg bentonite.

5.4.2.5 Electrode Area

The effect of electrode area was assessed in two direct electrocoagulation tests at a current density of 83.6 A/m^2. The currents and electrode areas were: 2.5 A, 299.1 cm^2; 5.0 A, 598.2 cm^2. The temperature and pH of the feed suspension were 21.8°C and 9.5.

In Figure 5-10, which depicts the enhanced settling behaviour of the treated bentonite, the greater enhancement was achieved with the smaller electrode area (*i.e.*, lower current). This result was duplicated by the current density tests (Figure 5-9). In both sets of tests, the AC/EC retention time was 15 minutes in the direct mode, and the initial settling rates were 1.9 cm/min for 2.5 A and 1.2 cm/min for 5.0 A. It, therefore, appears that the adsorption/floc-growth behaviour of bentonite was facilitated by the slower electrode reactions associated with the 2.5-A current. Moreover, the effects of electrode area and current density on electrocoagulation really reflect the effects of the current.

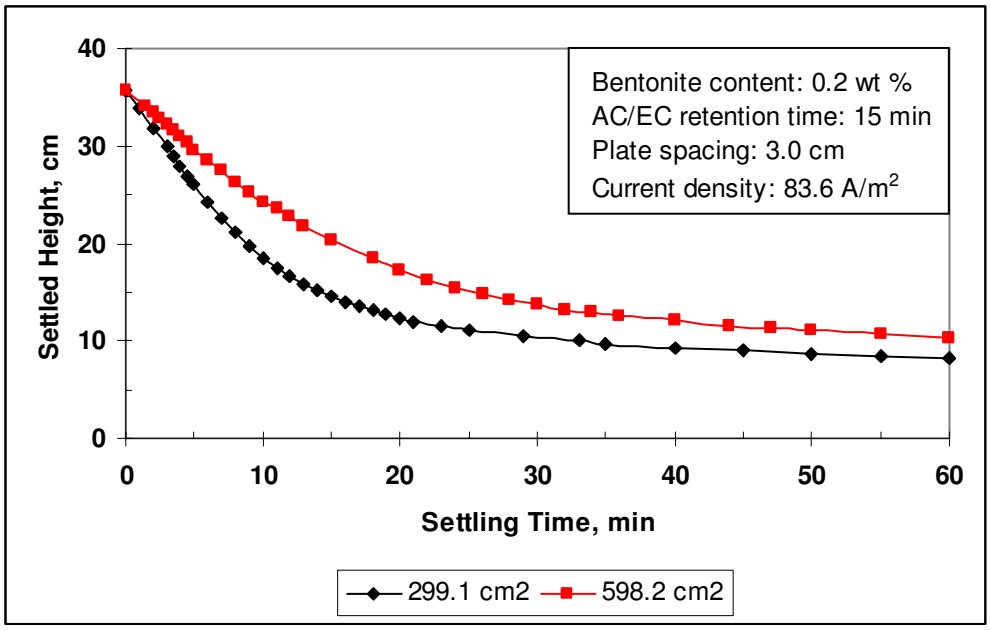

Figure 5-10. Effect of electrode area on the settling behaviour of bentonite.

Table 5-10 reports the pulp and water pH values.

Table 5-10. Pulp and water pH values from electrode area tests.

Electrode Area (cm^2)	Pulp pH		Water pH	
	Feed	Electrocoagulated	Feed	Supernatant
299.1	9.46	9.15	6.60	8.92
598.2	9.48	9.44	6.70	8.98

For both electrode areas, the net pH increase from the feed water to the supernatant was 2.3. The pulps registered net pH decreases of 0.3 (299.1 cm^2) and 0.04 (598.2 cm^2). Operating data are given in Table 5-11.

Table 5-11. Operating data from electrode area tests.

Electrode Area (cm^2)	Pulp ΔT (°C)	V_{avg} (V)	SEI (MJ/kg Bentonite)
299.1	6.3	52.2	14.6
598.2	12.2	51.4	28.8

The operating data suggest that doubling the current at the fixed density doubled the temperature rise and SEI value.

Operating data for the current density and electrode area tests at 5.0 A are compared in Table 5-12. The data indicate that, for a given AC/EC current and retention time, considerable energy savings can be realized by operating at a low current density. This provides a large electrode area which reduces the electrical resistance of the cell. Consequently, the Joule heating, applied voltage and SEI are all reduced.

Table 5-12. Comparison of operating data for 5.0 A current.

Test	C.D.[1] (A/m^2)	E.A.[2] (cm^2)	Pulp ΔT (°C)	V_{avg} (V)	SEI (MJ/kg)
Current density	167.2	299.1	21.2	90.6	50.8
Electrode area	83.6	598.2	12.2	51.4	28.8

[1]Current density [2]Electrode area

5.4.2.6 Quantity of Electricity

A fixed quantity of 3000 C of electricity was passed in two direct electrocoagulation tests as follows: 5.0 A for 10 minutes and 2.5 A for 20 minutes. The feed suspension temperature and pH were 21.6°C and 9.3. The settling test results are plotted in Figure 5-11.

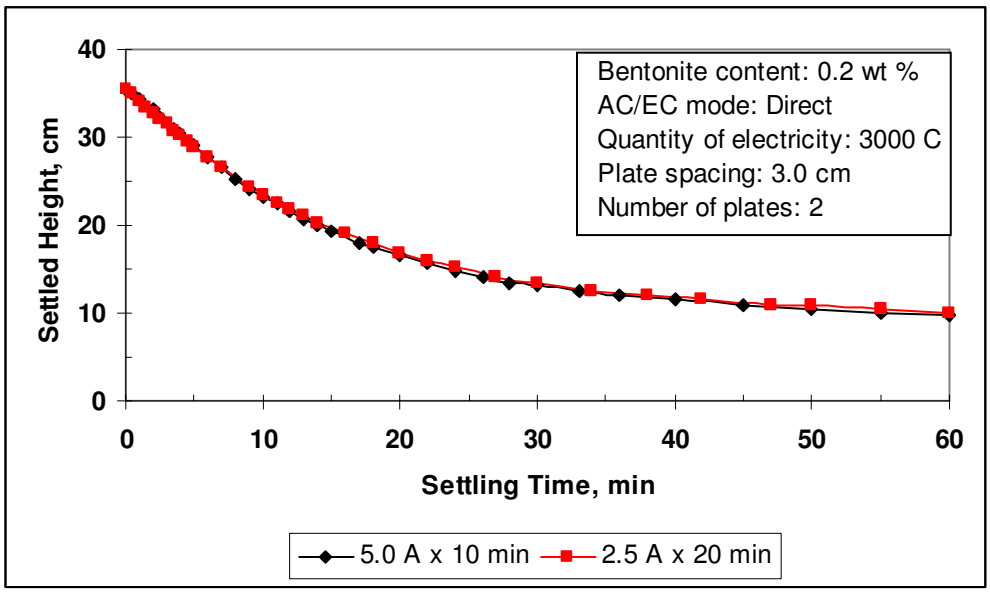

Figure 5-11. Effect of the quantity of electricity on the settling behaviour of bentonite.

The curves are coincident, with an initial settling rate of 1.3 cm/min. Table 5-13 lists pulp and water pH data.

Table 5-13. Pulp and water pH values from the coulomb tests.

Current (A) x Time (min)	Pulp pH		Water pH	
	Feed	EC*	Feed	Supernatant
5.0 x 10	9.26	9.37	6.56	8.99
2.5 x 20	9.34	9.21	6.63	8.95

* Electrocoagulated

The water pH rose during electrocoagulation from 6.6 to 9.0. The pulp pH increased from 9.3 to 9.4 in the 5.0 x 10 test, but dropped from 9.3 to 9.2 in the 2.5 x 20 test. It is noteworthy that the 2.5-A current produced an initial settling rate of 1.9 cm/min in 15 minutes of electrocoagulation in the current density test, but only 1.3 cm/min in 20 minutes in the coulomb test. This result again illustrates

the negative effect of increased retention time, as well as the sensitivity of the extent of bentonite settling behaviour enhancement to retention time.

Table 5-14. Operating data from the coulomb tests.

Current (A) x Time (min)	Pulp ΔT (℃)	V_{avg} (V)	SEI (MJ/kg Bentonite)
5.0 x 10	15.1	94.3	35.3
2.5 x 20	8.1	51.8	19.4

Table 5-14 shows that, in passing the same quantity of electric charge, doubling the current almost doubled the temperature increase, average applied voltage and SEI value, consistent with expectations.

5.5 STUDY OF SYNCRUDE MFT

5.5.1 Characterization of As-received MFT

The Syncrude MFT sample had a pulp density of 1281.9 kg/m^3 and a solids content of 38.7 wt %. It was a stable suspension in which three mineral phases became distinguishable upon dilution with de-ionized water to 4.6 wt % solids: dark-grey sand, dark-brown silt and light-brown clay. No settling could be discerned in the dilute suspension, even after three days. The hydrocarbon phase consisted mainly of oil and bitumen.

5.5.2 Electrocoagulation of MFT

For AC/EC testing, the MFT was diluted with de-ionized water to 4.6 wt % solids in simulation of tailings run-off into the pond. Also, solids concentrations greater than about 5 wt % proved too voluminous for the acquisition of meaningful settling test results. Four litres of the diluted MFT were electrocoagulated for 43 minutes and the current was allowed to vary from 3.4 to 9.6 A. Two electrodes were immersed 2.0 cm apart in the suspension. Continuous agitation was limited by frothing to a rate of about 0.5 m/s impeller tip speed for the first 25 minutes, and was discontinued as the frothing became heavy. Settling tests were performed on the electrocoagulate at 62° and 22℃.

Electrocoagulation was initially constrained by the reduced specific conductivity (~250 μS/cm) of the dispersion medium due to dilution. However, the

settling behaviour of the solids was enhanced. Figure 5-12 shows the settling curve for the first 7 of 140 h at 22°C.

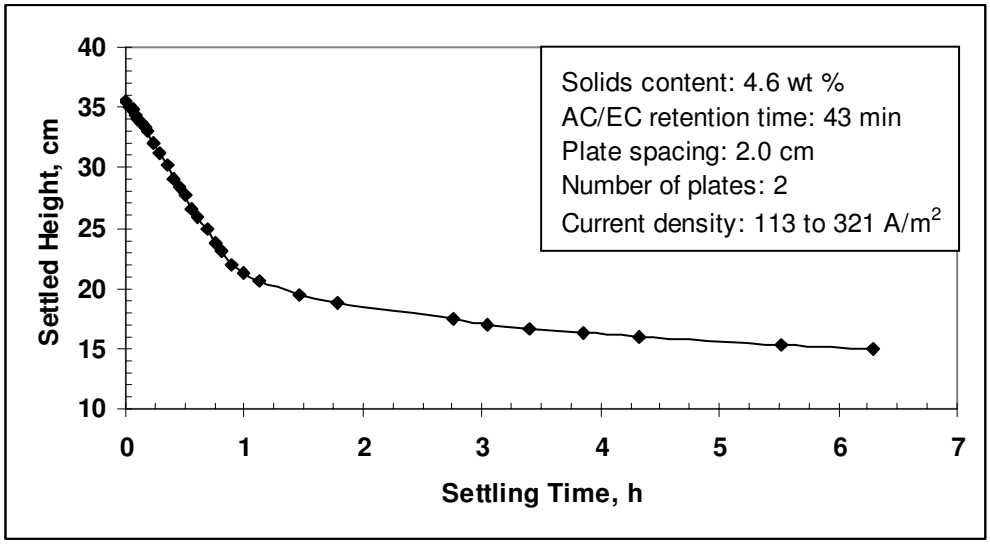

Figure 5-12. Enhanced settling behaviour of electrocoagulated Syncrude MFT.

The initial settling rate of the solids was 0.7 cm/min at 62°C and 0.3 cm/min at 22°C. In an industrial operation, thickening would be conducted at elevated temperature directly after electrocoagulation. Of the three mineral phases constituting the solids, the sand settled fastest, followed by the silt and then the clay. From an average applied voltage of 114.4 V, the specific energy input was calculated to be 7.83 MJ/kg solids.

In what was effectively a hot flotation process, electrocoagulation stripped the oil and bitumen from the suspended particles, while a bitumen-clay froth was floated off. The froth, which began forming immediately after power-up, was formed by gas evolved at the electrodes. Hence, the AC/EC technique is capable of recovering bitumen from Syncrude MFT while enhancing the settling behaviour of the solids. During the settling test, only traces of oil were discernible on the surface of the crystal-clear supernatant. The incorporation of flotation with electrocoagulation for the removal of pollutants has been championed by Holt *et al.* (2005).

After the bitumen had been recovered, flotation of the clay particles continued. The clay-laden froth was spray-washed with water and the particles settled quickly. Spray-washing with acetone or toluene gave similar results. With

toluene, however, further flocculation occurred, consistent with Fernandez and Quigley's (1985) finding that non-polar organic liquids are capable of flocculating the clays they permeate.

5.6 STUDY OF LUSCAR STERCO FINES UNDERSIZE

5.6.1 Characterization of Fines Undersize Slurry as Received

The fine coal slurry was a sample of thickener feed which contained 4.9 wt % solids. The solids had an initial settling rate of 0.2 cm/min, while the supernatant characteristics were as follows: pH 8.15, specific conductivity 1654 µS/cm, and density 996.7 kg/m^3.

5.6.2 Electrocoagulation of Fines Undersize

Four litres of the coal slurry were electrocoagulated without agitation. Over the 29-minute retention time, the current was allowed to increase from 8.0 to 10.0 A. Two electrodes were operated 6.0 cm apart.

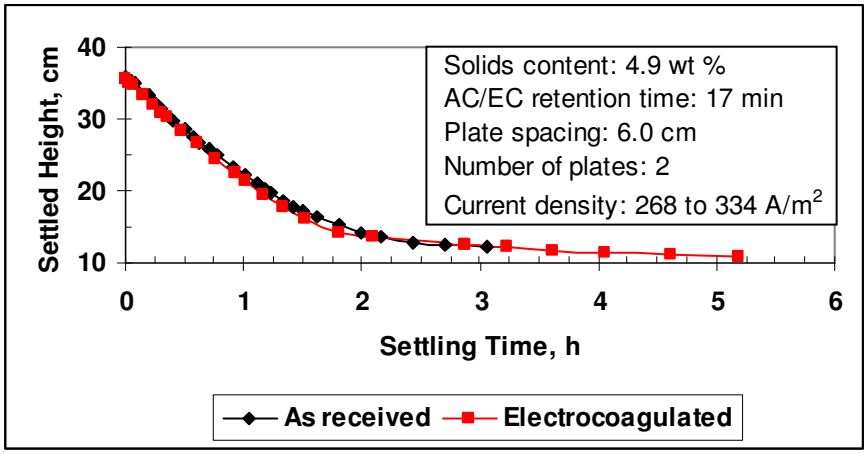

Figure 5-13. Settling behaviours of as-received and electrocoagulated fine coal.

Figure 5-13 shows the settling curve for the first 6 of 18 h. The settling behaviour of the solids was not enhanced significantly (0.25 cm/min vs. 0.22 cm/min as received). After electrocoagulation for an additional 20 minutes, the initial settling rate did not improve further. Why AC/EC did not have a more substantial effect is not clear, but the following explanation is offered. Since Luscar Sterco was not permitted to operate tailings ponds routinely, the company resorted to electrocoagulation (with aluminum electrodes) to boost thickener

performance. Hence, it is possible, even probable, that the sample obtained for this testwork had been contaminated by Luscar's electrocoagulation operation.

5.7 CHAPTER SUMMARY

Bentonite, whose particles were mostly of colloidal size (estimated 60% < 1 µm), was shown to be amenable to electrocoagulation. There appears to be an inverse relation between the solids concentration in the pulp and the specific energy input, the latter being comparable for bentonite and silica pulps of equal solids concentration. Although electrocoagulation was performed on pulps containing 0.2 wt % bentonite, it was found to be effective on more concentrated pulps. Upon dilution, these pulps demonstrated enhanced settling behaviour.

The settling behaviour of bentonite was enhanced with and without agitation, but the absence of shear favoured greater enhancement, probably because the flocs were inherently weak mechanically. Long electrocoagulation times were less effective than short times, perhaps due to the aluminum speciation or because of the formation of large, open flocs. Under-coagulated bentonite can be re-treated for further enhancement of its initial settling rate. As was observed for silica, the indirect mode of electrocoagulation is capable of producing the greater enhancement of initial settling rate in bentonite. That the initial settling rate was more enhanced by lower currents suggests that the aluminum adsorption and bentonite floc growth processes were slow. Hence, the effects of the intermission during cumulative electrocoagulation, and of the absence of shear during electrocoagulation on settling behaviour enhancement could be explained, at least in part.

Syncrude MFT is amenable to electrocoagulation as a method of improving the settling characteristics of the sludge formers, enabling better utilization of the tailings ponds. The crystal-clear supernatant produced can be recycled, minimizing the make-up water taken from the Athabasca River. Electrocoagulation facilitated the recovery of bitumen which would otherwise be lost to the tailings ponds. The environmental and economic advantages are evident. Bitumen and fine solids can be separated from the AC/EC-generated froth by simple spray-washing, with water or with naphta which already serves as a diluent at Syncrude. The design of the electrocoagulation cell for industrial application would conceivably incorporate some features of a flotation cell.

The settling characteristics of the coal sample could not be improved substantially by AC/EC treatment, perhaps because the sample had been contaminated by Luscar Sterco's electrocoagulation operation.

5.8 REFERENCES

Berkowitz N. (1994), An Introduction to Coal Technology, 2nd Edition. Academic Press, Inc., San Diego, California, pp. 101-144.

Brinker C.J. and Scherer G.W. (1990), Sol-Gel Science: The Physics and Chemistry of Sol-Gel Processing. Academic Press, Inc., New York, pp. 2-262.

Buettner W. (1985), Bentonite seepage control barriers. In First Canadian Engineering Technology Seminar on the Use of Bentonite for Civil Engineering Applications. March 18, Regina, Saskatchewan, pp. 22-32.

Cohen J.M. and Hannah S.A. (1971), Coagulation and flocculation. In Water Quality and Treatment – A Handbook of Public Water Supplies, Third Edition. McGraw-Hill Book Company, New York, pp. 66-122.

Cullen G.V. and Siviour N.G. (1981), Equilibrium relationships in the extraction of metals from ammoniacal solution with low rank coals. In Kuhn M.C. (Ed.), Process and Fundamental Considerations of Selected Hydrometallurgical Systems. SME (AIME), New York, pp. 371-377.

Fernandez F. and Quigley R.M. (1985), Hydraulic conductivity of natural clays permeated with simple liquid hydrocarbons. *Can. Geotech. J.*, **22**, 205-214.

Ghernaout D., Ghernaout B. and Boucherit, A. (2008), Effect of pH on electrocoagulation of bentonite suspensions in batch using iron electrodes. *J. Dispersion Sci. Technol.*, **29**, 1272-1275.

Grim R.E. and Güven N. (1978), Bentonites: Geology, Mineralogy, Properties and Uses. Elsevier Scientific Publishing Company, New York, 256 p.

Haug M.D. (1985), Slurry trench cutoffs. In First Canadian Engineering Technology Seminar on the Use of Bentonite for Civil Engineering Applications. March 18, Regina, Saskatchewan, pp. 33-52.

Holt P.K., Barton G.W. and Mitchell C.A. (2005), The future for electrocoagulation as a localised water treatment technology. *Chemosphere*, **59**, 355-367.

Hsu P.H. (1992), Reaction of OH-Al polymers with smectites and vermiculites. *Clays and Clay Minerals*, **40**, 300-305.

Kinniburgh D.G. and Jackson M.L. (1981), Cation adsorption by hydrous metal oxides and clay. In Anderson M.A. and Rubin A.J. (Eds.), Adsorption of Inorganics at Solid-Liquid Interfaces. Ann Arbor Science Publishers Inc., Ann Arbor, MI, pp. 91-160.

Kitchener J.A. (1978), Flocculation in mineral processing. In Ives K.J. (Ed.), The Scientific Basis of Flocculation. Sijthoff & Noordhoff, The Netherlands, pp. 283-328.

MacKinnon M.D. (1989), Development of the tailings pond at Syncrude's oil sands plant: 1978 – 1987. *AOSTRA J. Res.*, **5**, 109-133.

Oades J.M. (1984), Interactions of polycations of aluminum and iron with clays. *Clays and Clay Minerals*, **32**, 49-57.

Olin H.L. and Gauler J.V. (1938), The use of bentonite clays in water treatment. *JAWWA*, **30**, 498-506.

Olin H.L. and Peterson H.W. (1937), The use of bentonite as a coagulant in water treatment. *JAWWA*, **29**, 513-522.

Parekh B.K., Groppo J.G. and Justice J.G. (1992), Removal of fine particulates and metal ions from process discharge waste water using AC electro-coagulation technique. In Chandler S. (Ed.), Emerging Process Technologies for a Cleaner Environment. AIME Proceedings, Phoenix, Arizona, pp. 99-105.

Ross C.S. and Shannon E.V. (1926), Minerals of bentonite and related clays and their physical properties. *J Am. Ceram. Soc.*, **9**, 77-96.

Schindler P.W. (1981), Surface complexes at oxide-water interfaces. In Anderson M.A. and Rubin A.J. (Eds.), Adsorption of Inorganics at Solid-Liquid Interfaces. Ann Arbor Science Publishers Inc., Ann Arbor, MI, pp. 1-50.

Smart P. and Tovey N.K. (1982), Electron Microscopy of Soils and Sediments: Techniques. Clarendon Press, Oxford, pp. 1-38.

Snyder G.A. and Gregory M.J. (1979), Electrocoagulation of coal preparation plant waters. SME-AIME Fall Meeting and Exhibit, Tucson, AZ, October 17-19, 10 p.

Stumm W. (1992), Chemistry of the Solid-Water Interface. Wiley-Interscience, New York, pp. 47-51.

Tambo N. (1991), Basic concepts and innovative turn of coagulation/flocculation. *Water Supply*, **9**, Jönköping, 1-10.

van Olphen H. (1977), An Introduction to Clay Colloid Chemistry, 2nd Edition. John Wiley & Sons, New York, pp. 1-5.

van Olphen H. (1987), Dispersion and flocculation. In Newman A.C.D. (Ed.), Chemistry of Clays and Clay Minerals. Mineralogical Society Monograph No. 6, Longman Scientific & Technical, London, pp. 203-224.

van Veen W. (1985), Clay mineralogy. In First Canadian Engineering Technology Seminar on the Use of Bentonite for Civil Engineering Applications. March 18, Regina, Saskatchewan, pp. 6-21.

Xiao F., Zhang X. and Lee C. (2008), Is electrophoretic mobility determination meaningful for aluminum(III) coagulation of kaolinite suspension? *J. Colloid Interface Sci.*, **327**, 348-353.

CHAPTER 6

GENERAL DISCUSSION AND CONCLUSIONS

6.1 EFFECTIVENESS OF AC/EC TECHNIQUE

Alternating current electrocoagulation (AC/EC) has been demonstrated in this study to be an effective means of enhancing the settling behaviour of solids which possess naturally poor sedimentation characteristics. From a fundamental study of its effect on ground silica, the technique was successfully extended to the treatment of materials of industrial importance, namely, Syncrude MFT and bentonite, both of which are notorious for their poor settling behaviour.

Syncrude MFT is amenable to electrocoagulation as a method of enhancing the settling characteristics of the sludge formers (<22 μm particles) (MacKinnon, 1989), enabling better utilization of the tailings ponds. The crystal-clear supernatant produced can be recycled, minimizing the make-up water taken from the Athabasca River. Electrocoagulation facilitated the recovery of bitumen which would otherwise be lost to the tailings ponds. The environmental benefit of such recovery is evident. Bitumen and fine solids can be separated from the AC/EC-generated froth by simple spray-washing, possibly with naphtha which already serves as a diluent at Syncrude. The design of the electrocoagulation cell for industrial application would conceivably incorporate some features of a flotation cell.

Bentonite, whose particles were mostly of colloidal size (estimated 60% <1 μm), was demonstrated to be amenable to electrocoagulation. Although electrocoagulation was performed on pulps containing 0.2 wt % solids, it was also found to be effective on more concentrated pulps which, upon dilution, demonstrated the enhanced settling behaviour.

AC/EC did not augment the settling behaviour of the fine coal tailings (thickener feed) plant sample. It is suspected that the sample had been contaminated by Luscar Sterco's electrocoagulation operation, to the extent that further settling enhancement could not be achieved. It is worth noting that AC/EC has been reported (Parekh *et al.*, 1992) to be effective on coal of d_{50} size 1.8 μm.

The AC/EC process was found to consist of two developmental stages: coagulation and floc growth. Coagulation is the first stage which is characterized

by pH decrease in, and destabilization of, the suspension. The attainment of a minimum pH signified the end of coagulation; within about a further two minutes, enhanced settling became evident. Hence, the net pulp pH change in the first stage was always negative. Floc growth, the second stage, was accompanied by a pH increase from the minimum. Therefore, the terminal pulp pH could represent either a negative or positive net change.

6.2 INFLUENCE OF SHEAR DURING ELECTROCOAGULATION

The enhanced initial settling behaviour achieved by electrocoagulation of silica was marginally sensitive to shear. In other words, the silica flocs were strong and, over the range of agitation rates studied (0 to 4.97 m/s impeller tip speed), exhibited little fragmentation. Bentonite, in contrast, appeared to form weaker flocs whose settling behaviour improved in the absence of shear.

The silica study showed that agitation was beneficial to floc growth, especially at extended electrocoagulation times, but was not essential to electrocoagulation. Hence, in practical application, the flow of suspension through the electrocoagulation cell is expected to provide adequate agitation, making a dedicated mixer redundant. Agitation was also capable of decreasing the electrocoagulation time for achieving a given initial settling rate in silica.

In suspensions of high solids concentration, interparticle proximity facilitates collision for aggregation to occur. This was deduced from the enhancement of the settling behaviour of silica in the absence of shear, the bulk of the as-received material being coarser than colloidal size and, therefore, not transported by Brownian motion (Masliyah, 1994; Montgomery, 1985). Consequently, in the absence of shear, the mode of floc growth could be described neither as perikinetic nor as orthokinetic in the classical sense.

6.3 INDIRECT AND DIRECT ELECTROCOAGULATION

In the absence of aluminum hydroxide precipitation, silica and bentonite floc growth by indirect electrocoagulation was faster than by the direct mode because of the higher aluminum dosage in the treated water which engendered greater adsorption. Slower mass adsorption of aluminum during direct electrocoagulation resulted from aluminum being “metered” into the pulp. The initial settling rate of silica increased with electrocoagulation time in both

treatment modes and was controlled by floc size. In the direct electrocoagulation of bentonite, the initial settling rate declined with increasing electrocoagulation time.

When precipitation occurred, however, settling behaviour in the two modes of electrocoagulation was affected differently. Floc growth in indirect electrocoagulation was limited in accordance with the fraction of efficient coagulative species removed from solution, causing the initial settling rate to diminish. In direct electrocoagulation, floc size decreased, presumably the result of fragmentation at sites bridged by precipitate particles. The flocs became less porous as precipitate particles were adsorbed in the pores. Consequent to the general adsorption of precipitate particles onto the flocs, the increased floc density negated the effect of fragmentation on settling performance; indeed, the settling performance was enhanced, perhaps with assistance from enmeshment by the precipitate. Of the two electrocoagulation modes, therefore, the direct mode facilitated settling enhancement at longer electrocoagulation times. Energy requirements were similar for the two modes of electrocoagulation.

After having been stored dry for more than a year, electrocoagulated silica was effective in coagulating as-received silica. In this special case of indirect electrocoagulation, the electrocoagulated silica exhibited a long “shelf life”. This test was not repeated with chemically coagulated silica. In a continuous electrocoagulation process, therefore, a portion of the electrocoagulated slurry can be recycled to the cell, in a blend with fresh feed suspension, to reduce retention time and energy requirements. In addition, having demonstrated its capability of coagulating Syncrude MFT, electrocoagulated silica has qualified itself as a practical coagulant for other suspended solids. It possesses the added advantage of not introducing any noxious constituents to the process stream that it contacts.

Interruption of the electrocoagulation process was not detrimental to the enhancement of the settling behaviour of silica or bentonite. In fact, for the same AC/EC retention time, the initial settling rate was higher for cumulatively treated silica and bentonite than for the continuously treated materials. This implies that under-coagulated material can be re-treated to achieve a higher initial settling rate or larger floc size.

6.4 PARAMETERS DETERMINING ALUMINUM DOSAGE

The principal parameters determining aluminum dosage in electrocoagulation are retention time and current. Retention time has been reviewed in Section 6.3. The effect of current can be expressed in two ways: by the magnitude of the applied current, and by conditions which control the current effecting electrocoagulation. Increasing the current by either means would accelerate the electrode reaction kinetics.

6.4.1 Magnitude of Applied Current

In this study, the magnitude of the applied current was adjusted by varying the applied voltage, and has been expressed in terms of current density and the electrode area.

At low current densities, the system entered an induction phase, the duration of which shortened with increasing current density. The feed water pH (<5) was also observed to create the induction state. At sufficiently high current density, the induction phase was eliminated. The initial settling rate of silica increased with current density up to 117.0 A/m^2 ($I \leq 3.5$ A), but further current density increase to 167.2 A/m^2 ($3.5\ A < I \leq 5.0$ A) did not lead to further enhancement. The onset of enhanced settling was attained at progressively shorter electrocoagulation times as current density was increased. Hence, the electrocoagulation time required to achieve a given initial settling rate shortened with increasing current density, but the time savings was negated by the increased energy demand. Therefore, in the design of an electrocoagulation operation, an energy audit would be essential for optimizing selection of the process parameters. In the electrocoagulation of bentonite, settling performance improved with decreasing current.

The study of electrode area was conducted at constant current density, such that the current was increased in direct proportion to area. The initial settling rate of silica increased with increasing electrode area, and was controlled by floc size when electrocoagulation was effected with electrode areas in the approximate range of 300 to 900 cm^2 ($2.1\ A \leq I \leq 6.3$ A). For areas ≥ 1500 cm^2 ($I \geq 10.5$ A), initial settling rate was controlled jointly by floc size, floc densification (*i.e.*, reduction of porosity) and, possibly, enmeshment by aluminum hydroxide precipitate. The range of 900 to 1500 cm^2 of electrode area represented a

transition in the mode of initial settling rate control, as precipitation became more profuse. The transition range was also characterized by floc fragmentation, which is proposed to have occurred at sites where adsorbed precipitate formed mechanically weak inter-floc bridges, limiting the extent of multiple level aggregation.

6.4.2 Conditions Controlling Electrocoagulation Current

Conditions affecting the electrocoagulation current in this study were the specific conductivity and temperature of the feed water.

The initial settling rate of silica increased with specific conductivity up to 3840 µS/cm. At higher conductivities, aluminum hydroxide precipitated, seriously impairing settling performance. The onset of precipitation is inferred to have occurred progressively earlier with increasing feed water conductivity. The explanation for this observation is that an increasing proportion of the input electrical energy was utilized for anodic oxidation as conductivity was elevated. Thus, higher Al dosages resulted and aluminum solubility decreased against rising background ionic strength.

The settling behaviour enhancement for silica increased with feed water temperature (indirect AC/EC) and attained its maximum at ~45°C. At higher feed water temperatures, settling performance was affected by the temperature at which as-received silica was slurried with the treated water, tending to be enhanced by higher slurrying temperature. With rising water temperature, the conductivity increased, making a larger proportion of the input electrical energy available for anodic oxidation. Since the background ionic strength was relatively low, in contrast to the conductivity test series, the aluminum solubility did not decrease as it did at high conductivity. The decline in initial settling rate at temperatures above 45°C is considered to be related to changes in speciation of dissolved aluminum, aluminum hydroxide not having been precipitated. Temperature alters the kinetics of the hydrolysis reactions, as well as the pH range in which $Al(OH)_3$ precipitates (Duan and Gregory, 2003).

6.5 AGEING EFFECTS

One day's ageing was detrimental to the initial settling rate of silica that was electrocoagulated indirectly in the absence of precipitation. The settling rate

deterioration, which was as high as 50%, is attributed to degradation of the efficient coagulative aluminum species to species of lower molecular weight and, hence, lower coagulative capacity. Consequently, the flocs are considered to have collapsed, as indicated by their reduced porosity. On the other hand, ageing did not seriously affect the initial settling rate of silica that was indirectly electrocoagulated with water from which substantial quantities of aluminum had precipitated. Smaller decreases in floc porosity resulted.

Ageing for one day effected dramatic enhancement of initial settling rate of up to 178% in silica that had been electrocoagulated directly for periods between 15 and 110 minutes. Floc porosity decreased, and either growth or degeneration of flocs occurred in the aged electrocoagulates. Floc growth is ascribed to re-aggregation to a denser configuration possessing a larger limiting floc size. Floc degeneration has been addressed for aged, indirectly electrocoagulated silica. Porosity increase, observed in the 90- and 120-minute electrocoagulates, is attributed to redissolution of aluminum hydroxide precipitate. Floc growth in the 90-minute electrocoagulate is considered to have resulted from the formation of new, efficient coagulative species. Silica, electrocoagulated for 15 minutes and for longer than 110 minutes, displayed lower settling rates upon ageing.

6.6 FACTORS AFFECTING ENERGY CONSUMPTION

Apart from the energy required to produce elemental aluminum, the high electrical energy demand by the AC/EC process is viewed by some as the primary obstacle to industrial adoption on a wider scale (Scott and Cymerman, 1984). On the other hand, others have concluded that electrocoagulation is less expensive than chemical coagulation to operate. For example, Kobya *et al.* (2007) estimated the operating cost of DC/EC to be one-third that of chemical coagulation for treating 1000 m^3/day of textile plant wastewater. In the current study, factors affecting the energy demand have been identified.

Energy input depends primarily on the applied voltage, current and electrocoagulation time. Reducing the magnitude of these parameters reduces the energy input. Hence, AC/EC is expected to be the most economical when applied to treat hot suspensions consisting of solids at high concentration and an aqueous dispersion medium of high specific conductivity at the optimum pH. With

several, closely spaced electrodes per cell operating at an appropriate current, short retention times should be required. Recycle of a portion of the electrocoagulated pulp (to be blended with fresh feed) should advance the energy savings.

It is recognized that limited scope may exist for treating suspensions which possess all of the desired properties listed above. Suspensions normally have to be treated as they are produced from the main plant process. Nevertheless, optimization studies will elucidate the scope available for modifying certain properties of the suspension to reduce energy consumption in the AC/EC step.

Pretorius *et al.* (1991) reported that bipolar electrodes consumed less energy than the conventional power configuration (see Figure 1-1) employed in this study. Hence, proper cell design holds ample promise for reducing the energy consumed by the AC/EC process. Evidently, access to reasonably inexpensive sources of electric power would play a significant role in enhancing the economic feasibility of A.C. electrocoagulation.

6.7 FLEXIBILITY OF AC/EC TECHNIQUE

A.C. electrocoagulation has shown itself to be a remarkably flexible process. It can be operated in either the indirect or direct mode. In the indirect mode, the aqueous dispersion medium is subjected to AC/EC treatment and is then slurried with the solids outside the cell. In the direct mode, the suspension is electrocoagulated in the cell. In addition, an environmentally innocuous material (*e.g.*, silica) can be electrocoagulated and applied as a coagulant, even after dry storage for extended periods.

AC/EC was effective in enhancing the settling behaviour of silica in feed water of pH 3.0 to 9.1 — a range which far exceeds that of chemical coagulants. Owing to its determinative influence on aluminum speciation, pH is a key control for electrocoagulation and, hence, for floc growth and settling behaviour. AC/EC was also effective over a wide range of temperatures (23° to 85°C), making it applicable to the treatment of hot waste streams.

In the event of process upsets in the main plant, such that incremental electrocoagulation of the waste discharge is necessary, the waste can be re-

treated to achieve the desired settling performance and to establish, for example, the new retention time required.

When dispersed in water over a wide range of specific conductivities, silica was successfully treated by electrocoagulation. In an industrial setting, the shortest possible electrocoagulation time would be employed. Short times reduce the risk of aluminum hydroxide precipitation and its deleterious effect on settling behaviour in water of high specific conductivity.

This study has revealed the existence of an unusually extensive array of parameters that can be optimized to refine the electrocoagulation process, with respect to enhancing the settling characteristics of poorly settling solids.

6.8 REFERENCES

Duan J. and Gregory J. (2003), Coagulation by hydrolysing metal salts. *Advances Colloid Interface Sci.*, **100-102**, 475-502.

Kobya M., Bayramoglu M. and Eyvaz M. (2007), Techno-economical evaluation of electrocoagulation for the textile wastewater using different electrode connections. *J. Hazard. Mater.*, **148**, 311-318.

MacKinnon M.D. (1989), Development of the tailings pond at Syncrude's oil sands plant: 1978-1987. *AOSTRA J. Res.*, **5**, 109-133.

Masliyah J.H. (1994), Electrokinetic Transport Phenomena. AOSTRA Technical Publication Series #12, Edmonton, Canada, 363 p.

Montgomery J.M., Consulting Engineers, Inc. (1985), Water Treatment Principles and Design. John Wiley & Sons, New York, pp. 116-134.

Parekh B.K., Groppo J.G. and Justice J.G. (1992), Removal of fine particulates and metal ions from process discharge waste water using AC electro-coagulation technique. In Chandler S. (Ed.), Emerging Process Technologies for a Cleaner Environment. AIME Proceedings, Phoenix, Arizona, pp. 99-105.

Pretorius W.A., Johannes W.G. and Lempert G.G. (1991), Electrolytic iron flocculant production with a bipolar electrode in series arrangement. *Water SA*, **17**, 133-138.

Scott J.D. and Cymerman G.J. (1984), Prediction of viable tailings disposal methods. In Proceedings of a Symposium: Sedimentation Consolidation Models. ASCE, San Francisco, October, 522-544.

CHAPTER 7
SUGGESTIONS FOR FURTHER STUDY

Aluminum speciation and the design of the electrocoagulation cell are considered to be two of the most important topics for research. In recent years, illuminating studies of aluminum speciation by mass spectrometry have been conducted as a function of pH, and the research continues.

In cell design, the cell geometry and associated hydrodynamics, and electrode configuration are expected to be fruitful areas of work, with the objective of minimizing the energy consumption of AC/EC. Of particular interest would be a study of the effect of A.C. frequency on the rate of floc growth.

Investigation of the effect of ageing on electrocoagulates over longer terms than that studied here could hold implications for the operation of tailings ponds. The postulated degradation of silica flocs, originally produced by indirect electrocoagulation in the absence of aluminum hydroxide precipitation, deserves elucidation. Of added interest would be a study of the ageing of chemically coagulated silica.

Floc fragmentation, which has been partly attributed to weak inter-floc bridges formed by aluminum hydroxide precipitate, requires further study, as do the following additional topics:

- the effects of making chemical coagulant additions to feed water (indirect electrocoagulation) and to the suspension (direct electrocoagulation) in the separate presence of aluminum electrodes, carbon electrodes and mixed pairs of aluminum and carbon electrodes;
- AC/EC at a range of controlled temperatures and comparison with chemical coagulation at those temperatures;
- processes occurring in the retention time range of 0 to 15 minutes; and
- quantification of the electric charge required for the onset of enhanced settling with respect to total Al concentration, quantity of solids present, speciation and fixed operating temperature.

APPENDIX A

COMPILATION OF DATA PLOTTED IN GRAPHS

CHAPTER 1

Figure 1-4

h, nm	V_R, J	V_A, J
0.1	8.6×10^{-19}	7.1×10^{-18}
0.5	7.9×10^{-19}	1.4×10^{-18}
0.75	7.6×10^{-19}	9.4×10^{-19}
1.0	7.2×10^{-19}	7.1×10^{-19}
5.0	3.3×10^{-19}	1.4×10^{-19}
10	1.3×10^{-19}	7.1×10^{-20}
20	1.9×10^{-20}	3.5×10^{-20}
30	2.8×10^{-21}	2.4×10^{-20}
50	5.9×10^{-23}	1.4×10^{-20}
80	1.9×10^{-25}	8.9×10^{-21}
100	4.0×10^{-27}	7.1×10^{-21}

Figure 1-5

h, nm	Net Interaction Energy (V), J			
	κ^{-1} = 0.52 nm	κ^{-1} = 5.2 nm	κ^{-1} = 52 nm	κ^{-1} = 188 nm
0.1	-6.4×10^{-18}	-6.2×10^{-18}	-6.2×10^{-18}	-6.2×10^{-18}
0.5	-1.1×10^{-18}	-6.2×10^{-19}	-5.5×10^{-19}	-5.5×10^{-19}
0.75	-7.4×10^{-19}	-1.9×10^{-19}	-8.4×10^{-20}	-7.5×10^{-20}
1.0	-5.8×10^{-19}	1.2×10^{-20}	1.5×10^{-19}	1.6×10^{-19}
2.0	-3.4×10^{-19}	2.4×10^{-19}	4.9×10^{-19}	5.1×10^{-19}
3.0	-2.3×10^{-19}	2.5×10^{-19}	5.9×10^{-19}	6.2×10^{-19}
5.0	-1.4×10^{-19}	1.9×10^{-19}	6.5×10^{-19}	7.1×10^{-19}
10	-7.1×10^{-20}	5.7×10^{-20}	6.5×10^{-19}	7.6×10^{-19}
20	-3.5×10^{-20}	-1.7×10^{-20}	5.6×10^{-19}	7.5×10^{-19}
30	-2.4×10^{-20}	-2.1×10^{-20}	4.7×10^{-19}	7.2×10^{-19}

$kT = (1.381x10^{-23})(298) = 4.115x10^{-21}$ J

h, nm	Net Interaction Energy (V), J			
	κ^{-1} = 0.52 nm	κ^{-1} = 5.2 nm	κ^{-1} = 52 nm	κ^{-1} = 188 nm
0.1	-1555	-1507	-1507	-1507
0.5	-267	-151	-134	-134
0.75	-180	-46	-20	-18
1.0	-141	2.9	36	39
2.0	-83	58	119	124
3.0	-56	61	143	151
5.0	-34	46	158	173
10	-17	14	158	185
20	-8.5	-4.1	136	182
30	-5.8	-5.1	114	175

Figure 1-7

Al^{3+} Hydrolysis Equilibria, Equilibrium Constants and References

Line	Equilibrium Reaction	Eqm. Const.*	log (Eqm. Const.*)	Ref.
1	$Al(OH)_3(am) + 3\ H^+ \leftrightarrow Al^{3+} + 3\ H_2O$	$*K_{S0}$	10.8	1
2	$Al^{3+} + H_2O \leftrightarrow AlOH^{2+} + H^+$	$*K_1$	-5.02	2
3	$2\ Al^{3+} + 2\ H_2O \leftrightarrow Al_2(OH)_2^{4+} + 2\ H^+$	$*\beta_{2,2}$	-6.27	2
4	$6\ Al^{3+} + 15\ H_2O \leftrightarrow Al_6(OH)_{15}^{3+} + 15\ H^+$	$*\beta_{15,6}$	-47.00	2
5	$8\ Al^{3+} + 20\ H_2O \leftrightarrow Al_8(OH)_{20}^{4+} + 20\ H^+$	$*\beta_{20,8}$	-68.7	2
6	$13\ Al^{3+} + 34\ H_2O \leftrightarrow Al_{13}(OH)_{34}^{5+} + 34\ H^+$	$*\beta_{34,13}$	-97.39	2
7	$Al^{3+} + 4\ H_2O \leftrightarrow Al(OH)_4^- + 4\ H^+$	$*\beta_4$	-23.57	2
8	$Al^{3+} + 3\ H_2O \leftrightarrow Al(OH)_3^o + 3\ H^+$	$*\beta_3$	-15.0	1
9	$Al^{3+} + 2\ H_2O \leftrightarrow Al(OH)_2^+ + 2\ H^+$	$*\beta_2$	-9.3	1
10	$3\ Al^{3+} + 4\ H_2O \leftrightarrow Al_3(OH)_4^{5+} + 4\ H^+$	$*\beta_{4,3}$	-13.9	1
11	$13\ Al^{3+} + 28\ H_2O \leftrightarrow Al_{13}O_4(OH)_{24}^{7+} + 32\ H^+$	$*\beta_{32,13}$	-98.7	1
12	$7\ Al^{3+} + 17\ H_2O \leftrightarrow Al_7(OH)_{17}^{4+} + 17\ H^+$	$*\beta_{17,7}$	-48.8	3

*Equilibrium constant

References: 1 Stumm and Morgan (1981)

2 Kindzierski (1995)

3 Stumm and O'Melia (1968)

Plotting Equations for Al-H_2O pC-pH Diagram (25°C)

(1) $\log[Al^{3+}] = 10.8 - 3\ pH$

(2) $\log[AlOH^{2+}] = 5.78 - 2\ pH$

(3) $\log[Al_2(OH)_2^{4+}] = 15.33 - 4\ pH$

(4) $\log[Al_6(OH)_{15}^{3+}] = 17.8 - 3\ pH$

(5) $\log[Al_8(OH)_{20}^{4+}] = 17.7 - 4\ pH$

(6) $\log[Al_{13}(OH)_{34}^{5+}] = 43.01 - 5\ pH$

(7) $\log[Al(OH)_4^{-}] = pH - 12.77$

(8) $\log[Al(OH)_3^{o}] = -4.2$

(9) $\log[Al(OH)_2^{+}] = 1.5 - pH$

(10) $\log[Al_3(OH)_4^{5+}] = 18.5 - 5\ pH$

(11) $\log[Al_{13}O_4(OH)_{24}^{7+}] = 41.7 - 7\ pH$

(12) $\log[Al_7(OH)_{17}^{4+}] = 26.8 - 4\ pH$

Data Used to Plot Solubility Boundary

pH	9	9.3	9.5	10	10.5	11	12
log $C_{T,diss}$	-0.9	-2.4	-3.0	-2.8	-2.3	-1.8	-0.8

CHAPTER 2

Figure 2-5

Equivalent Particle Diameter, µm	Cumulative Wt % Passing
63.9	99.3
48.5	83.8
36.0	72.4
32.6	68.8
30.1	65.9
23.1	55.3
18.8	47.2
16.3	43.1
11.4	33.0
8.3	24.8
7.1	22.0
6.3	19.9
5.5	18.7
5.1	17.5
4.6	15.1
2.0	6.9

Figure 2-6

0 mg/L NaCl Addition		200 mg/L NaCl Addition	
pH	ζ, mV	pH	ζ, mV
3.01	-8.7	3.01	-8.8
5.13	-16.1	5.24	-19.2
7.02	-15.9	7.00	-21.9
8.57	-17.1	8.65	-21.3
9.20	-18.1	9.29	-26.5

Figure 2-7

Time, min	Settled Height, cm			
	30 min; no	30 min; yes	75 min; no	75 min; yes
0	35.5	35.6	35.6	35.6
0.5	33.7	33.5	33.5	31.7
1	30.9	31.0	31.0	27.1
1.5	28.9	28.5	28.7	no data
2	27.0	26.0	26.7	19.2
2.5	24.7	23.9	24.0	14.2
3	22.7	no data	21.4	10.3
3.5	20.6	18.9	19.6	5.7
4	18.3	16.4	17.4	3.5
4.5	16.5	13.9	15.3	3.1
5	13.8	11.4	13.2	2.9
5.5	11.9	8.9	10.7	2.8
6	10.3	7.1	8.5	2.8
6.5	8.2	4.6	6.1	no data
7	5.7	3.4	3.6	no data
7.5	3.2	3.2	3.4	no data
8	3.1	3.1	3.2	2.5
9	2.8	2.8	3.0	no data
10	2.6	2.7	2.8	2.4
11	no data	2.6	no data	no data
12	2.5	no data	2.7	no data
13	no data	2.5	no data	no data
15	2.4	2.5	2.5	2.1
20	2.3	2.3	2.5	2.1
25	no data	2.2	2.4	2.1
30	2.2	2.2	2.4	2.1
35	no data	2.2	no data	no data
40	2.2	2.2	2.4	2.1
50	2.2	2.2	2.4	2.1
60	2.2	2.2	2.4	2.1

Figure 2-8

Time (min)	Settled Height, cm					
	0 m/s	1.73 m/s	2.62 m/s	3.14 m/s	4.19 m/s	4.97 m/s
0	35.5	35.6	35.7	35.6	35.7	35.5
0.5	33.7	33.5	33.6	33.5	33.6	33.2
1	30.9	31.0	31.1	30.8	31.1	31.2
1.5	28.9	28.5	27.8	28.5	28.9	29.1
2	27.0	26.0	25.3	26.0	26.8	26.6
2.5	24.7	23.9	23.2	23.5	24.3	24.5
3	22.7	no data	21.1	21.7	21.8	22.7
3.5	20.6	18.9	18.2	no data	19.3	20.6
4	18.3	16.4	16.1	16.7	17.5	18.5
4.5	16.5	13.9	13.6	14.2	no data	16.0
5	13.8	11.4	11.1	11.6	12.5	14.2
5.5	11.9	8.9	8.6	9.3	10.4	11.7
6	10.3	7.1	6.1	7.1	7.9	9.9
6.5	8.2	4.6	3.6	4.5	5.4	7.8
7	5.7	3.4	3.2	3.2	3.0	5.3
7.5	3.2	3.2	3.0	3.0	2.9	3.1
8	3.1	3.1	2.9	2.8	2.8	3.1
8.5	no data	no data	no data	no data	no data	2.8
9	2.8	2.8	2.6	2.6	2.5	2.8
10	2.6	2.7	2.5	2.5	2.4	2.5
11	no data	2.6	no data	no data	no data	no data
12	2.5	no data	2.4	2.4	2.2	2.4
13	no data	2.5	no data	no data	no data	no data
15	2.4	2.5	2.3	2.2	2.1	2.2
20	2.3	2.3	2.1	2.1	no data	2.1
22	no data	no data	no data	no data	2.0	no data
25	no data	2.2	2.1	2.1	2.0	2.1
30	2.2	2.2	2.1	2.1	2.0	2.1
35	no data	2.2	no data	2.1	1.9	2.1
40	2.2	2.2	2.1	2.1	1.9	2.1
50	2.2	2.2	2.1	2.1	1.9	2.1
60	2.2	2.2	2.1	2.1	1.9	2.1

Figure 2-9

Impeller Tip Speed, m/s	Initial Settling Rate, cm/min
0	4.3
1.73	4.8
2.62	4.9
3.14	4.8
4.19	4.7
4.97	4.3

Figures 2-10, 2-20 and 2-27

Electrocoagulation Time, min	Initial Settling Rate, cm/min
15	3.6
45	6.4
75	3.8
90	3.6
120	3.4

Figure 2-11

Silica As Received		Electrocoagulated for 15 Minutes	
Equivalent Diameter (µm)	Cumulative Passing (wt %)	Equivalent Diameter (µm)	Cumulative Passing (wt %)
63.9	99.3	91.9	96.3
48.5	83.8	80.5	93.1
36.0	72.4	72.3	89.9
32.6	68.8	65.1	86.7
30.1	65.9	58.9	83.5
23.1	55.3	54.0	80.3
18.8	47.2	50.0	77.2
16.3	43.1	41.1	61.2
11.4	33.0	40.0	58.0
8.3	24.8	39.0	54.8
7.1	22.0	36.4	42.1
6.3	19.9	35.8	38.9
5.5	18.7	33.8	26.1
5.1	17.5	33.5	23.0
4.6	15.1	31.8	13.4
2.0	6.9	30.4	3.8

Figure 2-11 continued

Electrocoagulated for 45 Minutes		Electrocoagulated for 75 Minutes	
Equivalent Diameter (µm)	Cumulative Passing (wt %)	Equivalent Diameter (µm)	Cumulative Passing (wt %)
98.3	96.6	98.5	98.2
90.1	93.4	84.5	95.0
84.2	90.2	75.2	91.8
76.3	83.9	68.9	88.6
73.4	80.7	64.0	85.4
70.0	74.3	60.6	82.2
67.7	71.1	57.6	79.1
66.6	67.9	55.7	75.9
65.2	64.7	53.9	72.7
64.0	61.5	47.3	53.6
63.0	58.3	46.7	50.4
62.0	55.2	45.9	47.2
61.1	52.0	45.2	44.0
60.4	48.8	42.2	28.1
59.4	45.6	41.8	24.9
58.6	42.4	41.3	21.7
57.9	39.2	40.8	18.5
56.7	32.8	38.8	7.3
56.3	29.7	38.4	5.7
55.2	23.3	33.6	2.6
54.6	20.1	27.7	0.6
50.6	2.6	no data	no data
45.1	1.0	no data	no data

Figure 2-11 continued

Electrocoagulated for 90 Minutes		Electrocoagulated for 120 Minutes	
Equivalent Diameter (µm)	Cumulative Passing (wt %)	Equivalent Diameter (µm)	Cumulative Passing (wt %)
93.7	98.5	92.8	98.5
81.8	95.3	80.4	95.3
72.1	92.1	72.0	92.1
65.7	88.9	65.2	88.9
61.1	85.7	61.2	85.7
58.0	82.6	58.1	82.6
55.5	79.4	55.6	79.4
53.7	76.2	53.8	76.2
51.9	73.0	52.1	73.0
47.0	57.1	47.0	57.1
46.3	53.9	46.1	53.9
45.5	50.7	43.7	41.1
42.4	34.7	43.0	37.9
41.8	31.6	42.6	34.7
41.3	28.4	40.8	22.0
40.8	25.2	40.4	18.8
38.8	12.4	38.9	9.3
36.7	5.4	38.0	6.1
33.7	2.9	36.5	3.2
no data	no data	34.6	1.9
no data	no data	29.9	0.3

Figures 2-12, 2-22 and 2-29

Electrocoagulation Time, min	Equivalent Floc d_{50}, µm
0	20
15	38
45	60
75	47
90	45
120	46

Figures 2-13, 2-24 and 2-25

AC/EC Time (min)	T, ℃	pH			
		Feed Water	AC/EC-treated Water	EC* Slurry	Supernatant
15	21.2	8.50	8.14	8.52	8.03
45	21.2	8.45	8.34	8.37	8.19
75	21.2	8.46	8.58	8.37	8.36
90	21.2	8.50	8.62	8.26	8.04
120	21.3	8.49	8.59	8.08	7.93

*Electrocoagulated

Figures 2-14 and 2-23

AC/EC Time, min	Total Al Concentration, mg/L	
	AC/EC-treated Water	Supernatant
0	0	0
15	5.3	<1
45	17.3	1.4
75	22.3	2.7
90	28.5	2.6
120	21.4	1.5

Figures 2-15, 2-20 and 2-31

Electrocoagulation Time, min	Initial Settling Rate, cm/min
15	2.7
45	4.6
75	8.1
90	8.9
120	12.2

Figures 2-16, 2-22 and 2-33

Electrocoagulation Time, min	Equivalent Floc d_{50}, µm
0	20
15	34
45	65
75	92
90	79
120	77

Figures 2-17, 2-24 and 2-25

AC/EC Time (min)	T, ℃	pH			
		Feed Water	Feed Suspension	EC* Slurry	Supernatant
15	21.3	8.50	8.58	8.10	8.00
45	21.6	8.47	8.66	8.49	8.38
75	21.5	8.48	8.83	8.85	8.66
90	21.3	8.50	8.60	8.56	8.33
120	21.3	8.49	8.71	8.58	8.27

*Electrocoagulated

Figures 2-18 and 2-23

Electrocoagulation Time, min	Total Al in Supernatant, mg/L
0	0
15	0.7
45	2.5
75	3.6
90	2.9
120	2.2

Figure 2-21

AC/EC Time, min	Zeta Potential of Electrocoagulated Silica, mV	
	Indirect Mode	Direct Mode
0	-21.4	-21.4
15	-19.6	-19.2
45	-7.5	-10.3
75	-21.9	-5.5
90	-18.4	-9.5
120	-21.0	-0.9

Figure 2-26

Settling Time (min)	Settled Height, cm				
	15 min	45 min	75 min	90 min	120 min
0	35.6	35.5	33.8	35.7	35.0
0.5	no data	33.7	32.1	no data	no data
1	no data	32.7	29.7	no data	no data
1.5	no data	30.9	27.7	no data	no data
2	no data	28.8	26.0	28.2	28.0
2.5	no data	27.7	24.0	26.4	26.3
3	no data	25.6	21.6	24.6	24.9
3.5	no data	23.8	19.4	22.5	22.8
4	28.5	22.0	17.6	20.7	20.3
4.5	no data	20.6	15.2	18.9	18.6
5	26.7	19.2	13.2	16.8	17.2
5.5	no data	17.8	11.2	15.0	15.8
6	25.3	16.3	9.1	13.2	14.4
6.5	no data	14.2	7.4	11.4	13.0
7	23.1	12.4	5.7	9.5	11.2
7.5	no data	no data	3.4	no data	no data
8	21.7	9.6	2.7	no data	6.3
8.5	no data	7.8	no data	no data	4.9
9	20.3	6.0	2.5	2.8	no data
9.5	no data	no data	no data	no data	2.8
10	18.9	2.6	2.4	2.5	2.7
11	17.1	no data	no data	no data	no data
12	14.6	2.4	2.3	2.2	2.5
13	12.5	no data	no data	no data	no data
14	10.7	no data	no data	no data	no data
15	8.9	2.2	2.1	2.2	2.3
16	7.1	no data	no data	no data	no data
17	5.3	no data	no data	no data	no data
18	3.6	no data	no data	no data	no data
19	2.1	no data	no data	no data	no data
20	2.0	2.1	2.0	2.1	2.1
25	1.9	no data	no data	no data	no data
30	1.9	1.9	1.9	1.9	2.0
40	1.8	1.9	1.9	1.9	2.0
50	1.8	1.9	1.9	1.9	2.0
60	1.8	1.9	1.9	1.9	2.0

Figures 2-27 and 2-34

Electrocoagulation Time, min	Initial Settling Rate, cm/min
15	1.8
45	3.3
75	4.1
90	3.7
120	3.5

Figure 2-28

Silica As Received		Electrocoagulated for 15 Minutes	
Equivalent Diameter (µm)	Cumulative Passing (wt %)	Equivalent Diameter (µm)	Cumulative Passing (wt %)
63.9	99.3	92.9	96.3
48.5	83.8	70.5	86.7
36.0	72.4	65.5	83.6
32.6	68.8	58.9	80.4
30.1	65.9	54.7	77.2
23.1	55.3	46.7	70.8
18.8	47.2	37.6	61.2
16.3	43.1	30.3	45.3
11.4	33.0	26.4	29.3
8.3	24.8	24.0	14.0
7.1	22.0	21.6	4.8
6.3	19.9	19.2	3.2
5.5	18.7	17.6	2.2
5.1	17.5	15.3	0.6
4.6	15.1	12.4	0.6
2.0	6.9	no data	no data

Figure 2-28 continued

Electrocoagulated for 45 Minutes		Electrocoagulated for 75 Minutes	
Equivalent Diameter (µm)	Cumulative Passing (wt %)	Equivalent Diameter (µm)	Cumulative Passing (wt %)
107.3	97.2	112.2	96.0
84.0	94.0	87.2	92.8
69.9	87.7	77.3	89.6
57.1	81.3	57.7	80.0
52.2	78.1	54.0	76.8
43.9	65.4	51.3	73.7
39.5	52.6	46.1	60.9
36.4	38.3	44.7	57.7
36.0	36.7	43.6	54.5
33.9	23.9	42.8	51.3
31.4	9.2	41.8	48.1
28.9	4.8	39.3	35.4
26.2	1.9	37.4	24.6
20.0	1.9	36.7	22.6
no data	no data	36.6	19.5
no data	no data	34.9	9.9
no data	no data	34.6	6.7
no data	no data	33.0	3.5
no data	no data	25.6	0.3

Figure 2-28 continued

Electrocoagulated for 90 Minutes		Electrocoagulated for 120 Minutes	
Equivalent Diameter (µm)	Cumulative Passing (wt %)	Equivalent Diameter (µm)	Cumulative Passing (wt %)
99.8	98.2	92.4	98.2
87.7	95.0	75.1	91.8
65.9	85.4	66.0	88.6
60.3	82.2	56.0	82.2
55.1	79.1	51.3	79.1
52.2	75.9	47.2	75.9
45.3	69.5	41.5	63.1
43.3	66.3	40.4	59.9
39.8	59.3	39.8	56.7
39.2	56.7	36.7	44.0
38.5	53.6	36.0	40.8
36.0	47.2	34.1	30.3
34.8	44.0	34.0	28.1
32.2	34.4	32.3	18.5
31.7	31.2	29.9	6.4
30.2	24.9	24.0	6.1
29.4	21.7	18.9	2.6
27.9	15.9	no data	no data
26.3	12.1	no data	no data
24.2	8.9	no data	no data
22.3	6.4	no data	no data
19.9	6.1	no data	no data
15.9	5.7	no data	no data

Figures 2-29 and 2-35

Electrocoagulation Time, min	Equivalent Floc d_{50}, µm
0	20
15	32
45	38
75	42
90	37
120	38

Figure 2-30

Settling Time, min	Settled Height, cm				
	15 min	45 min	75 min	90 min	120 min
0	35.6	35.7	36.3	36.3	35.7
0.5	no data	30.0	30.1	29.0	30.3
0.75	no data	26.4	26.9	26.1	no data
1	no data	23.6	24.7	22.5	26.1
1.25	no data	19.6	21.4	19.6	23.9
1.5	no data	16.8	18.5	16.3	21.4
1.75	no data	12.9	15.2	12.7	18.6
2	no data	10.4	12.3	10.2	16.4
2.25	no data	6.8	9.1	6.5	14.3
2.5	no data	5.0	6.5	5.1	11.4
2.75	no data	4.6	4.7	no data	9.3
3	no data	4.3	4.4	4.4	6.8
3.25	no data	no data	no data	no data	4.6
3.5	no data	3.8	3.9	3.8	no data
4	26.7	3.5	3.6	3.6	3.9
4.5	no data	3.4	no data	no data	3.5
5	24.9	3.3	3.3	3.4	3.3
6	23.1	3.1	3.1	3.2	3.1
7	21.4	no data	no data	no data	no data
8	19.6	2.9	2.9	no data	2.9
9	17.8	no data	no data	2.9	no data
10	16.0	2.7	2.6	no data	2.7
12	11.4	no data	no data	2.8	2.6
14	6.1	no data	no data	no data	no data
15	3.9	2.5	2.5	2.6	2.5
16	2.1	no data	no data	no data	no data
20	2.1	2.4	2.5	2.6	2.4
30	2.0	2.4	2.4	2.6	2.3
40	1.9	2.3	2.4	2.6	2.3
50	1.9	2.3	2.4	2.5	2.3
60	1.9	2.3	2.4	2.5	2.3

Figures 2-31 and 2-34

Electrocoagulation Time, min	Initial Settling Rate, cm/min
15	2.1
45	12.8
75	11.9
90	12.5
120	9.6

Figure 2-32

Silica As Received		Electrocoagulated for 15 Minutes	
Equivalent Diameter (µm)	Cumulative Passing (wt %)	Equivalent Diameter (µm)	Cumulative Passing (wt %)
63.9	99.3	92.6	96.3
48.5	83.8	77.0	89.9
36.0	72.4	71.0	86.7
32.6	68.8	65.0	83.5
30.1	65.9	59.9	80.3
23.1	55.3	55.3	77.2
18.8	47.2	51.2	74.0
16.3	43.1	46.9	70.8
11.4	33.0	38.9	61.2
8.3	24.8	34.1	48.5
7.1	22.0	30.8	35.7
6.3	19.9	29.0	26.1
5.5	18.7	28.4	23.0
5.1	17.5	26.1	10.2
4.6	15.1	21.1	4.1
2.0	6.9	16.5	1.3

Electrocoagulated for 45 Minutes		Electrocoagulated for 75 Minutes	
Equivalent Diameter (µm)	Cumulative Passing (wt %)	Equivalent Diameter (µm)	Cumulative Passing (wt %)
114.9	97.2	112.0	97.2
98.2	87.7	96.6	87.7
94.8	81.3	89.9	81.3
88.6	71.7	85.1	74.9
85.4	65.4	83.1	68.5
82.7	55.8	80.8	62.2
80.7	49.4	77.9	52.6
79.0	43.0	75.6	43.0
77.6	36.7	74.1	36.7
76.3	33.5	72.9	30.3
74.7	20.7	72.1	23.9
72.8	14.3	71.3	20.7
72.5	8.0	70.2	17.5
71.4	4.8	69.1	11.2
66.6	1.6	67.2	4.8
50.0	0	53.8	1.6
no data	no data	46.3	0

Figure 2-32 continued

Electrocoagulated for 90 Minutes		Electrocoagulated for 120 Minutes	
Equivalent Diameter (µm)	Cumulative Passing (wt %)	Equivalent Diameter (µm)	Cumulative Passing (wt %)
117.9	95.0	101.2	96.9
110.5	88.6	92.5	90.5
106.7	82.2	87.7	87.4
101.3	75.9	83.2	81.0
97.3	69.5	79.9	74.6
96.1	66.3	77.7	71.4
93.2	59.9	76.8	68.2
92.3	53.6	75.5	65.0
89.6	47.2	73.9	61.9
87.9	40.8	73.3	58.7
86.9	34.4	72.4	55.5
86.0	31.2	71.6	52.3
85.6	28.1	70.5	49.1
84.8	24.9	69.8	45.9
83.8	18.5	69.2	42.7
82.9	12.1	68.6	39.5
81.6	8.9	68.1	36.3
46.9	1.6	67.6	33.2
no data	no data	66.9	30.0
no data	no data	66.4	26.8
no data	no data	65.8	23.6
no data	no data	65.2	20.4
no data	no data	64.7	17.2
no data	no data	64.2	14.0
no data	no data	63.7	10.8
no data	no data	62.9	7.7
no data	no data	61.7	4.5
no data	no data	46.4	1.3

Figures 2-33 and 2-35

Electrocoagulation Time, min	Equivalent Floc d_{50}, µm
0	20
15	35
45	81
75	77
90	90
120	70

Figure 2-36

Freshly Electrocoagulated

AC/EC Time (min)	Indirect Electrocoagulation			Direct Electrocoagulation		
	ρ_{bulk} (kg/m^3)	Wt % Solids	Porosity (%)	ρ_{bulk} (kg/m^3)	Wt % Solids	Porosity (vol. %)
15	1623	63.5	59.4	1519	56.6	66.2
45	1519	56.6	66.2	1521	56.7	66.1
75	1519	56.6	66.2	1464	52.6	69.7
90	1546	58.5	64.4	1458	52.0	70.1
120	1546	58.5	64.4	1502	55.4	67.3

Aged 1 Day

AC/EC Time (min)	Indirect Electrocoagulation			Direct Electrocoagulation		
	ρ_{bulk} (kg/m^3)	Wt % Solids	Porosity (%)	ρ_{bulk} (kg/m^3)	Wt % Solids	Porosity (vol. %)
15	1636	64.3	58.6	1611	62.7	60.2
45	1588	61.3	61.7	1556	59.2	63.8
75	1594	61.6	61.3	1556	59.2	63.8
90	1577	60.6	62.4	1444	51.0	71.0
120	1611	62.8	60.2	1494	54.8	67.8

Figure 2-37

Settling Time, min	Settled Height, cm	
	Continuous	Cumulative
0	29.9	35.7
0.5	28.8	33.9
1	28.1	31.4
1.5	26.3	29.3
2	25.6	27.8
2.5	23.9	25.0
3	22.4	22.8
3.5	21.0	21.1
4	19.2	19.6
4.5	17.8	17.9
5	17.1	15.7
5.5	15.7	13.9
6	14.6	12.1
6.5	12.8	10.0
7	11.4	8.6
7.5	10.3	6.4
8	9.3	4.3
8.5	7.8	2.7
9	no data	2.6
10	no data	2.5
11	2.7	no data
12	2.6	2.2
15	2.5	2.1
20	2.2	2.0
25	2.1	1.9
30	2.1	1.8
40	2.1	1.8
50	2.1	1.8
60	2.1	1.8

Figure 2-38

Settling Time (min)	Settled Height, cm				
	70.2 A/m^2	100.3 A/m^2	117.0 A/m^2	133.7 A/m^2	167.2 A/m^2
0	33.2	35.7	35.7	35.5	35.6
0.5	31.4	33.6	33.2	33.4	33.5
1	29.6	31.4	31.2	30.9	30.6
1.5	28.2	28.9	28.6	28.4	28.3
2	27.1	26.4	26.1	25.9	25.6
2.5	25.7	23.9	23.9	23.8	23.1
3	24.3	22.1	21.4	21.3	20.6
3.5	22.5	20.0	19.3	19.5	18.2
4	21.1	17.9	16.8	17.0	16.4
4.5	19.3	15.4	14.3	14.6	13.9
5	17.9	13.2	12.1	12.4	11.0
5.5	16.8	10.7	9.6	9.9	8.9
6	no data	8.9	7.1	7.8	6.8
6.5	13.6	6.4	4.6	5.3	3.9
7	11.8	4.3	2.6	3.1	3.0
7.5	10.7	2.8	no data	2.9	no data
8	9.3	2.5	2.3	2.8	2.6
8.5	8.2	no data	no data	no data	no data
9	7.1	2.3	2.1	2.5	2.5
9.5	6.1	no data	no data	no data	no data
10	5.0	2.2	2.1	2.4	2.3
10.5	3.4	no data	no data	no data	no data
11	2.7	no data	no data	no data	no data
12	2.5	2.1	no data	2.2	2.2
13	2.4	no data	no data	no data	no data
15	2.2	2.0	1.9	2.1	2.1
20	2.1	1.8	1.7	2.1	2.0
25	2.1	1.8	1.7	2.0	2.0
30	2.0	1.7	1.7	1.9	1.9
40	2.0	1.7	1.7	1.9	1.9
50	2.0	1.7	1.7	1.9	1.8
60	2.0	1.7	1.7	1.9	1.8

Figure 2-39

Current Density, A/m^2	Initial Settling Rate, cm/min
70.2	2.8
100.3	4.5
117.0	4.7
133.7	4.6
167.2	4.7

Raw Voltage Data for Tables 2-21 and 2-23

AC/EC Time (min)	Voltage, V				
	70.2 A/m^2	100.3 A/m^2	117.0 A/m^2	133.7 A/m^2	167.2 A/m^2
0	51.0	70.6	82.6	92.9	115.2
1	51.1	69.9	81.6	91.3	111.5
2	51.2	68.7	80.2	89.6	107.4
3	51.0	68.6	78.6	87.0	103.1
4	50.4	66.7	76.5	85.6	100.4
5	50.4	66.9	75.7	84.1	97.6
6	49.5	65.6	74.7	81.5	95.5
7	49.5	64.5	73.6	80.7	92.4
8	49.4	64.4	71.1	79.1	90.4
9	48.8	63.2	70.0	77.4	88.0
10	48.8	62.0	70.0	76.0	85.5
11	48.2	62.0	68.5	74.6	84.1
12	48.2	61.3	67.6	73.7	81.9
13	47.5	60.1	66.6	72.2	81.0
14	47.5	60.1	65.6	71.1	79.2
15	46.9	59.2	64.7	70.5	78.3

Figure 2-43

Current Density, A/m^2	pH	
	Electrocoagulated Slurry	Supernatant
0	8.8	7.5
70.2	8.5	8.4
100.3	8.2	8.3
117.0	8.4	8.3
133.7	8.5	8.5
167.2	8.6	8.4

Figure 2-44

Current Density, A/m^2	Zeta Potential, mV
0	-21.7
70.2	-19.9
100.3	-19.3
117.0	-7.6
133.7	-20.6
167.2	-1.9

Figure 2-45

Settling Time, min	Settled Height, cm	
	3.5 A, 15 min	5.0 A, 10.5 min
0	35.7	35.6
0.5	33.2	32.8
1	31.2	29.9
1.5	28.6	26.7
2	26.1	24.2
2.5	23.9	21.4
3	21.4	18.5
3.5	19.3	16.0
4	16.8	13.2
4.5	14.3	10.3
5	12.1	7.8
5.5	9.6	no data
6	7.1	2.9
6.5	4.6	no data
7	2.6	2.5
8	2.3	2.3
9	2.1	no data
10	2.1	2.1
12	no data	2.1
15	1.9	2.0
20	1.7	no data
21	no data	1.8
25	1.7	no data
30	1.7	1.8
40	1.7	1.8
50	1.7	1.8
60	1.7	1.8

Figure 2-46

Settling Time (min)	Settled Height, cm				
	10 mg/L Al	25 mg/L Al	40 mg/L Al	60 mg/L Al	100 mg/L Al
0	23.8	25.2	25.2	25.6	25.2
0.5	21.0	21.7	22.1	23.2	23.1
1	18.1	19.1	19.5	20.1	20.6
1.5	16.2	16.8	16.8	18.0	18.1
2	13.9	13.9	14.1	15.2	16.1
2.5	11.4	11.1	11.8	12.9	14.1
3	8.9	8.7	8.5	10.3	12.1
3.5	6.7	6.0	6.0	7.8	10.1
4	4.4	3.1	4.9	5.5	8.0
4.5	2.3	no data	3.5	4.5	6.8
5	2.1	2.6	3.1	4.3	6.3
5.5	no data	no data	2.9	no data	5.8
6	1.9	2.4	2.8	3.5	5.5
7	no data	no data	2.6	3.3	4.8
8	1.8	2.2	2.6	3.1	4.3
9	no data	no data	no data	no data	4.0
10	1.7	2.1	2.4	2.9	3.9
12	1.7	2.0	2.2	2.7	3.6
15	1.6	1.9	2.2	2.6	3.4
20	1.6	1.9	2.1	2.5	3.2
25	1.6	1.9	2.1	2.4	3.0
30	1.6	1.9	2.1	2.3	3.0
40	1.6	1.9	2.0	2.3	2.8
50	1.6	1.9	2.0	2.3	2.8
60	1.6	1.9	2.0	2.3	2.8

Figure 2-47

Settling Time (min)	Settled Height, cm				
	10 mg/L Al	25 mg/L Al	40 mg/L Al	60 mg/L Al	100 mg/L Al
0	23.8	25.6	25.2	23.8	25.2
0.5	21.3	23.2	22.1	21.4	23.1
1	18.9	20.3	19.7	18.9	20.9
1.5	17.2	17.2	17.1	16.2	18.9
2	14.9	14.6	14.5	13.7	16.5
2.5	13.2	11.3	11.7	11.6	14.3
3	11.1	8.6	8.9	8.8	12.3
3.5	9.3	6.2	6.6	6.7	10.5
4	7.2	3.1	4.0	4.2	8.0
4.5	4.8	2.9	3.4	3.8	6.4
5	2.7	2.7	3.1	3.4	5.7
5.5	2.2	no data	no data	3.0	no data
6	2.1	2.5	2.8	3.0	5.0
7	no data	2.3	no data	2.9	no data
8	1.8	2.3	2.5	2.7	3.9
10	1.7	2.1	2.4	2.5	3.6
12	no data	2.1	2.2	2.5	3.4
15	no data	1.9	2.2	2.3	3.2
20	1.6	1.9	2.2	2.3	3.0
25	1.5	1.8	2.1	2.2	2.9
30	1.5	1.8	2.1	2.2	2.8
40	1.5	1.8	2.1	2.2	2.7
50	1.5	1.8	2.1	2.1	2.7
60	1.5	1.8	2.1	2.1	2.7

Figure 2-48

Dosage, mg/L Al	Initial Settling Rate, cm/min	
	Alum	Aluminum Chloride
10	4.8	4.2
25	5.5	5.6
40	5.5	5.3
60	5.0	4.9
100	4.1	4.2

CHAPTER 3

Figure 3-1

Settling Time, min	Settled Height, cm
0	25.2
0.5	19.3
1	14.1
1.5	9.3
2	5.0
2.5	4.2
3	3.7
3.5	3.4
4	3.2
4.5	3.1
5	3.0
6	2.8
8	2.6
10	2.5
12	2.4
15	2.4
20	2.3
25	2.3
30	2.2
40	2.2
50	2.2
60	2.2

Figure 3-2

NaCl Addition (mg/L)	Specific Conductivity (µS/cm)	Initial Settling Rate (cm/min)
200	420	2.7
1080	2040	3.3
1510	2860	3.7
2000	3840	4.1
2470	4620	3.3
3000	5650	3.0
3400	6320	2.7

Figure 3-3

Water Conductivity (µS/cm)	pH		
	Feed Suspension	EC* Slurry	Supernatant
420	8.82	8.65	8.60
2040	8.79	8.67	8.33
2860	8.66	8.10	8.11
3840	8.61	8.16	8.03
4620	8.56	8.49	8.54
5650	8.75	8.13	8.09
6320	8.57	8.25	8.17

* Electrocoagulated

Figure 3-4

Specific Conductivity (µS/cm)	Zeta Potential, mV	
	EC* Silica	As-received Silica
0.3	-16.0	-16.0
420	-20.3	-21.4
2040	-13.3	-25.3
2860	-11.6	-25.4
3840	-10.4	-23.2
4620	-18.9	-22.0
5650	-21.5	-23.0
6320	-9.0	-21.8

* Electrocoagulated

Figure 3-5

h, nm	Net Interaction Energy, kT			
	0.3 µS/cm	420 µS/cm	2040 µS/cm	2860 µS/cm
0.1	-32000	-29000	-28000	-28000
1	-690	650	970	700
1.5	450	1400	1200	900
2	1000	1700	1100	740
2.5	1400	1700	870	520
3	1600	1600	650	320
5	2000	1200	41	-170
10	2300	400	-270	-300
15	2300	57	-220	-230
20	2300	-61	-170	-170

h, nm	Net Interaction Energy, kT			
	3840 µS/cm	4620 µS/cm	5650 µS/cm	6320 µS/cm
0.1	-29000	-29000	-29000	-30000
1	-280	-790	-740	-1100
1.5	37	-410	-440	-720
2	-2	-380	-440	-660
2.5	-110	-420	-500	-660
3	-210	-460	-540	-660
5	-410	-510	-550	-590
10	-330	-340	-340	-340
15	-230	-230	-230	-230
20	-170	-170	-170	-170

Figure 3-6

Settling Time (min)	Settled Height, cm				
	pH 3.00	pH 4.11	pH 5.44	pH 6.93	pH 9.07
0	35.5	35.5	35.7	35.6	35.7
0.5	no data	34.4	33.6	33.8	34.6
1	34.8	33.4	31.4	32.0	33.2
1.5	no data	31.6	28.6	30.3	31.4
2	33.7	30.5	26.1	28.8	30.0
2.5	no data	29.1	24.3	27.1	28.2
3	32.3	27.9	21.4	25.3	27.0
3.5	no data	26.3	19.3	23.5	25.3
4	31.2	25.2	16.8	22.1	23.9
4.5	no data	23.6	14.3	20.6	22.5
5	30.2	22.7	12.1	18.9	21.1
5.5	no data	20.9	10.0	17.3	19.3
6	28.8	19.5	6.8	16.0	17.9
6.5	no data	18.5	3.9	14.2	16.4
7	27.9	17.0	3.2	12.5	15.0
7.5	no data	15.6	3.1	10.7	13.6
8	26.6	14.9	2.9	9.3	12.3
8.5	no data	13.3	no data	7.5	10.7
9	25.2	11.7	2.7	6.1	9.3
9.5	no data	10.3	no data	4.3	8.0
10	23.8	9.2	2.5	4.0	6.8
10.5	no data	7.6	no data	3.7	5.2
11	22.4	6.4	no data	3.6	4.2
11.5	no data	4.6	no data	no data	3.9
12	20.6	3.0	2.5	3.2	3.7
13	20.4	2.8	no data	3.2	3.4
14	18.8	2.6	no data	no data	3.2
15	17.0	2.5	2.3	3.0	3.2
17	13.8	no data	no data	no data	no data
18	12.4	no data	no data	no data	no data
19	11.4	no data	no data	no data	no data
20	9.6	2.4	2.2	2.8	2.9
21	8.2	no data	no data	no data	no data
22	5.9	no data	no data	no data	no data
23	4.3	no data	no data	no data	no data
24	3.6	no data	no data	no data	no data
25	3.5	2.2	2.1	2.6	2.8
27	3.2	no data	no data	no data	no data
30	2.9	2.2	2.1	2.5	2.6
33	2.6	no data	no data	no data	no data
36	2.4	no data	no data	no data	no data
40	2.3	2.1	2.1	no data	2.5
45	2.3	no data	no data	2.4	no data
50	2.2	2.1	2.1	2.3	2.4
60	2.2	2.1	2.1	2.2	2.4

Figure 3-7

Feed Water pH	Initial Settling Rate, cm/min
3.00	1.2
4.11	2.7
5.44	4.9
6.93	3.3
9.07	2.9

Figure 3-8

Silica As Received		Electrocoagulated from pH 3.00	
Equivalent Diameter (µm)	Cumulative Passing (wt %)	Equivalent Diameter (µm)	Cumulative Passing (wt %)
63.9	99.3	91.1	95.4
48.5	83.8	74.4	85.9
40.3	79.8	65.8	82.7
36.0	72.4	56.2	75.6
32.6	68.8	49.8	71.8
30.1	65.9	45.6	67.7
23.1	55.3	42.4	64.2
18.8	47.2	31.4	55.2
16.3	43.1	25.7	48.8
13.4	35.0	23.3	45.0
11.4	33.0	21.2	40.5
8.3	24.8	18.9	33.2
7.1	22.0	17.4	25.9
6.3	19.9	16.3	18.8
5.5	18.7	14.7	8.3
5.1	17.5	13.3	3.5
4.6	15.1	12.2	2.9
2.0	6.9	11.1	1.0
no data	no data	10.0	0

Figure 3-8 continued

Electrocoagulated from pH 5.44		Electrocoagulated from pH 9.07	
Equivalent Diameter (µm)	Cumulative Passing (wt %)	Equivalent Diameter (µm)	Cumulative Passing (wt %)
93.1	97.6	109.9	99.7
68.9	91.5	89.6	96.9
60.0	82.3	79.8	93.5
56.9	78.5	67.2	89.4
54.9	73.0	55.6	80.0
53.0	68.9	52.6	74.4
51.8	63.5	50.7	70.6
48.9	56.5	49.0	67.5
44.5	31.3	48.1	65.0
41.9	14.4	47.5	61.6
38.9	2.2	46.6	59.7
35.0	0.6	41.1	35.6
30.4	0.3	38.7	17.8
23.6	0	36.9	5.3
no data	no data	34.5	4.4
no data	no data	32.5	0

Figure 3-9

Feed Water pH	Zeta Potential, mV	
	Electrocoagulated Silica	As-received Silica
3.00	+9.9	-8.8
4.11	-5.9	-15.5
5.44	+19.7	-19.5
6.93	-1.5	-21.8
9.07	-8.6	-24.0

Figure 3-10

Wt % Solids	Al Concentration in Supernatant, mg/L		
	pH 3.00	pH 5.44	pH 9.07
0	10.5	6.0	7.5
0.5	9.5	4.0	4.8
1.0	9.0	4.0	4.0
2.0	9.0	3.0	3.0
3.0	9.0	1.0	2.5
5.0	9.0	0.2	1.0

Figure 3-11

Wt % Solids	Zeta Potential, mV		
	pH 3.00	pH 5.44	pH 9.07
0.5	-5.3	-10.8	-12.6
1.0	-6.2	-9.5	-14.4
2.0	-3.7	-12.2	-14.9
3.0	-6.7	-13.4	-12.7
5.0	+9.9	+19.7	-8.6

Figure 3-12

Settling Time (min)	Settled Height, cm					
	23.2℃	29.8℃	44.6℃	61.0℃	70.4℃	85.0℃
0	35.7	35.6	35.5	35.6	35.7	35.7
0.5	33.2	32.8	31.6	32.4	32.8	32.5
1	30.7	30.3	27.3	29.5	28.9	30.3
1.5	27.8	27.8	23.4	26.7	25.9	27.1
2	25.3	24.9	19.9	23.5	23.2	24.6
2.5	22.5	22.1	16.0	20.5	19.6	21.4
3	20.0	19.6	12.1	17.8	16.4	19.3
3.5	17.5	17.1	7.8	15.0	13.2	no data
4	15.0	14.6	4.3	12.1	10.4	13.9
4.5	12.5	12.1	4.0	8.7	6.8	11.1
5	10.0	8.7	3.4	6.1	3.6	7.9
5.5	7.1	6.4	no data	3.6	3.2	6.1
6	4.5	4.3	3.2	3.2	3.0	3.7
6.5	3.1	3.1	no data	no data	no data	3.5
7	2.9	2.9	3.0	3.0	2.9	3.2
7.5	2.8	2.8	no data	no data	no data	no data
8	2.6	2.6	2.9	2.8	2.8	3.0
8.5	no data	2.6	no data	no data	no data	no data
9	2.5	2.5	no data	2.8	no data	no data
10	2.5	2.5	2.8	2.7	2.5	2.9
12	no data	2.3	2.7	2.5	no data	2.7
13	2.3	no data	no data	no data	no data	no data
15	2.2	2.2	2.5	2.5	2.4	2.5
20	2.1	2.1	2.4	2.3	2.2	2.5
25	2.1	2.1	2.4	2.2	2.1	2.4
30	2.1	2.1	2.3	2.2	2.1	2.3
40	2.1	2.1	2.3	2.1	2.1	2.2
50	2.1	2.0	2.3	2.1	2.1	2.2
60	2.1	2.0	2.3	2.1	2.1	2.2

Figure 3-13

Feed Water Temperature, ℃	Initial Settling Rate, cm/min
23.2	5.2
29.8	5.2
44.6	7.8
61.0	5.9
70.4	6.4
85.0	5.4

CHAPTER 4

Figure 4-1

Settling Time (min)	Settled Height, cm					
	299.1 cm^2	598.2 cm^2	897.3 cm^2	1196.4 cm^2	1495.5 cm^2	1794.6 cm^2
0	32.1	35.5	35.5	35.6	35.7	35.6
0.5	31.1	33.7	33.2	33.8	33.6	33.5
1	29.6	no data	31.2	31.5	31.4	31.0
1.5	28.6	30.2	29.1	29.2	29.3	28.5
2	27.1	28.4	26.8	27.4	27.0	26.0
2.5	26.1	26.3	24.7	24.9	24.6	23.1
3	24.6	24.9	22.4	23.0	22.7	20.8
3.5	23.9	22.7	20.2	21.0	20.3	17.8
4	22.3	21.3	18.1	18.9	18.2	16.0
4.5	20.9	19.3	16.2	16.7	15.9	13.4
5	20.0	17.6	14.0	14.6	13.6	11.0
5.5	18.2	16.0	11.7	12.5	11.6	8.7
6	17.1	14.2	9.6	10.3	9.3	6.6
6.5	16.1	12.4	7.5	8.5	7.5	6.0
7	15.0	10.7	5.3	6.4	5.7	5.6
7.5	13.9	8.9	4.6	5.3	5.3	5.1
8	12.5	7.1	4.3	4.9	4.9	4.7
8.5	11.4	5.5	3.9	4.6	4.6	4.5
9	10.0	5.0	3.8	4.4	4.3	4.2
9.5	8.9	4.8	no data	no data	4.1	no data
10	7.1	4.6	3.5	3.9	3.9	4.0
10.5	6.1	no data	no data	no data	no data	no data
11	5.0	4.2	3.3	3.7	3.7	no data
11.5	3.6	no data	no data	no data	no data	no data
12	3.2	3.8	no data	no data	3.6	3.8
13	3.0	3.6	3.2	3.5	no data	no data
14	2.8	no data	no data	no data	no data	no data
15	2.6	3.4	3.1	3.4	3.3	3.6
16	2.5	no data	no data	no data	no data	no data
17	no data	3.3	no data	no data	no data	no data
18	2.5	no data	no data	no data	no data	no data
20	2.5	3.2	2.8	3.2	3.1	3.2
25	2.3	3.0	2.8	2.9	2.9	3.1
30	2.2	2.9	2.7	2.8	2.9	2.9
35	2.2	no data	no data	no data	no data	no data
40	2.1	2.8	2.5	2.8	2.8	2.8
50	2.1	2.8	2.5	2.7	2.8	2.8
60	2.1	2.7	2.5	2.7	2.7	2.8

Figure 4-2

Electrode Area, cm^2	Initial Settling Rate, cm/min
299.1	2.5
598.2	3.5
897.3	4.3
1196.4	4.2
1495.5	4.3
1794.6	4.9

Figure 4-3

AC/EC Time (min)	Slurry pH					
	299.1 cm^2	598.2 cm^2	897.3 cm^2	1196.4 cm^2	1495.5 cm^2	1794.6 cm^2
0	8.68	8.78	8.74	8.72	8.65	8.73
1	8.41	8.60	8.27	8.19	8.05	8.15
2	8.28	8.29	8.06	8.01	7.95	8.18
3	8.09	8.09	8.05	8.05	8.08	8.27
4	7.98	8.08	8.09	8.09	8.17	8.43
5	7.91	8.08	8.15	8.15	8.24	8.49
6	7.92	8.12	8.21	8.22	8.27	8.52
7	7.90	8.20	8.30	8.30	8.36	8.57
8	7.92	8.28	8.33	8.34	8.37	8.62
9	7.93	8.32	8.38	8.39	8.40	8.63
10	7.97	8.35	8.41	8.43	8.50	8.65
11	8.01	8.38	8.44	8.45	8.46	8.67
12	8.07	8.41	8.50	8.43	8.48	8.66
13	8.08	8.44	8.50	8.51	8.53	8.70
14	8.09	8.46	8.52	8.52	8.54	8.69
15	8.12	8.46	8.52	8.52	8.54	8.70

Figure 4-4

Electrode Area, cm^2	Electrocoagulated Slurry pH	Supernatant pH
0	8.72	7.34
299.1	8.38	8.29
598.2	8.46	8.52
897.3	8.96	8.68
1196.4	8.89	8.73
1495.5	9.05	9.06
1794.6	8.70	8.90

Figure 4-5

Electrode Separation (cm)	V_{avg} (V)	Average Voltage Gradient (V/cm)	Initial Settling Rate (cm/min)
0.5	10.0	20.0	4.2
1	17.3	17.3	2.6
2	33.8	16.9	5.1
3	49.9	16.6	2.6
4	63.3	15.8	4.2
5	77.4	15.5	3.2
6	90.8	15.1	3.6
7	103.7	14.8	3.5

CHAPTER 5

Figure 5-1

Equivalent Particle Diameter, µm	Cumulative Passing, Wt %
69.0	99.9
54.0	97.9
44.3	96.6
40.5	96.2
35.2	95.3
31.6	94.9
22.5	93.7
17.8	93.3
13.3	92.4
10.2	91.2
8.1	89.1
6.6	88.2
5.5	86.6
4.8	85.3
4.3	84.5
3.9	83.2
2.2	74.4
2.0	69.8

Figure 5-2

pH	Zeta Potential, mV	
	0 mg/L NaCl	200 mg/L NaCl
3.30	no data	-10.2
3.44	-11.7	no data
5.30	no data	-11.9
5.41	-10.5	no data
7.27	-12.6	no data
7.50	no data	-13.4
9.74	no data	-14.5
9.99	-15.6	no data

Figure 5-3

Settling Time, min	Settled Height, cm	
	Quiescent	Agitated
0	35.7	35.6
0.5	no data	35.2
1	34.5	34.6
1.5	no data	34.1
2	32.5	33.5
2.5	no data	32.8
3	30.6	32.2
3.5	no data	31.6
4	28.7	31.0
4.5	no data	30.3
5	26.8	29.7
5.5	no data	29.1
6	25.4	28.5
6.5	no data	27.9
7	24.0	27.4
7.5	no data	26.8
8	22.7	26.3
8.5	no data	25.8
9	21.6	25.3
9.5	no data	24.9
10	20.6	24.4
11	19.6	23.5
12	18.8	22.5
13	18.0	21.8
14	no data	21.0
15	16.6	20.3
16	16.1	19.6
17	15.5	19.0
18	15.0	18.4
19	14.6	17.8
20	14.3	17.2
21	13.9	no data
22	13.6	16.4
23	13.4	no data
24	no data	15.7
25	12.9	no data
26	no data	15.1
27	12.5	no data
28	no data	14.6
30	12.0	14.2
33	11.6	13.7
36	11.2	13.2
39	10.9	no data

Figure 5-3 continued

Settling Time, min	Settled Height, cm	
	Quiescent	Agitated
40	no data	12.6
42	10.6	no data
45	no data	12.1
46	10.2	no data
50	10.0	no data
51	no data	11.5
55	9.6	11.1
60	9.3	10.8

Figure 5-4

Settling Time (min)	Settled Height, cm					
	6 min AC/EC	10 min AC/EC	15 min AC/EC	25 min AC/EC	35 min AC/EC	45 min AC/EC
0	34.5	35.5	35.6	35.7	35.6	35.7
0.5	33.8	35.1	35.2	no data	no data	35.1
1	33.1	34.4	34.6	34.8	34.6	34.4
1.5	32.0	no data	34.1	34.1	no data	33.7
2	30.3	33.2	33.5	33.5	33.3	33.0
2.5	29.4	32.3	32.8	32.8	32.6	32.1
3	28.1	no data	32.2	32.1	31.9	31.4
3.5	26.7	31.0	31.6	31.4	31.2	30.6
4	25.8	30.4	31.0	30.7	30.5	29.9
4.5	24.9	no data	30.3	30.1	29.9	29.1
5	23.5	29.0	29.7	29.4	29.1	28.4
5.5	no data	no data	29.1	28.7	28.4	no data
6	21.4	27.7	28.5	28.1	27.7	27.0
6.5	no data	no data	27.9	no data	27.1	no data
7	no data	26.5	27.4	26.8	26.4	25.7
7.5	no data	no data	26.8	no data	no data	no data
8	18.0	25.3	26.3	25.7	25.2	24.3
8.5	no data	no data	25.8	no data	no data	no data
9	16.7	24.2	25.3	24.6	24.0	23.2
9.5	no data	no data	24.9	no data	no data	no data
10	15.8	23.2	24.4	23.6	23.0	22.1
11	no data	22.4	23.5	22.6	22.0	21.1
12	14.2	21.5	22.5	21.8	21.1	20.3
13	no data	20.7	21.8	21.0	20.3	19.5
14	13.1	20.1	21.0	20.1	19.5	18.6
15	no data	19.3	20.3	no data	18.8	18.0
16	12.2	no data	19.6	18.7	18.1	17.4

Figure 5-4 continued

Settling Time (min)	Settled Height, cm					
	6 min AC/EC	10 min AC/EC	15 min AC/EC	25 min AC/EC	35 min AC/EC	45 min AC/EC
17	no data	17.9	19.0	18.1	17.5	16.8
18	11.6	17.6	18.4	no data	16.9	16.2
19	no data	no data	17.8	17.0	16.4	no data
20	no data	16.6	17.2	no data	15.9	15.3
21	10.9	no data	no data	16.1	no data	no data
22	no data	15.7	16.4	no data	15.1	14.5
23	no data	no data	no data	15.4	no data	no data
24	no data	14.8	15.7	no data	14.5	13.9
25	10.3	no data	no data	14.7	no data	no data
26	no data	14.1	15.1	no data	14.0	13.4
28	no data	13.5	14.6	no data	no data	no data
29	no data	no data	no data	13.9	13.4	12.9
30	9.7	13.1	14.2	no data	no data	no data
32	no data	no data	no data	13.4	no data	no data
33	no data	12.5	13.7	no data	12.8	no data
34	no data	no data	no data	no data	no data	12.1
35	9.3	no data	no data	12.9	no data	no data
36	no data	12.0	13.2	no data	no data	no data
37	no data	no data	no data	no data	12.3	no data
38	no data	no data	no data	12.5	no data	11.8
40	8.9	11.5	12.6	no data	no data	no data
41	no data	no data	no data	12.2	11.9	no data
45	no data	11.0	12.1	11.8	11.4	11.1
50	8.4	10.5	no data	11.3	11.1	10.7
51	no data	no data	11.5	no data	no data	no data
55	no data	10.1	11.1	11.0	10.8	10.4
60	7.9	9.8	10.8	10.6	10.5	10.1

Figure 5-5

Electrocoagulation Time, min	Initial Settling Rate, cm/min
6	2.2
10	1.3
15	1.2
25	1.3
35	1.3
45	1.4

Figure 5-6

Electrocoagulation Time, min	Zeta Potential. mV
0	-14.3
10	-15.5
15	-15.7
25	-16.1
35	-15.4
45	-14.5

Figure 5-7

Settling Time, min	Settled Height, cm	
	Continuous AC/EC	Cumulative AC/EC
0	35.6	35.6
0.5	35.2	no data
1	34.6	34.6
1.5	34.1	33.9
2	33.5	33.1
2.5	32.8	32.2
3	32.2	31.3
3.5	31.6	30.4
4	31.0	29.5
4.5	30.3	28.7
5	29.7	27.8
5.5	29.1	no data
6	28.5	26.3
6.5	27.9	no data
7	27.4	24.8
7.5	26.8	no data
8	26.3	23.5
8.5	25.8	no data
9	25.3	22.4
9.5	24.9	no data
10	24.4	21.3
11	23.5	20.3
12	22.5	19.5
13	21.8	18.7
14	21.0	17.9
15	20.3	17.2
16	19.6	16.6
17	19.0	16.0
18	18.4	no data
19	17.8	15.0
20	17.2	14.5

Figure 5-7 continued

Settling Time, min	Settled Height, cm	
	Continuous AC/EC	Cumulative AC/EC
22	16.4	13.9
24	15.7	13.2
26	15.1	12.8
28	14.6	no data
30	14.2	12.1
33	13.7	no data
35	no data	11.4
36	13.2	no data
40	12.6	10.8
45	12.1	10.4
50	no data	10.0
51	11.5	no data
55	11.1	9.6
60	10.8	9.3

Figure 5-8

Settling Time, min	Settled Height, cm	
	Direct AC/EC	Indirect AC/EC
0	35.7	35.3
0.5	35.1	no data
1	34.4	34.6
1.5	33.7	no data
2	33.0	no data
2.5	32.1	no data
3	31.4	no data
3.5	30.6	no data
4	29.9	no data
4.5	29.1	no data
5	28.4	24.3
6	27.0	22.1
7	25.7	19.6
8	24.3	17.5
9	23.2	15.7
10	22.1	no data
10.5	no data	13.9
11	21.1	13.6
11.5	no data	13.2
12	20.3	12.9
13	19.5	12.2
14	18.6	11.8

Figure 5-8 continued

Settling Time, min	Settled Height, cm	
	Direct AC/EC	Indirect AC/EC
15	18.0	11.4
16	17.4	11.0
17	16.8	10.7
18	16.2	10.5
20	15.3	10.1
22	14.5	no data
23	no data	9.7
24	13.9	no data
26	13.4	9.3
29	12.9	no data
32	no data	8.7
34	12.1	no data
36	no data	8.5
38	11.8	no data
40	no data	8.2
45	11.1	7.9
50	10.7	7.7
55	10.4	7.5
60	10.1	7.4

Figure 5-9

Settling Time, min	Settled Height, cm	
	83.6 A/m^2	167.2 A/m^2
0	35.7	35.6
0.5	no data	35.2
1	33.9	34.6
1.5	no data	34.1
2	31.8	33.5
2.5	no data	32.8
3	30.0	32.2
3.5	28.9	31.6
4	28.0	31.0
4.5	26.8	30.3
5	26.1	29.7
5.5	no data	29.1
6	24.3	28.5
6.5	no data	27.9
7	22.5	27.4
7.5	no data	26.8
8	21.1	26.3
8.5	no data	25.8

Figure 5-9 continued

Settling Time, min	Settled Height, cm	
	83.6 A/m^2	167.2 A/m^2
9	19.6	25.3
9.5	no data	24.9
10	18.4	24.4
11	17.5	23.5
12	16.6	22.5
13	15.8	21.8
14	15.2	21.0
15	14.6	20.3
16	14.0	19.6
17	13.6	19.0
18	13.1	18.4
19	12.7	17.8
20	12.3	17.2
21	12.0	no data
22	no data	16.4
23	11.5	no data
24	no data	15.7
25	11.1	no data
26	no data	15.1
28	no data	14.6
29	10.4	no data
30	no data	14.2
33	10.0	13.7
35	9.7	no data
36	no data	13.2
40	9.3	12.6
45	9.0	12.1
50	8.6	no data
51	no data	11.5
55	8.4	11.1
60	8.2	10.8

Figure 5-10

Settling Time, min	Settled Height, cm	
	299.1 A/m^2	598.2 A/m^2
0	35.7	35.7
1	33.9	no data
1.5	no data	34.1
2	31.8	33.5
2.5	no data	32.8
3	30.0	32.2
3.5	28.9	31.5
4	28.0	30.9
4.5	26.8	30.3
5	26.1	29.6
6	24.3	28.5
7	22.5	27.4
8	21.1	26.3
9	19.6	25.3
10	18.4	24.3
11	17.5	23.5
12	16.6	22.7
13	15.8	21.8
14	15.2	no data
15	14.6	20.3
16	14.0	no data
17	13.6	no data
18	13.1	18.5
19	12.7	no data
20	12.3	17.2
21	12.0	no data
22	no data	16.3
23	11.5	no data
24	no data	15.4
25	11.1	no data
26	no data	14.7
28	no data	14.2
29	10.4	no data
30	no data	13.7
32	no data	13.2
33	10.0	no data
34	no data	12.9
35	9.7	no data
36	no data	12.6
40	9.3	12.1
44	no data	11.5
45	9.0	no data
47	no data	11.2
50	8.6	11.0
55	8.4	10.6
60	8.2	10.2

Figure 5-11

Settling Time, min	Settled Height, cm	
	5.0 A x 10 min	2.5 A x 20 min
0	35.5	35.5
0.5	35.1	34.9
1	34.4	34.1
1.5	no data	33.5
2	33.2	32.8
2.5	32.3	32.1
3	no data	31.5
3.5	31.0	30.7
4	30.4	30.2
4.5	no data	29.5
5	29.0	28.9
6	27.7	27.7
7	26.5	26.5
8	25.3	no data
9	24.2	24.4
10	23.2	23.4
11	22.4	22.5
12	21.5	21.8
13	20.7	21.1
14	20.1	20.3
15	19.3	no data
16	no data	19.1
17	17.9	no data
18	17.6	18.0
20	16.6	16.9
22	15.7	16.0
24	14.8	15.2
26	14.1	no data
27	no data	14.1
28	13.5	no data
30	13.1	13.3
33	12.5	no data
34	no data	12.6
36	12.0	no data
38	no data	12.0
40	11.5	no data
42	no data	11.5
45	11.0	no data
47	no data	11.0
50	10.5	10.8
55	10.1	10.4
60	9.8	10.0

Figure 5-12

Settling Time, h	Settled Height, cm
0	35.5
0.03	35.1
0.06	34.8
0.08	34.4
0.10	34.1
0.13	33.7
0.16	33.4
0.18	33.0
0.24	32.0
0.29	31.2
0.35	30.2
0.41	29.1
0.45	28.4
0.50	27.7
0.56	26.6
0.61	25.9
0.69	24.9
0.76	23.8
0.80	23.1
0.89	22.0
0.99	21.3
1.13	20.6
1.46	19.5
1.79	18.8
2.76	17.4
3.05	17.0
3.40	16.7
3.85	16.3
4.33	16.0
5.52	15.3
6.29	14.9
140.1	10.2

Figure 5-13

Settling Time, h	Settled Height, cm	
	As Received	Electrocoagulated
0	35.7	35.5
0.04	no data	35.1
0.05	35.3	no data
0.06	no data	34.8
0.08	35.0	no data
0.15	no data	33.4
0.21	33.2	no data
0.24	no data	32.0
0.26	32.1	no data
0.30	no data	30.9
0.31	31.4	no data
0.35	no data	30.2
0.37	30.3	no data
0.41	29.6	no data
0.48	no data	28.4
0.50	28.6	no data
0.57	27.5	no data
0.60	no data	26.6
0.62	26.8	no data
0.71	25.7	no data
0.76	no data	24.5
0.77	25.0	no data
0.92	23.2	no data
0.93	no data	22.4
1.02	22.1	21.3
1.11	21.1	no data
1.17	no data	19.5
1.18	20.3	no data
1.24	19.6	no data
1.33	no data	17.8
1.34	18.6	no data
1.42	17.9	no data
1.50	17.1	no data
1.52	no data	16.0
1.62	16.4	no data
1.80	15.4	14.2
2.00	14.3	no data
2.10	no data	13.5
2.16	13.6	no data
2.43	12.9	no data
2.71	12.5	no data

Figure 5-13 continued

Settling Time, h	Settled Height, cm	
	As Received	Electrocoagulated
2.88	no data	12.4
3.06	12.1	no data
3.22	no data	12.1
3.62	no data	11.7
4.06	no data	11.4
4.62	no data	11.0
5.19	no data	10.7
18.06	8.0	no data
18.19	no data	7.6

APPENDIX B

CALCULATIONS

CHAPTER 1

Figure 1-4

A_{121} = 1.70x10^{-20} J [subscript 1, crystalline quartz; subscript 2, water]
(Masliyah,1994)
ε = 78.5 at 298°K
ε_o = 8.854x10^{-12} C/Vm
a = 5x10^{-7} m
ζ = -0.020 V
κ = 1.92x10^{8} m^{-1}
V_R was calculated from Equation 1-7 and V_A from Equation 1-12.

Figure 1-5

A_{121} = 1.70x10^{-20} J [subscript 1, crystalline quartz; subscript 2, water]
(Masliyah,1994)
ε = 78.5 at 298°K
ε_o = 8.854x10^{-12} C/Vm
a = 5x10^{-7} m
ζ = -0.020 V
V was calculated from Equation 1-14.

Figure 1-7

Derivation of Plotting Equations for Al-H_2O pC-pH Diagram (25°C)

These equations are developed on the condition that the aluminum species exist in thermodynamic equilibrium with amorphous $Al(OH)_3$.

For Line 1: $Al(OH)_3(am) + 3\ H^+ \leftrightarrow Al^{3+} + 3\ H_2O$ $\quad *K_{S0} = 10^{10.8}$

Hence, $[Al^{3+}] = 10^{10.8}\ [H^+]^3$

Thus, $\log [Al^{3+}] = 10.8 - 3\ pH$.

For Line 2: $Al^{3+} + H_2O \leftrightarrow AlOH^{2+} + H^+$ $\quad *K_1 = 10^{-5.02}$

Hence, $[AlOH^{2+}] = \dfrac{10^{-5.02}[Al^{3+}]}{[H^+]}$

$$\log [AlOH^{2+}] = -5.02 + \log [Al^{3+}] - \log [H^+]$$
$$= -5.02 + 10.8 - 3\,pH + pH$$
$$= 5.78 - 2\,pH$$

The equations for Lines 3 to 12 were calculated similarly.

Solubility Boundary Calculations

Line 1: $*K_{S0} = \dfrac{[Al^{3+}]}{[H^+]^3}$

Hence, $[Al^{3+}] = *K_{S0}[H^+]^3$

Line 2: $*K_1 = \dfrac{[AlOH^{2+}][H^+]}{[Al^{3+}]}$

Hence, $[AlOH^{2+}] = \dfrac{*K_1[Al^{3+}]}{[H^+]}$

Line 3: $*\beta_{2,2} = \dfrac{[Al_2(OH)_2^{4+}][H^+]^2}{[Al^{3+}]^2}$

Hence, $[Al_2(OH)_2^{4+}] = \dfrac{*\beta_{2,2}[Al^{3+}]^2}{[H^+]^2}$

Line 4: $*\beta_{15,6} = \dfrac{[Al_6(OH)_{15}^{3+}][H^+]^{15}}{[Al^{3+}]^6}$

Hence, $[Al_6(OH)_{15}^{3+}] = \dfrac{*\beta_{15,6}[Al^{3+}]^6}{[H^+]^{15}}$

Line 5: $*\beta_{20,8} = \dfrac{[Al_8(OH)_{20}^{4+}][H^+]^{20}}{[Al^{3+}]^8}$

Hence, $[Al_8(OH)_{20}^{4+}] = \dfrac{{}^*\beta_{20,8}[Al^{3+}]^8}{[H^+]^{20}}$

Line 6: ${}^*\beta_{34,13} = \dfrac{[Al_{13}(OH)_{34}^{5+}][H^+]^{34}}{[Al^{3+}]^{13}}$

Hence, $[Al_{13}(OH)_{34}^{5+}] = \dfrac{{}^*\beta_{34,13}[Al^{3+}]^{13}}{[H^+]^{34}}$

Line 7: ${}^*\beta_4 = \dfrac{[Al(OH)_4^-][H^+]^4}{[Al^{3+}]}$

Hence, $[Al(OH)_4^-] = \dfrac{{}^*\beta_4[Al^{3+}]}{[H^+]^4}$

Line 8: ${}^*\beta_3 = \dfrac{[Al(OH)_3^o][H^+]^3}{[Al^{3+}]}$

Hence, $[Al(OH)_3^o] = \dfrac{{}^*\beta_3[Al^{3+}]}{[H^+]^3}$

Line 9: ${}^*\beta_2 = \dfrac{[Al(OH)_2^+][H^+]^2}{[Al^{3+}]}$

Hence, $[Al(OH)_2^+] = \dfrac{{}^*\beta_2[Al^{3+}]}{[H^+]^2}$

Line 10: ${}^*\beta_{4,3} = \dfrac{[Al_3(OH)_4^{5+}][H^+]^4}{[Al^{3+}]^3}$

Hence, $[Al_3(OH)_4^{5+}] = \dfrac{{}^*\beta_{4,3}[Al^{3+}]^3}{[H^+]^4}$

Line 11: ${}^*\beta_{32,13} = \dfrac{[Al_{13}O_4(OH)_{24}^{7+}][H^+]^{32}}{\{Al^{3+}]^{13}}$

Hence, $[Al_{13}O_4(OH)_{24}^{7+}] = \dfrac{{}^*\beta_{32,13}[Al^{3+}]^{13}}{[H^+]^{32}}$

Line 12: ${}^*\beta_{17,7} = \dfrac{[Al_7(OH)_{17}^{4+}][H^+]^{17}}{[Al^{3+}]^7}$

Hence, $[Al_7(OH)_{17}^{4+}] = \dfrac{{}^*\beta_{17,7}[Al^{3+}]^7}{[H^+]^{17}}$

Let the concentration of the total dissolved aluminum in equilibrium with $Al(OH)_3(am) = C_{T,diss}$ mole/L. Thus,

$$C_{T,diss} = [Al^{3+}] + [AlOH^{2+}] + 2[Al_2(OH)_2^{4+}] + 6[Al_6(OH)_{15}^{3+}] + 8[Al_8(OH)_{20}^{4+}] + 13[Al_{13}(OH)_{34}^{5+}] + [Al(OH)_4^-] + [Al(OH)_3^o] + [Al(OH)_2^+] + 3[Al_3(OH)_4^{5+}] + 13[Al_{13}O_4(OH)_{24}^{7+}] + 7[Al_7(OH)_{17}^{4+}]$$

$$= [Al^{3+}]\left\{1 + \frac{{}^*K_1}{[H^+]} + 2\left(\frac{{}^*\beta_{2,2}[Al^{3+}]}{[H^+]^2}\right) + 6\left(\frac{{}^*\beta_{15,6}[Al^{3+}]^5}{[H^+]^{15}}\right) + 8\left(\frac{{}^*\beta_{20,8}[Al^{3+}]^7}{[H^+]^{20}}\right)\right\}$$

$$+ [Al^{3+}]\left\{13\left(\frac{{}^*\beta_{34,13}[Al^{3+}]^{12}}{[H^+]^{34}}\right) + \frac{{}^*\beta_4}{[H^+]^4} + \frac{{}^*\beta_3}{[H^+]^3} + \frac{{}^*\beta_2}{[H^+]^2} + 3\left(\frac{{}^*\beta_{4,3}[Al^{3+}]^2}{[H^+]^4}\right)\right\}$$

$$+ [Al^{3+}]\left\{13\left(\frac{{}^*\beta_{32,13}[Al^{3+}]^{12}}{[H^+]^{32}}\right) + 7\left(\frac{{}^*\beta_{17,7}[Al^{3+}]^6}{[H^+]^{17}}\right)\right\}$$

Substitution of $10^{10.8}[H^+]^3$ for $[Al^{3+}]$ and the respective values for the equilibrium constants allows $C_{T,diss}$ to be evaluated as follows.

$$C_{T,diss} = 10^{18.6}[H^+]^3 + 10^{5.8}[H^+]^2 + 10^{27.6}[H^+]^4 + 10^{44.1}[H^+]^5 + \frac{10^{-12.8}}{[H^+]} + 10^{-4.2} + 10^{1.5}[H^+] + 10^{42.8}[H^+]^7$$

$C_{T,diss}$ can now be calculated over a range of pH values, as the following example illustrates.

At pH 9, $[H^+] = 10^{-9}$ M. Hence, $C_{T,diss} = 10^{-8.4} + 10^{-12.2} + 10^{-8.4} + 10^{-0.9} + 10^{-3.8} +$

$$10^{-4.2} + 10^{-7.5} + 10^{-20.2} = 10^{-0.9} \text{ M}$$

Hence, log $C_{T,diss}$ = -0.9 at pH 9.

CHAPTER 2

Hydrometer Calculations

From measurements of the dimensions of the hydrometer, the effective depth of its centre of volume, L (m), was calculated from Equation B2-1.

$$L = L_1 + 0.5\left(BL - \frac{BV}{AR}\right) \qquad \text{(B2-1)}$$

where L_1 = distance from the top of the bulb to the reading on the stem, m
BL = bulb length, m
BV = bulb volume, m^3
AR = cross-sectional area of the graduated cylinder, m^3.

L_1 was calculated from Equation B2-2 as follows:

$$L_1 = SL - 1000DIV(\text{pulp SG} - 1.00) \qquad \text{(B2-2)}$$

where SL = stem length from the bulb to the 1.000 mark, m
DIV = length of 1 division (0.001 SG interval), m.

Following the calculation of L and the measurement of the absolute viscosity of de-ionized water (as described in Section 2.3.4), the Stokes Equation (Equation B2-3) enabled the calculation of the equivalent (*i.e.*, sphericity assumed) particle diameter, d (µm).

$$d = 10^6\left[\left(\frac{18\mu}{(\rho_s - \rho_\ell)g}\right)\left(\frac{L}{t}\right)\right]^{0.5} \qquad \text{(B2-3)}$$

where µ = absolute viscosity of de-ionized water, Pa.s
ρ_s = density of silica, kg/m^3
ρ_ℓ = density of de-ionized water, kg/m^3
g = gravitational constant, m/s^2
t = time, s.

The solids concentration, C (kg/m^3), was calculated from Equation B2-4.

$$C = \left(\frac{\rho_s}{\rho_s - \rho_\ell} \right) \left(\rho_p - \rho_\ell \right) \qquad \text{(B2-4)}$$

where ρ_p = pulp density, kg/m^3.

Values of C were used to calculate Y (wt %), the cumulative fraction of solids passing the size, d (μm), for a given hydrometer reading, as shown by Equation B2-5.

$$Y = \frac{100C}{C_o} \qquad \text{(B2-5)}$$

where C_o = initial solids concentration, kg/m^3.

Location of Stationary Positions

In the flat cell used: ℓ = 10.16 mm

d = 1.054 mm

Hence ℓ/d = 9.64.

Komagata's expression (Equation B2-6) for ℓ/d < 20 is:

$$\frac{s}{d} = 0.500 - \left[0.0833 + \frac{32}{\pi^5} \left(\frac{d}{\ell} \right) \right]^{0.5} \qquad \text{(B2-6)}$$

where s = distance of either stationary level from the closer cell wall, mm

d = internal cell width, mm

ℓ = internal height of cell, mm.

For the ℓ/d value of 9.64, the corresponding s/d ratio was 0.193. When the cell was filled with sample, the liquid caused the d value to become less than it was in air as a result of refraction. However, the s/d ratio was still valid (Rank Brothers, 1986), since the refractive index was the same for s and d.

Hence, s' = 0.193d', where the prime indicates refracted values.

Let x_1' = position of anterior (*i.e.*, closer to the objective lens) internal cell wall, mm

and x_2' = position of posterior (*i.e.*, closer to the light source) internal cell wall, mm.

Then, $d' = (x_2' - x_1')$ mm.

Hence, the location of the anterior stationary position is $(x_1' + s')$ mm, and
the location of the posterior stationary position is $(x_2' - s')$ mm.

The condenser was moved along its axis to focus on the respective internal wall, so that the related stationary position could be located with the micrometer.

Calculation of Zeta Potential

The Helmholtz-Smoluchowski equation for zeta potential, ζ (V), when $\kappa a >> 1$ is stated as Equation B2-7.

$$\zeta = \frac{\mu U}{\varepsilon \varepsilon_o E_\infty} \qquad \text{(B2-7)}$$

where μ = absolute viscosity of the aqueous medium, Pa.s
U = average electrophoretic velocity, m/s
ε = dielectric constant of water, dimensionless
ε_o = permittivity of vacuum, C/Vm
E_∞ = electric field strength, V/m.

In addition, $U = \frac{x}{t}$ m/s

where x = electrophoretic distance traversed by the particle in time t.

$$E_\infty = \frac{V}{3.27 \text{x} 10^{-2}\,\text{m}} \text{ V/m,}$$

where V = applied potential, V, and
$3.27 \text{x} 10^{-2}$ m = inter-electrode separation.

Estimation of Bulk Density of Electrocoagulated Silica

Basis of calculations: 1 m^3 of slurry

Mass of silica in slurry = 51.56 kg

Density of silica = 2534.8 kg/m^3

Silica volume = $\frac{51.56\ \text{kg}}{2534.8\ \text{kg/m}^3}$ = 0.0203 m^3

Measured bulk volume of sediment after 15 minutes' electrocoagulation = 0.0590 m^3.

Then, pore volume = 0.0590 – 0.0203 = 0.0387 m^3

Density of pore fluid (*i.e.*, supernatant) = 997.2 kg/m^3

Then, mass of pore fluid = 0.0387x997.2 = 38.59 kg

Bulk mass of sediment = 38.59 + 51.56 = 90.15 kg

Hence, bulk density of electrocoagulated silica = $\frac{90.15\ \text{kg}}{0.0590\ \text{m}^3}$ = 1528 kg/m^3

Wt % solids in the sediment = $\left(\frac{51.56}{90.15}\right)100$ = 57.2%

Volume % porosity of sediment = $\left(\frac{0.0387}{0.0590}\right)100$ = 65.6%

Errors in the Estimation of Bulk Density of Freshly Electrocoagulated Silica

Basis of calculations: 1.00 L of slurry in a 1-L graduated cylinder

Mass of silica in slurry =	51.56	g	
Density of silica =	2534.8	g/L	
Silica volume =	0.0203	L	
Sediment bulk volume error =	0.002	L	(± 2 mL)
Pore fluid density =	997.2	g/L	

Calculation of Sediment Bulk Volume

AC/EC Time (min)	Height per L of Slurry (cm)	Sediment	
		Height (cm)	Volume
15	35.6	2.1	0.0590
45	35.5	2.1	0.0592
75	35.7	2.4	0.0672
90	35.6	2.4	0.0674
120	36.3	2.5	0.0689

Calculation of Errors in Bulk Density, Wt % Solids and Vol % Porosity

Case	Sediment Bulk Volume (L)	Pore Volume (L)	Pore Fluid Mass (g)	Sediment Bulk Mass (g)	EC* Silica Bulk Density (kg/m^3)	Sediment Characteristics	
						Wt % Solids	Vol % Porosity
15 min, base	0.0590	0.0386	38.54	90.10	1527	57.2	65.5
15 min + 2 mL	0.0610	0.0406	40.53	92.09	1510	56.0	66.6
15 min - 2 mL	0.0570	0.0366	36.55	88.11	1546	58.5	64.3
45 min, base	0.0592	0.0388	38.71	90.27	1526	57.1	65.6
45 min + 2 mL	0.0612	0.0408	40.70	92.26	1509	55.9	66.7
45 min - 2 mL	0.0572	0.0368	36.71	88.27	1544	58.4	64.4
75 min, base	0.0672	0.0469	46.75	98.31	1462	52.4	69.7
75 min + 2 mL	0.0692	0.0489	48.75	100.31	1449	51.4	70.6
75 min - 2 mL	0.0652	0.0449	44.76	96.32	1477	53.5	68.8
90 min, base	0.0674	0.0471	46.94	98.50	1461	52.3	69.8
90 min + 2 mL	0.0694	0.0491	48.94	100.50	1448	51.3	70.7
90 min - 2 mL	0.0654	0.0451	44.95	96.51	1475	53.4	68.9
120 min, base	0.0689	0.0485	48.39	99.95	1451	51.6	70.5
120 min + 2 mL	0.0709	0.0505	50.39	101.95	1439	50.6	71.3
120 min - 2 mL	0.0669	0.0465	46.40	97.96	1465	52.6	69.6

*Electrocoagulated

Interparticle Separation in 5.0 wt % Suspension of As-received Silica

Assume a monodisperse suspension of spherical d_{50} particles of diameter 20 µm.

Volume of a d_{50} particle = 4.2×10^{-15} m^3

Mass of a d_{50} particle = 1.06×10^{-11} kg

Number of particles present in 210.5 g as-received silica = $\dfrac{0.2105 \text{ kg}}{1.06 \times 10^{-11} \text{ kg}}$

$= 2.0 \times 10^{10}$

Suspension volume = 4.083 L = 4.083×10^{-3} m^3

Hence, number concentration of particles = $4.9 \times 10^{12}/m^3$ of suspension

Water volume = 4.0 L = 4.0×10^{-3} m^3

Thus, ratio of particle volume:water volume = 0.0208

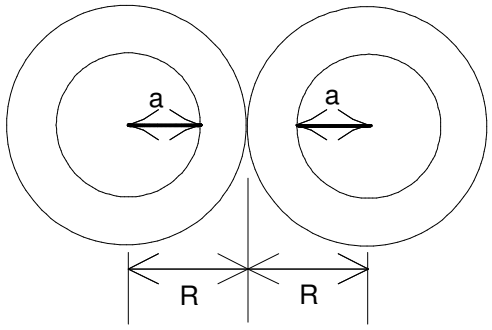

Assume that each spherical particle of radius a (metre) is enveloped in a sphere of water, such that the combined radius is R (metre), as sketched above.

Hence, volume of water containing 1 particle = $\dfrac{4.2 \times 10^{-15} \text{ m}^3}{0.0208} - 4.2 \times 10^{-15} \text{ m}^3$

$= 2.0 \times 10^{-13}$ m^3

Therefore, $\dfrac{4}{3}\pi\left(R^3 - a^3\right) = 2.0 \times 10^{-13}$ m^3

Thus, $R = 3.7 \times 10^{-5}$ m = 37 µm

Interparticle separation = 2(R – a) = 2(37 – 10) µm = 54 µm

Estimation of Collision Frequencies

Constants [Taken from Masliyah (1994) unless indicated otherwise]

Boltzmann constant, $k = 1.381 \times 10^{-23}$ J/°K

Feed suspension temperature, T = 294.5°K

$kT = 4.067 \times 10^{-21}$ J

Feed water viscosity, $\mu = 8.962 \times 10^{-4}$ Pa.s

Number concentration of silica particles, $n_s = 4.9 \times 10^{12}/m^3$

Radius of d_{50} size silica particle, $a_s = 10^{-5}$ m

Shear rate at impeller tip speed of 1.73 m/s, $\dot{\gamma} = 900\ s^{-1}$

Ionic radius of aluminum, $a_{Al} = 5.3 \times 10^{-11}$ m (Orvig, 1993)

Other Symbols

D_{Al}: diffusion coefficient of aluminum ion (m^2/s)

D_s: diffusion coefficient of d_{50} size silica particle (m^2/s)

$J_{Al\text{-}s}$: aluminum ion-silica particle collision frequency (collisions/m^3/s)

$J_{s\text{-}s}$: silica interparticle collision frequency (collisions/m^3/s)

n_{Al}: number concentration of aluminum ions (ions/m^3)

M: molar concentration (mol/L)

N_a: Avogadro's number (6.02×10^{23} ions/mole)

Simple Brownian Motion: Ion-Particle Collision Frequency

At infinite dilution: $D_{Al} = \dfrac{kT}{6\pi\mu a_{Al}} = \dfrac{4.067 \times 10^{-21}}{6\pi(8.962 \times 10^{-4})(5.3 \times 10^{-11})} = 4.5 \times 10^{-9}\ m^2/s$

A similar calculation of D_s gives a value of 2.4×10^{-14} m^2/s, five orders of magnitude less than D_{Al}, consistent with the non-colloidal particle size. Hence, D_s is negligible in comparison to D_{Al}. It should be noted that the actual value of D_{Al} would be modified by the presence of the silica particles, by diffusing Na^+ and Cl^- ions, by dispersive and electrostatic interactions, and by the oscillating AC electric field. Complex corrections can be made for these influences on D_{Al} (Masliyah, 1994) but, for the present purpose, they are not justifiable. As electrocoagulation proceeded, D_{Al} increased as a result of its direct dependence on temperature and its inverse dependence on the water viscosity.

The frequency of collision between aluminum ions and silica particles is given by:

$$J_{Al\text{-}s} = 4\pi(a_{Al} + a_s)(D_{Al} + D_s)n_{Al}n_s.$$

Since $D_{Al} >> D_s$ and $a_{Al} << a_s$,

$$J_{Al\text{-}s} = 4\pi a_s D_{Al} n_{Al} n_s.$$

Data for Figure 2-14 given in Appendix A allow the aluminum dosing rate to be estimated at 0.4 mg/min or $2.3\text{x}10^{-7}$ mol/s. Therefore, the concentration increased by $5.7\text{x}10^{-8}$ mol/L/s.

Hence, the number concentration rate of change = $10^3 M N_a$ ions/m^3/s

$= 10^3(5.7\text{x}10^{-8})(6.02\text{x}10^{23})$ ions/m^3/s

$= 3.4\text{x}10^{19}$ ions/m^3/s

$= n_{Al}$

The collision rate is estimated to have been:

$$J_{Al\text{-}s} = 4\pi(10^{-5})(4.5\text{x}10^{-9})(3.4\text{x}10^{19})(4.9\text{x}10^{12}) = 9.4\text{x}10^{19} \text{ collisions/m}^3\text{/s}.$$

Simple Shear: Interparticle Collision Frequency

The collision frequency among silica particles is estimated as follows.

$$J_{s\text{-}s} = \frac{32}{3}(a_s)^3 \dot{\gamma}(n_s)^2$$

$$= \frac{32}{3}\left(10^{-5}\right)^3(900)\left(4.9\times10^{12}\right)^2$$

$= 2.3\text{x}10^{14}$ collisions/m^3/s

Simple Shear: Ion-Particle Collision Frequency

The frequency of collision between aluminum ions and silica particles is estimated by:

$$J_{Al\text{-}s} = \frac{4}{3}(a_{Al} + a_s)^3 \dot{\gamma} n_{Al} n_s$$

Since $a_{Al} << a_s$,

$$J_{Al\text{-}s} = \frac{4}{3}(a_s)^3 \dot{\gamma} n_{Al} n_s$$

$$= \frac{4}{3}\left(10^{-5}\right)^3 (900)\left(3.4\times10^{19}\right)\left(4.9\times10^{12}\right)$$

$$= 2.0\text{x}10^{20} \text{ collisions/m}^3\text{/s}$$

Hence, the ion-particle collision rate was doubled by the agitation rate that was applied.

Theoretical Aluminum Concentrations in AC/EC-treated Water

I = current, A

t = electrocoagulation time, min

C_T = theoretical total Al concentration in AC/EC-treated water, mg/L

$$C_T = \frac{(60\times It)C\times 26.98\dfrac{\text{g Al}}{\text{mol Al}}\times 1000\dfrac{\text{mg}}{\text{g}}}{96{,}485\dfrac{C}{\text{eq}}\times 3\dfrac{\text{eq Al}}{\text{mol Al}}\times 4.0\text{ L}} = 1.398\ It \text{ mg/L}$$

For I = 2.1 A, C_T = 2.936t mg/L Al.

Hence, for t = 15 min, C_T = 44.0 mg/L Al.

CHAPTER 3

Aluminum Mass Balance on AC/EC Treatment of Water

Basis of Aluminum Balance

Total Al input = Al released from electrodes

Total Al output = Al dissolved in AC/EC-treated water + Al in precipitate + Al in solids recovered from electrode surfaces

Masses and Volumes

Mass lost from electrodes = 0.22 g

Volume of AC/EC-treated water = 4.0 L

Mass of precipitate recovered = 524.0 mg

Mass of solids recovered from electrode surfaces = 251.2 mg

Analyses

Electrode material: 91.8% Al

AC/EC-treated water: 3.0 mg/L Al

Precipitate: 36.5% Al

Solids recovered from electrode surfaces: 34.8% Al

Aluminum Masses

Al released from electrodes = (0.22)(0.918) g = 0.202 g = 202.0 mg

Total Al input = 202.0 mg

Al dissolved in AC/EC-treated water = (4.0)(3.0) mg = 12.0 mg

Al in precipitate = (524)(0.365) mg = 191.3 mg

Al in solids recovered from electrode surfaces = (251.2)(0.348) mg = 87.4 mg

Total Al output = 290.7 mg, equivalent to 143.9% of the total input.

Aluminum Distribution

Relative to the total output, the mass distribution of Al is as follows:

Al dissolved in AC/EC-treated water : 4.1%

Al in precipitate: 65.8%

Al in solids recovered from electrode surfaces: 30.1%

Total Al output: 100.0%

Aluminum Mass Balance on Indirect Electrocoagulation of Silica

Basis of Aluminum Balance

Total Al input = Al in precipitate + Al dissolved in AC/EC-treated water + Al in as-received silica

Total Al output = Al in electrocoagulated silica + Al in supernatant

Masses and Volumes

Mass of precipitate/L AC/EC-treated water = 131.0 mg

Volume of AC/EC-treated water = 1.00 L

Mass of as-received silica = 52.63 g

Mass of electrocoagulated silica = 52.63 g

Volume of supernatant = 1.00 L

Analyses

Precipitate: 36.5% Al

AC/EC-treated water: 3.0 mg/L Al

As-received silica: 0.59% Al

Electrocoagulated silica: 0.34% Al

Supernatant: 1.5 mg/L Al

Aluminum Masses

Al in precipitate = (131.0)(0.365) mg = 47.8 mg

Al dissolved in AC/EC-treated water = 3.0 mg

Al in as-received silica = (52.63)(0.0059)(1000) mg = 310.5 mg

Total Al input = 361.3 mg

Al in electrocoagulated silica = (52.63)(0.0034)(1000) mg = 178.9 mg

Al in supernatant = 1.5 mg

Total Al output = 180.4 mg, equivalent to 49.9% of the total input.

Aluminum Distribution

Inputs

Al in precipitate: 13.3%

Al dissolved in AC/EC-treated water: 0.8%

Al in as-received silica: 85.9%

Total Al input: 100.0%

Outputs

Al in electrocoagulated silica: 99.2%

Al in supernatant: 0.8%

Total Al output: 100.0%

Specific Mass Adsorption Calculations

Volume of sphere = $\frac{\pi d^3}{6}$

Equivalent diameter of d_{50} particle in as-received silica = 2×10^{-5} m

Thus, volume of d_{50} particle = $\frac{\pi}{6}\left(2\times10^{-5}\right)^3 \text{ m}^3 = 4.2\times10^{-15} \text{ m}^3$

Density of as-received silica = 2534.8 kg/m^3

Hence, mass of a d_{50} particle = $(4.2 \times 10^{-15})(2534.8)$ kg = 1.1×10^{-11} kg

Let the mass of as-received silica slurried with 0.50 L AC/EC-treated water be W g.

Then, number of particles = $\frac{W\times10^{-3}}{1.1\times10^{-11}} = (9.4 \times 10^7)W$

Surface area of sphere = πd^2

Surface area of a d_{50} particle = $\pi(2 \times 10^{-5})^2$ m^2 = 1.3×10^{-9} m^2

Hence, specific surface area of a d_{50} particle = $\left(\frac{1.3\times10^{-9}}{1.1\times10^{-11}}\right)$ m^2/kg = 118.2 m^2/kg

= 0.12 m^2/g

Total surface area of W g as-received silica = 0.118W m^2

Volume of AC/EC-treated water = 0.50 L

Al concentration in AC/EC-treated water = C_o mg/L

Al concentration in supernatant water = C mg/L

Mass of Al adsorbed = $0.50(C_o - C)$ mg

Hence, specific mass adsorption =

$$\left[\frac{0.50(C_o - C)}{0.118W}\right] \text{mg/m}^2 = 4.24\left(\frac{C_o - C}{W}\right) \text{mg/m}^2$$